Fundamental Investigation of Localised Forced Ignition in Turbulent Homogeneous and Stratified Mixtures: A Direct Numerical Simulation Analysis

Dipal Patel

School of Mechanical and Systems Engineering

Newcastle University

This thesis is submitted for the degree of

Doctor of Philosophy

March 2017

गुरुर्ब्रह्मा गुरुर्विष्णु गुरुर्देवो महेश्वरः।
गुरुः साक्षात् परब्रह्मा तस्मै श्री गुरुवे नमः।

Gurur Brahma Gurur Vishnu Gurur Devo Maheshvara |
Gurur Shashaath Para-Brahma Tasmai Shri Guruve Namah |

I prostrate to that Sri Guru (the teacher),
who is himself Brahma (the force of creation),
Vishnu (the force of preservation),
and God Maheshvara (the force of destruction or transformation),
and who is verily the Supreme Absolute itself.

Declaration

I hereby declare that this thesis is my own work and that I have correctly acknowledge the work of others. This submission is in accordance with Newcastle University and School of Mechanical and Systems Engineering guidance on good academic conduct. I certify that no part of the material offered has been previously submitted by me for a degree or other qualification in this or any other University. I confirm that the word length is within the prescribed range as advised by my school and faculty. I confirm that this thesis does not contain collaborative work. This thesis contains approximately 58,000 words[1], 103 figures and 19 tables.

Dipal Patel
March 2017

[1] Using LyXProcessor

Acknowledgements

I would like to express my gratitude to **Prof. Nilanjan Chakraborty** for his continuous support and guidance throughout this study. I also wish to thank him for his help, his constructive criticisms, and above all for providing many opportunities for conferences. I am grateful to **Dr. David Swailes** for all his help and for his invaluable suggestions during critical moments. I would like to express my sincere thanks to Dr. Daniel Wacks and Dr. Tamir Brosh for their help and interest in my work. I would like to offer my thanks to Mr. Ian Pitcher and Mr. David Wall for their help and support.

I am grateful to the Engineering and Physical Sciences Research Council (EPSRC) for the financial support through the course of this PhD. Additionally, I am grateful to the Combustion Institute for the travel grant, which have allowed me to attend and present part of this work.

I would like to thank Jiawei Lai, Sahin Yigit and Bruno Machado for their wonderful company and great discussions during this PhD, who are dear to me and I hope to preserve their priceless friendship in the future.

My sincere thanks go to my wife Dipika for her deep thoughts, endless patience and encouragements that has kept me motivated. The most important of all, I thank my parents for being a source of constant moral courage and inspiration. Without their support this would never been possible.

Abstract

Localised forced ignition (e.g. spark or laser ignition) of combustible mixtures has a number of important applications ranging from Gasoline Direct Injection (GDI) engines, Lean Premixed Prevaporised (LPP) combustors to high-altitude relight in aero-gas turbines. An improved understanding of localised ignition of combustible mixtures is essential for fire/explosion safety and also for designing a reliable ignition system in Internal Combustion (IC) engines and gas turbines so that self-sustained combustion subsequent to ignition can be achieved without compromising on emissions and energy-efficiency. The aforementioned importance of forced ignition serves the motivation behind the current analysis.

In this thesis, localised forced ignition of turbulent homogeneous and stratified mixtures has been analysed in detail using three-dimensional compressible simple chemistry Direct Numerical Simulations (DNS) for range of different parameters (e.g. root-mean-square (rms) values of turbulent velocity (u') and equivalence ratio fluctuations, and the length scales of turbulent fluid motion and mixture inhomogeneity). The influences of energy deposition characteristics on localised forced ignition of turbulent homogeneous mixtures have been analysed for different turbulent velocity fluctuations in order to identify the favourable conditions in terms of the characteristic width and duration of ignition energy deposition ignition for the purpose of achieving self-sustained combustion. Moreover, the ignitability of turbulent homogeneous mixtures and the corresponding value of Minimum Ignition Energy (MIE) in the case of localised forced ignition have been numerically analysed for different values of Karlovitz number Ka. It has been found that for the given values of equivalence ratio and u', an increase in the energy deposition width leads to an increase the magnitude of minimum energy requirements for successful ignition and self-sustained combustion.

Additionally, the influences of initial mixture distributions for both globally stoichiometric and fuel-lean stratified mixture on localised forced ignition of stratified mixtures have been analysed for different rms values of equivalence ratio, turbulent velocity fluctuations, and the Taylor micro-scale of equivalence ratio variation for ini-

tial presumed Bi-modal and Gaussian distribution of equivalence ratio. It has been demonstrated that the initial equivalence ratio distribution has significant effects on the early stages of burning of stratified mixtures following successful localised forced ignition. The results show that the rate of heat transfer from hot gas kernel increases with increasing turbulent intensity, which acts to reduce the extent of burning, and in some extreme cases may lead to flame extinction. The results demonstrated that favourable conditions in terms of initial mixture distribution, equivalence ratio variation, length scale of mixture inhomogeneity, and rms turbulent velocity fluctuation are required for self-sustained combustion on following successful ignition of stratified mixtures.

Furthermore, the effects of fuel Lewis number Le_F (ranging from 0.8 to 1.2) on ignitability of both homogeneous and stratified mixtures and early stage of burning following localised forced ignition have been analysed based on DNS data. It has been found that the ignition energy which leads to successful ignition and subsequent self-sustained flame propagation increases with increasing Le_F for both stratified and homogeneous mixtures. Detailed physical explanations have been provided for the influences of the various parameters which significant affect the performance of localised forced ignition. Qualitative similarities between computational findings and experimental observations have been indicated, where possible, and limited number DNS simulations of localised forced ignition in n-heptane-air mixture with detailed chemistry have been carried out to confirm qualitative similarities between simulation results obtained using simple and detailed chemical mechanisms.

Keywords: localised forced ignition, Direct Numerical Simulations, equivalence ratio, fuel Lewis number, equivalence ratio distribution, homogeneous mixtures, stratified mixtures

Publications

Some portion of the work from this thesis are published and presented.

Journal Papers

1. **Patel, D.**, Chakraborty, N., (2016), Effects of Mixture Distribution on Localised Forced Ignition of Stratified Mixtures: A Direct Numerical Simulation Study, Combustion Science and Technology 188.11-12 (2016): 1904-1924. [153]

2. **Patel, D.**, Chakraborty, N., (2016), Effects of Fuel Lewis Number on Localised Forced Ignition of Globally Stoichiometric Stratified Mixtures: A Numerical Investigation, Flow Turbulence and Combustion, 96(4), 1083-1105. [151]

3. **Patel, D.**, Chakraborty, N., (2016), Effects of Fuel Lewis Number on Localised Forced Ignition of Turbulent Homogeneous Mixtures: A Numerical Investigation, International Journal of Spray and Combustion Dynamics, 8(3), 183-196. [152]

4. **Patel, D.**, Chakraborty, N., (2015), Effects of Energy Deposition Characteristics on Localised Forced Ignition of Homogeneous Mixtures, International Journal of Spray and Combustion Dynamics 7(2), 151-174. [150]

5. Brosh, T., **Patel, D.**, Wacks, D., Chakraborty, N., (2015), Numerical Investigation of Localised Forced Ignition of Pulverised Coal Particle-laden Mixtures: A Direct Numerical Simulation (DNS) Analysis, Fuel , 145, 50-62. [37]

6. **Patel, D.**, Chakraborty, N., (2014), Localised Forced Ignition of Globally Stoichiometric Stratified Mixtures: A Numerical Investigation, Combustion Theory and Modelling, 18(6), 627-651. [149]

Conference Proceedings

1. **Patel, D.**, Chakraborty, N., Effects of mixture fraction on localised forced ignition of stratified mixtures: A Numerical Investigation, 25th International Colloquium on the Dynamics of Explosions and Reactive Systems, August 2-7, 2015, Leeds, UK.

2. Brosh, T., Marincola, F.C., **Patel, D.**, Wacks, D., Chakraborty, N., On Conditions for Self-sustained combustion of pulverised coal particle-laden mixtures following localised forced ignition: A Direct Numerical Simulation Analysis, 25th International Colloquium on the Dynamics of Explosions and Reactive Systems, August 2-7, 2015, Leeds, UK.

3. **Patel, D.**, Chakraborty, N., Effects of Fuel Lewis Number with Energy Deposition Characteristics on Localised Forced Ignition of Homogeneous Mixtures: A Direct Numerical Simulation Analysis, 12th International Conference on Energy of a Clean Environment, July 5-9, 2015, Lisbon, Portugal.

4. **Patel, D.**, Chakraborty, N., Effects of Lewis Number on Localised Forced Ignition of Globally Stoichiometric Stratified Mixtures: A Numerical Investigation, in Ninth Mediterranean Combustion Symposium, June 7-11, 2015, Rhodes, Greece.

5. **Patel, D.**, Chakraborty, N., Effects of Combustion Regime On Localised Forced Ignition Of Turbulent Homogeneous Mixtures: A Direct Numerical Simulation Analysis, in 7th European Combustion Meeting, March 30 – April 02, 2015, Budapest, Hungary.

6. **Patel, D.**, Chakraborty, N., Effects of Mixture Distribution on Localised Forced Ignition of Globally Stoichiometric Stratified Mixtures: A Direct Numerical Simulation Study, in An International Meeting Towards Sustainable Combustion, November 19-21, 2014, Lisbon, Portugal.

7. **Patel, D.**, Chakraborty, N., Effects of Energy Deposition Characteristics in Localised Forced Ignition of Turbulent Homogeneous Mixtures: A Direct Numerical Simulation (DNS) Analysis, in International Conference on Heat Transfer and Fluid Flow (HTFF'14), August 11-12, 2014, Prague, Czech Republic.

8. Brosh, T., **Patel, D.**, Wacks, D., Chakraborty, N., Localised Forced Ignition of Pulverised Coal Particle-laden Mixtures: A Direct Numerical Simulation Analysis, in International Conference on Heat Transfer and Fluid Flow (HTFF'14), August 11-12, 2014, Prague, Czech Republic.

9. **Patel, D.**, Chakraborty, N., Localised Forced Ignition Of Stratified Mixtures: A Direct Numerical Simulation (DNS) Analysis, in Joint Meeting of the British and Scandinavian Nordic Section of the Combustion Institute, March 27-28, 2014, Cambridge, UK.

Contents

List of Figures

List of Tables

Nomenclature

Roman Symbols

a	Sonic speed
A_H	Parameter originating due to reactant inhomogeneity
A_m	Frequency factor for a given step m
A_q	Constant in the Gaussian distribution equation
a_{sp}	Parameter that determined the total energy deposited by the igniter
B	Pre-exponential factor
b_{sp}	Energy duration parameter
c	Reaction progress variable
C_P	Specific heat capacity at constant pressure
C_V	Specific heat capacity at constant volume
D	Diffusivity
D_i	Mass Diffusivity of given species i
d_q	Quenching distance
D_{mol}	Molecular thermal diffusivity
D_{th}	Thermal diffusivity
D_t	Eddy thermal diffusivity
Da	Damköhler number
E	Stagnation internal energy
E_m	Activation energy for a given step m
E_{ac}	Activation energy
F	Flammability Factor
h_α	Enthalpy of formation of the species α
H_ϕ	Heat release per unit mass of fuel
I_c	Takeno's flame index
Ka	Karlovitz numbers
L	Computational domain length

l_f	Laminar flame thickness (Zel'dovich flame thickness for the stoichiometric mixture)
L_i	Wave amplitude variation
L_{11}	Integral length scale
l_δ	Reaction layer thickness
l_ϕ	Length scale of mixture inhomogeneity (Taylor micro-scale of the equivalence ratio variation)
l_T	Length scale of thermal inhomogeneity
Le_F	Fuel Lewis number
Le_i	Lewis number of given species i
Le_O	Oxidiser Lewis number
M	Number of steps in reaction mechanism
m	Given step in reaction mechanism
M_b	Normalised burned gas mass
m_b	Burned gas mass
Ma	Mach number
N	Number of species
N_g	Number of grid points
n_m	Temperature exponent for a given step m
N_ξ	Scalar dissipation rate of the mixture fraction
P	Pressure
Pr	Prandtl number
Q	Elementry cells
R	Width of the Gaussian profile
r	Radial distance from the centre of the igniter
R_0	Universal Gas constant
R_{fk}	Radius of a flame kernel
Re	Reynolds number
Re_t	Turbulent Reynolds number
Re_λ	Reynolds number based on Taylor micro scale
s	Mass of oxidiser consumed per unit mass of fuel consumption
$S_{b(\phi)}$	Laminar burning velocity at Equivalence ratio ϕ
$S_{L,0}\,(S_L)$	Unstrained laminar burning velocity of the stoichiometric mixture
Sc	Schmidt number
T_0	Initial temperature

T_C	Critical temperature
t_e	Large eddy turn over time
t_f	Flame time scale (characteristic chemical time scale)
T_P	Temperature of products
T_R	Temperature of reactants
t_η	Life time for the small eddies of turbulence
T_{ad}	Adiabatic flame temperature
T_{ref}	Reference temperature
t_{sp}	Time duration over which energy is deposited by the igniter
u_i	i^{th} component of the velocity vector
$V_{\alpha j}$	Diffusion velocity of the species α
W_α	Molar mass of species α
Y_F	Fuel mass fraction
Y_O	Oxidiser mass fraction
Y_α	Mass fraction of the species α
$Y_{F\infty}$	Fuel mass fraction in the pure fuel stream
$Y_{Fb(\phi)}$	Fuel mass fraction in the burned gas corresponding to ϕ
$Y_{Fu(\phi)}$	Fuel mass fraction in the unburned gas corresponding to ϕ
$Y_{O\infty}$	Oxidiser mass fraction in air

Accents

$\bar{\rho}$	Mean density
$\bar{\vec{q}}$	Mean heat flux from the hot gas kernel
$\dot{\Omega}_F$	Normalised fuel reaction rate magnitude
$\dot{Q}$	Ignition power
$\dot{w}_c$	Reaction progress variable reaction rate
$\dot{w}_T$	Source term origination from heat release due to combustion
$\dot{w}_\alpha$	Chemical reaction rate
$\hat{T}$	Instantaneous temperature
$\langle \ldots \rangle$	Global mean evaluated over the entire computational domain
$\langle T \rangle$	Global mean of temperature
$\langle \phi \rangle$	Global mean of equivalence ratio
$\tilde{\hat{T}}$	Density-weighted mean (Favre-mean) temperature
$\vec{\kappa}$	Linear wave number vector
$\vec{N}$	Flame normal vector
$\vec{n}$	Local flame normal vector

$\vec{r}$	Unit radial vector from the centre of the hot gas kernel
$B^{\star}$	Pre-exponential factor related constant
q'''	Ignition source term accounting heat addition in the energy transport equation
T'	Temperature fluctuation
$T^{\star}$	Instantaneous dimensional temperature
u'	RMS of Turbulent Velocity
$v''_{\alpha,m}$	Product stoichiometric coefficient for a given step m
$v'_{\alpha,m}$	Reactant stoichiometric coefficient for a given step m
ϕ'	RMS of equivalence ratio
ξ'	RMS of mixture fraction driven by ϕ fluctuations
${N_{\xi}}^{+}$	Normalised scalar dissipation rate

Abbreviations

3D	Three-Dimensional
CFD	Computational Fluid Dynamics
DI	Direct Injection
DNS	Direct Numerical Simulations
GDI	Gasoline Direct Injection
IC	Internal Combustion
LPP	Lean Premixed Prevaporised
MIE	Minimum Ignition Energy
PDF	Probability Density Function
RMS	Root Mean Square
SI	Spark Ignition

Greek Symbols

α_i	Thermal conductivity of given species i
α_{T_0}	Thermal diffusivity in the unburned reactant
β	Zel'dovich number
Δx	Grid spacing
δ_D	Diffusive flame thickness
δ_{th}	Thermal flame thickness
η	Kolmogorov length scale
γ	Ratio of specific heats
κ_0	Wave number magniture at which $E(\kappa)$ attains its maximum value
κ_1 , κ_2	Two principle curvature of the concerned flame surface

κ_m	Arithmetic mean of principle curvatures
λ	Taylor micro scale
λ_0	Thermal conductivity
λ_i	Characteristic wave velocities
μ	Dynamic viscosity
ν	Kinematic viscosity
ϕ	Equivalence ratio
ρ	Density
τ	Heat release parameter
τ_{ij}	Viscous stress tensor
ε	Dissipation rate
ξ	Mixture fraction
ξ_{lean}	Lean flammability limit
ξ_{rich}	Rich flammability limit
ξ_{st}	Stoichiometric mixture fraction

Chapter 1

Introduction

In this Chapter, the combustion and ignition are defined from a fundamental point of view. Then, various kinds of ignition sources are presented and discussed. Finally, this Chapter ends with the research objectives and structure of this thesis.

1.1 Combustion

Burning fossil fuels play predominant role for providing energy in domestic use, industrial use and in transportation. With recent evolvement of alternative sources (e.g. wind and solar), the energy production by means of combustion for high-power density applications is expected to remain dominant for many years to come. With the modern trends of conventional Internal Combustion (IC) engines and aircraft gas turbines to use lean mixture and to reduce the emission levels, the solution to the efficient ignition system becomes a high priority for the automobile and aircraft industries.

Generally, combustion can be divided into two categories: premixed and non-premixed combustion. Figure 1.1 shows Venn diagram representing different combustion modes. Each of these categories has their advantages and disadvantages, but premixed combustion offers advantages in terms of pollutant emission because the maximum burned gas temperature can be controlled by the mixture composition. Thus fuel lean premixed combustion can potentially lead to reduction of burned gas temperature which offers reduction in thermal NO_X emission [95, 136, 179]. In the demand to reduce harmful emissions, industrial combustors are designed to operate under fuel lean conditions and with inhomogeneous mixtures, which increasingly often leads to stratified combustion [8, 67]. Many engineering combustion systems including: lean premixed prevaporised (LPP) gas turbine combustor, afterburners,

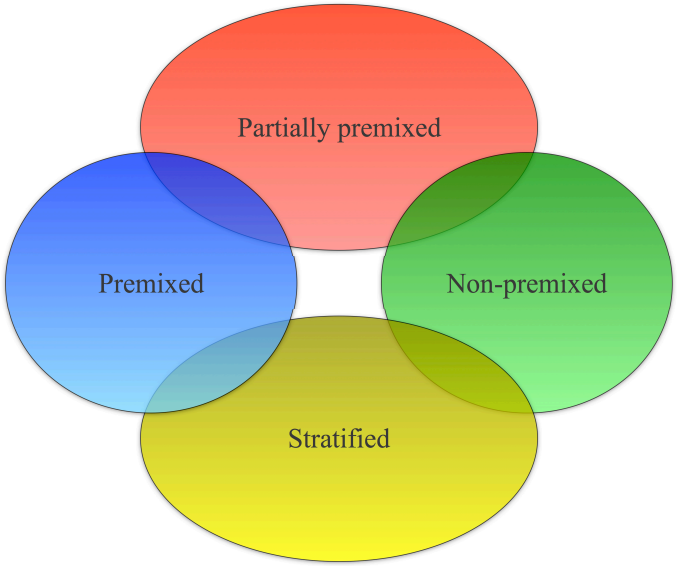

Figure 1.1: Venn diagram representing combustion modes.

and direct-injection spark-ignition internal combustion engines, all operate in inhomogeneous reactants mode to gain full advantages of a spatially varying mixture field [37, 92, 119, 139].

The premixed combustion has cleaner burnt products but it has a smaller range of operating conditions, making this mode of flame difficult to control. On the contrary, having a wider operating range, a non-premixed combustion is easier to control [119]. Stratified premixed combustion combines advantages of both premixed and non-premixed combustion modes (see Figure 1.1). In stratified combustion a premixed flame originated from ignition source travels through mixture field of varying equivalence ratio, which may be either all lean or all rich and the flame propagation is strongly affected by local gradient of mixture field [193]. For instance, in a Gasoline Direct Injection (GDI) spark ignition engine, the time interval between fuel being injected into the combustion chamber and the spark ignition may be too short for the mixture composition to be homogeneous at the instant of ignition, but it is long enough for most of the fuel to be mixed with air before burning. The flame kernel originated by the spark propagates through a highly inhomogeneous mixture field characterised by large fluctuations in the equivalence ratio, with the ensemble-averaged mixture composition being lean (and even beyond lean flammability limit) in some spatial regions and rich (and even beyond the rich flammability limit) in other regions. Such burning regime is sometimes called premixed/nonpremixed combustion [27, 122]. In such ex-

ample inhomogeneously premixed combustion is important, as it controls majority of the total heat release, while the afterburning of the lean and rich products in the diffusion mode may be of significant importance as far as pollutant (e.g. soot formation) is concerned. By contrast, in a diesel engine, the time interval between fuel injection and autoignition is so short that only a small amount of the fuel is mixed with air before autoignition of mixture due to compression. Here, also lean and rich premixed turbulent flames coexist with diffusion flames, but contrary to GDI engine, the total heat release is mainly controlled by the non-premixed mode of burning, and such regime is called nonpremixed/premixed combustion [27, 122]. All aforementioned combustion modes (stratified, premixed/nonpremixed, and nonpremixed/premixed burning) are commonly absorbed under partially-premixed flames [122].

Direct Numerical Simulations (DNS) is a computational fluid dynamics (CFD) tool which resolves all flow features explicitly and is widely adopted in combustion research. Cant [40] presented the feasibility and challenges of DNS in tackling the problems of turbulent combustion. DNS often demands a very large computational power, especially when resolving the forced ignition process of turbulent reacting flows. Additionally DNS is a powerful tool for capturing important quantities (e.g. Takeno's index (discussed in 3.4.1.1), displacement speed etc.), which are not easily measured through experimental data. Despite the computation cost, DNS is highly accurate and provides an enormous amount of detailed information in comparison to experiments because it is either extremely expensive or impossible to obtain three-dimensional temporally and spatially resolved data by experimental means.

1.2 Ignition

Forced ignition involves an external energy that leads to exothermic reactions and ultimately a flame in a combustible mixture. Ignition not only initiates combustion but also influences subsequent combustion. Ignition can be caused with the help of an external stimulus such as an electric spark, or spontaneously due to high temperature without any external source such as auto-ignition in a compression ignition engine. This thesis mainly concentrates on forced ignition with an external source. The external source that provides localised heating in a combustible mixture may be an electric spark or another kind of a laser or plasma jet [2]. Ignition is a crucial event in the operation of many systems such as gas turbines, Spark Ignition (SI) engines, industrial furnaces and boilers. The ignition in jet engine combustors is an important

phenomenon due to the desirability of fast ignition and its relation to the issue of flame stabilization. Similar considerations apply to spark ignition engines, where fast well-controlled ignition is important to engine efficiency and emissions (as incomplete combustion can be avoided which forms soot and NO_X). For aircraft gas turbine, the importance of reliable ignition is the need for easy light-up during ground starting and rapid relighting in the event of flameout [3]. The successfulness of an ignition can be indicated by continued burning after the ignition source has been switched off, and such definition is considered in the present thesis.

1.2.1 Various Ignition Sources

The forced ignition is the only source of ignition considered in the present thesis, other different means of ignition sources are briefly discussed in this section.

Spark Ignition

For gas turbines, the most satisfactory and convenient mode of ignition is some form of electrical discharge, such as a spark or an arc discharge [116]. In spark ignition, the electrical energy is converted in fairly efficient manner into heat that is concentrated into small volume. Another feature of spark ignition is the transient deposition of ignition energy in a very short duration (in terms of microseconds). The next stage is to examine whether or not this energy deposition leads to appearance of flame, identifying conditions which supports successful ignition rather than misfire. Moreover, complete control can be exercised over the duration, amount of energy and characteristic width of ignition energy distribution in each discharge [116]. The parameters affecting the forced ignition will be discussed in more details in Chapter 4.

Laser Ignition

The roots of laser ignition research may be traced back to the first discovery of laser-induced optical breakdown by R.W. Terhune in 1960's [63]. It has been known that the focused output of a powerful Q-switched laser beam can cause the electrical breakdown of gases [116]. The focused laser beam creates an electric field of sufficient intensity to cause dielectric breakdown of the air-fuel mixture. The process steps are: multi-photon ionization of a few molecules to release electrons; 'inverse bremsstrahlung' to increase the electron kinetic energies, collision with and ionization of other molecules; electron avalanche and breakdown of the gas mixture [63]. At atmospheric pressure,

the electric field strength necessary for laser induced breakdown in gases is higher than for SI and, for ns duration pulses, the threshold optical intensity for non-resonant breakdown is of the order $10^{11}\,{}^{W}/_{cm^2}$. Increasing the pressure to levels representative of real engine conditions reduces the MIE [140]. This phenomenon has potential advantages over conventional methods of ignition. It offers ignition location to be accurately positioned, also reduces flame kernel quenching (due to lack of an intruding electrodes). Laser ignition can be advantageous for obtaining successful ignition and self-sustained combustion in fuel-lean mixtures where laser can offer great control and independent alteration between energy deposition width, duration of energy deposition and input ignition energy [63, 65, 66]. With recent advances made in laser research, the laser ignition parameters includes: laser pulse energy, pulse duration, wavelength and pulse selection for spatial and temporal distribution of laser energy in single and multiple ignition events [63]. The advantages of laser ignition will be discussed in Chapter 4.

Plasma Jet

This method of ignition has been studied by Weinberg *et al.* [214] and Orrin *et al.* [147]. The very high pressures and temperatures generated by the discharge cause the plasma to be ejected as a supersonic jet through an orifice located at the downstream end of the cavity. It is possible to vary the temperature of the plasma jet and its velocity by varying the feed to the cavity, input energy, and size of the discharge orifice [116]. Furthermore, Warris and Weinberg investigated ignition performance of pulsed plasma jets, and found that the electrical equipment tends to be lighter as large currents are required only transiently [213]. The results from pulsed plasma jets shown that ignition and stable combustion can be achieved at fuel/air ratios much lower than the normal lean blowout limit . Furthermore Guan *et al.* [83] studied a plasma jet ignition technology for aeroengine combustor and demonstrated that the plasma jet igniter could produce a continuous plasma jet, giving stable and reliable ignition better than the conventional one.

Torch Igniter

The torch igniter incorporates a spark plug and an auxiliary fuel jet in a common housing. The juxtaposition of these two components is such that ignition of the fuel spray by the spark creates a “torch” of burning droplets that ignites the main fuel spray

[116]. However, the performance of a torch igniter is fairly insensitive to its location. The major issue with this kind of ignition is that of fuel cracking and gumming [116]. This issue can be avoided by fitting solenoid valves, which stops the fuel after lightup, and by the provision of clean purging air. This solution, however creates additional weight and complexity. This kind of ignition performance is affected by inlet air temperature, fuel volatility and fuel/air ratio.

Hot Surface Ignition

The ignition of a fuel spray by a hot surface is technically feasible, but not normally regarded as a practical solution in gas turbines because of very high heat transfer rate [116]. And that is why spark ignition is very successful, as it provides instantaneous heat transfer to the fresh reactants. However, hot surface igniter is used in some applications such as the PT6 (Pratt & Whitney Canada) engine [164]. Recently Colwell and Reza investigated hot surface ignition of automotive and aviation fluids [57].

Chemical Ignition

There are many chemicals, so-called pyrophoric fuels (even 2cc is enough) that ignite spontaneously on contact with air and produce a high rate of energy release[116]. Tests show that pyrophoric fuels are very powerful sources of ignition, however storage and practical means of injection remain challenging. They are obviously very dangerous in the event of a crash, and this would appear to restrict their use in military aircraft [116].

Oxygen Injection

It is well known that effects of oxygen addition to all aspects of combustion performance is beneficial. Recently Chin [55] demonstrated that increasing the oxygen content of a propane-air mixture (from 21% to 50%), the ignition energy requirement was reduced by a factor 40. This effect is found to also apply in the gas turbine combustors, where ignition at low pressure is greatly facilitated by the injection of oxygen into the primary zone [116]. Moreover, work by Chin [55] on engine combustor simulated at high-altitudes conditions showed that flame blowout and relight performance were improved by adding small amount of oxygen. As, oxygen is normally carried on aircraft for various obvious reasons, this method is an attractive option for

high-altitude relight, where more conventional methods have been proved inadequate [55].

Despite the different means of ignition system, localised forced ignition (e.g. spark or laser) is still the most common way used to produce ignition in the engineering practical systems. In addition, the localised forced ignition has well defined characteristics (e.g. ignition energy, characteristic width of energy deposition, energy deposition time etc.), which they can be controlled easily. This present thesis concentrates on localised forced ignition.

1.3 Ignition Problem

From transportation industries to energy production, the problem of forced ignition is crucial. The demand of making combustors with improved fuel economy and reduced emission are one of the top priorities for automotive and aerospace industries. Experiments on gas turbine and IC engines are extremely expensive while computational models used in industry have not been thoroughly validated for such complicated problem. Forced Ignition in different combustion modes (Figure 1.1) has been the subject of numerous analyses [3, 4, 27, 44, 134, 146, 149, 171]. In laminar flows, ignition mechanism is well known [44]. However, when the flow becomes turbulent, ignition becomes more complex. Minimum Ignition Energy (MIE) is the energy that has to be deposited in the mixture in order to ignite a flame kernel which subsequently leads to self-sustained flame propagation[13]. With increasing level of turbulence intensity, the flame kernel is subjected to more intense disruption from these eddies and leads to high heat loss by diffusion to surrounding unburned gas, leading to an increase of MIE [182, 184]. Ignition energy is an important parameter as it influences the size of the early flame kernel and the early stages of flame propagation [21]. Moreover different hydrocarbon-air mixtures requires different ignition system, as ignition system designed for lighter hydrocarbon-air mixtures may not be suitable for heavier hydrocarbon-air mixtures [151, 152].

Despite these attentions in the literature, the effects of energy deposition characteristics, combustion regimes, equivalence ratio stratification and fuel Lewis number (Le_F) on localised forced ignition of both homogeneous and stratified mixtures are yet to be numerically analysed in detail. This thesis aims to provide a thorough understanding of physical mechanism of localised forced ignition and subsequent flame propagation in turbulent homogeneous and stratified combustible mixtures using

three-dimensional DNS.

1.4 Research Objectives

This project aims to conduct DNS based analysis of forced ignition process of turbulent combustible mixtures. In this analysis the effects of background turbulence intensity, integral length scale of turbulence, RMS (root-mean-square) and mean values of mixture equivalence ratio, length scale of mixture inhomogeneity, energy deposition time and characteristic width of energy deposition will be analysed based on an intense parametric analysis using three-dimensional DNS simulations. In this respect, the main objectives of this project are as follows:

- To understand the effects of energy deposition characteristics (i.e. ignition power, ignition energy deposition period and the energy deposition width) by the igniter on localised forced ignition of turbulent homogeneous mixtures.
- To understand the effects of combustion regimes on localised forced ignition of turbulent homogeneous mixtures.
- To understand the effects of equivalence ratio stratification on the localised forced ignition and subsequent early stages of burning process.
- To understand the effects of fuel Lewis number (Le_F) on localised forced ignition of both homogeneous and stratified mixtures.

1.5 Thesis Structure

Chapter 2 provides background review on parameters influencing ignition performance, ignition probability, forced ignition in both premixed and non-premixed mixtures and turbulent combustion. Before discussing results, the necessary mathematical background and numerical implementation are presented in Chapter 3. The basic assumptions, numerical methods together with the boundary conditions and DNS initial conditions are also presented in Chapter 3.

Results and related discussion is presented in the subsequent three chapters, organised according to the nature of fuel-air mixtures. Chapter 4 deals with localised forced ignition of homogeneous fuel-air mixtures. In Chapter 4 DNS simulation data of

forced ignition of homogeneous gaseous mixtures will be presented to demonstrate effects of energy deposition characteristics, along with effects of the regimes of turbulent combustion.

Once the effects of energy deposition characteristics and turbulent combustion regimes have been understood, the ignition parameters can be chosen to ensure successful ignition and self-sustained combustion. Chapter 5 deals with localised forced ignition in stratified mixtures where the effects of mixture inhomogeneity length scale, equivalence ratio variance, turbulence intensity and integral length scale are discussed for different initial mixture distributions. Chapter 6 discusses the effects of fuel Lewis number on localised forced ignition for both homogeneous and stratified mixtures.

Finally, the main findings of this work are summarised and conclusion are drawn in Chapter 7 along with the the preliminary analysis of localised forced ignition in the presence of complex chemistry and suggestion of future direction of research.

The outline of the thesis is presented in a flow diagram as below.

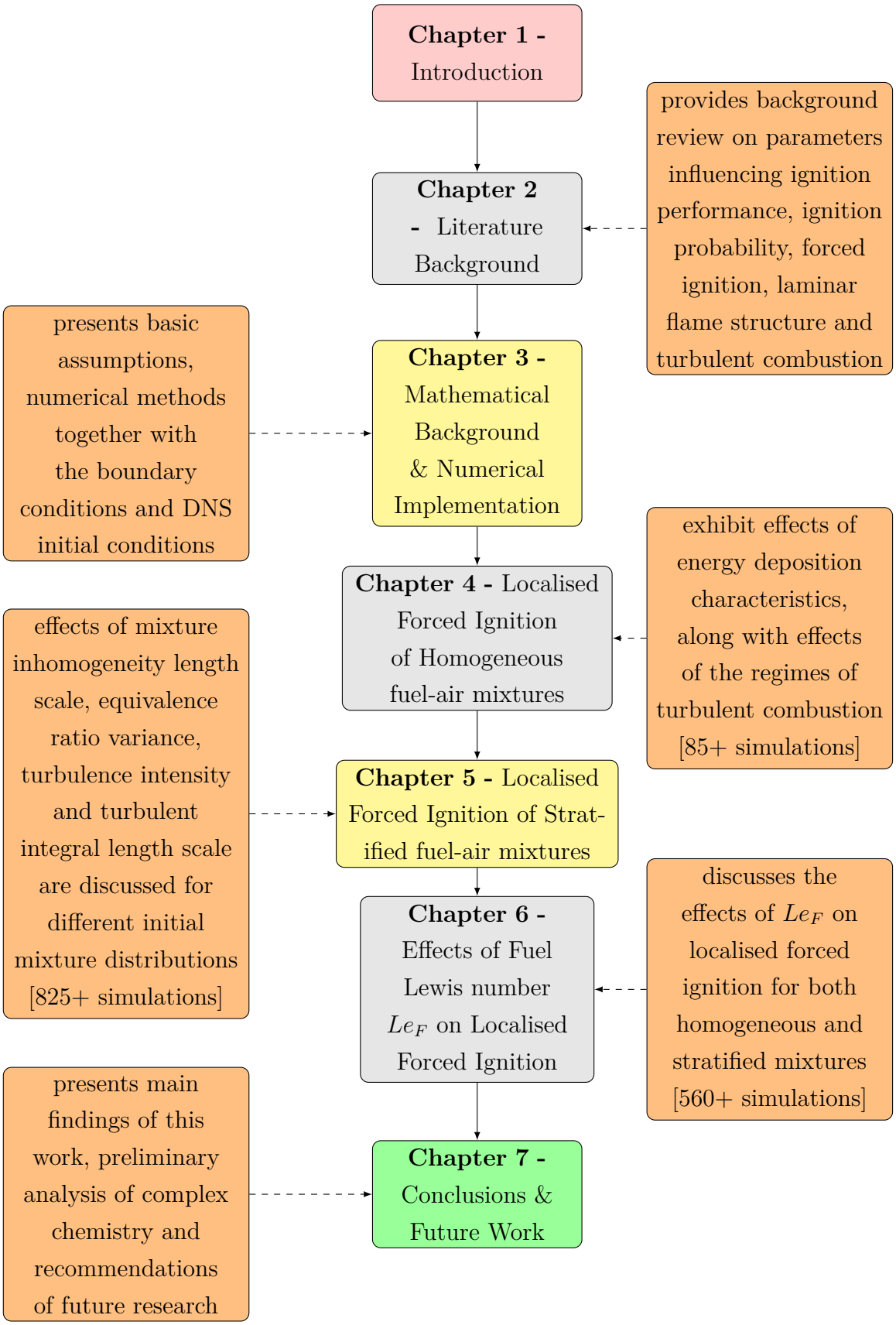
Chapter 1 - Introduction
Chapter 2 - Literature Background
provides background review on parameters influencing ignition performance, ignition probability, forced ignition, laminar flame structure and turbulent combustion
Chapter 3 - Mathematical Background & Numerical Implementation
presents basic assumptions, numerical methods together with the boundary conditions and DNS initial conditions
Chapter 4 - Localised Forced Ignition of Homogeneous fuel-air mixtures
exhibit effects of energy deposition characteristics, along with effects of the regimes of turbulent combustion [85+ simulations]
Chapter 5 - Localised Forced Ignition of Stratified fuel-air mixtures
effects of mixture inhomogeneity length scale, equivalence ratio variance, turbulence intensity and turbulent integral length scale are discussed for different initial mixture distributions [825+ simulations]
Chapter 6 - Effects of Fuel Lewis number Le_F on Localised Forced Ignition
discusses the effects of Le_F on localised forced ignition for both homogeneous and stratified mixtures [560+ simulations]
Chapter 7 - Conclusions & Future Work
presents main findings of this work, preliminary analysis of complex chemistry and recommendations of future research

Chapter 2

Literature Background

This Chapter 2 investigates the parameters influencing ignition performance and measurements of ignition probability. Additionally it presents a review of forced ignition of homogeneous and inhomogeneous mixtures. Furthermore a review of laminar premixed flame structure and turbulent combustion is provided.

A vast number of studies focused on the growth of the initial flame kernel of premixed flames following localised forced ignition. Clearly the growth of this initial kernel is influenced by the flame nature itself. In many automobile engines the mixing of the fuel and oxidiser occurs after injection into the combustion chamber. Combustion is therefore not only dictated by activation energies of the fuel and oxidiser and their characteristic reaction times, but also by the mixing characteristics, ignition system, background fluid velocities, mixture strength and ignition input energy etc.

2.1 Parameters Influencing Ignition Performance

A certain minimum energy is always required to ignite a combustible mixture. However, there are a number of physical variables which affect the ignition and combustion of fuel-air mixtures. Therefore, it is possible to pass small amount of electric energy through an explosive gas without producing ignition. When ignition energy increased, a threshold energy is eventually obtained at which the spark/laser becomes incendiary in the sense that a combustion wave propagates from the spark/laser through the volume of gas.

A successful ignition event generally begins with an "ignition kernel", a localised region of high reactivity and heat release, followed by the establishment of a flame. This depends upon a number of parameters, such as the local flow field, the mixture

composition, and the mode of deposition of ignition energy etc. These parameters have been extensively investigated in flowing flammable mixtures [13, 116, 196] and also inside a combustion vessel [30, 34, 202]. These parameters can further be categorised into two groups; one group is related to the ignition system which includes: ignition energy, ignition duration, ignition rate, electrode diameter and ignition gap-width. And the other group is related to the flow field which includes: mixture strength, flow velocity, flow pressure, turbulence scale and turbulence intensity.

Ignition Energy

It has been found that the minimum energy required to ignite the flowing mixture depends upon a number of parameters such as turbulence intensity, mixture strength, etc.[13, 116]. This thesis discusses the effect of these parameters individually to find the optimum value for each parameter which corresponds to the minimum ignition energy of the flow. However, increasing the spark energy increases the probability of ignition of the flowing mixture. A detailed discussion on the effects of ignition energy deposition characteristics will be provided in Chapter 4.

Ignition Duration

Of the total energy stored in the condenser, only a small amount is needed in heating the combustible mixture, where some is accounted for by losses in the ignition unit [116]. These energy losses are very high when the spark discharge is rapid, by contrast if the spark duration is too long, the energy is distributed over a large volume and ignition may not even occur, causing misfire. Ballal and Lefebvre [18] conducted a number of experiments on gaseous fuels, and from their findings, expressions were derived for calculating the optimum spark duration for any specified mixture and flow conditions. From range of conditions investigated, Ballal and Lefebvre [13, 167] found that the optimum ignition duration to fall between $30\mu s$ and $90\mu s$. Furthermore, it was found that optimum ignition duration was unaffected by turbulence, however it decreased with an increase in velocity. A detailed discussion on the effects of energy deposition duration based on present DNS study can be found in Chapter 4 (Section 4.2).

Ignition Rate (Frequency)

Ignition can only occur if the spark discharge coincides with a local mixture strength that is well inside the limits of flammability. Under these conditions, an increase in spark rate is likely to be far more effective for ignition than an increase in ignition spark energy, especially for problems like start-up and relight of the aircraft gas turbine [116]. An alternative method is by changing the mixture strength condition in the ignition zone. Additionally Foster [77] examined the influence of ignition frequency on altitude ignition performance in J-33 combustion chamber, and demonstrated a slight improvement in relighting capability as the spark ignition rate was increased from 2 to 150 per seconds. Presumably, the effect of igniting rate can only be really significant if it is sufficiently high for sparks to be generated in gas which has already been heated as a result of previous sparks [77]. Additionally, Lefebvre [116] shown that a ignition frequency of between one and two per seconds, depending on the application, generally entails the minimum expenditure of power and gives the most compact ignition unit.

Electrode Diameter & Ignition Gap-Width

The electrode's size and shape can affect both quenching distance and ignition energy. The effects of electrode diameter on the MIE of flowing propane air mixture was studied by Ballal and Lefebvre [13], and they found that MIE increases with electrode diameter because of a high heat loss developed by the large area of exposed metal surface. Moreover, more rapid increase of ignition energy with electrode diameter was observed for fuel-rich mixtures. The electrode materials has very little influence on MIE, and therefor can be neglected [13]. It is well known that the spark electrodes can have strong quenching effect on the spark kernel. It has been recognized for many years that the spark electrodes can have a powerful quenching effect on the spark kernel. As the gap width is increased, the quenching effect is diminished, but if the gap becomes too wide, then energy is wasted in creating a larger spark kernel than is needed to achieve ignition [3]. Therefore, for every combustible mixture, there is an optimum gap width corresponding to MIE. Furthermore, Roberts and Eichenberger [73] used an electrode with 1 mm diameter and 2 mm diameter gap width in studying the ignition of turbulent methane-air mixture to reduce thermal losses and disruption to the flow. A detailed discussion on the effects of the width of ignition energy deposition can be found in Chapter 4 (Section 4.2).

Ignition Location

The location of the igniter plug in early gas turbines was determined in a somewhat arbitrary manner, because of its accessibility for fitting and replacement[116]. The position of the igniter plays an important role in both ignition performance and igniter plug life [33, 116, 218]. Obvious choice of the position for the igniter is that it restricted to the primary zone, so that hot gas kernel originating from spark reaches upstream by the flow reversal action. This means, the burned pocket of gas is retained, continuously rotated and at the same time propagating outward until the primary zone is filled with flame. Investigation from Wilsted and Armstrong [215] has shown that an excellent location for the igniter is close to the centreline of the liner, adjacent to the fuel nozzle, however this is very inconvenient for accessibility and igniter plug life. In context of aircraft engines, a common practice is to fit igniter that can be withdrawn when not in use. This approach serves most advantageous position for ignition and avoids problem of plug life [116]. In the present thesis, the ignition location is kept geometrically at the centre of the domain for all the cases investigated here.

Mixture Strength

It is well known that optimum conditions for ignition are when the mixture strength is roughly stoichiometric (i.e. when flame speed and flame temperature are at peak). Ballal and Lefebvre [12] and Danis *et al.* [61] confirmed this theory in their studies on effects of mixture strength on the MIE of pre-vaporised n-heptane and methanol. A detailed analysis on the effects of mixture strength based on the present DNS analysis will be presented in Chapter 5.

Flow Velocity

Beneficial advantage of an increase in velocity is from stretching of the spark in a downstream direction, which increases the energy release during spark discharge. However, offsetting these advantages is the convective heat loss suffered by the spark kernel during the initial phase of its development. This loss of heat increases with increasing velocity, decreasing ignition performance unless it is accompanied by an increase in spark energy. Another detrimental effect of an increase in velocity is that it provides spark kernel less time in which to propagate before being swept downstream [116].

Flow Pressure

It has been highlighted that in all the existing experimental data obtained from stagnant mixtures, idealised flowing systems and practical combustor, an increase in pressure reduces the MIE [3]. The effects of pressure on MIE could be less for heterogeneous fuel-air mixtures, depending on the fuel evaporation rates. In the cases where ignition process if fully controlled by chemical reaction rates, MIE $\propto P^{-2.0}$, where if the evaporation rates are controlled by ignition process, then MIE $\propto P^{-0.5}$, where P is the pressure. Therefore the pressure exponent is always between -0.5 to -2.0. Additionally, the gas heat capacity increases with pressure, whereas the gas thermal conductivity is roughly independent of the pressure, this further leads to reduction in the heat losses and thus reduction in MIE [114, 199]. Practical combustor experimental data obtained by Foster[77] also suggested that the adverse effect of a reduction in pressure on ignition performance.

Turbulence Scale and Turbulence Intensity

When the spark kernel separates itself from the igniter and enters the recirculation zone. Now, as the spark kernel being airborne it is no longer subject to the influence of velocity, per se. However, it suffers from the heat loss to its surrounding fresh reactants. The adverse effects of turbulence on ignition is well documented in the literature [116, 166]. Moreover, the experimental data by Ballal and Lefebvre [116] show that the net effect of an increase in turbulence intensity is to increase MIE. Ballal and Lefebvre [116] also noted that under low turbulence conditions, MIE either decreases slightly with an increase in RMS turbulent velocity (u') or remains independent of u', whereas at high turbulence levels there was a clear tendency towards higher values of MIE with an increase in u'. Bradley and Lung [34] also reported that the main effect of turbulence was to convect the ignition kernel bodily rather than to spread it at the early stage of ignition.

2.2 Ignition Probability

The ignition probability is defined as the ratio of the number of successful ignition events divided by the total number of sparks. Ignition probability is most important parameter for the high altitude relight of the aircraft gas turbine combustor. Determining the igniter location that give high probability of successful ignition at different

flow conditions is essential for increasing the relighting capabilities of the engine [3].

The ignition probability for turbulent non-premixed flow (e.g. turbulent jet), depends upon a number of parameters, related to the flow and the igniter. When the fuel jet emerges into quiescent air, the jet expands and entrains air. The entrained air mixes with the fuel to create combustible mixtures with different mixture fractions across the flow field. The location of the optimum mixture fraction for successful ignition will change when the flow conditions changes. In addition, the mixture fraction fluctuation in the same flow conditions causes randomness in the ignitability of this non-premixed flow.

Relatively limited number of studies investigated the ignition probability of turbulent reacting flows. Some of them examined the ignition probability of turbulent jets [28, 189], and the ignition probability of flowing mixtures [111] by using electric spark ignition. Others investigated the ignition probability of laminar jets using laser ignition. Smith *et al.* [189] have studied the ignition probability along the axis of turbulent free jets of natural gas, propane and simulated town gas (containing 50% hydrogen) by using an electric spark igniter, with spark energy of 100 mJ , and spark duration of 20 ms at a repetition rate of 2 Hz . In addition Smith *et al.* [189] defined the estimated flammability factor F as:

$$F = \int_{\xi_{lean}}^{\xi_{rich}} P(\xi)\ \ d(\xi) \tag{2.1}$$

where ξ_{rich} and ξ_{lean} are the rich and lean flammability limits respectively, and $P\,(\xi)$ is the Probability Density Function (PDF) of the mixture fraction. It should be noted that the flammability factor F , which is presented by Equation (2.1) is the cumulative probability of a potentially flammable mixture occurring at a given point in a turbulent free jet. This factor may be defined as the area under the PDF of the volume fraction concentration of fuel gas between the static flammability limits ξ_{rich} and ξ_{lean}. The previous work by Smith *et al.* [189] concentrated to examine the ignition probability in turbulent free jets for only on the jet axis. Moreover, Smith *et al.* [189], Birch *et al.* [28], Kono *et al.* [111] and Ahmed *et al.* [4] have not investigated the effects of energy deposition characteristics (i.e. ignition energy , ignition duration and width of ignition energy distribution) and mixture conditions on the ignition probability, which are highlighted in the present thesis.

2.3 Forced Ignition of Homogeneous and Inhomogeneous Mixtures

According to Lefebvre [116], ignition of a combustor can be characterises into three distinct phases: kernel development, flame propagation and flame stabilisation. In order to obtain successful ignition, the fulfillment of these three phases is necessary. The success of ignition also relies on the flow in which the energy is deposited [116]. The MIE is required to generate a growing flame kernel is a key parameter to quantify ignition success [144].

2.3.1 Flame Kernel Growth

Generally a spark ignition involves two electrodes which produces capacitance sparks [117]. From an electrical perspective, three phases will contribute in the appearance of a spark. These phases are plasma phase (usually $1 - 10\,ns$), arc phase and lastly glow phase [144]. Although the plasma and the electrodes play a role in the actual energy provided to the kernel, limited effort has been directed to its computation investigation [202]. It is important to note that the aspects of momentum modification contribution, plasma formation and shock wave are kept beyond the scope of the present study in order to keep this study computationally feasible. This study only concentrates on the thermal aspect of ignition and on the fluid dynamic aspect of the kernel growth.

In a homogeneous turbulent mixture, the kernel growth also follows three different phases. First phase is a pressure wave (breakthrough) phase, where the kernel growth is dominated by this phase. Due to large pressure increase inside the small plasma volume, as a shockwave leaves at about $1\mu s$ and transports spark energy and heats up the surrounding mixtures [34]. This results in a fast kernel growth between 1 and $10\mu s$. If the energy during the breakdown phase is very high, this shockwave can also act as an ignition source but this is unlikely [6]. Hence, the shockwave can be considered as a loss to the fresh reactants since this energy is not used to increase the kernel temperature [13]. Following to this phase, the kernel growth slows down and the thermal spread is now supported by the spark energy. The kernel grows spherically through the diffusion of the spark energy from the hot kernel to the fresh mixture [34]. At early times, the kernel is similar to a laminar one because the influence of turbulent eddy diffusivity is very weak. Between about $50\mu s$ and $300\mu s$ after the breakdown, the kernel growth is dominated by molecular diffusion of energy and reactive species [13, 34]. When

sufficient heat has been lost to the fresh mixture so that the kernel temperature has dropped near the adiabatic flame temperature T_{ad}, its size will determine in the case of self-propagating kernel. At this stage, the heat release has to overcome the heat transfer by the kernel. This happens if the kernel reaches a critical size according to Lefebvre [116]. A third phase starts where the kernel growth is determined by the heat release and it becomes a self-propagating flame. Finally, the ignition process will be successful if the flame propagates towards the fresh mixtures and is not swept away either by the background fluid motion or by high turbulence intensity.

2.3.2 MIE for Homogeneous Mixtures

A vast number of papers investigated the problem of spark ignition in homogeneous mixtures using analytical [6, 34, 52], experimental [13, 68, 116, 131, 132, 182, 205] and numerical [51, 79, 113, 201, 202] means. Here MIE relates to the total energy deposited by the igniter. Experiments by Ballal and Lefebvre [13, 14, 116, 144] suggested that only a small amount of this energy contributes to the flame kernel, where the rest is lost through the initial shockwave propagation and radiation. The experimental analyses by Lefebvre [116] suggest that the high temperature kernel is obtained as a result of input ignition energy, but also due to the heat release arising from combustion.

2.3.2.1 MIE based on Critical Kernel Size

Lewis and von Elbe [117] defined the MIE, in association with the energy required to heat a sphere of critical radius to T_{ad} [116]. According to Lewis and von Elbe [117], the kernel must reach to a critical size to exhibit self-propagating behaviour. Lewis and von Elbe [117] and Lefebvre [116] showed that, an ideal spherical kernel is subjected to a high stretch rate due to its curvature which increases the heat loss, which eventually get compensated by the heat release inside the kernel. Theory of Bradley and Lung [34], Akindele *et al.* [6], Lefebvre [116] and Champion *et al.* [52] suggested that this critical radius is of the order of the flame thickness. Accordingly, Glassman [80] defined the MIE as:

$$\text{MIE} \sim \left[\frac{D_{th}}{S_{L,0}}\right]^3 \rho C_P \left(T_{ad} - T_0\right) \tag{2.2}$$

where $\frac{D_{th}}{S_{L,0}}$ provides a measure of the flame reaction zone thickness.

2.3.2.2 MIE based on Quenching Distance

Ballal and Lefebvre [17, 116] suggested the critical kernel size in the order of the quenching distance d_q. Lefebvre's work [116] suggested that the quenching distance is the length scale at which heat release is same as heat dissipation and $d_q \sim 10 \times \frac{D_{th}}{S_{L,0}}$ [13, 14, 17]. Additionally Calcote *et al.* [39] also provided that MIE $\sim d_q^{2.5}$. Since the effects of turbulence provides additional strain rate and an increase in turbulence intensity augments the heat transfer rate which increases the critical radius and MIE [34, 62]. Additionally Lefebvre indicted that an increase in equivalence ratio (ϕ) reduces the critical dimension d_q, whereas this critical dimension d_q (MIE) increases with an increase in turbulence intensity [116].

2.3.2.3 MIE based on Flow Parameters

A higher initial temperature can result in lower MIE as suggested by Swett [196]. Additionally MIE can be lower for close to stoichiometric mixture, as the laminar flame speed is maximum here (see Figure 3.1) [72, 158]. Lewis and Von Elbe [117] demonstrated that in quiescent mixtures, the mixture strength can control MIE as:

$$\text{MIE} \sim \begin{cases} \text{lowest} & \text{for slightly lean fuel with low carbon number: e.g. } CH_4 \\ \text{highest} & \text{for richer with higher hydrocarbon: e.g. } C_7H_{16} \end{cases} \tag{2.3}$$

Additionally, the effect of pressure on the MIE has been investigated as [13, 116, 196]:

$$\text{MIE} \sim P^{-n} \quad \text{where} \qquad 1 \leq n \leq 2 \tag{2.4}$$

The negative exponent relates to the effect of the reduced flame thickness $\frac{D_{th}}{S_{L,0}}$ with higher pressure and the higher density ρ which leads to more mass to heat in the kernel [115]. Ballal and Lefebvre [12] showed that n varied from 2 in stagnant mixture to about 1.25 at high flow velocity.

The detrimental effect of turbulence on ignition leads to increase in MIE [13, 51, 196]. The effects of turbulence on MIE was further investigated by Shy *et al.* [182, 185] and Ballal and Lefebvre [13, 116] and found that the increase in MIE with increasing u' is mild in low turbulence region and large in region of high turbulence intensity. In the low turbulence region, the turbulence simply wrinkles the flame surface while

for intensively turbulent condition eddies penetrate into the burning zone. Ballal and Lefebvre [13, 116] showed that the transition between the two region occurs at $\frac{u'}{S_{L,0}} = 2$. Additionally, as mentioned earlier the igniter diameter and ignition duration also influences the MIE. The optimum igniter gap is a compromise between a distance small enough to reduce the air electrical resistance [196] and large enough to prevent excessive heat losses [116].

2.4 Laminar Premixed Flame Structure

The generic structure of a planar laminar premixed flame is shown in Figure 2.1. The area around the flame front is divided into three distinct zones namely preheat zone, reaction zone and equilibration zone by Zel'dovich and Frank-Kamenetzki [43, 80]. In the Figure 2.1, T_R is the reactants temperature and T_P is the temperature of the products.

2.4.1 Preheat Zone

In this region the temperature of the reactant rises due to the diffusion of heat from the reaction zone. The heat release in this zone is too small and can be neglected. No chemical reaction takes place in this region, as the temperature remains too low to overcome the high activation energy.

2.4.2 Reaction Zone

This is where most of the chemical reaction take place. This zone is very thin ($\ll 0.1\,mm$) and made up of overlapping reaction and diffusion layers where reaction progresses through long and complex sequence of species. In this zone most of the chemical energy is released in the form of heat, and decomposition of fuel takes place which leads to intermediate radical formation. The temperature and concentration gradient are high in this zone.

2.4.3 Equilibration Zone

In this zone the most of the heat release occurs, where CO_2 and H_2O are formed. The temperature in this zone is very high and chemical equilibrium is attained. The equilibration zone is comparably thick in comparison to reaction zone and often equilibration

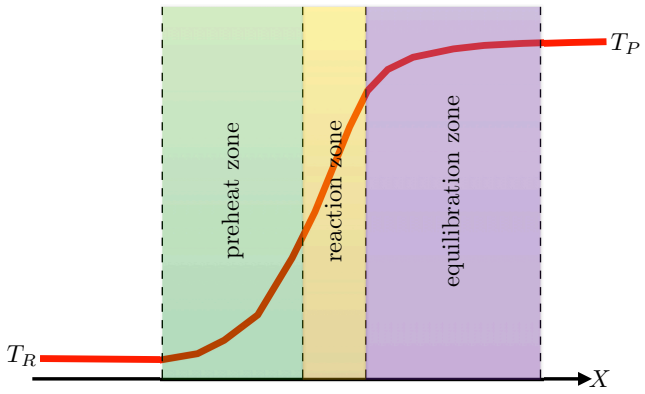

Figure 2.1: Generic structure of a premixed laminar flame.

and reaction zone are considered as one. The chemistry in this zone is relatively slow in comparison to reaction zone.

The flame structure is maintained by a dynamic balance of reaction and diffusion of heat and mass. Chemical reaction takes place within the reaction zone at a rate which is determined by the supply of preheated reactants transported by molecular diffusion from the preheat zone. At the same time, heat release from the chemistry within the reaction and equilibration zones results in heat conduction down the temperature gradient into the preheat zone. The rate of propagation is controlled by the molecular processes of transport and reaction. These are generally slow, and hence the laminar burning velocity is usually much less than $1\,ms^{-1}$ (typical values of the laminar burning velocity for most hydrocarbon–air mixtures with reactants at ambient conditions are in the range 0.3-0.6 ms^{-1}) [43]. For most hydrocarbon fuels the reaction zone thickness under typical conditions is much less than a millimeter, and the entire flame thickness is rarely more than a few millimeters [43].

2.5 Turbulent Combustion

Combustion requires fuel and oxidiser to mix at the molecular level. How this takes place in turbulent combustion depends on the turbulent mixing process. The general view is that once a range of different size eddies has developed, strain rate at the interface between the eddies enhances the mixing. During the eddy break-up process and the formation of smaller eddies, strain rate increases and thereby steepens the concentration gradients at the interface between reactants, which in turn enhances their molecular diffusion rate. Molecular mixing of fuel and oxidizer, a prerequisite of

combustion, takes place at the interface between small eddies [161].

The subject of turbulent combustion spans a broad range of disciplines ranging from turbulent flows to combustion chemistry, which makes the analysis of turbulent combustion a daunting task. At the heart of the challenge is the presence of a broad range of length and time scales spanned by the various processes governing combustion and the degree of coupling between these processes across all scales [71].

2.5.1 Turbulent Length and Time Scales

In order to estimate whether chemistry is fast or slow compared to turbulent mixing, it is useful to define time, length and velocity scales associated with physical processes. First consider the range of length scale (eddy sizes) that one may expect to encounter in turbulent flows. The largest length scale of turbulence is known as the integral length scale (L_{11}), which is the length scale at which most of the energetic eddies are associated. By contrast, the smallest length scale of turbulence known as Kolmogorov length scale, is determined by viscous dissipation of turbulent kinetic energy. From Kolmogorov's hypothesis, the only factors influencing the behavior of the small scale motions are the overall kinetic energy dissipation rate (ε) and the viscosity (ν). The length scale which governs these physical mechanisms is given by:

$$\eta = \left(\frac{\nu^3}{\varepsilon}\right)^{1/4} \tag{2.5}$$

This length scale is called the Kolmogorov length scale (η) and is the smallest hydrodynamic scale in turbulent flows. To relate this length scale to the largest length scale in the flow, it requires an estimation for the dissipation rate in terms of the large scale flow features. The kinetic energy of the flow is proportional to $(u')^2$. The time scale of the life time of the large eddies (commonly referred to as the large eddy turnover time) can be estimated as $\frac{L_{11}}{u'}$. Thus, it is reasonable to assume that the kinetic energy dissipation rate scales as:

$$\varepsilon \sim \frac{u'u'}{\left(\frac{L_{11}}{u'}\right)} \sim \frac{(u')^3}{L_{11}} \tag{2.6}$$

Using Eq. 2.6 for ε in Eq. 2.5 yields:

$$\eta = \left(\frac{\nu^3 L_{11}}{u'^3}\right)^{1/4} \tag{2.7}$$

The ratio of the largest to smallest length scales in the turbulent flow is given by:

$$\frac{L_{11}}{\eta} \sim \left(\frac{u' L_{11}}{\nu}\right)^{3/4} \sim Re_t^{3/4} \tag{2.8}$$

where $Re_t \sim \frac{u' L_{11}}{\nu}$ is the turbulent Reynolds number.

Another commonly encountered length scale in turbulence is the Taylor micro-scale. This length scale does not have the same easily understood physical significance as the Kolmogorov or internal length scale but provides a convenient estimate for the fluctuating strain rate field. The Taylor micro-scale(λ) is defined through the relation:

$$\varepsilon \sim \nu \frac{\partial u_i'}{\partial x_j} \frac{\partial u_i'}{\partial x_j} \sim \frac{u'^2}{\lambda^2} \tag{2.9}$$

Taylor micro-scale is also known as turbulence length scale. An alternative Reynolds number can be computed based on the Taylor micro-scale and the RMS turbulent velocity fluctuation in the following manner:

$$Re_\lambda \sim \frac{u' \lambda}{\nu} \tag{2.10}$$

The large eddy turnover time (t_e) is defined by:

$$t_e \sim \frac{L_{11}}{u'} \tag{2.11}$$

The life time for the small eddies of turbulence can be estimated using the viscosity and the dissipation rate:

$$t_\eta \sim \left(\frac{\nu}{\varepsilon}\right)^{1/2} \tag{2.12}$$

Now using Eq. 2.6 one can obtain:

$$t_\eta \sim \left(\frac{\nu L_{11}}{u'^3}\right) \tag{2.13}$$

And the ratio of time scales is therefore:

$$\frac{t_e}{t_\eta} \sim \left(\frac{u' L_{11}}{\nu}\right)^{1/2} = Re_t^{1/2} \tag{2.14}$$

The large scale structures in the flow are seen to have a much larger time scale (duration) than the smallest energy dissipating eddies. As the turbulent Reynolds number of the flow increases, the magnitude of the separation between both time and

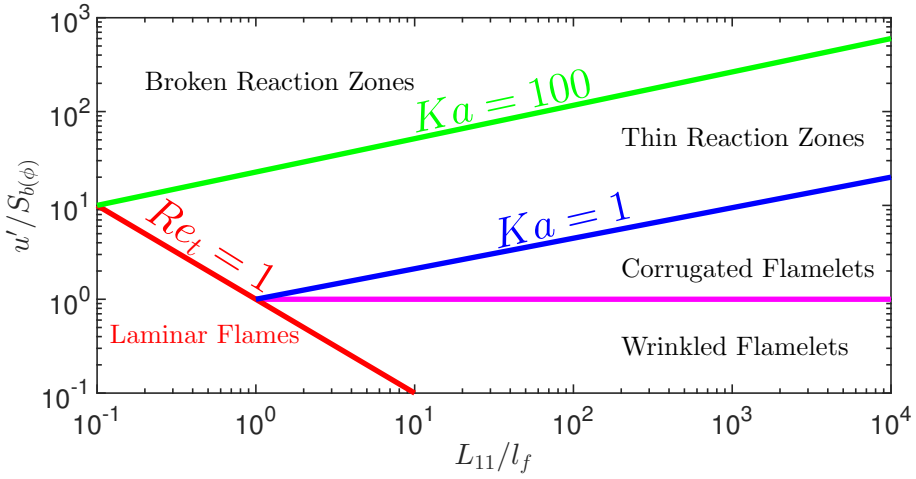

Figure 2.2: Regime diagram for premixed turbulent combustion

length scales increases.

2.5.2 Premixed Turbulent Combustion Regimes

Diagrams defining regimes of premixed turbulent combustion in terms of velocity and length scale ratio have been proposed in a number of previous analyses [34, 122, 158, 161]. For scaling purposes it is useful to assume equal diffusivities for all reactive scalars, Schmidt number $Sc = \nu/D$ equal to unity, and to define the flame thickness (l_f) and the flame time (t_f) as:

$$l_f = \frac{D}{S_{b(\phi)}}; \qquad t_f = \frac{D}{S_{b(\phi)}^2} \tag{2.15}$$

where $S_{b(\phi)}$ is the laminar burning velocity at equivalence ratio ϕ. Then using the turbulent velocity u' and the integral length scale L_{11} , one can estimate the turbulent Reynolds number as:

$$Re_t \sim \frac{u' L_{11}}{S_{b(\phi)} l_f} \tag{2.16}$$

Furthermore, the turbulent Damköhler number can be estimated as:

$$Da \sim \frac{t_e}{t_f} \sim \frac{S_{b(\phi)} L_{11}}{u' l_f} \tag{2.17}$$

Furthermore, one can quantify the separation between chemical time scale to the

Kolmogorov time scale in the following manner:

$$Ka \sim \frac{t_f}{t_\eta} \sim \frac{l_f^2}{\eta^2} \tag{2.18}$$

where Ka is Karlovitz number. Now, using $\nu = D$, one can further show that,

$$Re_t \sim Da^2 Ka^2 \tag{2.19}$$

Figure 2.2 shows the regime diagram for premixed turbulent combustion using the definition of Kolmogorov length scale, where the ratios $\frac{u'}{S_{b(\phi)}}$ and $\frac{L_{11}}{l_f}$ may be expressed in terms of the two non-dimensional numbers Re_t and Ka as:

$$\frac{u'}{S_{b(\phi)}} = Re \left(\frac{L_{11}}{l_f} \right)^{-1} = Ka^{2/3} \left(\frac{L_{11}}{l_f} \right)^{1/3} \tag{2.20}$$

The lines $Re = 1$ and $Ka = 1$ represent boundaries between different regimes of premixed turbulent combustion in Figure 2.2. Other boundaries of interest are the line $\frac{u'}{S_{b(\phi)}} = 1$, which separated the wrinkled flamelets from the corrugated flamelets, and the line denoted by $Ka = 100$, which separates the thin reaction zones from broken reaction zones.

The line $Re_t = 1$ separates all turbulent flame regimes characterized by $Re_t > 1$ from the laminar flame regime ($Re_t < 1$), which is situated in the lower-left corner of the diagram.

In the wrinkled flamelet regime, where $u' < S_{b(\phi)}$, the turnover velocity u' of even the integral eddies is not large enough to compete with the advancement of the flame front with the laminar burning velocity $S_{b(\phi)}$. Laminar flame propagation therefore dominates over flame front corrugations by turbulence [158].

The corrugated flamelet regime is characterized by the inequalities $Re_t > 1$ and $Ka < 1$. The inequality indicates that $l_f < \eta$ (see Eq. 2.18), which means that the entire reactive-diffusive flame structure is embedded within the eddies of the size of the Kolmogorov scale, where the flow is quasi-laminar. Therefore the flame structure is not perturbed by turbulent fluctuation and retains its quasi-laminar structure [158].

The boundary of the corrugated flamelets regime to the thin reaction zones regime is given by $Ka = 1$, which is equivalent to the condition that the flame thickness is equal to Kolmogorov length scale and the burning velocity is equal to the Kolmogorov velocity.

The thin reaction zones regime is characterised by $Re_t > 1$ and $1 < Ka < 100$, the

Laminar flames	$Re_t \leq 1.0$
Wrinkled flamelets	$Re_t \geq 1.0$; $\frac{u'}{S_{b(\phi=1)}} \leq 1$
Corrugated flamelets	$Re_t \geq 1.0$; $\frac{u'}{S_{b(\phi=1)}} > 1$; $Ka < 1$
Thin reaction zones	$Re_t \geq 1.0$; $1 \leq Ka < 100$
Broken reaction zones	$Re_t \geq 1.0$; $Ka \geq 100$

Table 2.1: Summary of regimes

last inequality indicating that the smallest eddies of size η can enter into the reactive-diffusive flame structure since $\eta < l_f$ (see Eq. 2.18). These small eddies are still larger than the reaction layer thickness l_δ and can therefore not penetrate into that layer. The thickness δ of the inner layer in a premixed flame is typically one tenth of the flame thickness, such that l_δ is one tenth of the preheat zone thickness which is of the same order of magnitude as the flame thickness l_f . The line $Ka = 100$ indicates the condition where the Kolmogorov length scale becomes equal to the reaction layer thickness (i.e. $l_\delta \sim 0.1 l_f$). This value used in Figure 2.2 for the upper limit of the thin reaction zones regime, was considered as the limit of the flamelet boundary based on numerical studies [122, 158, 161]. The analyses argued that since quenching by vortices occurs only for large Karlovitz numbers, the region below the limiting value of the Karlovitz number should corresponds to the flamelet regime.

Beyond the line $Ka = 100$ there is a regime called the broken reaction zones regime where Kolmogorov eddies are smaller than the inner layer thickness l_δ. These eddies may therefore enter into the inner layer and perturb it with the consequence that chemical processes are disturbed locally owing to enhanced heat loss to the preheat zone followed by temperature decrease and the loss of radicals. When this happens the flame will extinguish and fuel and oxidizer will inter diffuse and mix at lower temperatures where combustion reaction has ceased to take place. Nevertheless, regime diagram provides a useful purpose in allowing the classification of turbulent premixed flames, different premixed turbulent combustion regimes are summarised in Table 2.1.

This chapter summarised research material on parameters influencing ignition performance, forced ignition of both homogeneous and inhomogeneous mixtures, laminar premixed flame structure and turbulent combustion. Substantial knowledge has been collected for forced ignition in premixed mixtures and a large amount of MIE data is available for forced ignition. However, the physics associated with a forced ignition process, subsequent flame propagation and burning process is little understood. There

is a gap in the literature for detailed parametric analysis of ignition energy deposition characteristics on forced ignition in turbulent homogeneous mixtures. Relatively limited effort has been directed to MIE requirement and forced ignition of homogeneous mixture under highly turbulent environments. Furthermore, understanding of the effects of mixture strength on localised forced ignition and subsequent burning process is still required for the design of efficient combustion engines. A parametric study of the energy deposition characteristics and the effects of combustion regimes on localised forced ignition in homogeneous mixtures is performed in Chapter 4 using 3D DNS. Moreover, the effects of equivalence ratio stratification on localised forced ignition and subsequent burning process is numerically studied in Chapter 5. Furthermore, forced ignition with different hydrocarbon mixtures has received very little attention. It is expected that findings with this regards helps designing ignition system for alternative fuel types. Effects of fuel Lewis number (Le_F) on forced ignition in both homogeneous and stratified environment is numerically studied in Chapter 6.

Chapter 3

Mathematical Background and Numerical Implementation

In this Chapter 3, the mathematical formulations used in this thesis and the numerical implementations are introduced. The governing equations and ignition modelling for the simulations are outlined along with the assumptions that are made in the current study, followed by a brief introduction on composition variables and resolution of different scales. Initialisation of the turbulent flow field and scalar fluctuations for 3D DNS are outlined. Finally the specification of boundary conditions are presented.

3.1 Governing Equations

All the simulations presented in this thesis are performed using a well known compressible DNS code SENGA [42]. This DNS code solves the full compressible Navier-Stokes equations on a cartesian grid. The governing equations that describe the three-dimensional (3D) gaseous reacting flow consists of mass (Equation 3.1), momentum (Equation 3.2), energy (Equation 3.3) and species (Equation 3.4) conservation equations. These equations in dimensional form are as follows:

$$\frac{\partial}{\partial t}\rho + \frac{\partial}{\partial x_j}\rho u_j = 0 \tag{3.1}$$

$$\frac{\partial}{\partial t}\rho u_i + \frac{\partial}{\partial x_j}\rho u_j u_i = -\frac{\partial}{\partial x_i}P + \frac{\partial}{\partial x_j}\tau_{ji} \tag{3.2}$$

$$\frac{\partial}{\partial t}\rho E + \frac{\partial}{\partial x_k}\rho u_k E = -\frac{\partial}{\partial x_k}u_k P + \frac{\partial}{\partial x_k}\tau_{ki}u_i + \frac{\partial}{\partial x_k}\left[\lambda_0 \frac{\partial \hat{T}}{\partial x_k}\right] - \frac{\partial}{\partial x_i}\rho \sum_{k=1}^{N} h_{s,k} Y_k V_{k,i} + \dot{w}_T \quad (3.3)$$

$$\frac{\partial}{\partial t}\rho Y_\alpha + \frac{\partial}{\partial x_j}\rho u_j Y_\alpha = \dot{w}_\alpha - \frac{\partial}{\partial x_j}\rho V_{\alpha j} Y_\alpha \qquad \text{where } \alpha = 1, \ldots, N \quad (3.4)$$

In the above equations, ρ is the density, u_i is the i^{th} component of the velocity vector, P is the pressure, E is the stagnation internal energy and Y_α is the mass fraction of the species α in the reacting mixture containing total number of species N. The viscous stress tensor τ_{ij} is defined as:

$$\tau_{ij} = \mu\left[\left(\frac{\partial u_i}{\partial x_j} + \frac{\partial u_j}{\partial x_i}\right) - \frac{2}{3}\delta_{ij}\frac{\partial u_k}{\partial x_k}\right] \quad (3.5)$$

where μ is the dynamic viscosity. The source term $\dot{w}_T$ originating from heat release due to combustion is defined as:

$$\dot{w}_T = H_\phi \left|\dot{w}_F\right| \quad (3.6)$$

where λ_0 is the thermal conductivity, $\hat{T}$ is the temperature, h_α is the enthalpy of formation of the species α and $V_{\alpha j}$ is the diffusion velocity of the species α depending on the mixture. The chemical reaction rate $\dot{w}_\alpha$ is defined by following Equation 3.7 for N species and M steps reaction mechanism.

$$\dot{w}_\alpha = W_\alpha \sum_{m=1}^{M}\left[\left(v''_{\alpha,m} - v'_{\alpha,m}\right) A_m \hat{T}^{n_m} \exp\left(-\frac{E_m}{R_0 \hat{T}}\right) \prod_{\beta=1}^{N}\left(\frac{\rho Y_\beta}{W_\beta}\right)^{v'_{\beta,m}}\right] \quad (3.7)$$

In the above equation, W_α is the molar mass of species α and R_0 is the universal gas constant. For a given step m, $v''_{\alpha,m}$, and $v'_{\alpha,m}$ are the product and reactant stoichiometric coefficients, respectively. Additionally E_m is the activation energy, n_m is the temperature exponent and A_m is the frequency factor. The compatibility condition of the species mass fraction $\sum_{\alpha=1}^{N} Y_\alpha = 1$, the thermal equation of state is $P = \rho R_0 \hat{T} \sum_{\alpha=1}^{N} \frac{Y_\alpha}{W_\alpha}$, whereas the specific stagnation internal energy is defined as: $E = \int_{T_{ref}}^{T} C_V d\hat{T} + 0.5 u_k u_k$, here C_V is the mixture heat capacity at constant volume and T_{ref} is the reference temperature.

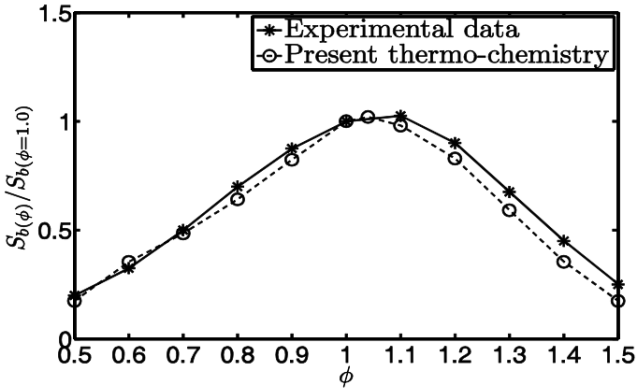

Figure 3.1: The variation of laminar burning velocity $S_{b(\phi)}/S_{b(\phi=1)}$ with equivalence ratio ϕ for the present thermo-chemistry along with the experimental variation [72].

3.2 Assumptions

The following assumptions have been considered for the analysis presented in this thesis:

1. A modified single-step irreversible type chemical reaction [197]

   $Fuel + s \cdot Oxidiser \rightarrow (1+s)Products$

   where s is the mass of the oxidiser consumed per unit mass of fuel consumption.

2. The reactants are fuel and oxidiser, where the fuel reaction rate is expressed as:

$$\dot{w}_F = -\rho B^{\star} Y_F Y_O \exp\left[-\frac{\beta\,(1-T)}{1-\alpha\,(1-T)}\right] \tag{3.8}$$

   where ρ is the gas density and the non-dimensional temperature $T = \frac{\hat{T}-T_0}{T_{ad}-T_0}$ where $\hat{T}$ is the instantaneous dimensional temperature, T_0 is the initial reactant temperature and T_{ad} is the adiabatic flame temperature for stoichiometric mixture. Additionally,

   Zel'dovich number:

$$\beta = \frac{E_{ac}\,(T_{ad}-T_0)}{R_0 T_{ad}^2} \tag{3.9}$$

   Heat release parameter:

$$\alpha = \frac{\tau}{1+\tau} = \frac{T_{ad}-T_0}{T_{ad}} \tag{3.10}$$

and pre-exponential factor related constant:

$$B^{\star} = B \exp\left(-\frac{\beta}{\alpha}\right) \tag{3.11}$$

where E_{ac} is the activation energy, B is the pre-exponential factor and τ is the heat release parameter.

3. The equivalence ratio is defined as $\phi = \frac{\text{FAR}}{(\text{FAR})_{st}}$, where FAR and $(\text{FAR})_{st}$ are the actual and stoichiometric fuel-air ratios respectively. The activation energy E_{ac} and the heat of combustion are taken to be function of equivalence ratio ϕ according to Tarrazo *et al.* [197]. The normalised laminar burning velocity $S_{b(\phi)}/S_{b(\phi=1)}$ variation with equivalence ratio ϕ is shown in Fig. 3.1 which shows that the present thermo-chemistry satisfactorily captures the experimentally obtained laminar burning velocity variation with ϕ for typical hydrocarbon-air mixtures (e.g. CH_4-air mixtures) [72]. The flame Mach number $Ma = \frac{S_{b(\phi=1)}}{\sqrt{\gamma R_0}}$ for all is taken to be 0.014 and the Zel-dovich numer $\beta = \frac{T_{ac}\left(T_{ad(\phi=1)} - T_0\right)}{T^2_{ad(\phi=1)}}$ is taken to be a function of ϕ according to the suggestion by Tarrazo *et al.* [197]:

$$\beta = 6\, f\left(\phi\right) \tag{3.12}$$

where,

$$f\left(\phi\right) = \begin{cases} 1 + 8.25\ \left(\phi - 1\right)^2 & \phi \leq 0.64 \\ 1 + 1.443\ \left(\phi - 1.07\right)^2 & \phi \geq 1.07 \\ 1 & 0.64 < \phi < 1.07 \end{cases} \tag{3.13}$$

The heat release per unit mass of fuel $H_{\phi} = \frac{\left[T_{ad(\phi)} - T_0\right] C_P}{\left(Y_{Fu(\phi)} - Y_{Fb(\phi)}\right)}$ is given by:

$$\frac{H_{\phi}}{H_{\phi=1}} = \begin{cases} 1 & \phi \leq 1 \\ 1 - \alpha_H\left(\phi - 1\right) & \phi > 1 \end{cases} \tag{3.14}$$

where $\alpha_H = 0.21$ for $CH_4 - \text{Air}$ flames [197], $Y_{Fu(\phi)}$ and $Y_{Fb(\phi)}$ is the fuel mass-fraction in the unburned and burned gas respectively for premixed flame corresponding to the ϕ, and C_P is the specific heat at constant pressure.

4. The transport quantities including viscosity μ, thermal conductivity λ_0 and the

density-weighted mass diffusivity ρD are taken to be same for all species and independent of temperature. The combustion is assumed to be taking place in the gaseous phase where all species are perfect gases, which satisfy the following state relations:

Stagnation internal energy:

$$E = C_V \hat{T} + \frac{1}{2} u_k u_k \tag{3.15}$$

Pressure:

$$P = \rho R_0 \hat{T} \tag{3.16}$$

Gas constant:

$$R_0 = C_P - C_V = (\gamma - 1) C_V \tag{3.17}$$

Ratio of specific heats:

$$\gamma = \frac{C_P}{C_V} = 1.4 \tag{3.18}$$

Prandtl number:

$$Pr = \frac{\mu C_P}{\lambda_0} = 0.7 \tag{3.19}$$

Schmidt number:

$$Sc = \frac{\mu}{\rho D} \tag{3.20}$$

Reynolds number:

$$Re = \frac{\rho u l}{\mu} \tag{3.21}$$

According to the above assumptions, the non-dimensional form of the governing equations take the following form:

$$\frac{\partial \rho}{\partial t} + \frac{\partial (\rho u_j)}{\partial x_j} = 0 \tag{3.22}$$

$$\frac{\partial(\rho u_i)}{\partial t} + \frac{\partial(\rho u_j u_i)}{\partial x_j} = -\frac{\partial P}{\partial x_i} + \frac{1}{Re}\frac{\partial(\tau_{ji})}{\partial x_j} \tag{3.23}$$

$$\frac{\partial(\rho E)}{\partial t} + \frac{\partial(\rho u_j E)}{\partial x_j} = -(\gamma-1)\,Ma^2\frac{\partial(P u_j)}{\partial x_j} + \frac{1}{Re}(\gamma-1)\,Ma^2\frac{\partial(\tau_{ji}u_i)}{\partial x_j} + \frac{\tau}{Re\,Pr}\frac{\partial}{\partial x_j}\left[\lambda_0\frac{\partial T}{\partial x_j}\right] + \dot{w}_T \tag{3.24}$$

$$\frac{\partial(\rho Y_\alpha)}{\partial t} + \frac{\partial(\rho u_j Y_\alpha)}{\partial x_j} = \dot{w}_\alpha + \frac{1}{Re\,Sc}\frac{\partial}{\partial x_j}\left[\rho D\frac{\partial Y_\alpha}{\partial x_j}\right] \qquad \text{where } \alpha = 1,\ldots,N \tag{3.25}$$

Additionally, the Lewis number is defined as:

$$Le_i = \frac{\alpha_i}{D_i} \tag{3.26}$$

where i is a given species, α_i is the thermal diffusivity and D_i is the species diffusivity. This non-dimensional number represents the differential diffusion of heat and mass.

3.3 Ignition Modelling

A source term q''' has been added for accounting the heat addition to the energy transport Eq. 3.3.

$$\frac{\partial}{\partial t}\rho E + \frac{\partial}{\partial x_k}\rho u_k E = -\frac{\partial}{\partial x_k}u_k P + \frac{\partial}{\partial x_k}\tau_{ki}u_i + \frac{\partial}{\partial x_k}\left[\lambda\frac{\partial \hat{T}}{\partial x_k}\right] - \frac{\partial}{\partial x_i}\rho\sum_{k=1}^{N} h_{s,k}Y_k V_{k,i} + \dot{w}_T + q''' \tag{3.27}$$

The specific heats at constant pressure and constant volume (i.e. C_P and C_V) are taken to be constant and the same for all species in the present analysis. Therefore the term $\sum_{k=1}^{N} h_{s,k}Y_k V_{k,i} = C_P(T-T_0)\sum_{k=1}^{N} Y_k V_{k,i} = 0$. The source term q''' is assumes to follow a Gaussian distribution [48, 155] in the radial direction away from the centre of

the igniter and can be expressed in the following manner:

$$q'''(r) = A_q \exp\left(-\frac{r^2}{2R^2}\right) \tag{3.28}$$

where r is the radial distance from the centre of the igniter and R is the width of the Gaussian profile. The choice of R [149, 150] in the present analysis allows sufficient resolution of the temperature gradient and guarantees the rapid disappearance of any artificial effects introduced by the ignition source. The constant A_q is determined by the following volumetric integration [48]:

$$\dot{Q} = \int_V q''' dV \tag{3.29}$$

where $\dot{Q}$ is the ignition power, which can be defined as:

$$\dot{Q} = a_{sp}\rho_0 C_P \tau T_0 \left(\frac{4}{3}\pi l_f^3\right)\left[\frac{H(t) - H(t - t_{sp})}{t_{sp}}\right] \tag{3.30}$$

where a_{sp} is a parameter that determined the total energy deposited by the igniter, the t_{sp} is the time duration over which the energy is deposited by the igniter, which is expressed as $t_{sp} = b_{sp} \times t_f$, where b_{sp} is the energy duration parameter and t_f is a characteristic chemical time scale given by $t_f = \frac{l_f}{S_{b(\phi=1)}}$. The parameter b_{sp} varies between 0.2 and 0.4 for optimum spark duration according to experimental findings by Ballal and Lefebvre [14]. Here l_f is the Zel-dovich flame thickness for the stoichiometric mixture, which is defined as $l_f = \frac{\alpha_{T_0}}{S_{b(\phi=1)}}$, where α_{T_0} is the thermal diffusivity in the unburned reactants and $S_{b(\phi=1)}$ is the unstrained laminar burning velocity of the stoichiometric mixture.

It is important to note that the details of the spark formation (momentum modification contribution, plasma formation and shock wave) remain beyond the scope of the present analysis to keep this study computationally feasible. Understanding of such aspects for DNS simulation methodology is still remain an active area of research. Moreover, DNS simulations are computationally expensive so these simulations are not ideally suited to identify the exact values of minimum ignition energy and optimum energy deposition duration. Furthermore, some simplifications are adopted in representing the localised ignition in analytical [52, 90, 207, 208] and numerical simulation [51, 210, 212] studies, which often preclude a direct comparison of the minimum ignition energy and the optimum energy deposition duration obtained from experiments with computational results. Despite of the above limitations, important qualitative

conclusions can be drawn from the DNS simulations. In Chapter 4, Sections 4.2.7 and 4.3.7 shows that present DNS study results are in satisfying agreement with experimental findings of Huang *et al.* [96] and Shy *et al.* [184].

Parametric study of the effects of energy deposition characteristics (a_{sp} [parameter determining total energy deposition], b_{sp} [energy duration parameter] and R [parameter determining characteristic width of ignition energy deposition]) on localised forced ignition and early stages of burning following successful ignition in homogeneous turbulent mixtures using 3D DNS are presented in Chapter 4.

3.4 Composition Variables

Premixed combustion can be described in terms of two composition variables [35]: one variable to describe the mixture composition and another to describe the progress of the premixed reaction [91].

3.4.1 Mixture Fraction ξ

The knowledge of both active and passive (conserved) scalar fields (e.g. fuel mass fraction Y_F and mixture fraction ξ) are often required for describing the turbulent combustion of stratified mixtures [127]. The mixture fraction is often expressed using both fuel and oxidiser mass fraction and can be expressed as [27]:

$$\xi = \frac{Y_F - \frac{Y_O}{s} + \frac{Y_{O\infty}}{s}}{Y_{F\infty} + \frac{Y_{O\infty}}{s}} \tag{3.31}$$

where Y_F and Y_O are local fuel and oxidiser mass fractions, $Y_{F\infty}$ is the fuel mass fraction in the pure fuel stream and $Y_{O\infty}$ is the oxidiser mass fraction in air. The equivalence ratio ϕ can be expressed in terms of ξ using Burke-Schumann solution [158] as:

$$\phi = \frac{1-\xi_{st}}{\xi_{st}} \times \frac{\xi}{1-\xi} \qquad \text{where} \qquad \xi_{st} = \frac{Y_{O\infty}}{sY_{F\infty} + Y_{O\infty}} \tag{3.32}$$

3.4.1.1 Takeno's Flame Index I_c

In order to understand the flame structure originating from localised forced ignition, the Takeno flame index [86, 118, 175, 219] can be used to identify the local combustion

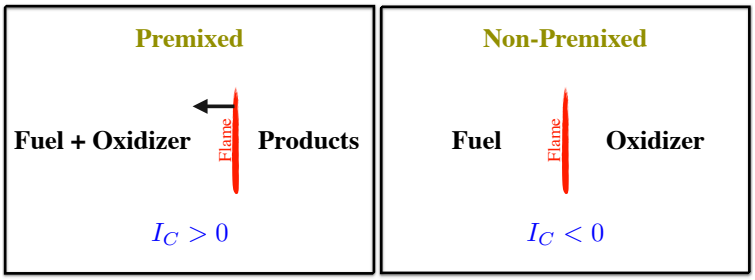

Figure 3.2: Takeno's flame index to determine combustion mode

mode:

$$I_c = \frac{\nabla Y_F}{|\nabla Y_F|} \bullet \frac{\nabla Y_O}{|\nabla Y_O|} \tag{3.33}$$

Based on the Equation 3.33, the Takeno flame index obtains positive value in premixed mode of combustion and negative value in non-premixed mode of combustion (see Figure 3.2).

3.4.2 Reaction Progress Variable c

The active scalars which are often considered for analysing turbulent combustion are the fuel mass fraction Y_F and the reaction progress variable c [127]. The extent of the completion of chemical reaction can be quantified in terms of a reaction progress variable c, defined as:

$$c = \frac{Y_{Fu} - Y_F}{Y_{Fu} - Y_{Fb}} \tag{3.34}$$

where Y_{Fu} is the fuel mass fractions in the unburned gas and Y_{Fb} is the fuel mass fraction in the burned gas. Both Y_{Fu} and Y_{Fb} are the function of ξ. The role of the reaction progress variable c, in the turbulent stratified mixtures has been discussed in detail by Bray *et al.* [35]. In the context of stratified combustion, the reaction progress variable can be defined in the following manner [91, 127–130, 149, 153]:

$$c = \frac{\xi Y_{F\infty} - Y_F}{\xi Y_{F\infty} - \max\left[0, \frac{\xi - \xi_{st}}{1 - \xi_{st}}\right] Y_{F\infty}} \tag{3.35}$$

According to Equations 3.34 and 3.35, c rises monotonically from zero in the fully unburned reactants to unity in the fully burnt products.

3.4.2.1 Reaction Progress Variable Reaction Rate

The transport equation of the reaction progress variable c in the context of turbulent premixed flames is:

$$\rho\frac{\partial}{\partial t}c+\rho u_j\frac{\partial}{\partial x_j}c=\frac{\partial}{\partial x_j}\left[\rho D\frac{\partial c}{\partial x_j}\right]+\dot{w}_c \tag{3.36}$$

where $\dot{w}_c$ is the reaction progress variable reaction rate [35, 93]:

$$\dot{w}_c=\begin{cases}-\frac{\dot{w}_F}{\xi Y_{F\infty}} & \text{for} \quad \xi\leq\xi_{st}\\ \\ -\frac{\dot{w}_F(1-\xi_{st})}{\xi_{st}(1-\xi)Y_{F\infty}} & \text{for} \quad \xi>\xi_{st}\end{cases} \tag{3.37}$$

Now, the The transport equation of the reaction progress variable c in the context of turbulent stratified flames is:

$$\rho\frac{\partial}{\partial t}c+\rho u_j\frac{\partial}{\partial x_j}c=\frac{\partial}{\partial x_j}\left[\rho D\frac{\partial c}{\partial x_j}\right]+\dot{w}_c+A_H \tag{3.38}$$

The term A_H originates due to reactant inhomogeneity [35, 93]:

$$A_H=\begin{cases}\frac{2\rho D\vec{N}.\nabla\xi|\nabla c|}{\xi} & \text{for} \quad \xi\leq\xi_{st}\\ \\ \frac{2\rho D\vec{N}.\nabla\xi|\nabla c|}{(1-\xi)} & \text{for} \quad \xi>\xi_{st}\end{cases} \tag{3.39}$$

where $\vec{N}$ is the flame normal vector, which can be defined as:

$$\vec{N}=-\frac{\nabla c}{|\nabla c|} \tag{3.40}$$

3.5 Resolution of Scales

For the purpose of turbulent combustion simulations, DNS grids must meet the following requirements:

1. total number of grid points in DNS should be large enough to ensure the largest scales of flow are captured and enough number of samples then can be used for obtaining statistically converged results.

2. DNS mesh should be fine enough to ensure that the smallest scales of flow (i.e. the Kolmogorov length scale) are fully resolved.

3.5.1 Turbulent Scales

In numerical simulation a turbulent flow can be considered to be fully resolved when the smallest scales of flow (i.e. Kolmogorov length scale) are fully resolved by the computational mesh. For example a cubic computational domain with side length L requires $N_g + 1$ grid points on each side for full resolved flow in DNS with cell size $\Delta x = \frac{L}{N_g}$. The turbulent flow field can be characterised with the integral length scale L_{11}, RMS of velocity u' and therefore the size of the computational domain should be at least on the order of one integral length scale $L = N_g \Delta x \geq L_{11}$. Additionally the Kolmogorov length scale can be estimated:

$$\eta \sim \frac{L_{11}}{(Re_t)^{3/4}} \tag{3.41}$$

Therefore the cell size needs to be smaller than the Kolmogorov scale (*i.e.* $\eta \geq \Delta x$). Based on above, following relationships can be obtained:

$$\frac{L_{11}}{\eta} < N_g \tag{3.42}$$

$$N_g > (Re_t)^{3/4} \Longrightarrow Re_t < N_g^{4/3} \tag{3.43}$$

The number of grid points can be determined from the above equation (3.43), i.e. grid points N_g+1 are necessary in each direction for carrying out a DNS at a turbulent Reynolds number Re_t.

3.5.2 Chemical Scales

DNS of turbulent combustion not only resolves the turbulent scale but chemical structure also requires the same resolution. Therefore the computational mesh should resolve the inner flame structure. This present study adopts simplified Arrhenius-type chemistry and the inner flame structure should extend over about 10 grid points. The flame thickness δ_{th} should extend over Q elementary cells (where $Q \approx 10$) and in terms

of the flame thickness, the computational domain length L can be expressed as:

$$L \approx \frac{N_g}{Q}\delta_{th} \tag{3.44}$$

The expression shown in Equation 3.44 can be used to compute an upper limit for the integral length scale of turbulence L_{11} (as discussed in sub-section 3.5.1), which should be less than L in order to provide converged statistics:

$$\frac{L_{11}}{\delta_{th}} < \frac{L}{\delta_{th}} < \frac{N_g}{Q} \tag{3.45}$$

By replacing δ_{th} with the diffusive flame thickness $\delta_D \approx \frac{\nu}{S_{b(\phi)}}$, the product of Re_t and Da is given by:

$$Re_t\, Da \sim \frac{L_{11}^2 S_{b(\phi)}}{\nu \delta_D} \sim \left(\frac{L_{11}}{\delta_D}\right)^2 \tag{3.46}$$

leading to the following condition (since δ_D and $\frac{D}{S_{b(\phi)}}$ are generally of same order):

$$Re_t\, Da < \left(\frac{N_g}{Q}\right)^2 \tag{3.47}$$

Thus, for a given Re_t that satisfies Equation 3.43, the Damköhler number Da is bounded by Equation 3.47.

3.5.3 Resolution of Scales in the Present Study

For all simulations performed in this present thesis, the uniform grid spacing Δx is smaller than Kolmogorov length scale η (i.e. $\eta \geq 1.2\Delta x$). The grid spacing is determined using the resolution of the flame structure. In all the simulations at least about 10 grid points are situated within the thermal flame thickness of the stoichiometric unstrained laminar flame:

$$\delta_{th} = \frac{T_{ad} - T_0}{\max |\nabla T^\star|_L} \tag{3.48}$$

3.6 Initialisation of Turbulent Velocity Flow Field

The present thesis adopts the DNS code SENGA [42] to initialise the turbulent flow field. The code generates a homogeneous, isotropic, incompressible, turbulent and periodic velocity field with a specified energy spectrum [41]. The energy spectrum

is generated in Fourier space and is then inverse Fourier transformed into real space. This methodology follows the familiar pseudo-spectral method proposed by Rogallo [174] and brief description is provided here. This method generates a velocity field in Fourier space $\hat{u}$ which satisfies the continuity for an incompressible flow:

$$\nabla \cdot \vec{u} = 0 \tag{3.49}$$

In Fourier space,

$$\vec{\kappa} \cdot \hat{u} = 0 \tag{3.50}$$

where $\vec{\kappa}$ is the linear wave number vector. Equation 3.50 indicates that $\vec{\kappa}$ and $\hat{u}$ are orthogonal to each other, and therefore $\hat{u}$ can be expressed as:

$$\hat{u} = \alpha(\kappa)\ \vec{e_1} + \beta(\kappa)\ \vec{e_2} \tag{3.51}$$

where κ is the magnitude of the linear wave number vector $\vec{\kappa}$, $\vec{e_1}$ and $\vec{e_2}$ are basis vectors ($\vec{e_1}$ is chosen arbitrary in such a manner that it is normal to $\vec{e_3}$, where $\vec{e_3}$ is aligned with $\vec{\kappa}$). The coefficients $\alpha(\kappa)$ and $\beta(\kappa)$ are generated with random phase in such manner that each of the Fourier modes is in accordance with the average energy described by the energy spectrum $E(\kappa)$. Under this case, $E(\kappa)$ is taken to present the final period of decay in decaying isotropic turbulence as described by Batchelor-Townsend energy spectrum [22–24]:

$$E(\kappa) = C_0 \left(\frac{\kappa}{\kappa_0}\right)^4 \exp\left[-\left(\frac{\kappa}{\kappa_0}\right)^2\right] \tag{3.52}$$

where C_0 is a parameter determining the global turbulent kinetic energy and the wavelength κ_0 corresponds to the wave number magnitude at which $E(\kappa)$ attains its maximum value. Thus, κ_0 determines the integral length scale. The coefficients $\alpha(\kappa)$ and $\beta(\kappa)$ can be expressed as:

$$\alpha(\kappa) = \left(\frac{E(\kappa)}{4\pi\kappa^2}\right)^{1/2} e^{i\theta_1} \cos\vartheta \quad \text{and;} \quad \beta(\kappa) = \left(\frac{E(\kappa)}{4\pi\kappa^2}\right)^{1/2} e^{i\theta_2} \sin\vartheta \tag{3.53}$$

where θ_1, θ_2 and ϑ are uniformly-distributed random angles. If, $\vec{e_1}$ is to lie on the

$x_1 - x_2$ plane then,

$$\vec{e_1} = \left(\frac{\kappa_2}{N_\kappa} , -\frac{\kappa_1}{N_\kappa} , 0 \right) \tag{3.54}$$

$$\vec{e_2} = \left(\frac{\kappa_1 \kappa_3}{\kappa N_\kappa} , -\frac{\kappa_2 \kappa_3}{\kappa N_\kappa} , -\frac{\kappa_1^2 + \kappa_2^2}{\kappa N_\kappa} \right) \tag{3.55}$$

$$\vec{e_3} = \left(\frac{\kappa_1}{\kappa} , \frac{\kappa_2}{\kappa} , \frac{\kappa_3}{\kappa} \right) \tag{3.56}$$

where $N_\kappa = \sqrt{\kappa_1^2 + \kappa_2^2}$, and κ_1, κ_2, κ_3 are the wave number components in the x_1, x_2 and x_3 directions respectively. The Fourier space velocities $\hat{u}_1(\kappa)$, $\hat{u}_2(\kappa)$ and $\hat{u}_3(\kappa)$ vectors are:

$$\hat{u}_1(\kappa) = \frac{\alpha \kappa \kappa_2 + \beta \kappa_1 \kappa_3}{\kappa N_\kappa} \tag{3.57}$$

$$\hat{u}_2(\kappa) = \frac{-\alpha \kappa \kappa_1 + \beta \kappa_2 \kappa_3}{\kappa N_\kappa} \tag{3.58}$$

$$\hat{u}_3(\kappa) = \frac{-\beta N_\kappa^2}{\kappa} \tag{3.59}$$

The code SENGA generates the velocity field in Fourier space for only half of the computational domain, as only half is necessary, since $\hat{u}(\kappa) = \hat{u}^\star(-\kappa)$ (where $\star$ indicates the complex conjugate, which ensures that the inverse Fourier transformed physical domain velocities are real). The x_3-direction is kept as a special direction and the upper half of the wave number domain is filled with computational data using Equations 3.57, 3.58 and 3.59. An inverse Fourier transform is carried out on all $\kappa_1-\kappa_2$ planes in this range to produce a partial inverse Fourier transform defined below:

$$\hat{u}_i^{(1,2)}(x_1, x_2, \kappa_3) = \int\int \hat{u}_i(\kappa_1, \kappa_2, \kappa_3)\, e^{-i2\pi(\kappa_1 x_1 + \kappa_2 x_2)} \quad d\kappa_1 d\kappa_2 \tag{3.60}$$

The remaining Fourier coefficients required in the x_3-direction are set using the symmetry condition. A final inverse Fourier transform in the x_3-direction is used to complete the initilisation procedure, which shown below:

$$u_i(x_1, x_2, x_3) = \int \hat{u}_i^{(1,2)}(x_1, x_2, \kappa_3)\, e^{-i2\pi\kappa_3 x_3} \quad d\kappa_3 \tag{3.61}$$

In the current study, the Fast Fourier Transform algorithm [42, 200] is used for all

Fourier transform operations. The initial turbulent velocity field provides good approximation of incompressible homogeneous isotropic turbulence. To simulate turbulent premixed/stratified combustion, the initial turbulent velocity field is superimposed. The reacting flow is neither isotropic nor homogeneous, thus, the initial velocity field can no longer provide a satisfactory solution. However, the decay rate is large in comparison to flame time scale and therefore the effects on the initial condition should not be important as long as the results of the simulations are taken at sufficiently late times.

3.7 Initialisation of Scalar Fluctuations

The current analysis investigates localised forced ignition process of stratified fuel-air mixtures. The mixture inhomogeneity in the unburned reactants have been specified using a random Bi-modal and Gaussian distribution of equivalence ratio ϕ for specified values of the global mean equivalence ratio $\langle\phi\rangle$,the RMS of equivalence ratio ϕ' and the Taylor-micro scale of mixture inhomogeneity l_ϕ following the methodology proposed by Eswaran and Pope [76] and further used by Hélie and Trouvé [91] and Grout *et al.* [81].

The methodology for generating the equivalence ratio fluctuations according to Eshwaran and Pope [76] can be summarised in the following manner [149]:

Step 1

The Fourier phase scalar field is expressed as:

$$\Phi\left(\vec{\kappa}\right) = \left(\frac{f_\phi}{4\pi\kappa^2}\right)^{\frac{1}{2}} \exp\left[2\pi i\,\theta\left(\vec{\kappa}\right)\right] \tag{3.62}$$

where $\vec{\kappa}$ is the wavenumber vector and κ is its magnitude, $\theta\left(\vec{\kappa}\right)$ is a uniformly distributed random number between 0 and 1, which is independently chosen for each node and f_ϕ is a top-hat function, which is defined as:

$$f_\phi = \begin{cases} 1.0 & \text{when} \quad \left(\frac{\kappa_s-\kappa_0}{2}\right) \leq \kappa \leq \left(\frac{\kappa_s+\kappa_0}{2}\right) \\ 0 & \text{otherwise} \end{cases} \tag{3.63}$$

where κ_0 is the lowest non-zero wave number magnitude, which is given by $\kappa_0 = \frac{2\pi}{L}$ with L being the domain size. The parameter $\frac{\kappa_s}{\kappa_0}$ determines the integral length scale

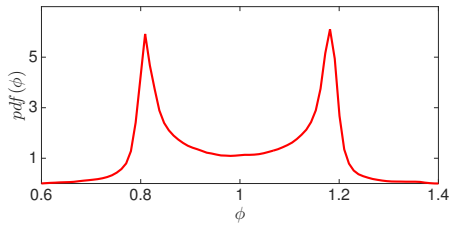

(a) at the central $x_1 - x_2$ plane

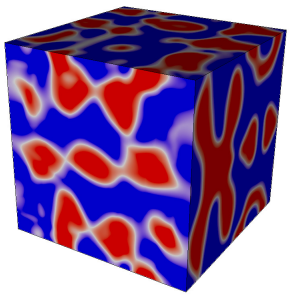

(b) in the cubic domain.

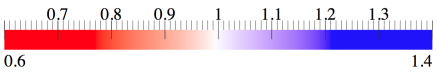

Figure 3.3: Example of an initial PDF (ϕ) initialised using the methodology proposed by Eswaran and Pope [76] in (a) at the central $x_1 - x_2$ plane (b) in the cubic domain, with $\langle\phi\rangle = 1.0$, $\phi' = 0.4$ and $\frac{l_\phi}{l_f} = 2.1$.

of the scalar fluctuations. Based on Equation 3.62, the scalar energy spectrum can be expressed as:

$$E_\phi(n\kappa_0) = \alpha_\phi \sum_{K_n} \Phi(\vec{\kappa})\,\Phi^\star(\vec{\kappa}), \qquad \text{where } n = 0, 1, 2, \ldots, N_{\max} \tag{3.64}$$

where $\Phi^\star$ is the complex conjugate of Φ, K_n is the set of wave numbers given by $n\kappa_0 - \kappa_0/2 \leq |\vec{\kappa}| \leq n\kappa_0 + \kappa_0/2$, and α_ϕ is a normalisation factor. Equation 3.64 leads to an initial scalar spectrum of the following form:

$$E(n\kappa_0) = \alpha_\phi \sum_{K_n} \frac{f_\phi}{4\pi\kappa^2} \tag{3.65}$$

Step 2

The scalar field produced in Fourier space in Step 1 is inversely transformed in physical space and the positive (negative) values are converted to +1 (-1) to ensure Bi-modal distribution.

Step 3

The scalar field is now retransformed into the spectral space and the Fourier amplitudes are multiplied by a filter function $F(\vec{\kappa})$, given by:

$$F(\vec{\kappa}) = \begin{cases} 1 & \text{if } \kappa \leq \kappa_c \\ \left(\frac{\kappa}{\kappa_c}\right)^{-2} & \text{if } \kappa > \kappa_c \end{cases} \tag{3.66}$$

where κ_c is a specified cut-off wave number. This step removes poorly resolved high wavenumber fluctuations. Here, $\frac{\kappa_c}{\kappa_s}$ is taken to be 2.0 following the recommendation of Eshwaran and Pope [76].

Step 4

The scalar field produced in Fourier space in Step 3 is inversely transformed in physical space and the fluctuations are scaled to obtain the desired value of ϕ'. These fluctuations are superimposed on top of the homogeneous field of mean equivalence ratio $\langle\phi\rangle$.

Here, the length scale of mixture inhomogeneity is taken as the Taylor micro-scale

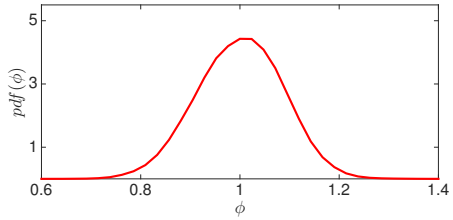

(a) at the central $x_1 - x_2$ plane

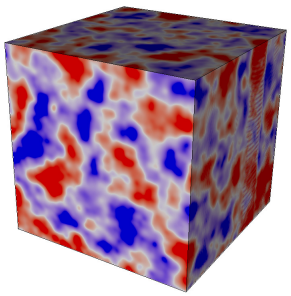

(b) in the cubic domain.

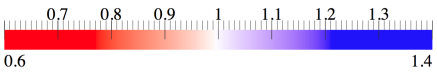

Figure 3.4: Example of an initial PDF (ϕ) initialised following Gaussian profile [81] in (a) at the central $x_1 - x_2$ plane (b) in the cubic domain, with $\langle\phi\rangle = 1.0$, $\phi' = 0.4$ and $\frac{l_\phi}{l_f} = 2.1$.

of the equivalence ratio variation l_ϕ and is defined as [76]:

$$l_\phi = \left(\frac{6 \left\langle [\phi - \langle \phi \rangle]^2 \right\rangle}{\langle \nabla [\phi - \langle \phi \rangle] \cdot \nabla [\phi - \langle \phi \rangle] \rangle} \right)^{1/2} \tag{3.67}$$

where the angle brackets $\langle \ldots \rangle$ indicate the global mean evaluated over the entire computational domain.

The Gaussian distribution is produced using the same method used for initial turbulent velocity field generation. Figure 3.4 shows the initial condition for equivalence ratio ϕ at the central $x_1 - x_2$ plane and in the cubic domain following Gaussian profile. The effects of mixture inhomogeneity length scale, equivalence ratio fluctuation and the nature of initial equivalence ratio distribution (i.e. Bi-modal and Gaussian distribution) on localised forced ignition of stratified mixtures are presented and discussed in Chapter 5.

3.8 Boundary Conditions

Selection of appropriate boundary conditions for DNS of turbulent combustion is a critical requirement. The interaction between combustion and acoustic waves can cause combustion instabilities in gas turbine applications [46, 127]. Therefore, boundary conditions require an acoustic wave propagation treatment. Numerical investigation by Schönfield and Poinsot [181] found combustion instabilities in gas turbine burner geometry where the self-sustained oscillation was strongly dependent on the boundary conditions. Numerical waves are originated because of the discrete treatment of the boundaries. These waves can lead to a coupling between inlet and outlet boundaries, and even unphysical oscillations [160]. The formulation of Navier Stokes Characteristic Boundary Conditions (NSCBC) attempts to provide well-posed boundary conditions that eliminate numerical instabilities and spurious wave reflection at the boundary. The NSCBC method is well documented by Poinsot and Lele [160] and here a brief discussion is provided.

The boundary conditions used for the solution of compressible Navier-Stokes equations can be categorised into two broad classes. The first class consists of physical boundary conditions, which employ the known physical behaviour of one or more of the dependent variables at the boundaries. The second class consists of numerical ('soft') boundary conditions, which are required by the discretised system to close the equations. This can be viewed as compatibility relations required by the numerical

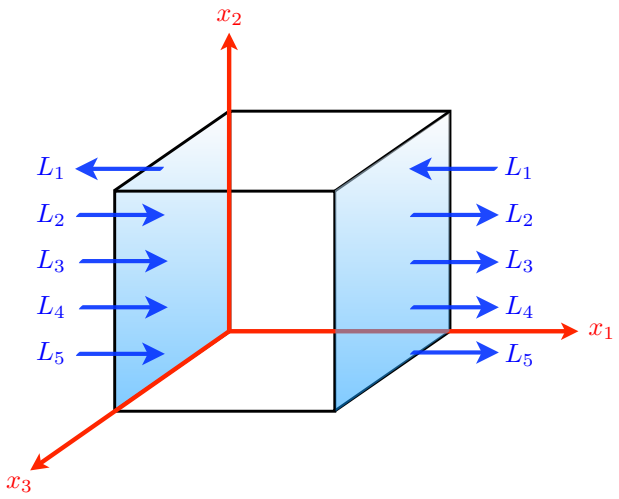

Figure 3.5: Wave amplitude variations into and out of the domain at the inflow and outflow boundaries.

method, and not as physical conditions. To achieve this, extrapolation from inside the domain is used in many works but this approach is arbitrary and leads to over constrained boundary conditions. Hence, this approach can not be used for acoustic wave reflection.

The NSCBC technique gives sound strategy for providing the physical and numerical boundary conditions. The physical boundary conditions are specified according to well-posedness of the Euler equations. The viscous conditions are then added to the inviscid Euler conditions to obtain correct number of boundary conditions for the Navier Stokes equations. The numerical boundary conditions are constructed using a local one-dimensional inviscid (LODI) approximation [204] for the wave crossing the boundary in either direction. The amplitude variations of the outgoing waves are dependent on the internal solution of the domain and are estimated according to the LODI scheme [204]. Incoming waves cannot be estimates from the internal solution, therefore are estimated by the specification of physical boundary conditions where necessary. The amplitude variations are then used to construct a reduced set of conservation equations to solve any left over variables which are not specified by the physical boundary conditions.

The LODI scheme is specified by a characteristic analysis of a locally one-dimensional

conservative system of equations:

$$\frac{\partial \psi_i^*}{\partial t} + \frac{\partial F_i}{\partial x} + C_i' = 0 \text{where } i = 1 \text{ to } n \tag{3.68}$$

where ψ_i^* is a conservative variable factor, F_i is a representative flux vector and C_i' is a non-homogeneous term without derivatives. Equation 3.68 can be rewritten based on dependent variables ψ_i as:

$$\frac{\partial \psi_i}{\partial t} + A_{ij}\frac{\partial \psi_j}{\partial x} + C_i = 0 \tag{3.69}$$

Equations 3.68 and 3.69 are related by the following relationship:

$$\frac{\partial \psi_i^*}{\partial t} = P_{ij}\frac{\partial \psi_j}{\partial t} \; ; \; \frac{\partial F_i}{\partial x} = Q_{ij}\frac{\partial \psi_j}{\partial x} \qquad \text{where} \qquad P_{ij} = \frac{\partial \psi_i^*}{\partial \psi_j} \; ; \; Q_{ij} = \frac{\partial F_i}{\partial \psi_j} \tag{3.70}$$

where $A_{ij} = \frac{Q_{kj}}{P_{ij}}$, $C_i = \frac{C_k'}{P_{ik}}$, and A_{ij}, P_{ij}, Q_{ij} are the components of the $n \times n$ matrices. It is expected for the matrix A_{ij} to have n linearly independent eigenvectors, which follows:

$$S_{ik}A_{kp}S_{pj} = \Lambda_{ij} \tag{3.71}$$

where S_{ij} is the eigenvector matrix and Λ_{ij} is the diagonal matrix($\Lambda_{ij=i} = \lambda_i$ where λ_i is the eigenvalues). Therefore, using the eigenvector matrix, Equation 3.68 can be rewritten as:

$$S_{ij}\frac{\partial \psi_j}{\partial t} + \Lambda_{ik}S_{kj}\frac{\partial \psi_j}{\partial x} + S_{ij}C_j = 0 \tag{3.72}$$

Now, it is possible to define the new vector $\vec{\varsigma}$ such that:

$$d\varsigma_i = S_{ij}\, d\psi_j + S_{ij}\, C_j\, dt \tag{3.73}$$

which further transforms as:

$$\frac{\partial \varsigma_i}{\partial t} + \Lambda_{ik}\frac{\partial \varsigma_k}{\partial x} = 0 \qquad \text{or} \qquad \frac{\partial \varsigma_i}{\partial t} + \lambda_i\frac{\partial \varsigma_i}{\partial x} = 0 \tag{3.74}$$

which is a series of wave equations which have a characteristic velocity of λ_i and

wave amplitude variation L_i can be defined as:

$$L_i = \Lambda_{ik} S_{kj} \frac{\partial \psi_j}{\partial x} \tag{3.75}$$

The LODI scheme is used for specifying numerically soft boundary conditions to ensure well-posedness of the numerical problem. Furthermore the LODI scheme is required to evaluate the derivatives normal to the boundary. The NSCBC technique replaces such derivatives with equivalent expressions of L_i. It is worth noting that each L_i corresponds to different characteristic physical waves that cross the boundary in inviscid flow situations. The expressions for different L_i can be found using characteristic analysis of the 3D extension of Equations 3.68-3.75 following Thompson [204]. If x_1-direction is normal to the boundary the L_i expressions are:

$$L_1 = \lambda_1 \left(\frac{\partial P}{\partial x_1} - \rho a \frac{\partial u_1}{\partial x_1} \right) \qquad \text{where} \qquad \lambda_1 = u_1 - a \tag{3.76}$$

$$L_2 = \lambda_2 \left(a^2 \frac{\partial \rho}{\partial x_1} - \frac{\partial P}{\partial x_1} \right) \qquad \text{where} \qquad \lambda_2 = u_1 \tag{3.77}$$

$$L_3 = \lambda_3 \frac{\partial u_2}{\partial x_1} \qquad \text{where} \qquad \lambda_3 = u_1 \tag{3.78}$$

$$L_4 = \lambda_4 \frac{\partial u_3}{\partial x_1} \qquad \text{where} \qquad \lambda_4 = u_1 \tag{3.79}$$

$$L_5 = \lambda_5 \left(\frac{\partial P}{\partial x_1} + \rho a \frac{\partial u_1}{\partial x_1} \right) \qquad \text{where} \qquad \lambda_5 = u_1 + a \tag{3.80}$$

where λ_i are characteristic wave velocities associated with L_i and a is the sonic speed. The wave amplitude variation L_1 corresponds to the wave travelling in the negative x_1-direction, whereas L_5 corresponds to the wave travelling in the positive x_1-direction. The wave amplitude variation L_2 is the entropy wave, whereas L_3 and L_4 correspond to the advection in the x_2 and x_3 directions, respectively. Figure 3.5 illustrates the various waves entering and leaving the computational domain at the inflow and outflow boundary. In the current study, partially non-reflecting boundary conditions are considered following the NSCBC technique outlined by Poinsot and Lele [160]. The boundaries in the transverse direction are considered to be periodic in nature, thus do not require any special boundary conditions.

The NSCBC technique can be used to specify a wide range of different boundary

Boundary type	Euler (Non-reacting)	Navier-Stokes (Non-reacting)	Navier-Stokes (Reacting)
Supersonic inflow	5	5	5+N
Subsonic inflow	4	5	5+N
Supersonic outflow	0	4	4+N
Subsonic outflow	1	4	4+N

Table 3.1: The number of physical boundary conditions required for well-posedness (for three-dimensional flow), where N is the number of reacting species.

conditions and are outlined by Poinsot and Lele [160] and also listed in Poinsot and Veynante [161]. The expressions for L_1 gives the necessary requirement of boundary conditions for the Euler equations and in the context of the Navier-Stokes equations, additional viscous boundary conditions are needed to ensure well-posedness. The required number of boundary conditions for different kinds of boundaries is presented in Table 3.1 [160]. Although boundary conditions specification is an established field in CFD research, it is still remains an active area of research [165, 192].

3.8.1 Boundary Conditions in the Current Study

A cubic domain is considered in which a mixture is ignited and a flame kernel is allowed to expand and freely propagate. Suitable boundary conditions are necessary to ensure the generation of acoustic waves does not affect simulation results. The boundaries in the x_1- direction are taken to be partially non-reflecting and specified by the NSCBC as described by Poinsot and Lele [160]. The other boundaries are considered to be periodic in nature and thus do not need any further boundary conditions.

A sub-sonic non-reflecting inflow boundary has been assigned for when the velocity component normal to the boundary is directed inwards, following Poinsot and Lele [160]. Imposing a fixed velocity section at the inlet leads to full reflection of any incident acoustic waves. Therefore, the boundary condition must be able to maintain a recommended temperature (i.e. T^r) and recommended velocity (i.e. u^r, v^r and w^r) whilst acting as partially non-reflecting in nature. This can be done by following wave

	Navier-Stokes with N species			
	ECBC (Inviscid) conditions	Viscous conditions	Reaction conditions	Total number of conditions
Partially Non-Reflecting inflow	No reflecting wave $(4+N)$	$\frac{\partial \tau_{11}}{\partial x_1} = 0$ (1)	None (0)	$5+N$
Partially Non-Reflecting Outflow	Pressure at infinity imposed (1)	$\frac{\partial \tau_{12}}{\partial x_1} = 0$; $\frac{\partial \tau_{13}}{\partial x_1} = 0$; $\frac{\partial q_{x_1}}{\partial x_1} = 0$ (3)	$\frac{\partial M_{k_1}}{\partial x_1} = 0$ (N)	$4+N$

Table 3.2: The boundary conditions for 3D reacting flows for partially non-reflecting inlet-outlet boundaries following NSCBC technique [160].

amplitude variations at the inlet:

$$\begin{aligned} L_2 &= \sigma_2 \left(T - T^r\right) \\ L_3 &= \sigma_3 \left(v - v^r\right) \\ L_4 &= \sigma_4 \left(w - w^r\right) \\ L_5 &= \sigma_5 \left(u - u^r\right) \end{aligned} \tag{3.81}$$

where σ_2, σ_3, σ_4 and σ_5 are relaxation parameters. These parameters are chosen to match the impedance of the inlet boundary and for low or zero values of these coefficients, the inlet will act as a fully non-reflecting boundary. When the σ_i are close to zero the boundary behaves similar to a perfectly non-reflecting boundary (i.e. the acoustic waves are not reflected but that recommended values begin to drift). If large values of σ_i are chosen then acoustic waves are reflected and the recommended values do not drift. For intermediate values of σ_i, the mean values of the inlet velocity and temperature vary about the recommended predefined velocity and temperature values but still allow acoustic waves to propagate through the inlet boundary with little reflection occurring. Therefore the intermediate values of σ_i has been adopted in the current study. Additionally, Poinsot and Lele [160] proposed that $\frac{\partial \tau_{11}}{\partial x_1} = 0$, in order to account for viscous terms which ensures a well-posed problem. The necessary physical boundary conditions are presented in Table 3.2.

The production of acoustic waves in combustion DNS with reflecting boundaries leads to erroneous results, thus sub-sonic partially non-reflecting outflow boundary conditions are used [160]. Fully non-reflecting boundary is a good option but under

such conditions a mean pressure drift can also occur [160]. Therefore corrections can be made to such boundary conditions to allow them to be partially non-reflecting in nature following NSCBC outlined by Poinsot and Lele [160].

A given outflow boundary has four characteristic waves with wave amplitude variations L_2, L_3, L_4 and L_5. They all leave the domain (see Figure 3.5) and thus can be calculated from one-sided differences using the internal solution. The wave amplitude variation L_1 enters the domain (see Figure 3.5) and will need to be specified. The specification of an inviscid boundary condition for one variable will create reflection and therefore a numerical 'soft' boundary condition is needed. To create a fully non-reflecting outflow boundary, L_1 can be set to zero, but then the pressure at the boundary cannot be determined. Another option for determining pressure at the boundary is to allow waves propagating into the domain from outside of the domain, but this cannot take place for fully non-reflecting boundaries and thus pressure drift takes place. Poinsot and Lele [160] proposed a method by which downstream pressure P_∞ can be supplied. In this method L_1 is specified in such a way that it forces the mean pressure at the outflow boundary towards the target value of P_∞.

$$L_1 = K_r \left(P - P_\infty\right) \tag{3.82}$$

where K_r is a constant, $K_r = \left[s\, a(1 - (Ma)^2_{\max}\right] / L$, here s is a constant, $Ma_{\max}$ is the maximum Mach number in the flow and L is the domain size. The selection of s determines the nature of the boundary (e.g. $s = 0$ corresponds to a fully non-reflecting boundary). The specification of L_1 is only sufficient to specify the outflow boundary for an inviscid flow. To deal with viscous terms a set of 'viscous' conditions are imposed. Poinsot and Lele [160] suggest that the derivatives of τ_{12}, τ_{13}, heat flux $\left(q_{x_1} = -\lambda \frac{\partial \hat{T}}{\partial x_1}\right)$ and scalar flux (M_{K_1}) in x_1-direction are set to zero. These boundary conditions are given in Table 3.2.

In the following Chapter 4, the localised forced ignition of homogeneous fuel-air mixtures using 3D DNS are studied and simulations results are discussed.

Chapter 4

Localised Forced Ignition of Homogeneous Fuel-Air Mixtures

This Chapter 4 presents the numerical investigation of localised forced ignition of turbulent homogeneous mixtures. The Chapter 4 starts with an introduction about the existing literature and the purpose of this study. In the Section 4.2 a parametric analysis has been performed to study the effects of energy deposition characteristics on localised forced ignition of turbulent homogeneous mixtures. And Section 4.3 deals with the effects of combustion regime on localised forced ignition of turbulent homogeneous mixtures. The results are presented and subsequently discussed. This chapter ends with main findings.

4.1 Introduction

The parameters which influence the ignition performance are briefly identified in the Chapter 2 (Section 2.1). Moreover, it has already been identified [116] that the ignition energy, ignition duration and the width of ignition energy distribution have important effects on obtaining successful ignition and subsequent flame propagation. Localised forced ignition in homogeneous turbulent mixtures in the form of spark or laser plays vital role in the design of efficient and reliable Spark Ignition and Direct Injection engines. This has been an extensive area for research and has been studied analytically [52, 90, 207, 208], experimentally [26, 34, 96, 116, 202] and numerically [25, 45, 51, 78, 105, 109, 159, 202, 203]. An extensive review on localised forced ignition of homogeneous mixtures with or without the presence of turbulence has been conducted by Mastorakos [134]. As mentioned in Chapter 1 DNS has become an important

Parameter	Value
Zel'dovich number β	6.0
Prandtl number Pr	0.7
Ratio of specific heats $\gamma = \frac{C_P}{C_V}$	1.40
Stoichiometric air fuel ratio $(AFR)_{st}$	17.16
Heat release parameter τ	3.0
Stoichiometric fuel mass fraction $Y_{F_{st}}$	0.055
Lewis number of fuel Le_F	1.0
Lewis number of oxidiser Le_O	1.0

Table 4.1: Thermochemical parameters used for all simulations in sections 4.2 and 4.3.

tool for fundamental physical understanding and modelling for complex combustion phenomena including localised forced ignition of homogeneous [105, 109, 202] , inhomogeneous [47, 48, 51] gaseous and droplet-laden mixtures [210–212]. An extensive experimental analysis for the evaluation of ignition energy, optimum ignition duration time and ignition diameter on localised forced ignition for homogeneous mixture has been done by Lefebvre [116]. Additionally, Lefbvre [116] proposed a relation between MIE and spark kernel critical dimension d_q for successful ignition (see Section 2.3.2.1). Moreover experimental study by Lefebvre [116] for spark ignition of flowing mixture of fuel droplet and air suggests that a high temperature kernel is obtained due to input ignition energy but also due to the heat released by combustion. Existing experimental results indicate that the equivalence ratio (ϕ) of the mixture strongly influences the spark kernel critical dimention d_q. Also d_q increases with an increase in turbulence intensity [116], which further increases MIE in order to obtain successful ignition. The detrimental effects of turbulent velocity fluctuation on ignition and early stages of flame development in homogeneous mixures have been analysed in detail by various researchers [25, 26, 34, 45, 68, 78, 97, 109, 116, 134, 202]. Wandel [210, 211] indicated that the absence of a substantial region containing hot products with small values of scalar dissipation rate could be inimical to the ignition of droplet laden mixtures based on DNS analysis. Although Wandel's analysis was restricted for droplet-laden mixtures, such an important extinction predictor can also be relevant to the ignition in gaseous homogeneous mixtures.

Despite this attention in the literature, the effects of energy deposition characteristics (i.e. ignition energy , ignition duration and width of ignition energy distribution) on localised forced ignition and early stages of burning following successful ignition in homogeneous turbulent mixtures are yet to be numerically analysed in detail. The first

$\frac{L_{11}}{l_f} = 3.36$			$\phi = 1.0$ [S]		$\phi = 0.8$ [L]	
			$\frac{u'}{S_{b(\phi=1)}} = 0$	$\frac{u'}{S_{b(\phi=1)}} = 4$	$\frac{u'}{S_{b(\phi=1)}} = 0$	$\frac{u'}{S_{b(\phi=1)}} = 4$
			[T0]	[T4]	[T0]	[T4]
$b_{sp} = 0.2$ $R = 1.10l_f$	$a_{sp} = 2.7$	[A]	ST0A	ST4A	LT0A	LT4A
	$a_{sp} = 3.5$	[B]	ST0B	ST4B	LT0B	LT4B
	$a_{sp} = 4.3$	[C]	ST0C	ST4C	LT0C	LT4C

Table 4.2: List of parameters to analyse the effects of ignition energy (i.e. a_{sp}).

$\frac{L_{11}}{l_f} = 3.36$			$\phi = 1.0$ [S]		$\phi = 0.8$ [L]	
			$\frac{u'}{S_{b(\phi=1)}} = 0$	$\frac{u'}{S_{b(\phi=1)}} = 4$	$\frac{u'}{S_{b(\phi=1)}} = 0$	$\frac{u'}{S_{b(\phi=1)}} = 4$
			[T0]	[T4]	[T0]	[T4]
$a_{sp} = 3.5$ $R = 1.10l_f$	$b_{sp} = 0.1$	[D]	ST0D	ST4D	LT0D	LT4D
	$b_{sp} = 0.2$	[E]	ST0E	ST4E	LT0E	LT4E
	$b_{sp} = 0.3$	[F]	ST0F	ST4F	LT0F	LT4F

Table 4.3: List of parameters to analyse the effects of ignition duration (i.e. b_{sp}).

half of the chapter (Section 4.2) fulfills the deficit in existing literature. In this Section 4.2, the findings for effects of energy deposition characteristics (i.e. parametric study of the effects of ignition energy, ignition duration and width of ignition energy distribution) will be discussed for localised forced ignition of stoichiometric and fuel-lean homogeneous mixtures.

Efficient and reliable localised forced ignition of homogeneous mixtures is important for increased fuel economy and reduction in NO_X emissions in Spark Ignition (SI) engines and industrial gas turbines [58, 96, 97, 178]. Experimental study by Lefebvre and his co-workers [116] analyses the mechanism of localised forced ignition and the MIE for laminar and weakly turbulent flows, but relatively limited effort was directed to localised forced ignition of homogeneous mixtures under highly turbulent environments where the internal structure of the flame is severely modified by ener-

$\frac{L_{11}}{l_f} = 3.36$			$\phi = 1.0$ [S]		$\phi = 0.8$ [L]	
			$\frac{u'}{S_{b(\phi=1)}} = 0$	$\frac{u'}{S_{b(\phi=1)}} = 4$	$\frac{u'}{S_{b(\phi=1)}} = 0$	$\frac{u'}{S_{b(\phi=1)}} = 4$
			[T0]	[T4]	[T0]	[T4]
$a_{sp} = 3.5$ $b_{sp} = 0.2t_f$	$R = 0.93l_f$	[G]	ST0G	ST4G	LT0G	LT4G
	$R = 1.10l_f$	[H]	ST0H	ST4H	LT0H	LT4H
	$R = 1.41l_f$	[I]	ST0I	ST4I	LT0I	LT4I

Table 4.4: List of parameters to analyse the effects of characteristic width of ignition energy deposition (i.e. R).

getic turbulent eddies. Under this conditions the flame kernel is subjected to a high rate of turbulent heat transfer, which requires an increase of MIE [44, 96, 184]. The MIE increases gradually with increasing $\frac{u'}{S_{b(\phi=1)}}$ but the requirement for MIE increases abruptly with an increase in $\frac{u'}{S_{b(\phi=1)}}$ when $Ka \sim 10$ is reached, recent experimental studies of Huang *et al.* [96] and Shy *et al.* [184] have revealed.

On the regime diagram (see Figure 2.2 in Section 2.5.2), traditionally the condition given by $Ka = 1$ distinguishes between corrugated flamelet ($Ka < 1$) and distributed regimes ($Ka > 1$) [32, 157, 158]. Although, several arguments in literature [53, 163, 173] reveals that $Ka = 1$ does not adequately represents the boundary of the flamelet regime of combustion, and which may occur at $Ka > 1$. Additionally, Peters [158] declared that flamelet combustion condition remains valid even for $100 > Ka > 1$, and under this condition energetic turbulent eddies can enter into flame and significantly disturb the preheat zone but reaction zone retains its quasi-laminar structure. In turbulent premixed combustion, the Ka can significantly affect the statistics of flame displacement speed and flame surface area [84, 85, 128]. These minimum energy requirements are extremely important for safety standards as well as for the fundamental understanding of the ignition process of combustible homogeneous mixtures.

Several previous [26, 34, 44, 52, 68, 78, 90, 96, 150, 184, 202, 207, 208] findings focused on various aspects of localised forced ignition, but the effects of Ka on the requirements of MIE for ignition and self-sustained combustion are yet to be analysed using DNS in existing literature. The analysis provided in the second half of this Chapter (Section 4.3) address the aforementioned gap by studying the influences of Ka, u' and energy deposition characteristics on MIE requirement for successful localised forced ignition and obtaining self-sustained combustion using DNS data. It is important to note that, this chapter not only identifies the conditions for successful ignition but also demonstrates the effects of energy deposition characteristics on early stages of flame development following successful ignition. Much of the previous literature [47, 48, 51, 90, 207, 208, 210–212] adopted an ignition model using a source term in the energy transport equation, which deposits energy in a Gaussian manner from the centre of the igniter over a stipulated time duration. The similar approach has been adopted here (for ignition modelling refer to Section 3.3).

4.2 Effects of Energy Deposition Characteristics

This section starts with brief discussion on the numerical formulation adopted for this study and then the results for effects of energy deposition characteristics on localised forced ignition and early stages of flame propagation for both stoichiometric and fuel-lean homogeneous mixtures are presented and discussed. Temporal evolution of maximum temperature and reaction rate magnitude is shown first to analyse the effects of energy deposition characteristics. Spatial distribution of different quantities and flame wrinkling analysis is then presented. The temporal evolution of the burned gas mass has been analysed for cases where self-sustained combustion following successful ignition was achieved. Ignition parameters have been modified to achieve self-sustained combustion for fuel-lean mixtures. Finally, the section ends with qualitative comparison with experimental findings and a summary is provided.

4.2.1 Numerical Formulation

The localised forced ignition is modelled using a source term and is already explained in Section 3.3. The boundary conditions used here are specified in Section 3.8.1. All the first- and second-order derivatives are evaluated using a 10^{th} - order central difference scheme for the internal grid points. The order of differentiation gradually drops to a second-order one-sided finite difference scheme at the non-periodic boundaries. The time advancement is carried out using a 3^{rd}-order low-storage Runge–Kutta scheme [103, 107]. The simulation domain is taken to be a cube of size $33l_f \times 33l_f \times 33l_f$ which in Cartesian grid size of $200 \times 200 \times 200$ with uniform grid spacing Δx. For all simulations, the grid spacing is smaller than Kolmogorov length scale (i.e. $\eta \geq 1.2\Delta x$). The desired simulation time for decaying turbulence: $t_{sim} = \max(t_e, t_f)$, where $t_e = \frac{L_{11}}{\sqrt{k}}$ is the eddy turn over time, L_{11} is the longitudinal integral length scale and k is the turbulent kinetic energy. The centre of igniter is taken to be placed at the geometric centre of the computational domain. The statistics for all cases are presented for a time $t = 1.68t_f$, which corresponds to about $2t_e$ and $3t_e$ for initial values of $\frac{u'}{S_{b(\phi=1)}} = 4.0$ and $\frac{u'}{S_{b(\phi=1)}} = 6.0$ respectively. It will be shown in section 4.2.2 that one can infer whether a particular case will give rise to self-sustained combustion following successful ignition by the time $t = 1.68t_f$. Several previous DNS studies [48, 50, 51, 85, 155] with comparable or smaller simulation time contributed significantly to the fundamental understanding of turbulent combustion. For the present analysis both stoichiometric (i.e. $\phi = 1.0$) and fuel-lean (i.e. $\phi = 0.8$) mixtures have been considered where ϕ is

the equivalence ratio defined as:

$$\phi = \frac{(\mathrm{AFR})_{st}}{\mathrm{AFR}} \tag{4.1}$$

where AFR and $(\mathrm{AFR})_{st}$ are the actual and stoichiometric air-fuel ratios respectively. Here $(\mathrm{AFR})_{st}$ is taken to be 17.16 and this value is representative of a methane-air binary mixture. The values of thermochemical parameters used in the current analysis are summarised in Table 4.1.

The effects of ignition energy, ignition duration and width of ignition energy distribution have been analysed by the parametric variation of parameters a_{sp}, b_{sp} and R respectively (see Section 3.3). The parametric variation of a_{sp}, b_{sp} and R for both stoichiometric and fuel-lean mixtures are summarised in Tables 4.2, 4.3 and 4.4 respectively. The case names are chosen in such manner so that S stands for stoichiometric mixtures; L stands for fuel-lean mixtures; T0 and T4 indicate increasing turbulent level; A, B, and C indicate increasing values of parameter a_{sp}; D, E, and F denote increasing values of parameter b_{sp}; and G, H, and I denote increasing values of parameter R (e.g. ST0G corresponds to a case for stoichiometric mixtures with initial values of $\frac{u'}{S_{b(\phi=1)}} = 0.0$; $a_{sp} = 3.5$; $b_{sp} = 0.2t_f$ and $R = 0.93l_f$).

4.2.2 Temporal Evolution of Maximum Temperature and Reaction Rate Magnitude

The temporal evolution of the maximum non-dimensional temperature ($T_{\max}$) and normalised fuel reaction rate magnitude ($\left(\dot{\Omega}_F\right)_{\max}$) for all the cases in Table 4.2, 4.3 and 4.4 are shown in Figure 4.1, 4.2 and 4.3 respectively. The non-dimensional temperature is defined as:

$$\begin{aligned} T &= \tfrac{T^\star - T_0}{T_{ad(\phi=1)} - T_0} \quad \text{for} \quad \phi = 1.0 \text{ mixtures} \\ T &= \tfrac{T^\star - T_0}{T_{ad(\phi=0.8)} - T_0} \quad \text{for} \quad \phi = 0.8 \text{ mixtures} \end{aligned} \tag{4.2}$$

where $T^\star$ is the instantaneous dimensional temperature. The normalised fuel reaction rate magnitude is defined as:

$$\left(\dot{\Omega}_F\right)_{\max} = |\dot{w}_F|_{\max} \times \frac{l_f}{\rho_0 S_{b(\phi=1)}} \tag{4.3}$$

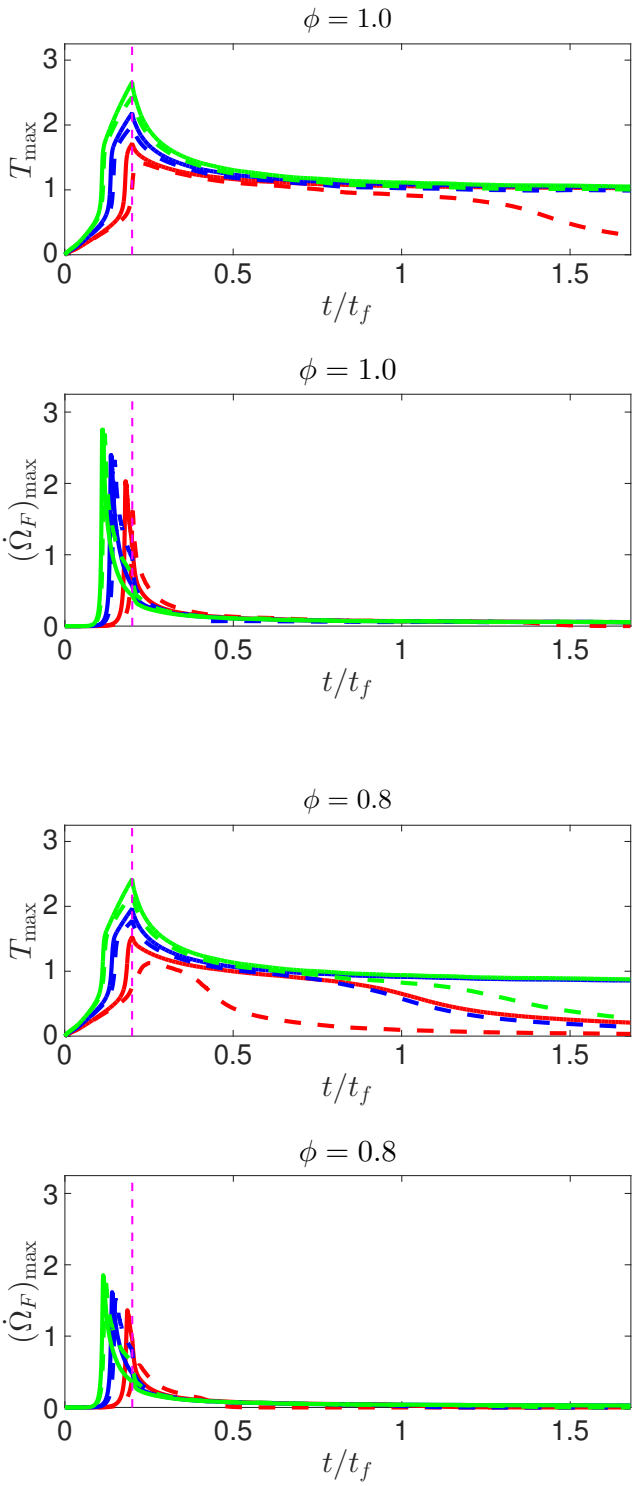

Figure 4.1: Temporal evolution of $T_{\max}$ and $\left(\dot{\Omega}_F\right)_{\max}$ for all the cases listed in Table 4.2.

[where $a_{sp} = 2.7$; $a_{sp} = 3.5$; $a_{sp} = 4.3$; magenta broken line shows $t = t_{sp}$; $\frac{u'}{S_{b(\phi=1)}} = 0$ (——) and $\frac{u'}{S_{b(\phi=1)}} = 4$ (- - - - - -)]

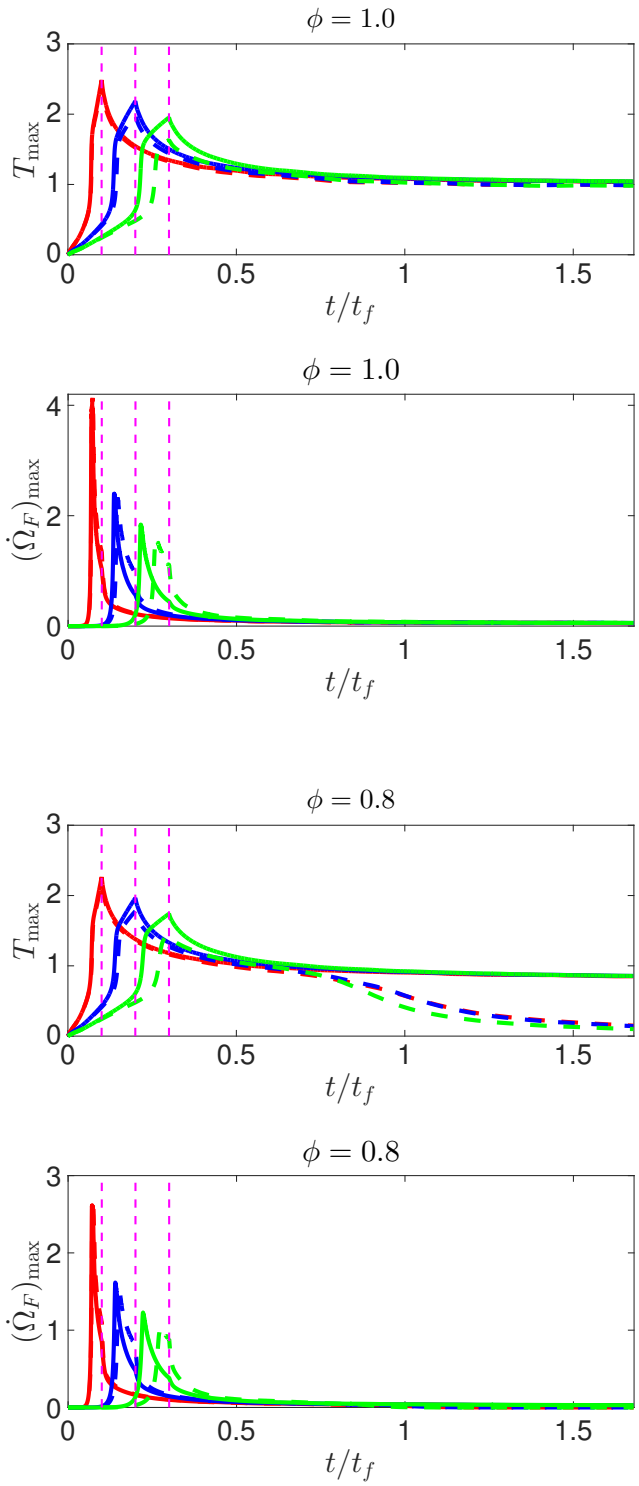

Figure 4.2: Temporal evolution of $T_{\max}$ and $\left(\dot{\Omega}_F\right)_{\max}$ for all the cases listed in Table 4.3.

[where $b_{sp} = 0.1$; $b_{sp} = 0.2$; $b_{sp} = 0.3$; magenta broken line shows $t = t_{sp}$; $\frac{u'}{S_{b(\phi=1)}} = 0$ (——) and $\frac{u'}{S_{b(\phi=1)}} = 4$ (- - - - - -)]

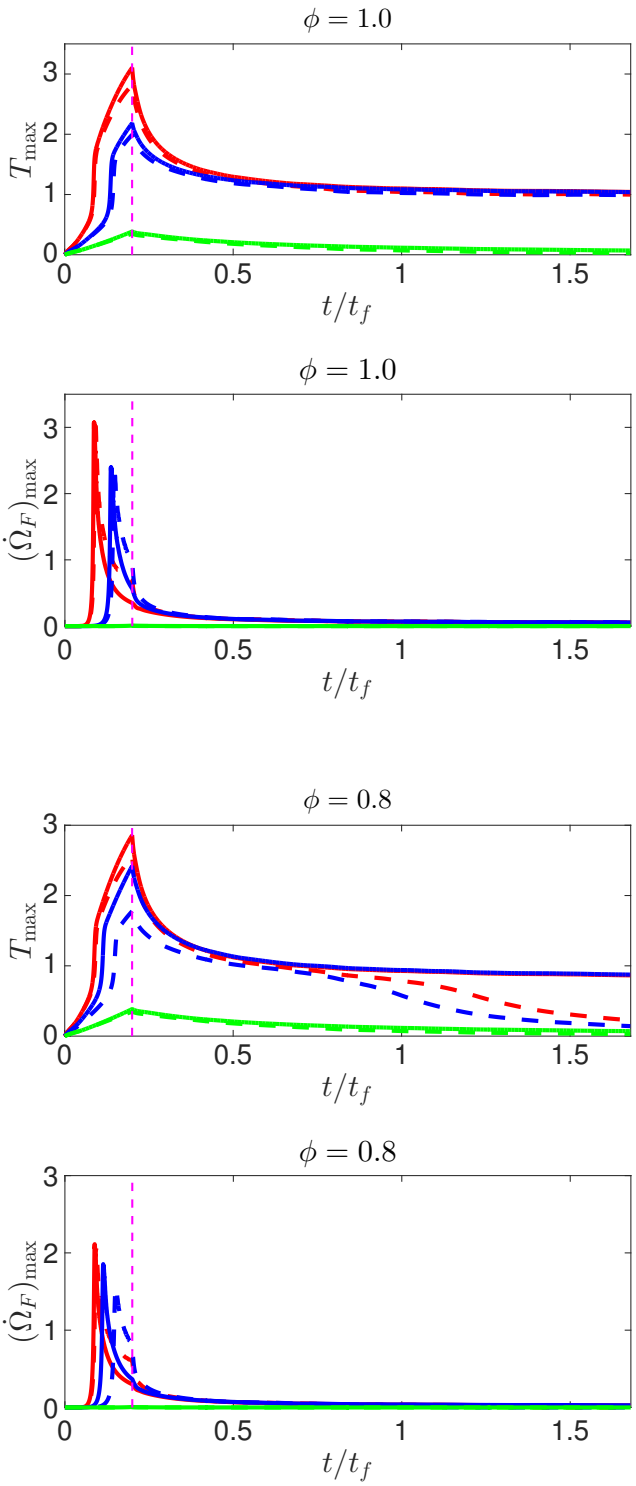

Figure 4.3: Temporal evolution of $T_{\max}$ and $\left(\dot{\Omega}_F\right)_{\max}$ for all the cases listed in Table 4.4.

[where $R = 0.93 l_f$; $R = 1.10 l_f$; $R = 1.41 l_f$; magenta broken line shows $t = t_{sp}$; $\frac{u'}{S_{b(\phi=1)}} = 0$ (——————) and $\frac{u'}{S_{b(\phi=1)}} = 4$ (– – – – – –)]

It can be seen from Figures 4.1, 4.2 and 4.3 that $T_{\max}$ rises with time due to energy deposition during $0 \leq t \leq t_{sp}$ and thermal runaway takes place when $T_{\max}$ reaches value close to $T_c \approx 1 - (1/\beta)$ and at this point both $T_{\max}$ and $\left(\dot{\Omega}_F\right)_{\max}$ increase rapidly with time. At $t = t_{sp}$ the energy deposition (igniter) has been switched off, at this point the high thermal gradient between hot gas kernel and surrounding gas leads to heat transfer from the kernel, which in turn leads to decrease in $T_{\max}$, unlike $\left(\dot{\Omega}_F\right)_{\max}$ starts to decrease even before $t = t_{sp}$. As the quantity $\left(\dot{\Omega}_F\right)_{\max}$ rises with time during energy deposition until the fuel is available at the maximum temperature location to support chemical reaction, but when the fuel is consumed at this location, $\left(\dot{\Omega}_F\right)_{\max}$ starts to decrease despite energy deposition continuing until $t = t_{sp}$. The $T_{\max}$ approaches the non-dimensional adiabatic flame temperature $T \approx 1.0$ ($T \approx 0.8$) for $\phi = 1.0$ ($\phi \approx 0.8$) at $t \gg t_{sp}$, where heat release overcomes the heat transfer from the hot gas kernel and confirming the self-sustained combustion is obtained. The $\left(\dot{\Omega}_F\right)_{\max}$ settles to a non-negligible value, which no longer changes appreciably with time for $t \gg t_{sp}$ for the cases where self-sustained combustion is obtained.

Additionally Figure 4.1 shows that successful ignition has been obtained for all cases, but in the ST4A, LT0A, LT4A, LT4B, LT4C cases $T_{\max}$ fails to settle at the adiabatic flame temperature, suggesting self-sustained combustion has not been achieved. For the cases ST4A, LT0A, LT4A, LT4B and LT4C, where successful ignition but failed self-sustained combustion has been obtained, $T_{\max}$ drops continuously for $t > t_{sp}$ and $\left(\dot{\Omega}_F\right)_{\max}$ drops sharply once $T_{\max} < [1 - (1/\beta)]$. It is evident from Figure 4.1 that the cases with $a_{sp} = 2.7$ are more prone to failure than the cases with $a_{sp} = 3.5$ and $a_{sp} = 4.3$. This findings are consistent agreement with the expectation that the probability of obtaining successful ignition and self-sustained combustion increases with increasing ignition energy for given set values of R and b_{sp} [51, 116]. Moreover Figure 4.1 shows that the cases with $\phi = 0.8$ mixture are more sensitive to flame extinction compare with $\phi = 1.0$ cases (compare cases ST0A, ST4B, ST4C with LT0A, LT4B, LT4C) as the chemical reaction rate is smaller in magnitude in the $\phi = 0.8$ cases than in corresponding $\phi = 1.0$ cases. Figure 4.2 suggests that successful ignition has been obtained for all cases from Table 4.3 but $T_{\max}$ settles to adiabatic flame temperature for cases except LT4D, LT4E and LT4F. The ignition duration parameter b_{sp} has influences on the possibility of self-sustained combustion following successful ignition. Furthermore, it can be seen from Figure 4.3 that, successful ignition has bee obtained for all the cases from Table 4.4 except cases ST0I, ST4I, LT0I and LT4I. However the cases with $R = 0.93l_f$ and $R = 1.10l_f$ obtained successful ignition but only the cases

ST0G, ST0H, ST4G, ST4H, LT0G and LT0H achieved self-sustained combustion.

The higher value (e.g. $R = 1.41l_f$) has a detrimental effect on the possibility of having successful ignition irrespective of the mixture conditions and/or values of $\frac{u'}{S_{b(\phi=1)}}$. Additionally Figure 4.3 shows that the choice of R has significant influences on the possibility of having successful ignition and thus can affect the MIE. This is especially crucial for fuel-lean mixtures.

4.2.3 Spatial Distributions of Temperature, Fuel Mass Fraction and Reaction Rate Magnitude

The distribution of non-dimensional temperature (T), fuel mass fraction (Y_F) and magnitude of fuel consumption rate $\left(\dot{\Omega}_F\right)$ for selected cases from Tables 4.2, 4.3 and 4.4 at the central $x_1 - x_2$ plane are shown in Figures 4.4, 4.5 and 4.6 respectively at times $t = 0.2t_f$ and $t = 1.68t_f$.

It is important to observe that temperature contours remain circular during the period of energy deposition but they become increasingly distorted as time progresses for all turbulent cases. During the energy deposition period (i.e. $t \leq t_{sp}$) the evolution of the temperature field is principally determined by the diffusion of energy deposited, but after the ignition is initiated, the flame propagation depends on the local reaction-diffusion balance, which is affected by local flame stretching mechanism induced via the background fluid motion.

Additionally Figure 4.4 shows that the fuel mass fraction Y_F is depleted at the regions associated with high values of T due to consumption of fuel as a result of chemical reaction. The reaction rate is vanishingly small for case LT4D at the time $t = 1.68t_f$ (see subfigure (f) in the Figure 4.5) as this case did not obtained self-sustained combustion following successful ignition, and the flame was already extinguished by this time. It can be seen from Figure 4.6 that the choice of characteristic width of energy deposition (characterised by R) can determine the possibility of achieving successful ignition for given set values of a_{sp} and b_{sp}. Clearly the choice of $R = 1.41l_f$ is shown to be more prone to unsuccessful ignition. The value of $T_{\max}$ during energy deposition time for $R = 1.41l_f$, did not reach to adiabatic flame temperature and thus negligible $\dot{\Omega}_F$ values are found in subfigures (e) and (f) in Figure 4.6.

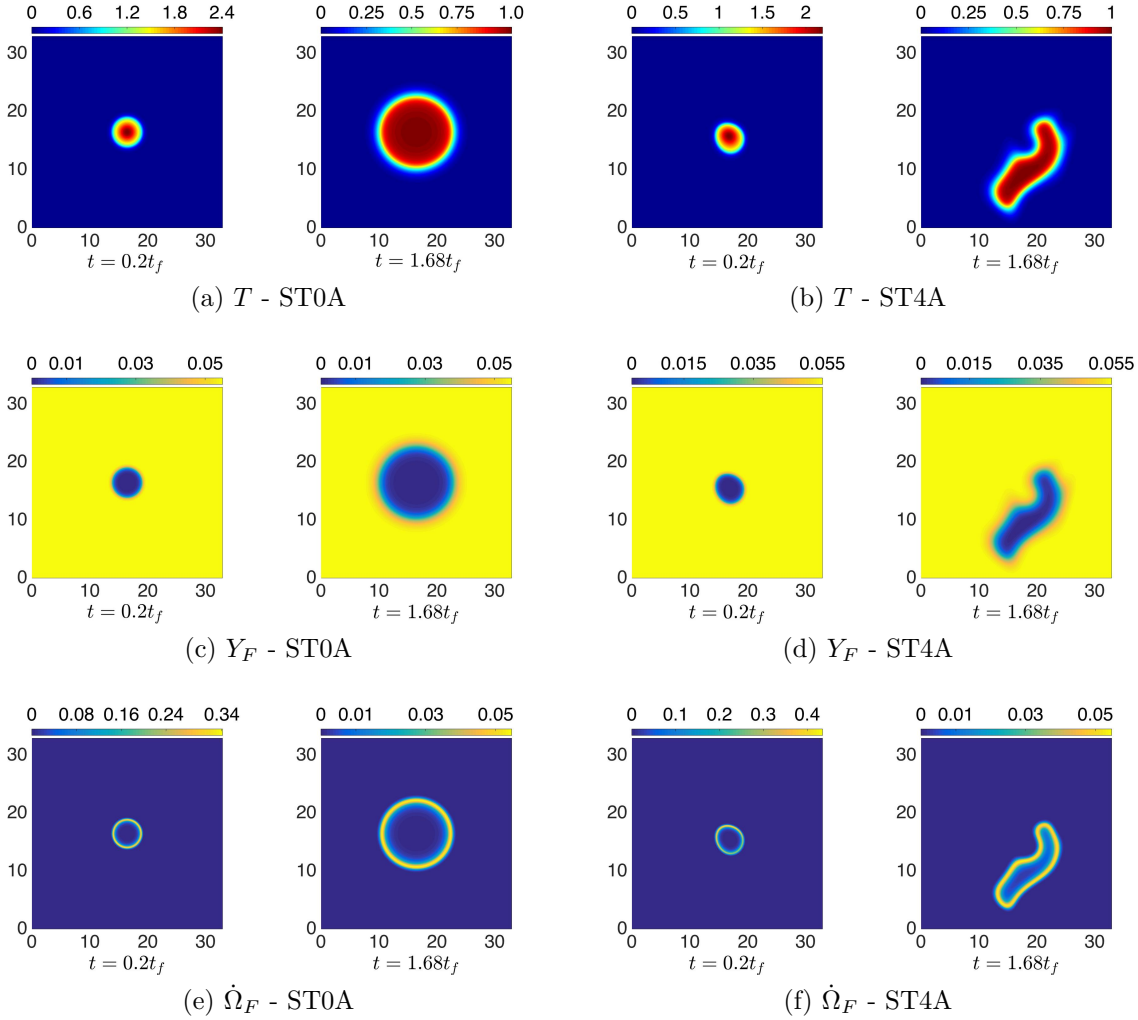

(a) T - ST0A (b) T - ST4A

(c) Y_F - ST0A (d) Y_F - ST4A

(e) $\dot{\Omega}_F$ - ST0A (f) $\dot{\Omega}_F$ - ST4A

Figure 4.4: Distribution of T [(a) and (b)], Y_F [(c) and (d)] and $\dot{\Omega}_F$ [(e) and (f)] on central $x_1 - x_2$ plane with domain size $33l_f \times 33l_f \times 33l_f$ for cases ST0A and ST4A from Table 4.2.

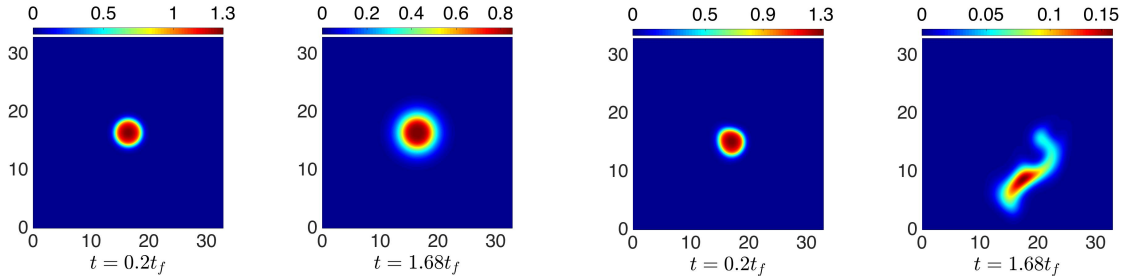

(a) T - LT0D

(b) T - LT4D

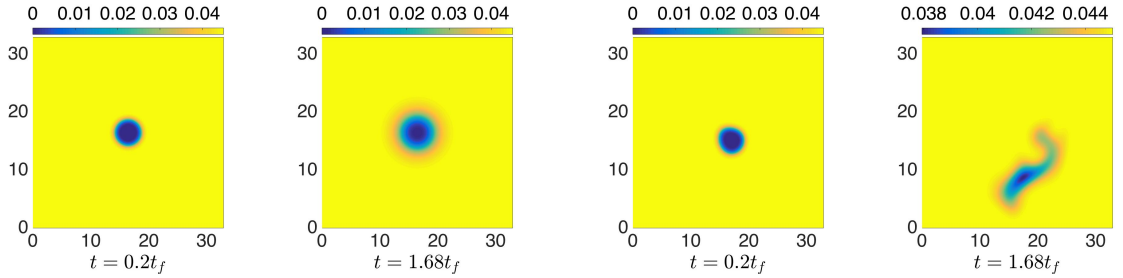

(c) Y_F - LT0D

(d) Y_F - LT4D

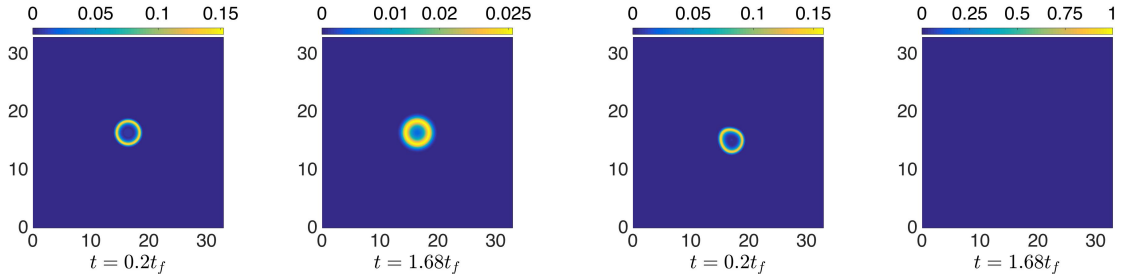

(e) $\dot{\Omega}_F$ - LT0D

(f) $\dot{\Omega}_F$ - LT4D

Figure 4.5: Distribution of T [(a) and (b)], Y_F [(c) and (d)] and $\dot{\Omega}_F$ [(e) and (f)] on central $x_1 - x_2$ plane with domain size $33l_f \times 33l_f \times 33l_f$ for cases LT0D and LT4D from Table 4.3.

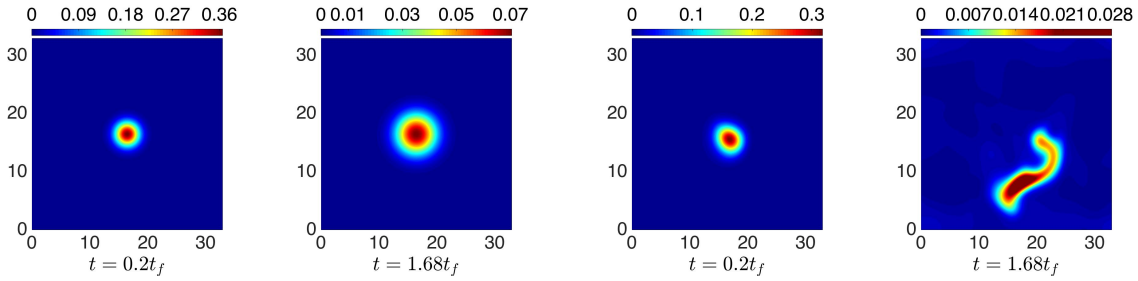

(a) T - ST0I

(b) T - ST4I

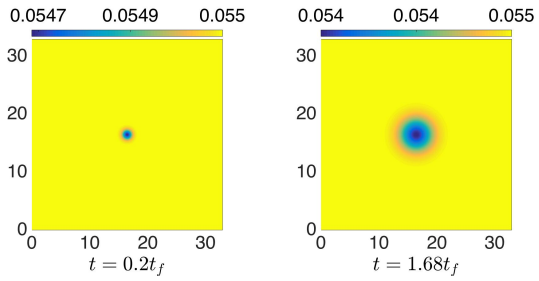

(c) Y_F - ST0I

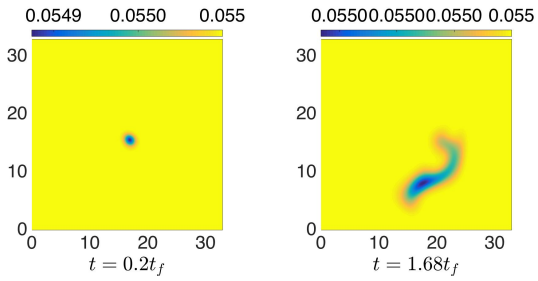

(d) Y_F - ST4I

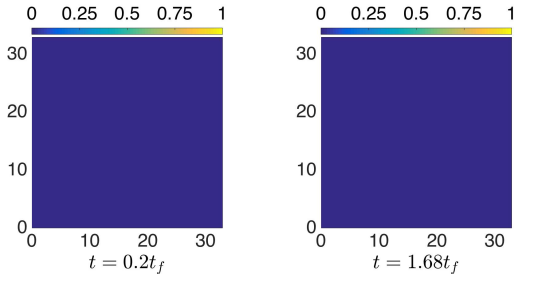

(e) $\dot{\Omega}_F$ - ST0I

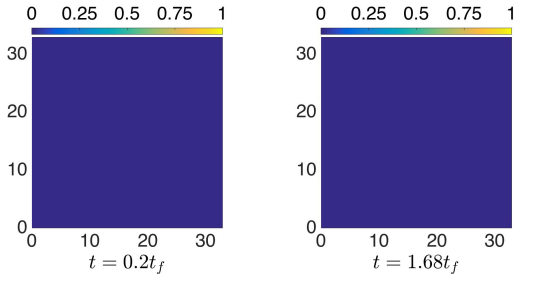

(f) $\dot{\Omega}_F$ - ST4I

Figure 4.6: Distribution of T [(a) and (b)], Y_F [(c) and (d)] and $\dot{\Omega}_F$ [(e) and (f)] on central $x_1 - x_2$ plane with domain size $33l_f \times 33l_f \times 33l_f$ for cases ST0I and ST4I from Table 4.4.

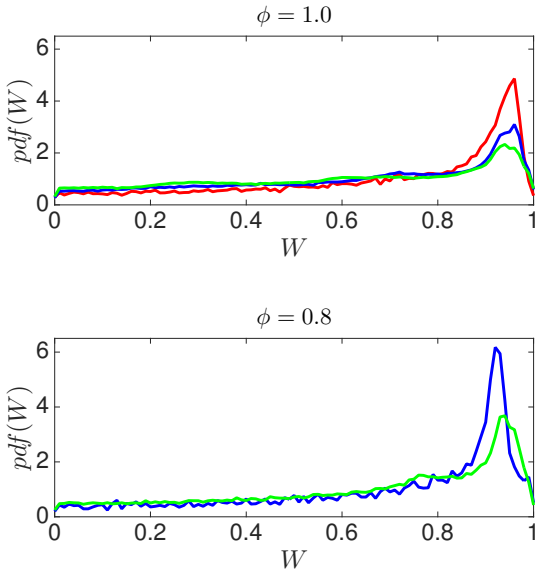

Figure 4.7: Temporal evolution of PDFs of the wrinkling indicator W for the region corresponding to $0.01 \leq c \leq 0.99$ at $t = 1.68t_f$ for selected $\frac{u'}{S_{b(\phi=1)}} = 4$ cases listed in Table 4.2.

[where $a_{sp} = 2.7$; $a_{sp} = 3.5$; $a_{sp} = 4.3$]

4.2.4 Flame Wrinkling

The successful ignition originates the flame, and the high heat release rate from that leads to a fully developed flame kernel (in favorable environment). Once the fully propagated flame kernel has been achieved, it is then possible to quantify the extent of wrinkling using a wrinkling indicator [155]:

$$W = |\,\vec{r} \cdot \vec{n}\,| \tag{4.4}$$

where $\vec{r}$ is the unit radial vector from the centre of the hot gas kernel and $\vec{n}$ is local flame normal vector already defined in Equation 3.40. The extent of the completion of chemical reaction can be quantified using reaction progress variable c, which is already defined in Section 3.4.2. The PDFs of W for the region corresponding to $0.01 \leq c \leq 0.99$ can give qualitative indication of the extent of flame wrinkling originating from localised forced ignition. According to Equation 4.4, a perfect spherical flame kernel without any wrinkled will give rise to a single delta function at $W = 1.0$ whereas the departure of the peak value of PDFs from $W = 1.0$ provides the measure of flame wrinkling.

The PDFs of W for the region corresponding to $0.01 \leq c \leq 0.99$ at $t = 1.68t_f$ are

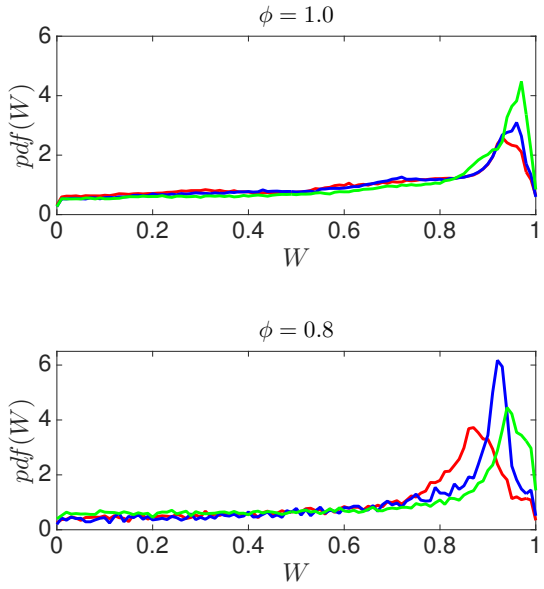

Figure 4.8: Temporal evolution of PDFs of the wrinkling indicator W for the region corresponding to $0.01 \leq c \leq 0.99$ at $t = 1.68t_f$ for selected $\frac{u'}{S_{b(\phi=1)}} = 4$ cases listed in Table 4.3.

[where $b_{sp} = 0.1$; $b_{sp} = 0.2$; $b_{sp} = 0.3$]

shown in Figure 4.7, 4.8 and 4.9 for all the cases from Table 4.2, 4.3 and 4.4 respectively where self-sustained combustion is obtained. It is evident from Figure 4.4 that the contours of T and Y_F in $\frac{u'}{S_{b(\phi=1)}} = 4$ cases are wrinkled. The flame kernel retains is spherical shape for all the quiescent cases (see Figure 4.4 for case ST0A). It can be seen from Figure 4.7 that the extent of flame wrinkling decreases with decreasing ignition energy (i.e. a_{sp}). A decrease in a_{sp} contributes in decrease radius of the hot gas kernel for the cases where self-sustained combustion obtained. This further decreases the extent of flame wrinkling because small flame kernels interact with less energetic small-scale eddies which do not sufficiently wrinkle the flame. Thus, the extent of flame wrinkling decreases with decreasing a_{sp}. This trend is evident in both $\phi = 1.0$ and $\phi = 0.8$ cases.

Furthermore, Figure 4.8 shows that a decrease in energy duration (i.e. b_{sp}) leads to an increase in flame wrinkling. An increase in b_{sp} acts as to reduce the size of the hot gas kernel, which leads to decrease the extent of flame wrinkling due to interaction of the flame kernel with less energetic small-scale eddies. Figure 4.9 suggests that an increase in R reduces the size of the hot gas kernel and hence only less energetic small eddies act to wrinkle the flame, where on the other side, the large scale eddies tend to convect the kernel. For the small values of R, the increase in flame radius due

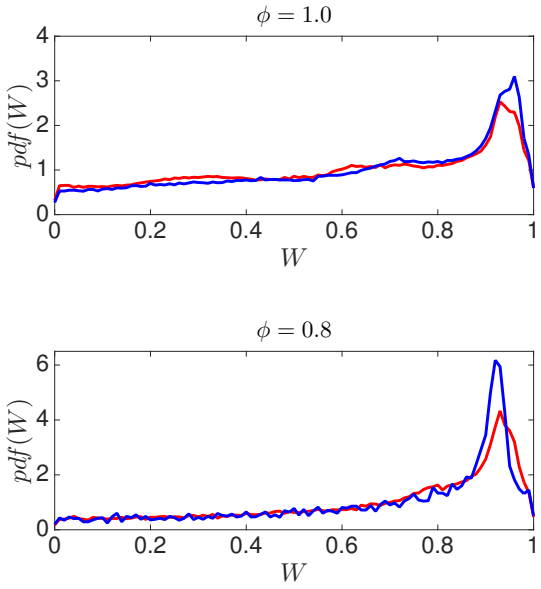

Figure 4.9: Temporal evolution of PDFs of the wrinkling indicator W for the region corresponding to $0.01 \leq c \leq 0.99$ at $t = 1.68t_f$ for selected $\frac{u'}{S_{b(\phi=1)}} = 4$ cases listed in Table 4.4.

[where $R = 0.93l_f$; $R = 1.10l_f$; $R = 1.41l_f$]

to kernel growth enables more energetic large scale eddies to interact with the flame surface, resulting great extent of flame wrinkling. It is evident from Figure 4.9 that an increase in R leads to decrease in the extent of wrinkling for both stoichiometric and fuel-lean mixture cases.

4.2.5 Temporal Evolution of the Burned Gas Mass

Once the flame kernel successfully originated from ignition source and freely propagating, then the extent of burning can be characterised by burned gas mass with $c \geq 0.9$.

$$M_b = \frac{m_b\,(c \geq 0.9)}{\frac{4}{3}\pi\rho_0 l_f^3} \tag{4.5}$$

The burned gas mass in Equation 4.5 is normalised by the mass of unburned gas in a sphere with radius equal to Zel-dovich flame thickness l_f. Moreover, the critical radius of ignition kernel scales with l_f [206]. It is important that the accuracy of M_b depends on the choice of $c \geq 0.9$, as $\int_V \rho c\, dV$ provides the measure of total burned gas mass but not accurately capture the extent of burning. For example, a flame that is about to extinguish can have a value of $\int_V \rho c\, dV$ comparable with a case where

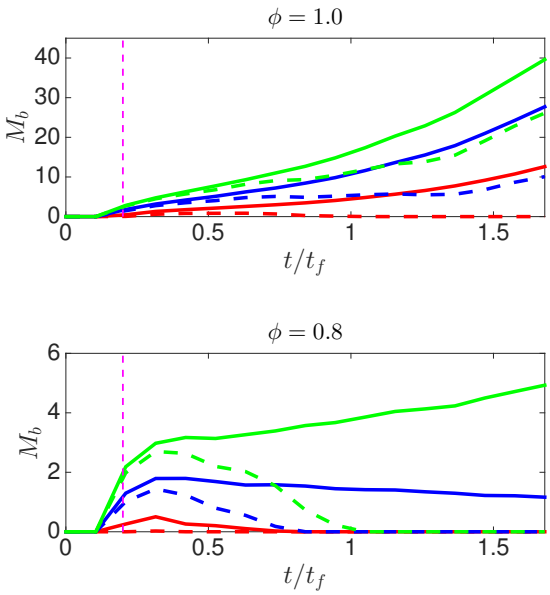

Figure 4.10: Temporal evolution of M_b for all cases listed in Table 4.2. [where $a_{sp} = 2.7$; $a_{sp} = 3.5$; $a_{sp} = 4.3$; magenta broken line shows $t = t_{sp}$; $\frac{u'}{S_{b(\phi=1)}} = 0$ (——) and $\frac{u'}{S_{b(\phi=1)}} = 4$ (– – – –)]

the fully propagated flame is in self-sustained combustion. This can happen as the flame which is just about to extinguish can show a high probability of finding $c \geq 0.5$ samples with negligible values of reaction rate magnitude but high values of density. This can eclipse the high probability of finding samples with small (high) values of $\rho\,(c)$ in a fully propagated flame in self-sustained combustion. For this reason, it is useful to consider the mass of the gas corresponding to $0.9 \leq c \leq 1.0$ region for the purpose of comparing the extent of burning because an increase of this mass indicates self-sustained combustion, and the density drop in the burned gas cannot eclipse the progress of chemical reaction. The same procedure has been adopted in several previous DNS analyses [48, 51, 127, 149, 150].

Ignition not only initiates the combustion, but also influences the subsequent combustion including the extent of burning. The temporal evolution of the burned gas mass M_b for all the cases listed in Table 4.2, 4.3 and 4.4 are shown in Figure 4.10, 4.11 and 4.12 respectively. The effects of a_{sp}, b_{sp} and R for stoichiometric and fuel-lean mixtures have been demonstrated in Figure 4.10, 4.11 and 4.12 respectively. It can be seen from Figures 4.10, 4.11 and 4.12 that the burning rate is the highest for the quiescent cases (i.e. $\frac{u'}{S_{b(\phi=1)}} = 0$) for stoichiometric cases (i.e. ST0A, ST0B, ST0C, ST0D, ST0E, ST0F, ST0G and ST0H) for a given set of values of a_{sp}, b_{sp} and R.

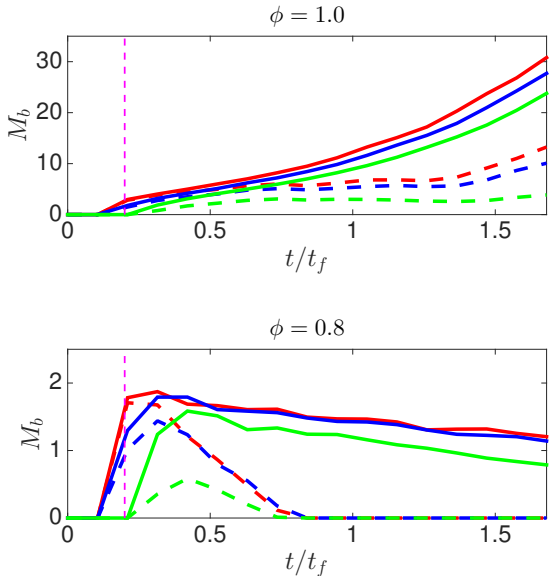

Figure 4.11: Temporal evolution of M_b for all cases listed in Table 4.3. [where $b_{sp} = 0.1$; $b_{sp} = 0.2$; $b_{sp} = 0.3$; magenta broken line shows $t = t_{sp}$; $\frac{u'}{S_{b(\phi=1)}} = 0$ (——) and $\frac{u'}{S_{b(\phi=1)}} = 4$ (- - - - -)]

Moreover, the extent of burning is greater in stoichiometric mixtures than in fuel-lean mixtures cases for a given set of values of a_{sp}, b_{sp} and R due to higher rate of chemical reaction in the stoichiometric mixture.

It can be seen from Figure 4.10 that the burning rate is the strongest for quiescent cases (i.e. $\frac{u'}{S_{b(\phi=1)}} = 0.0$) in comparison to turbulent (i.e. $\frac{u'}{S_{b(\phi=1)}} = 4.0$) cases. Furthermore it can be seen from Figure 4.10 that an increase in a_{sp} for a given set of values of R, b_{sp} and $\frac{u'}{S_{b(\phi=1)}}$ increases the probability of finding high temperature and $\dot{\Omega}_F$ values. This leads to higher burning rate with increasing a_{sp} and improves the chance of successful ignition and self-sustained combustion, which is very crucial for fuel-lean mixture cases. Figure 4.10 also indicates that high values of a_{sp} provide favorable conditions in order to achieve self-sustained combustion following successful ignition. The findings from Figure 4.10 further shows that M_b decreases with increasing value of $\frac{u'}{S_{b(\phi=1)}}$ for both stoichiometric and fuel-lean mixtures. It is possible to obtain either misfire or flame extinction for high values of u'.

The heat release due to chemical reaction needs to overcome heat transfer from the hot gas kernel to surrounding cold gas in order to have self-sustained combustion and growth of the flame kernel. By contrast, the hot kernel shrinks and eventually flame extinguishes once the heat transfer overcomes the chemical heat release. The

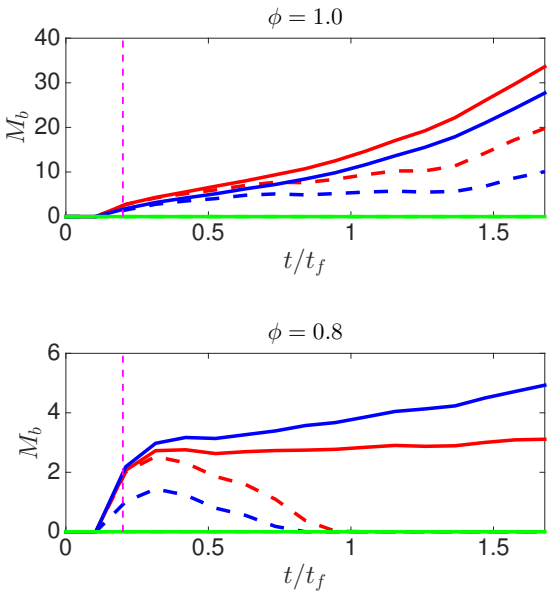

Figure 4.12: Temporal evolution of M_b for all cases listed in Table 4.4. [where $R = 0.93l_f$; $R = 1.10l_f$; $R = 1.41l_f$; magenta broken line shows $t = t_{sp}$; $\frac{u'}{S_{b(\phi=1)}} = 0$ (——) and $\frac{u'}{S_{b(\phi=1)}} = 4$ (– – – –)]

eddy thermal diffusivity in turbulent flows scales as:

$$D_t \sim u' L_{11} \tag{4.6}$$

The Equation 4.6 indicates that an increase in u' for a given value of L_{11} augments the rate of heat transfer from the hot gas kernel. Thus the mass of the hot gas kernel decreases with increasing u', and large values of u' give rise to either misfire or eventual flame extinction. As the rate of heat release in the fuel-lean cases is smaller than in the stoichiometric cases, the rate of augmented heat transfer for the turbulent cases is more likely to overcome chemical heat release in the fuel-lean cases than in the stoichiometric cases. Thus, the fuel-lean cases are more susceptible to flame extinction than the stoichiometric cases and this behaviour is particularly prominent especially for turbulent flows. The adverse effects of u' on ignition and early stages of burning are consistent with previous experimental [15, 96, 116] and computational [45, 48, 50, 51, 78] findings.

Figure 4.11 demonstrates that the effects of b_{sp} on the extent of burning in both stoichiometric and fuel-lean mixtures. An increase in b_{sp} gives rise to a reduction in ignition power for given set values of ignition energy (i.e. a_{sp}) and the characteristic width of ignition energy deposition (i.e. R), which further reduces the probability of

finding of high temperature which leads to high values of $\dot{\Omega}_F$. Thus, the probability of finding high $\dot{\Omega}_F$ and chemical heat release decreases with increasing value of b_{sp}, which leads to reduction in the extent of burning and the flames are more prone to extinction for high values of b_{sp} especially for fuel-lean mixture cases (see Figures 4.2 and 4.11). The effects of b_{sp} are qualitatively similar in both stoichiometric and fuel-lean mixtures. The detrimental effects of increasing $\frac{u'}{S_{b(\phi=1)}}$ on the possibility of successful ignition can be seen in Figure 4.11 as well.

It can be confirmed from Figure 4.3 that the cases with $R = 1.41l_f$ (i.e. ST0I, ST4I, LT0I and LT4I) fail to ignite, whereas a reduction in R gives rise to successful ignition and self-sustained combustion. Furthermore, Figure 4.12 shows that smaller values of R (i.e. $0.93l_f$ and $1.10l_f$) leads to increase in the burning rate. An increase in R for a given set values of a_{sp} and b_{sp} deposits ignition energy over a larger volume of gas, and this leads to reduction in the probability of finding high temperature (probably around adiabatic flame temperature) to support chemical reaction to take place. This further leads to reduction in the overall rate of fuel consumption (see subfigure (c) and (d) in Figure 4.6) and heat release within the flame kernel for higher value of R and flame eventually extinguishes when heat transfer overcomes the chemical heat release. The detrimental effects of $\frac{u'}{S_{b(\phi=1)}}$ are still present here irrespective of the choice of R. It can be concluded from the results shown in Figures 4.10, 4.11 and 4.12 that high (small) values of a_{sp} (b_{sp} and R) provide favorable condition in order to achieve self-sustained combustion following successful ignition.

4.2.6 Ignition and Self-Sustained Combustion for Fuel-Lean Mixtures

The results presented above show that it is more difficult to obtain self-sustained combustion following successful ignition for turbulent fuel-lean mixture cases than for stoichiometric mixtures, but this can be achieved with the proper choice of ignition parameters a_{sp}, b_{sp} and R. In order to demonstrate this, the cases summarised in Table 4.5 have been considered.

The temporal evolution of $T_{\max}$ for all the cases listed in Table 4.5 are shown in Figure 4.13. It can be seen from Figure 4.13 (subfigure (c)) that $T_{\max}$ settles to the adiabatic flame temperature for $t \gg t_{sp}$ for all [M] cases from Table 4.5 except the LT6M case which shows failed self-sustained combustion following successful ignition due to high values of u'. Although, comparing subfigures (a) and (c) in Figure 4.13,

$\frac{L_{11}}{l_f} = 3.36$		$\phi = 1.0$			$\phi = 0.8$		
		$\frac{u'}{S_{b(\phi=1)}} = 0.0$	$\frac{u'}{S_{b(\phi=1)}} = 4.0$	$\frac{u'}{S_{b(\phi=1)}} = 6.0$	$\frac{u'}{S_{b(\phi=1)}} = 0.0$	$\frac{u'}{S_{b(\phi=1)}} = 4.0$	$\frac{u'}{S_{b(\phi=1)}} = 6.0$
		[T0]	[T4]	[T6]	[T0]	[T4]	[T6]
$a_{sp} = 4.5$ $R = 1.10l_f$ $b_{sp} = 0.2t_f$	[M]	ST0M	ST4M	ST6M	LT0M	LT4M	LT6M
$a_{sp} = 13.0$ $R = 1.55l_f$ $b_{sp} = 0.2t_f$	[N]	ST0N	ST4N	ST6N	LT0N	LT4N	LT6N

Table 4.5: List of parameters that provides self-sustained combustion for some fuel-lean mixtures cases.

it can be seen that successful self-sustained combustion has been obtained for the very same [M] cases and same level of u' for the stoichiometric mixture. Additionally Figure 4.13 shows that the choice of $R = 1.55l_f$ with higher ignition energy $a_{sp} = 13.0$ leads to successful self-sustained combustion following successful ignition for all the stoichiometric as well as fuel-lean cases for all values of u' considered here.

The temporal evolution of M_b for all the cases listed in Table 4.5 are shown in Figure 4.14. Although the case LT4M shows successful ignition, the burned gas mass M_b decreases with time suggesting this case may eventually extinguish with time. Additionally cases with $R = 1.55l_f$; $a_{sp} = 13.0$; $b_{sp} = 0.2t_f$ yields successful self-sustained combustion for all cases, however the burned gas mass M_b continues to increase with time for fuel-lean mixture cases LT0N and LT4N, but M_b decreases with time at $t \gg t_{sp}$ for the LT6N case.

The observation from Figures 4.13 and 4.14 shows that it is possible to achieve self-sustained combustion following successful ignition even for fuel-lean cases with higher value of u' by judicious choice of a_{sp}, b_{sp} and R. These parameters can be altered independently of each other in the case of laser ignition. The findings presented above are in qualitative agreement with recent experimental findings [26, 31, 65, 66] and analytical review findings [63, 141, 198] that laser ignition can be effective in igniting fuel-lean mixtures by altering the laser power (i.e. equivalent to the variation of a_{sp}), laser bean radius (i.e. equivalent to the variation of R) and laser pulse duration (i.e. equivalent to the variation of b_{sp}).

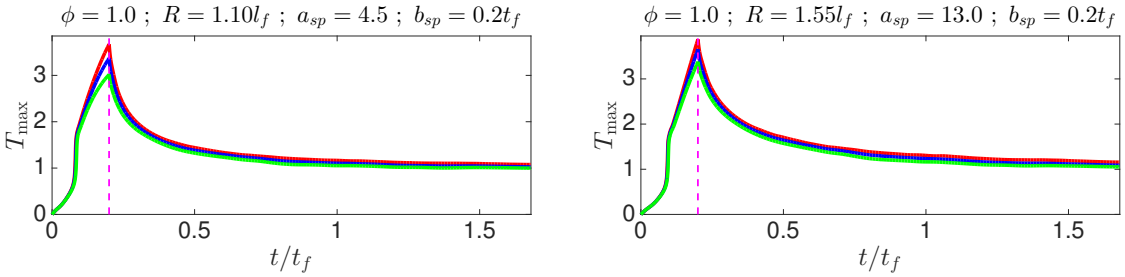

(a) Case M with $\phi = 1.0$

(b) Case N with $\phi = 1.0$

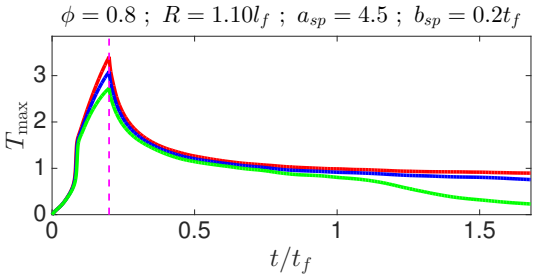

(c) Case M with $\phi = 0.8$

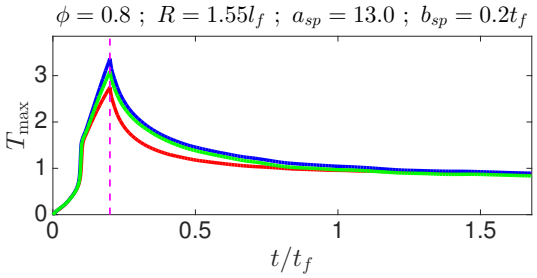

(d) Case N with $\phi = 0.8$

Figure 4.13: Temporal distribution of $T_{\max}$ for all the cases listed in Table 4.5. [where $\frac{u'}{S_{b(\phi=1)}} = 0$; $\frac{u'}{S_{b(\phi=1)}} = 4$; $\frac{u'}{S_{b(\phi=1)}} = 6$; magenta broken line shows $t = t_{sp}$]

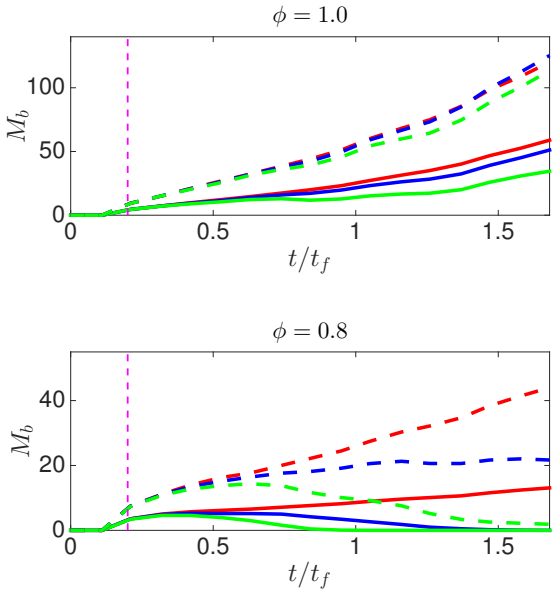

Figure 4.14: Temporal distribution of M_b for all the cases listed in Table 4.5. [where $\frac{u'}{S_{b(\phi=1)}} = 0$; $\frac{u'}{S_{b(\phi=1)}} = 4$; $\frac{u'}{S_{b(\phi=1)}} = 6$; magenta broken line shows $t = t_{sp}$; cases:$[M]$ (——) and cases:$[N]$ (- - - - -)]

4.2.7 Qualitative Comparison with Experimental Findings

The present analysis has been carried out under decaying turbulence in a canonical configuration, which is different from the experimental flow conditions analysed by Lefebvre [116]. Moreover, DNS simulations are computationally expensive so these simulations are not ideally suited to identify the exact values of minimum ignition energy and optimum energy deposition duration. Furthermore, some simplifications are adopted in representing the localised ignition in analytical [52, 90, 207, 208] and numerical simulation [51, 210, 212] studies, which often preclude a direct comparison of the minimum ignition energy and the optimum energy deposition duration obtained from experiments with computational results. Despite of the above limitations, important qualitative conclusions can be drawn from the DNS simulations, which are discussed here.

4.2.7.1 Expression of E_{min}

Experimental investigation from Ballal and Lefebvre [16] concluded that igniter generated hot gas kernel needs a critical diameter (see Sections 2.3.2.1 and 2.3.2.2), in order to survive without the aid of any further external energy addition. According to Ballal and Lefebvre [16], the critical diameter is given by:

$$d_q \approx \begin{cases} \frac{A\, l_f}{\left(S_{b(\phi)}/S_L\right) - 0.16\left(u'/S_L\right)} & \text{for} \quad u' < 2S_{b(\phi)} \\ \\ \frac{B\, l_f}{\left(S_T/S_L\right) - 0.63\left(u'/S_L\right)} & \text{for} \quad u' \gg 2S_{b(\phi)} \end{cases} \tag{4.7}$$

Here $S_{b(\phi)}$ is the unstrained laminar burning velocity for the mixture with given equivalence ratio ϕ , S_L is the unstrained laminar burning velocity of the stoichiometric mixture and S_T is the turbulent flame speed. Moreover,

$$S_{b(\phi)} \approx \begin{cases} S_L & \text{for} \quad \phi = 1.0 \\ 0.6S_L & \text{for} \quad \phi = 0.8 \end{cases} \tag{4.8}$$

Thus,

$$\frac{u'}{S_L} = 4.0 \xrightarrow{\text{correspond to}} \begin{cases} 4.0\, S_{b(\phi)} & \text{for} \quad \phi = 1.0 \\ 7.0\, S_{b(\phi)} & \text{for} \quad \phi = 0.8 \end{cases}$$
$$\frac{u'}{S_L} = 6.0 \xrightarrow{\text{correspond to}} \begin{cases} 6.0\, S_{b(\phi)} & \text{for} \quad \phi = 1.0 \\ 10.0\, S_{b(\phi)} & \text{for} \quad \phi = 0.8 \end{cases} \tag{4.9}$$

Now, it is possible to evaluate the MIE ($E_{\min}$) based on energy required to heat the mass of unburned gas with diameter d_q to its adiabatic flame temperature, which leads to the following expression:

$$E_{\min} = \rho_0\, C_P \left(T_{ad(\phi)} - T_0\right) \frac{\pi d_q^3}{6} \tag{4.10}$$

Ballal and Lefebvre [16] proposed an expression of $E_{\min}$ using Equation 4.7 :

$$E_{\min} = \begin{cases} \rho_0 C_P \left(T_{ad(\phi)} - T_0\right) \frac{\pi l_f^3}{6} \left[\frac{A S_L}{S_{b(\phi)} - 0.16\, u'}\right]^3 & \text{for} \quad u' < 2S_{b(\phi)} \\ \\ \rho_0 C_P \left(T_{ad(\phi)} - T_0\right) \frac{\pi l_f^3}{6} \left[\frac{B S_L}{S_T - 0.63\, u'}\right]^3 & \text{for} \quad u' \gg 2S_{b(\phi)} \end{cases} \tag{4.11}$$

Here A and B are constants of the order of unity. It is important to note that Equation 4.11 is applicable for all the u' cases considered here in this Section 4.2, although u' decays during the energy deposition in this configuration. Additionally Equation 4.11 suggests that an increase in u' acts to increase in $E_{\min}$, and decrease in $S_{b(\phi)}$ with decreasing ϕ leads to increase in $E_{\min}$ for fuel-lean mixtures. For example, $E_{\min}$ for the $\phi = 0.8$ mixture is about 4.0 times greater than that for the stoichiometric (i.e. $\phi = 1.0$) mixtures according to Equation 4.11. This indicates that higher a_{sp} are needed for successful ignition and self-sustained flame for fuel-lean mixtures in comparison to stoichiometric mixture, which is in consistent agreement with findings in this Section 4.2.6. Additionally, Figure 4.1 shows that the stoichiometric case ST0A obtained successful self-sustained combustion for $a_{sp} = 2.7$, whereas the corresponding fuel-lean case LT0A fails to sustain combustion once the ignition source is switched off. As another example, compare case ST4A (see Table 4.2 and Figure 4.1) and case ST4M, ST6M (see Table 4.5 and Figure 4.13), which suggests that $a_{sp} = 2.7$ fails to sustain combustion for higher value of u', whereas $a_{sp} = 4.5$ gives rise to self-sustained

combustion even for $\frac{u'}{S_{b(\phi=1)}} = 6$ (same set of values of b_{sp} and R). Again this findings are in agreement with Equation 4.11, which suggests that $E_{\min}$ is expected to rise with increasing u'. The increasing demand of $E_{\min}$ with decreasing ϕ is also consistent with previous experimental findings (please refer to Figure 5.38 in [116]). The Equation 4.11 provides information about the MIE for successful ignition and subsequent flame propagation, whereas Section 4.2 demonstrates the characteristics of energy deposition have profound influences on the success of ignition and subsequent flame propagation. For example cases ST0G and ST0H in Table 4.4 exhibit self-sustained combustion for $R = 0.93l_f$ and $1.10l_f$ respectively for $a_{sp} = 3.5$ but the corresponding cases with $R = 1.41l_f$ in Table 4.4 did not even ignite (see Figure 4.3).

4.2.7.2 Energy Deposited by the Igniter

In this sub-section, the comparison between $E_{\min}$ (Equation 4.11) and the total energy deposited by the igniter $\dot{Q}$ (Equation 3.30) has been analysed to draw the comparison with experimental findings. This comparison reveals that:

$$\rho_0 C_P \left(T_{ad(\phi)} - T_0\right) \frac{\pi l_f^3}{6} \left[\frac{AS_L}{S_{b(\phi)} - 0.16\,u'}\right]^3 = a_{sp}\rho_0 C_P \tau T_0 \left(\frac{4}{3}\pi l_f^3\right) \tag{4.12}$$

which further becomes:

$$a_{sp} = \begin{cases} 0.125A^3 & \text{for } \phi = 1.0 \\ 0.5A^3 & \text{for } \phi = 0.8 \end{cases} \tag{4.13}$$

The values of $a_{sp}\,(\geq 2.7)$ used in this analysis are sufficient to ignite both stoichiometric and fuel-lean mixtures except for $R = 1.41l_f$, however a direct quantitative comparison between the experimentally obtained empirical relations with present DNS results is beyond the scope of current analysis, as the exact evaluation of MIE will be made prohibitively expensive by the necessity of carrying out several computationally intensive DNS simulations. The experimentally achieved MIE also includes the heat loss through the electrode, which is not addressed in present DNS based analysis. Additionally, different researchers have used different values of A, B (see Equation 4.11) and different expression of S_T [141, 206], so the qualitative prediction of $E_{\min}$ is not entirely unambiguous, and can potentially form the basis of further analyses.

4.2.7.3 Energy Deposition Time Interval and Igniter Diameter

Lefebvre [116] defined the optimum energy deposition duration as a time interval, which leads to lowest measured value of ignition energy when the background fluid flow remains unchanged. In current DNS analysis the energy deposition time t_{sp} is modified independently of other parameters in order to change ignition power in isolation. The present analysis deals with homogeneous mixtures, hence the chemical time-scale remains unchanged and thus the parameter $b_{sp} = \frac{t_{sp}}{t_f}$ can be defined as a function of t_f and is independent of other parameters. Considering zero mean flow, the time scale for the diffusion of energy deposited over distance R is:

$$t_{diff} \sim \frac{R^2}{D_{ref} + D_t} \sim \left(\frac{R}{l_f}\right)^2 \left[\frac{t_f}{1 + a\left(\frac{u'}{S_L}\right)\left(\frac{L_{11}}{l_f}\right)}\right] \tag{4.14}$$

where D_{ref} is the reference unburned gas diffusivity and D_t is the thermal diffusivity. Experimental findings by Ballal and Lefebvre suggests that the constant parameter $a \sim 0.16$ [16]. Therefore Equation 4.14 can be further recast as:

$$t_{diff} \sim \frac{a_e^2\, t_f}{\left(\frac{l_f}{L_{11}}\right)^2 + 0.2\left(\frac{t_f}{t_e}\right)} \qquad \text{where} \quad a_e = \frac{R}{L_{11}} \tag{4.15}$$

which further leads to:

$$a_e = \begin{cases} 0.27 & \text{for } R = 0.93 l_f \\ 0.33 & \text{for } R = 1.10 l_f \\ 0.42 & \text{for } R = 1.41 l_f \end{cases} \tag{4.16}$$

In the present analysis, $\frac{L_{11}}{l_f}$ is constant, this suggests that the diffusion timescale t_{diff} decreases with increasing $\frac{u'}{S_L}$ and thus $\left(\frac{t_e}{t_f}\right)$ also decreases with increasing $\frac{u'}{S_L}$. This suggests that an increase in $\frac{u'}{S_L}$ leads to more rapid heat transfer (due to thermal diffusion) from hot gas kernel in comparison to the rate of chemical heat release. These detrimental effects of u' on extent of burning are in favorable agreement in the present findings (see cases in Table 4.5 and Figure 4.14).

A decrease in b_{sp} leads to more rapid energy deposition than the rate of diffusion of heat, which can increase the temperature of hot gas kernel and increase the extent of burning. This effect is also present in current DNS findings, as higher values of $T_{\max}$ and M_b are obtained in the cases [D] than the cases [F] from Table 4.3 (see Figures 4.2

and 4.11). Additionally, an increase in R acts as an increase in the diffusion timescale (see Equations 4.15 and 4.16). This effect can be seen in the cases [I] with $R = 1.41l_f$, where larger R leads to decrease in temperature (faster diffusion timescale) in the hot gas kernel because the energy is deposited over a larger mass of gas, which leads to failed ignition for $R = 1.41l_f$ (see Figure 4.3).

However this reduced temperature rise for large values of R can be eclipsed by increasing a_{sp}, which can be substantiated by cases [N] in Table 4.5 and leads to self-sustained combustion following successful ignition as well as higher extent of burning (see cases [N] in the Table 4.5 and corresponding Figures 4.13 and 4.14). These findings are also consistent with the recent results by Wandel [210] in the context of ignition of turbulent droplet-laden mixtures, which revealed that a large region of hot gas with small equivalence ratio variation can be advantageous from the viewpoint of localised forced ignition when sufficient ignition energy is supplied.

4.2.8 Summary

The section 4.2 analyses the effects of energy deposition characteristics (i.e. ignition energy, ignition duration and the width of ignition energy distribution) on localised forced ignition of both stoichiometric ($\phi = 1.0$) and fuel-lean ($\phi = 0.8$) turbulent homogeneous mixtures based on DNS. It has been found that higher amount of ignition energy is necessary to obtain self-sustained combustion in fuel-lean cases than in the stoichiometric cases. The detrimental effects of u' are more critical in the fuel-lean mixture than in the stoichiometric mixture because of weaker heat release effects in the fuel-lean mixture. An increase in R and b_{sp} for a given a_{sp} has been found to have detrimental effects on the extent of burning and these effects can be critical for the ignition of fuel-lean mixtures. The above findings clearly indicate that laser ignition can be advantageous for obtaining successful ignition and self-sustained combustion in fuel-lean mixtures where a laser can offer great control and independent alteration between energy deposition width, duration of energy deposition and input ignition energy. The above DNS based findings are in qualitatively consistent with previous experimental findings [16, 96, 116].

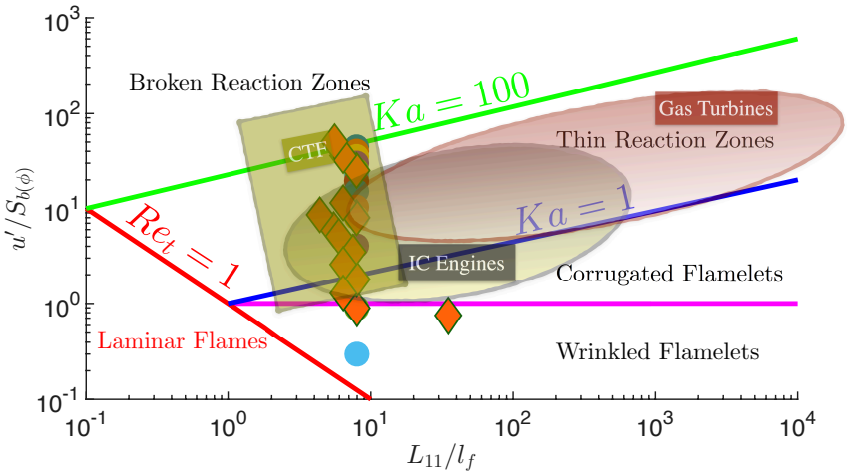

Figure 4.15: Premixed turbulent combustion regime diagram accentuating areas for engineering applications IC engines, gas turbines and counterflow regime and indicating simulations cases for the present study.

4.3 Effects of Combustion Regimes

This section starts with brief review of premixed turbulent combustion regimes and characterisation of Karlovitz number (Ka) for this study. Modifications in numerical formulation are highlighted and then the results for effects of combustion regime on localised forced ignition of turbulent homogeneous mixtures are presented and discussed. Temporal evolution of maximum temperature is shown first to analyse the effects of different combustion regimes on MIE. Isosurfaces of the temperature field and reaction-diffusion balance analysis of flame kernel are then presented. The temporal evolution of the burned gas mass was analysed for cases where self-sustained combustion following successful ignition was achieved. The width of ignition energy distribution has been modified to reduce MIE. Finally, qualitative comparison with experimental findings is presented and the section ends with summary.

Regimes of premixed turbulent combustion as functions of velocity and length scale ratios have been proposed by Borghi [32], Peters [158], Abdel-Gayed *et al.* [1], Poinsot *et al.* [162] and many others and has already been explained in Section 2.5.2. Findings of Section 4.2 suggests that the MIE plays a critical role in obtaining successful ignition and subsequent flame propagation.

Here the MIE is defined as the minimum amount of energy supplied by the igniter which confirms successful ignition as well as the self-sustained combustion. The ig-

Ka	$\frac{u'}{S_{b(\phi)}}$	$\frac{L_{11}}{l_f}\Big\vert_{\phi}$	ϕ	Case
44.2	25	8.0	1.0	STR_1
8.0	8.0	8.0	1.0	STR_2
6.3	6.0	5.5	1.0	STR_3
2.4	3.6	7.5	1.0	STR_4
0.90	1.8	8.0	1.0	SCR
0.30	0.9	8.0	1.0	SWR
84.4	35.7	6.4	0.8	LTR_1
15.3	11.4	6.4	0.8	LTR_2
12.0	8.6	4.4	0.8	LTR_3
4.8	5.1	6.0	0.8	LTR_4
1.7	2.6	6.4	0.8	LCR
0.6	1.3	6.4	0.8	LWR
149.4	50.0	5.6	0.7	LBR

Table 4.6: Simulation parameters to analyse the effects of different combustion regimes (different values of Ka).

nitability of turbulent homogeneous mixtures and the corresponding value of MIE in the case of localised forced ignition have been analysed for different values of Karlovitz number (Ka) using DNS. The flame-turbulence interaction in turbulent premixed combustion is often characterised in terms of a non-dimensional number known as the Karlovitz number. In this study the Karlovitz number is defines as:

$$Ka = \frac{\left(\frac{u'}{S_{b(\phi)}}\right)^{\frac{3}{2}}}{\sqrt{\frac{L_{11}}{l_f}}} \tag{4.17}$$

where L_{11} and l_f is the longitudinal integral length scale and Zel'dovich flame thickness respectively. The Karlovitz number also provides the measure of the ratio of the chemical time scale t_f to the Kolmogorov time scale t_η (i.e. $Ka \sim t_f/t_\eta$) [158]. Alternatively, the Karlovitz number can be interpreted as the ratio of flame thickness l_f to the Kolmogorov length scale η $\left(\text{i.e. } Ka \sim l_f^2/\eta^2\right)$ (see Section 2.5.2).

In order to emphasize the area for engineering applications, Figure 2.2 from Section 2.5.2 has been repeated in Figure 4.15. Moreover, Figure 4.15 shows the typical working conditions realised in IC engines, gas turbines and counter flow regime on the regime diagram. It is crucial to study the localised forced ignition for different combustion regimes to understand the impact of the combustion regimes on MIE. In the following section the results will be presented and subsequently discussed. The

numerical formulation remains similar to as described in Section 4.2.1 except for few modifications. The simulation domain is taken to be a cubic with size $53l_f \times 53l_f \times 53l_f$ which in Cartesian grid size of $320 \times 320 \times 320$ with uniform grid spacing Δx. Simulations have been carried out for $t_{sim} \sim 12.60 t_{sp} \sim 2.40\, t_f$ in all cases, and this simulation time has been found to be sufficient to determine whether or not a particular case will give rise to self-sustained combustion. It is important to note that the energy deposition duration ($t_{sp} = 0.2 t_f$) has been kept constant for all the cases studied here.

4.3.1 Ignition in Different Combustion Regimes

The most important application of premixed turbulent combustion is to SI engines and lean-burn gas turbines [158]. Since turbulent flow exists in nearly all engineering applications, it becomes a challenge to obtain successful ignition and self-sustained combustion when $Ka \geq 100$. Therefore the present Section 4.3 analyses the effects of different combustion regimes (different values of Ka) on MIE and requirement for successful localised forced ignition and obtaining self-sustained combustion using DNS. The simulation parameters are listed in Table 4.6 and the case names are chosen in such manner that S... Stoichiometric mixtures, L... Fuel-lean mixtures, BR... Broken reaction regime, TR... Thin reaction regime, CR...Corrugated flamelet regime, WR...Wrinkle flamelet regime (e.g. LCR corresponds to a case for Corrugated flamelet regime with fuel-lean mixtures).

4.3.2 Temporal Evolution of Maximum Temperature

The temporal evolution of the non-dimensional maximum temperature $T_{\max}$ and corresponding turbulence decay profile is shown in Figures 4.16 and 4.17 for both stoichiometric and fuel-lean cases as listed in Table 4.6.

Additionally, Figures 4.16 and 4.17 shows $T_{\max}$ for different values of ignition energy (i.e. a_{sp}) for the characteristic energy deposition width (igniter diameter) $R = 2.45 l_f$. The values of a_{sp} are chosen in such manner that it demonstrates the ignition energy needed to ignite the mixture, but does not guarantee self-sustained combustion. The ignition energy which confirms self-sustain combustion is different from the ignition energy which simply just ignites the mixture. For example in case STR_1 ($Ka = 44.20, \phi = 1.0$), the $a_{sp} = 32.5$ is enough to obtain successful ignition but once the igniter is switched off (i.e. $t = t_{sp}$), the $T_{\max}$ falls below the adiabatic flame temperature and flame eventually extinguishes. On the other hand, for the vary same

case STR_1 for $a_{sp} = 36.75$, $T_{\max}$ settles to $T_{\max} \approx 1.0$ even at $t \gg t_{sp}$ confirming the heat release from hot gas kernel is higher enough to overcome the heat transfer and self-sustained combustion has been achieved.

The smallest a_{sp} (i.e. the multiplier in ignition power Equation 3.30 in Section 3.3) value in Figures 4.16 and 4.17 for a given case indicates the minimum amount of ignition energy required just to ignite the given mixture. The ignition event can be differentiated from Figures 4.16 and 4.17 by the sharp change in slope of the temporal evolution of $T_{\max}$ at $t = t_{sp}$, which is accompanied by a thermal runaway leading to a value of $T_{\max}$ around adiabatic temperature. However successful ignition does not guarantee self-sustained combustion once the igniter has been switched off. For example see case LTR_3, the $a_{sp} = 18.8$ is enough to ignite the mixture but $T_{\max}$ decreases sharply after $t \gg t_{sp}$, whereas $a_{sp} = 21.3$ provides self-sustained combustion following successful ignition. Another example see case LTR_1 for $a_{sp} = 28.2$, the surface area to volume ratio of the hot gas kernel decreases with the expansion of the flame kernel.

Furthermore, in this DNS configuration u' decays with time and therefore the eddy thermal diffusivity $D_t \sim u' L_{11}$ also decreases with time. The combined effects of the reduction of thermal diffusivity and surface area to volume ratio with time for growing flame kernels leads to more reduction in the magnitude of heat transfer rate from the hot gas kernel as time progresses providing more favorable condition for thermal runaway at high value of $T_{\max}$. Therefore background fluid turbulence has influences on the duration over which the high value of $T_{\max}$ is obtained after igniter is switched off .

The cases STR_1 and LTR_1 represents $Ka = 44.2$ ($\phi = 1.0$) and $Ka = 84.4$ ($\phi = 0.8$) respectively, which are high Karlovitz number cases corresponding to thin reaction zones of regime combustion. In this thin reaction zone regime turbulent eddies penetrate into the flame structure and significantly disturb the thermodiffusive balance in the preheat zone and therefore the flame starts to show some attributes of the broken reaction regime (as described in Section 2.5.2). This can be seen in the fluctuation in the $T_{\max}$ profiles for both cases STR_1 and LTR_1 in Figure 4.16. The increase requirement of the ignition energy with increasing Ka are clearly evident from Figures 4.16 and 4.17.

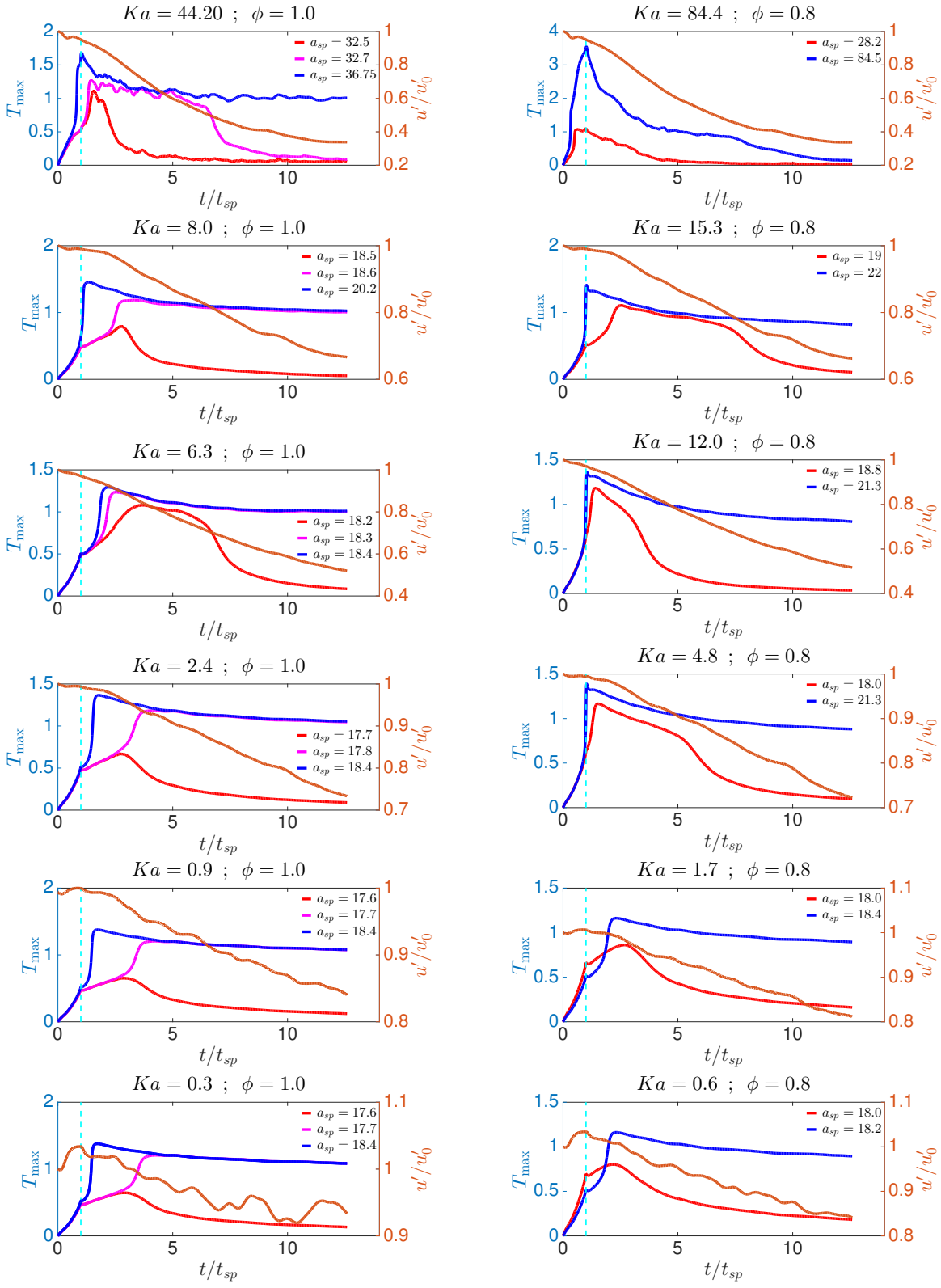

Figure 4.16: Temporal evolution of $T_{\max}$ and corresponding turbulence decay profile for $\phi = 1$ (1^{st}column) and $\phi = 0.8$ (2^{nd}column) cases listed in Table 4.6 with $R = 2.45 l_f$, where cyan broken line shows $t = t_{sp}$.

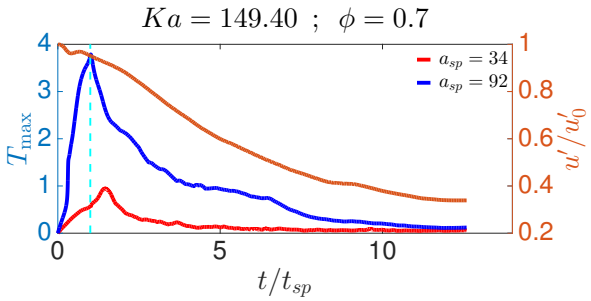

Figure 4.17: Temporal evolution of $T_{\max}$ and corresponding turbulence decay profile for $\phi = 0.7$ case LBR listed in Table 4.6 with $R = 2.45l_f$, where cyan broken line shows $t = t_{sp}$.

4.3.3 Isosurface of Temperature Field

The aforementioned behaviour can be substantiated from Figures 4.18 and 4.19 where 3D volume rendered view of non-dimentional temperature T is shown for selected cases from Table 4.6 at different time instants. It is evident from Figures 4.18 and 4.19 that the isosurfaces of T remains approximately spherical during the period of energy deposition (except cases STR_1 ($Ka = 44.20$, $\phi = 1.0$) and LBR ($Ka = 149.40$, $\phi = 0.7$) - where turbulence tends to fragment the flame surface), but they become increasingly wrinkled as time progresses for all the cases except for case STR_1. Further interesting observations can be drawn from Figure 4.18 that in case STR_1 ($Ka = 44.20, \phi = 1.0$), when $t \gg t_{sp}$, the high temperature region has been fragmented thanks to energetic eddies of turbulence penetrating into the flame. This tendency is more prominent for the case LBR (see Figure 4.19) for $Ka = 149.4$, where turbulent eddies enters into flame and start breaking the reaction zone and flame eventually extinguishes (see Figure 4.17).

4.3.4 Reaction-Diffusion Balance Analysis of the Flame Kernels

It is extremely important that heat release due to chemical reaction should overcome the heat transfer from the hot gas kernel in order to obtain self-sustained combustion following successful ignition. Although Figures 4.16-4.19 provides clear indication of both growing and broken (leading to extinction) flame kernels, it is important to examine the reaction-diffusion balance in order to understand the difference in flame kernels which are growing in an unperturbed manner and those which are fragmented

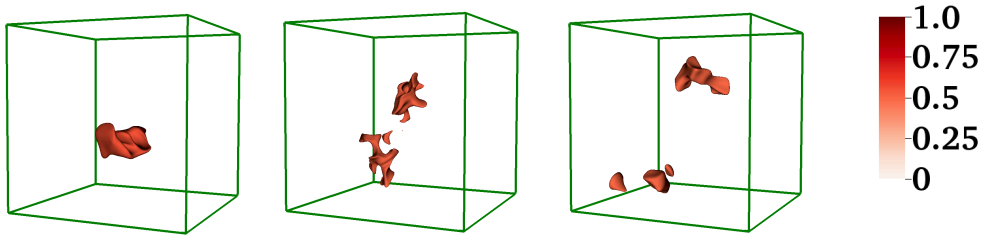

(a) case - STR_1 ($Ka = 44.2$; $a_{sp} = 36.75$; $\phi = 1.0$)

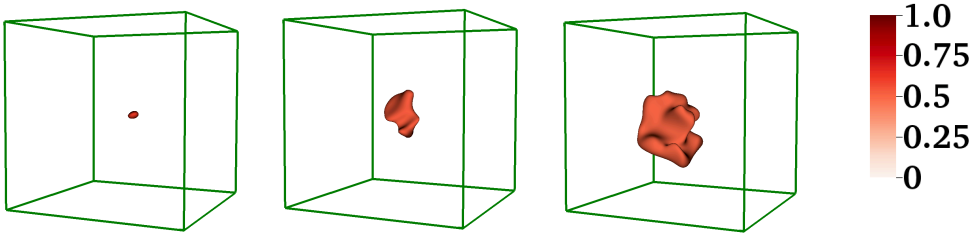

(b) case - STR_3 ($Ka = 6.3$; $a_{sp} = 18.4$; $\phi = 1.0$)

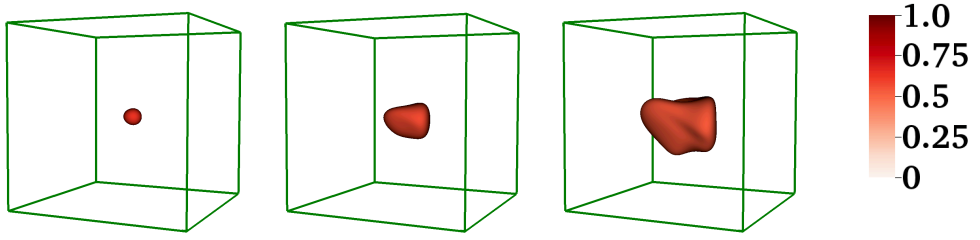

(c) case - SCR ($Ka = 0.9$; $a_{sp} = 18.4$; $\phi = 1.0$)

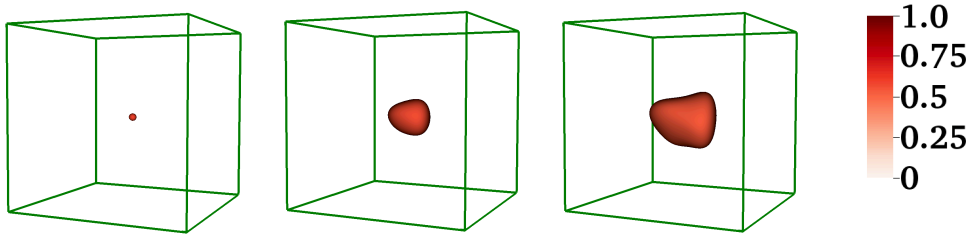

(d) Case - SWR($Ka = 0.3$; $a_{sp} = 18.4$; $\phi = 1.0$)

Figure 4.18: Volume rendered view of non-dimensional temperature field (T) within the domain $53l_f \times 53l_f \times 53l_f$ for the $\phi = 1.0$; $R = 2.45l_f$ selected cases from Table 4.6. [where 1^{st}column - $2.10t_{sp}$, 2^{nd}column - $6.30t_{sp}$ and 3^{rd}column - $12.60t_{sp}$]

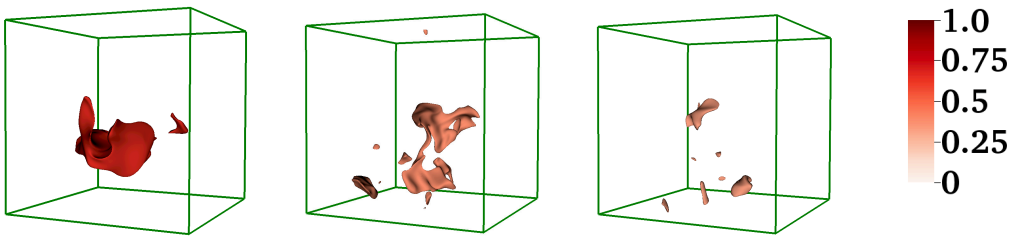

(a) Case - LBR ($Ka = 149.4$; $a_{sp} = 92.$; $\phi = 0.7$)

Figure 4.19: Volume rendered view of non-dimensional temperature field (T) within the domain $53l_f \times 53l_f \times 53l_f$ for the $\phi = 1.0$; $R = 2.45l_f$ LBR case from Table 4.6. [where 1^{st}column - $2.10t_{sp}$, 2^{nd}column - $4.20t_{sp}$ and 3^{rd}column - $5.25t_{sp}$]

and about to be quenched by turbulence. In that respect, the following terms are defined to explain the reaction-diffusion balance within the flame (see Section 3.4.2.1).

$$\text{reaction term:} \quad \dot{w}_c \tag{4.18}$$

$$\text{molecular diffusion term:} \quad \nabla \cdot (\rho D \nabla c) \tag{4.19}$$

$$\text{flame normal diffusion rate term:} \quad \vec{N} \cdot \nabla \left(\rho D \vec{N} \cdot \nabla c \right) \tag{4.20}$$

$$\text{tangential diffusion rate term:} \quad -\rho D \nabla \cdot \vec{N} \, |\nabla c| \tag{4.21}$$

Figure 4.20 (1^{st} row) shows the temporal evolution of maximum non-dimensional temperature $T_{\max}$ and normalised fuel reaction rate magnitude $(\dot{\Omega}_F)_{\max}$ for the case STR_3 ($Ka = 6.30$, $\phi = 1.0$) with $R = 2.45l_f$ for different values of a_{sp}.

It can be seen from Figure 4.20 (1^{st} row) that both $T_{\max}$ and $(\dot{\Omega}_F)_{\max}$ rises with time due to energy deposition during $0 < t < t_{sp}$ and thermal runaway takes place when $T_{\max}$ reaches value close to $T_c \approx 1 - (1/\beta)$, at this point both $T_{\max}$ and $(\dot{\Omega}_F)_{\max}$ increase rapidly with time. In the case STR_3 with $a_{sp} = 18.2$, both $T_{\max}$ and $(\dot{\Omega}_F)_{\max}$ reach to their maximum after $3.0t_{sp}$ whereas the same case with $a_{sp} = 18.4$, both $T_{\max}$ and $(\dot{\Omega}_F)_{\max}$ reach to their maximum values at $1.80t_{sp}$ indicating a delay for the successful ignition in the case STR_3 with $a_{sp} = 18.2$.

It is worth nothing that here c is the reaction progress variable (already defined in Section 3.4.2), which rises monotonically from zero in the fully unburned reactants to

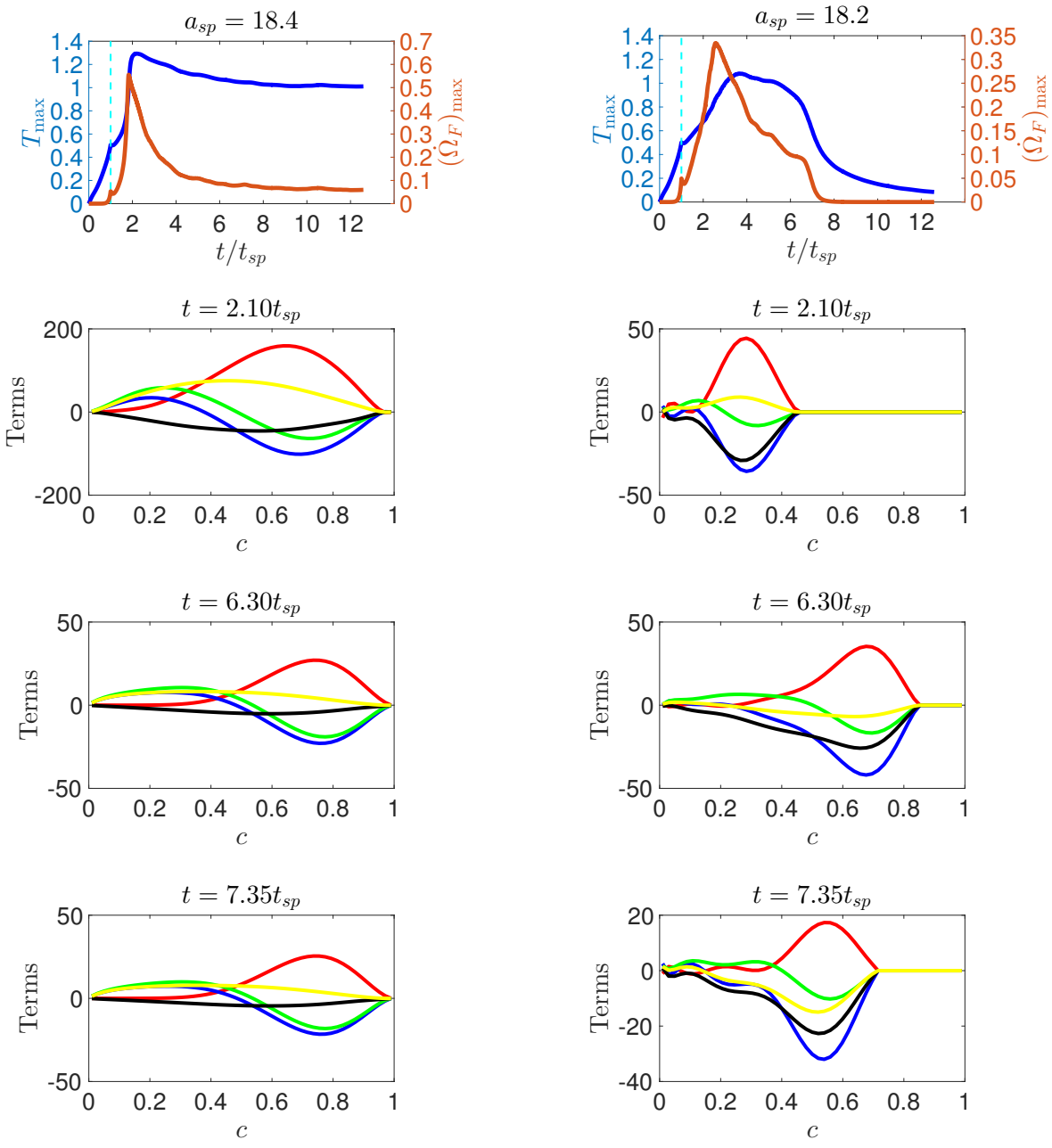

Figure 4.20: Temporal evolution of $T_{\max}$ and $(\dot{\Omega}_F)_{\max}$ along with the mean variation of different terms with reaction progress variable at different time instances for case STR_3 ($Ka = 6.30$, $\phi = 1.0$) with $R = 2.45l_f$, where cyan broken line shows $t = t_{sp}$. [$a_{sp} = 18.4$ (1^{st} column) and $a_{sp} = 18.2$ (2^{nd} column)]

unity in the fully burned products. Moreover, Figure 4.20 suggests that the term $\dot{w}_c$ [■] remains negligible in unburned side and increases sharply towards the burned side before decreasing to zero in the fully burned products. The magnitude of the term $\dot{w}_c$ [■] decreases with time, once the igniter is switched off, which is principally due to the decrease in fuel reaction rate magnitude with time. Additionally, it can be seen from Figure 4.20 that the positive value of the term $\dot{w}_c + \nabla\cdot(\rho D\nabla c)$ [■] suggesting a self-sustained propagation of the flame kernel. The term $\vec{N}\cdot\nabla\left(\rho D\vec{N}\cdot\nabla c\right)$ [■] remains positive in unburned side but becomes negative towards burned side. It can be seen from Figure 4.20 that the term $-\rho D\nabla\cdot\vec{N}\,|\nabla c|$ [■] remains negative for the flame brush. In Section 3.4.2.1, Equation 3.40 defines the flame normal vector $\vec{N}$. Now, N_j is the jth component of flame normal which can be defined in terms of flame curvature [49].

$$\kappa_m = \frac{1}{2}\nabla\cdot\vec{N} = \frac{\kappa_1+\kappa_2}{2} \sim \frac{1}{R_{fk}} \tag{4.22}$$

where κ_1 and κ_2 are the two principle curvature of the concerned flame surface, κ_m is the arithmetic mean of these two principle curvatures and R_{fk} is the radius of a flame kernel. As the flame kernel increases in size (i.e. R_{fk} increases), the probability of high values of κ_m decreases (see Equation 4.22). Furthermore according to Equation 4.22, positively curved location (i.e. $\kappa_m > 0$) are convex towards the reactant. The flame is initiated as a spherical kernel from the localised forced ignition (see Figure 4.18), which has a positive mean curvature. In this respect the term $-\rho D\nabla\cdot\vec{N}\,|\nabla c|$ [■] will attain negative values in the case of expanding flame kernel (i.e. self-sustained propagating flame kernel). The case STR_3 with $a_{sp} = 18.4$ provides self-sustained combustion following successful ignition (see Figures 4.16 and 4.20), where the hot gas kernel expands, which provides the probability of finding large magnitudes of positive curvature decreasing with time (see Figure 4.20).

The growth of the kernel leads to a decrease in the magnitude of the negative contribution of the term $-\rho D\nabla\cdot\vec{N}\,|\nabla c|$ [■], whereas the term $-\rho D\nabla\cdot\vec{N}\,|\nabla c|$ [■] is expected to assume large negative values in the kernels which are quenching. The above findings observations are in good agreement with the previous both DNS [49, 99, 100, 220] and experiment studies [5, 56, 108, 110, 216].

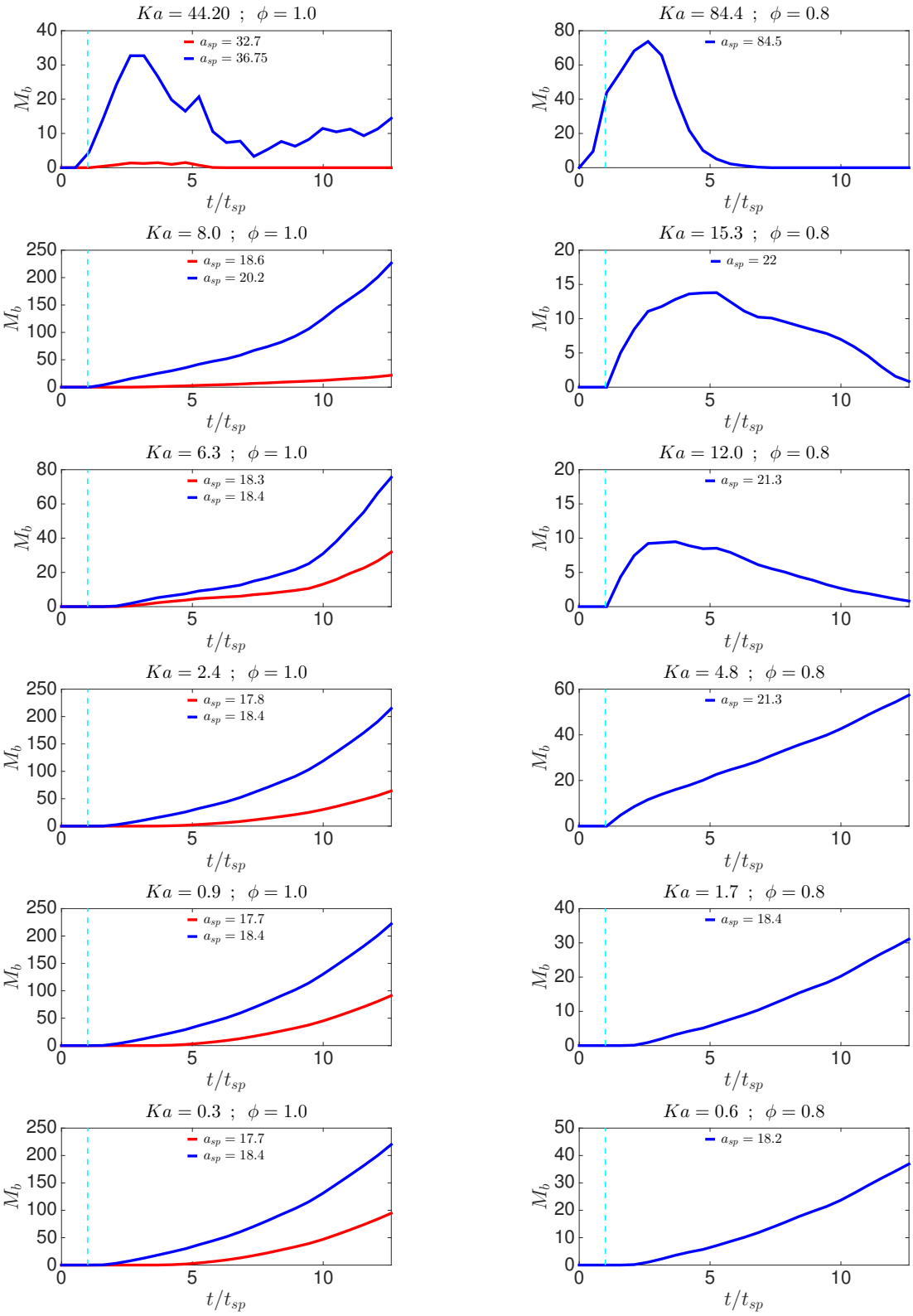

Figure 4.21: Temporal evolution of M_b for all $\phi = 1$ (1^{st}column) and $\phi = 0.8$ (2^{nd}column) cases listed in Table 4.6 with $R = 2.45l_f$, where cyan broken line shows $t = t_{sp}$.

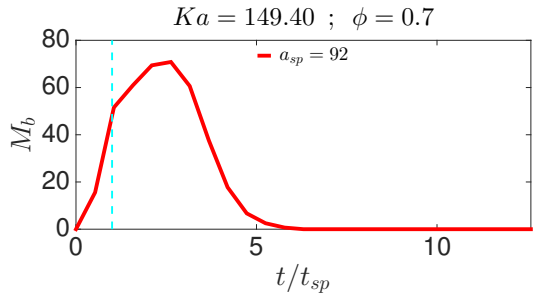

Figure 4.22: Temporal evolution of M_b for $\phi = 0.7$ case LBR listed in Table 4.6 with $R = 2.45l_f$, where cyan broken line shows $t = t_{sp}$.

4.3.5 Temporal Evolution of the Burned Gas Mass

Although the temporal evolution of $T_{\max}$ provides the signature of successful/failed ignition, it is necessary to assess the temporal evolution of the burned gas mass increasing with time in order to ascertain the possibility of obtaining self-sustained combustion following successful ignition. The temporal evolution of burned gas mass M_b for all cases listed in Table 4.6 is shown in Figures 4.21 and 4.22. By comparing Figures 4.16 and 4.17 with 4.21 and 4.22, it can be seen that M_b increases with time for the cases where $T_{\max}$ settles to adiabatic flame temperature for $t \gg t_{sp}$ indicating self-sustained combustion without any external energy addition following successful ignition. In the fuel-lean cases LTR_2 $(Ka = 15.3, \phi = 0.8)$ and LTR_3 $(Ka = 12.0, \phi = 0.8)$, M_b starts to decreases at $t \geq 5t_{sp}$, indicating the flame will eventually extinguishes long after $t \gg 12.60t_{sp}$. Figures 4.16, 4.17, 4.21 and 4.22 reveal that the higher values of a_{sp} is needed to ignite fuel-lean homogeneous mixtures in comparison to stoichiometric homogeneous mixtures and the same is true for sustaining combustion. The laminar burning velocity attains higher value in stoichiometric ($\phi = 1.0$) in comparison to fuel-lean (ϕ =0.8 and 0.7) mixtures as considered here (see Figure 3.1 in Chapter 3) and fuel-lean mixtures are less reactive than stoichiometric mixtures as discussed in previous Section 4.2.

Moreover, it can be demonstrated from Figures 4.21 and 4.22 that M_b assumes a non-zero value around $t = 5t_{sp}$ for the case LTR_1 $(Ka = 84.4, \phi = 0.8, a_{sp} = 84.5)$, and then eventually vanishes for $t \gg 5t_{sp}$ due to flame extinction (refer Figure 4.16). Additionally, Figure 4.21 reveals that M_b in the case STR_1 $(Ka = 44.20, \phi = 1.0, a_{sp} = 36.75)$ does not rises monotonically with time similar to other cases with $Ka < 20$ for $\phi = 1$. The heat transfer from hot gas kernel overcomes the chemical heat release at early stages of flame development, which results in reduction of M_b with time between

$2t_{sp} < t < 8t_{sp}$. The turbulent heat transfer rate decreases with time due to reduction in the magnitude of eddy thermal diffusivity $D_t \sim u'L_{11}$ as a results of decaying turbulence level (see the temporal evolution of u' for case STR_1 in Figure 4.16). Therefore the chemical heat release now starts to exceed the heat transfer from hot gas kernel at $t \geq 8t_{sp}$ for the case $\mathrm{STR}_1(Ka = 44.20, \phi = 1.0,\ a_{sp} = 36.75)$, which further gives rise to an increment in M_b with time for $8t_{sp} \leq t \leq 12.60t_{sp}$.

It is important to notice that the cases STR_1, STR_2, SCR and SWR have the same value of $\frac{L_{11}}{l_f} = 8.0$ but different values of u'. Figures 4.21 and 4.22 reveals that M_b obtains comparable values for $a_{sp} = 18.4$ in the cases SCR and SWR, whereas it is not even possible to ignite the mixture with same amount of a_{sp} in the cases STR_1 and STR_2. The probability of achieving high values of c decreases with increasing value of $\frac{u'}{S_{b(\phi)}}$ due to enhanced heat transfer rate from hot gas kernel, as $\frac{u'}{S_{b(\phi)}}$ can be expressed in the following manner (see Section 2.5) :

$$\frac{u'}{S_{b(\phi)}} \sim Ka^{1/2} Re_t^{1/4} \tag{4.23}$$

Even though case SCR $(Ka = 0.90, \phi = 1.0)$ corresponds to greater value of $\frac{u'}{S_{b(\phi=1)}}$ in comparison to case SWR $(Ka = 0.30, \phi = 1.0)$, Figure 4.16 indicates that the flame kernel in these both cases are subjected to similar temporal evolution of u'. Therefore the evolution of M_b in Figure 4.21 for the cases SCR and SWR with $a_{sp} = 18.4$ shows similar trend values. Additionally Figure 4.21 reveals that an increase in a_{sp} leads to an increase in burned gas mass irrespective of the values of Ka and $\frac{u'}{S_{b(\phi=1)}}$. For example M_b attains higher value for the case $\mathrm{STR}_2(Ka = 8.0, \phi = 1.0, a_{sp} = 20.2)$ in comparison to the case $\mathrm{STR}_3(Ka = 6.3, \phi = 1.0, a_{sp} = 18.4)$, even though the values of $\frac{u'}{S_{b(\phi=1)}}$ is higher in the case $\mathrm{STR}_2(\frac{u'}{S_{b(\phi=1)}} = 8.0)$ than the case $\mathrm{STR}_3(\frac{u'}{S_{b(\phi=1)}} = 6.0)$.

The findings from Figures 4.16, 4.17, 4.21 and 4.22 indicate that the minimum value of a_{sp} for successful ignition and subsequent self-sustained combustion increases significantly with increasing value of Ka. Additionally the minimum values of a_{sp} to obtain self-sustained combustion following successful ignition for the cases STR_1 and STR_2 are found to be significantly greater than the corresponding minimum value for just igniting the mixture. However, the minimum energy content for successful ignition in cases STR_2, STR_4, SCR and SWR is sufficient to lead to self-sustained combustion. Furthermore, the a_{sp} values in Figures 4.16, 4.17, 4.21 and 4.22 indicate that the minimum ignition energy requirement increases sharply once Ka reaches a value of the order of 10, which is in agreement with previous experimental findings

[96, 97, 184]. The findings obtained in this DNS study and the existing experimental findings are compared and analysed further in Section 4.3.7.

4.3.6 Effects of Width of Ignition Energy Deposition on MIE

As discussed and seen in Section 4.2, a reduction in energy deposition width (i.e. R) may lead to favorable condition for obtaining self-sustained combustion following successful ignition of turbulent homogeneous mixtures. And the energy deposition width can be controlled in the case of laser ignition [26, 31, 63, 65, 66, 141, 198]. Further DNS analysis reveals that the reduction choice of R may not only provide favorable conditions for self-sustained combustion but also helps to reduce MIE for successful ignition and self-sustained combustion. These findings can be demonstrated in the Figure 4.23, where temporal evolution of $T_{\max}$ for all the cases listed in Table 4.6 are shown for $R = 1.55l_f$.

Although the choice of R helps to reduce the value of a_{sp}, for $Ka = 84.4$ and $Ka = 149.4$ in fuel-lean case, the $T_{\max}$ profile fails to maintain adiabatic flame temperature after $t \sim 6.0t_{sp}$ and eventually extinguishes. This fragmented high temperature region is indicative of disturbance of the reaction zone by turbulence under high values of Karlovitz number. It can be seen from Figure 4.23 that new choice of reduced $R = 1.55l_f$ helps to scale down the MIE requirement for ignition and self-sustained combustion by nearly 75% (compare Figures 4.16 and 4.17 with Figure 4.23)

The heat release from the source term can be scaled as:

$$q''' \sim \rho C_P \left(T_{ad} - T_0\right) \frac{\alpha_{T0} + u' L_{11}}{R} \tag{4.24}$$

According to Equation 4.24, reduction in R leads to higher thermal difference which further reduces the demand of q'''. Additionally one can extend the Equation 4.24 for the ignition energy:

$$\dot{Q} t_{sp} \sim t_{sp} \int_V q''' \, dV \tag{4.25}$$

which further leads to,

$$\dot{Q} t_{sp} \sim \rho C_P \left(T_{ad} - T_0\right) \left[\alpha_{T0} + u' L_{11}\right] t_{sp} R^2 \tag{4.26}$$

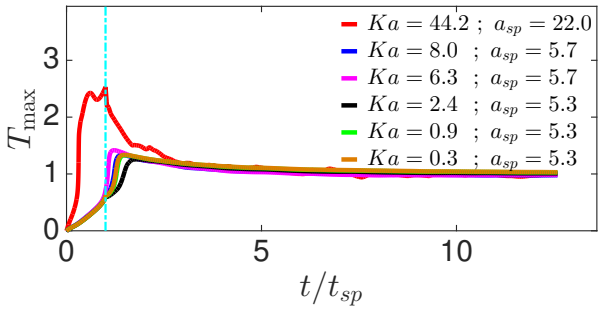

(a) $\phi = 1.0$

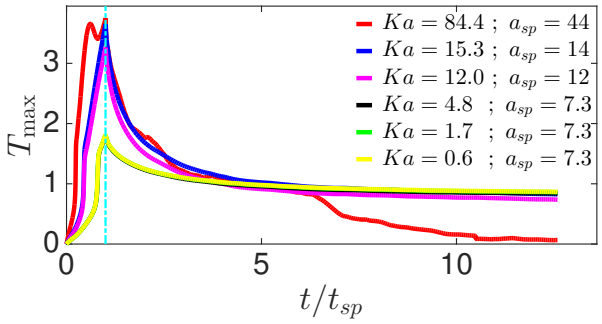

(b) $\phi = 0.8$

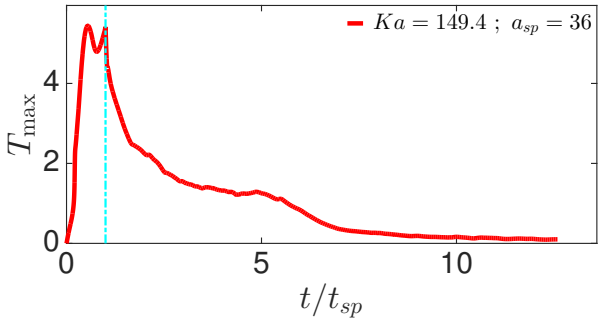

(c) $\phi = 0.7$

Figure 4.23: Temporal evolution of $T_{\max}$ for $\phi = 1$ (a) , $\phi = 0.8$ (b) and $\phi = 0.7$ (c) cases listed in Table 4.6 with $R = 1.55 l_f$, where cyan broken line shows $t = t_{sp}$.

From Equations 4.24 and 4.26, it can be seen that reduced choice of $R = 1.55l_f$ (compared to $R = 2.45l_f$) reduces the demand of ignition energy in order to obtain self-sustained combustion following successful ignition. The findings from Figure 4.23 concludes that it is possible to obtain self-sustained combustion and successful ignition even in fuel-lean environment by judicious choice of R and a_{sp}. These parameters can be altered independently of each other in case of laser ignition. Hence, laser ignition can be more advantageous than the conventional spark ignition for the purpose of reducing MIE requirement and pollutant emission [63] (agreement with findings from Section 4.2).

Recently Huang *et al.* [96, 97] reported that MIE can be scale as function of $\frac{u'}{S_{b(\phi)}}$ and l_f (see Figure 4.24):

$$\text{MIE} \sim \begin{cases} \left(\frac{u'}{S_{b(\phi)}}\right)^{0.7} & \text{for} \quad Ka < 10 \\ \left(\frac{u'}{S_{b(\phi)}}\right)^{7.0} & \text{for} \quad Ka > 10 \\ l_f^3 \end{cases} \tag{4.27}$$

The study from Huang *et al.* [96] was reported for $\phi = 0.6$ methane-air mixtures, moreover Huang *et al.* [96, 97] argued that MIE depends on the flame thickness (i.e. l_f^3). The findings of present analysis show that the MIE is not only dependent on $\frac{u'}{S_{b(\phi)}}$ and l_f but width of ignition energy deposition R also has very important influences on MIE.

4.3.7 Comparison with Experimental Results

According to Ballal and Lefebvre [16], the MIE can be predicted based on the critical igniter diameter to its adiabatic flame temperature. Based on the findings by Ballal and Lefebvre [16], the expression for MIE is given by Equation 4.11 which was discussed in Section 4.2.7. Equation 4.11 suggests that an increase in u' leads to increase in MIE, where on the other side decrease in $S_{b(\phi)}$ with decreasing ϕ acts to increase in MIE for fuel-lean mixtures. The findings in Section 4.2 and the experimental data by Ballal and Lefebvre [16] suggests that it is possible to ignite and achieve self-sustained combustion following successful ignition for fuel-lean mixtures.

The case $\text{LTR}_3(Ka = 12.0, \phi = 0.8)$ requires $a_{sp} = 21.3$ in order to obtain self-sustain combustion following successful ignition, whereas for the case $\text{LTR}_1(Ka = 84.4, \phi = 0.8)$ the value $a_{sp} = 84.5$ can successfully ignite the fuel-lean mixture but is

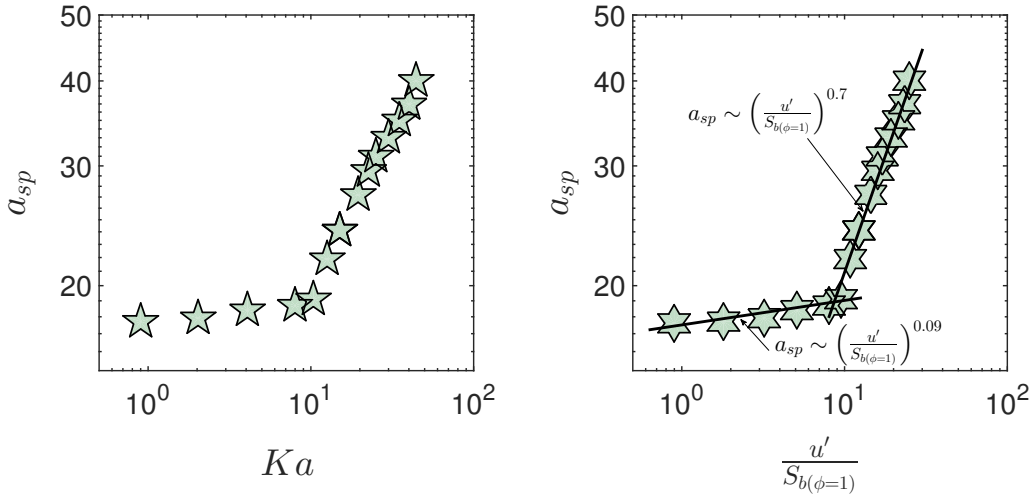

(a) a_{sp} as a function of Ka (left) and as a function of $\frac{u'}{S_{b(\phi=1)}}$ (right) for $\frac{L_{11}}{l_f} = 8.0$ and $\phi = 1.0$ in the current DNS study.

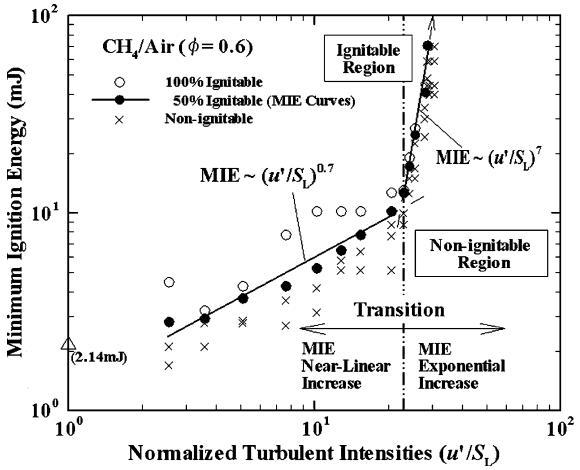

(b) Turbulent minimum ignition energy as a function of normalized turbulent intensities for methane–air mixtures at $\phi = 0.6$, showing a transition of MIE. (extracted from Huang *et al.* [96])

Figure 4.24: Qualitative comparison with experimental study.

still not sufficient to achieve self-sustained combustion (see Figure 4.16). The findings obtained from the discussion of Figures 4.16-4.22 indicate that the demand of MIE increases with decreasing ϕ, which is in good agreement with previous experimental findings [13, 16, 116].

Recently, Shy and his co-workers [96, 154, 184, 185] reported turbulent ignition transition based MIE measurements for premixed turbulent methane-air mixture combustion with equivalence ratio ranging $0.6 < \phi < 1.3$, and each covering a wide range of Karlovitz number (Ka). The reduction of MIE with reducing characteristic width of the energy deposition (Section 4.3.6) is in agreement with Shy *et al.* [184] (where Shy *et al.* [184] used electrode thickness as an energy deposition width). Shy *et al.* [184] and Huang *et al.* [96] shown the MIE as a function of Ka and u' to demonstrate their effects. Figure 4.24 shows a_{sp} as a function of Ka and as a function of $\frac{u'}{S_{b(\phi=1)}}$ for $\frac{L_{11}}{l_f} = 8.0$ and $\phi = 1.0$ in the current DNS study. It is worth noting that the values of a_{sp} in Figure 4.24 confirms both successful ignition as well as sustaining combustion.

Moreover Figure 4.24 (2^{nd} row) shows MIE as a function of $\frac{u'}{S_L}$ for lean methane-air mixtures ($\phi = 0.6$) from an experimental study by Huang *et al.* [96]. It can be seen from Figure 4.24 that a transition on MIE (a_{sp} in current study) of $\phi = 0.6$ ($\phi = 1.0$ in current study) premixed methane-air combustion exists due to different modes of combustion. Below the transition, values of MIE (a_{sp}) increase gradually for which MIE$\sim \left(\frac{u'}{S_L}\right)^{0.7}$ ($a_{sp} \sim \left(\frac{u'}{S_{b(\phi=1)}}\right)^{0.09}$ in current study). The transition occurs at $Ka > 8$ in the experiments by Huang *et al.* [96] ($Ka > 10$ in current study), when relatively large values of u' are achieved. Across the transition, the slope of MIE (a_{sp}) as a function of $\frac{u'}{S_L}\left(\frac{u'}{S_{b(\phi=1)}}\right)$ increases abruptly by a factor 10 (8 in current study), corresponding to different regimes varying from corrugated flamelets or thin reaction zones to possibly broken reaction regimes. It is important to note here that experimental study by Huang *et al.* [96] was carried out for lean methane-air mixtures ($\phi = 0.6$), whereas present DNS study corresponds to stoichiometric methane-air mixtures ($\phi = 1.0$) and it is known that the MIE (a_{sp}) demand increases with decreasing ϕ [13, 16, 116, 150].

The present DNS study results are in satisfying agreement with experimental findings of Huang *et al.* [96] and Shy *et al.* [184] (see Figures 6 and 7 in reference from Shy *et al.* [184] and Figure 4.24). Additionally the flame kernel formation in different regimes are also in qualitative agreement with experimental findings of Shy *et al.* [184].

4.3.8 Summary

The effects of different Karlovitz number (Ka), rms value of turbulent velocity u' and energy deposition characteristics on MIE requirements for successful ignition and self-sustained combustion has been investigated using DNS in Section 4.3. The discussion here suggests that MIE required for obtaining self-sustained combustion increases with increasing Ka and decreasing ϕ. Additionally, increase in u' decreases extent of burning and may lead to misfire for larger values of u'. The detrimental effects of high values of u' are more critical for high values of Ka. It is possible to reduce MIE requirement for obtaining self-sustained combustion following successful ignition by judicious choices of the characteristic width of energy deposition R. These findings obtained from present DNS study are in qualitative agreement with the findings in Section 4.2 for the effects of ignition energy and the width of ignition energy distribution. Additionally present findings suggests that the requirement of MIE increases abruptly when Ka reaches transition value of $Ka \sim 10$ for given $\frac{L_{11}}{l_f} = 8.0$ and stoichiometric ($\phi = 1.0$) turbulent homogeneous mixtures, and this findings are in qualitative agreement with previous experimental results (see Figure 4.24) [96, 154, 184, 185].

4.4 Main Findings

Localised forced ignition and early stages of flame propagation of turbulent homogeneous mixtures have been investigated based on three-dimensional DNS simulations to study the effects of energy deposition characteristics and the effects of combustion regimes. The main findings can be summarised as follows:

- The MIE requirement can be reduced by judicious choice of R and b_{sp}(which can be altered independently of each other in case of laser ignition).
- It is possible to ignite (i.e. successful ignition) fuel-lean mixtures with very high values of Ka and u', where MIE is dependent on u', Zel'dovich flame thickness l_f and also characteristic width of ignition energy deposition profile [characterised by R].
- The MIE requirement increases abruptly once Ka reaches a value of the order of ~ 10 for a given ${}^{L_{11}}/_{l_f} = 8.0$ and stoichiometric turbulent homogeneous mixtures. These findings are in qualitative agreement with experimental results (see Sections 4.2.7 and 4.3.7).

- The parameters of energy deposition characteristics (i.e. ignition energy [characterised by a_{sp}], characteristic width of ignition energy deposition profile [characterised by R] and duration of ignition energy deposition [characterised by b_{sp}]) play important roles in obtaining MIE and subsequent early stages of flame development.

- It has been found that higher amount of ignition energy is necessary to obtain self-sustained combustion in fuel-lean cases than in stoichiometric cases. Moreover, the results showed that increase in u' decreases the extent of burning and may lead to misfire for larger values of u'.

- It has been demonstrated that increases in Ka and u' have detrimental effects on mass burning process after successful ignition. The results showed that increase in a_{sp} leads to increase in extent of burning irrespective of the values of Ka and u'.

In this Chapter 4, the localised forced ignition of turbulent homogeneous mixtures have been investigated to study the effects of energy deposition characteristics and the effects of combustion regimes. The DNS work is now extended to study localised forced ignition of stratified fuel-air mixtures using 3D DNS in the next Chapter 5 and simulations results are discussed.

Chapter 5

Localised Forced Ignition of Stratified Fuel-Air Mixtures

This Chapter 5 presents the numerical investigation of localised forced ignition of stratified fuel-air mixtures. The chapter starts with an introduction about the existing literature and the purpose of the study. The effects of mixture inhomogeneity length scale and equivalence ratio fluctuation are presented and discussed in Section 5.2. In Section 5.3, the effects of nature of initial mixture distribution are presented. The effects of turbulent integral length scale are analysed in Section 5.4. Finally the effects of global mean equivalence ratio are studied in Section 5.5. The main findings are summarised at the end of this Chapter.

5.1 Introduction

For the design of efficient combustion engines (e.g. GDI, high-altitude relight in gas turbines etc.), localised forced ignition (e.g. spark or laser ignition) of inhomogeneous mixtures plays a pivotal role. Premixed combustion offers an option of controlling flame temperature and reducing pollutant emission such as nitrogen oxides (NO_X) but, in practice, perfect mixing is often difficult to achieve and thus combustion in many engineering applications takes place in turbulent stratified mixtures. A large number of both numerical [88, 89, 104, 128, 149, 155, 193, 224] and experimental [10, 19, 59, 82, 91, 106, 142, 170, 176, 194, 195, 223] analyses focuses on flame propagation in stratified mixtures, where the findings show that the flame propagation statistics are strongly influenced by the local equivalence ratio ϕ gradient.

Inhomogeneous mixtures produced by evaporating droplets in turbulent air streams

have been experimentally studied by Ballal and Lefebve [13, 14, 16, 17] to analyse the effects of critical spark energy, optimum spark duration and spark radius for successful ignition. Localised forced ignition in turbulent non-premixed jet flames has been studied by many previous DNS analyses [3–5, 9, 28]. A number of 3D simplified chemistry DNS studies [48, 50, 51] analysed the effects of turbulence on localised forced ignition of inhomogeneous mixtures, where influences of fuel Lewis number, mixture fraction value and its gradient at igniter location on the success of ignition and self-sustained combustion, have been investigated in detail. Richardson and Mastorakos [172] investigated the effects of laminar fluid-dynamic straining on localised forced ignition of non-premixed methane-air mixtures using detailed chemistry simulations, where results are qualitatively similar to the effects of turbulent straining indicated by Chakraborty *et al.* [51]. All the recent numerical studies [48, 50, 51, 94, 99, 134, 168, 169, 172, 193] concentrated on localised forced ignition of inhomogeneous mixtures for a mixture distribution that is characterised by a mean variation of equivalence ratio ϕ.

In a recent DNS study, Pera *et al.* [155] analysed the effects of heterogeneities induced by residual burned gas dilution and temperature fluctuation on early stages of flame propagation under SI engine conditions using mainly 2D semi-detailed chemistry of globally stoichiometric iso-octane-air mixtures. DNS investigation by Pera *et al.* [155] concluded that the mixture inhomogeneity can potentially increase the extent of flame wrinkling and may significantly affect the cycle-to-cycle variation of heat release. The findings from Pera *et al.* [155] are in consistent agreement with a preliminary analysis by Swaminathan *et al.* [193]. Experimental results suggest that the local variation of equivalence ratio has significant influences on the statistical behavior of Surface Density Function (SDF) and flame curvature for moderate values of turbulent Reynolds number [10] , but the same affects seems to varnish when turbulence intensity increases [194, 195]. Moreover, DNS analysis by Chakraborty *et al.* [48, 51] and Chakraborty and Mastorakos [50] concluded that an increase in turbulence intensity for a given value of integral length scale of turbulence has a detrimental effect on the success of localised forced ignition of single-phase gaseous inhomogeneous mixtures. In addition to that, experimental analyses by Ahmed and Mastorakos [3–5] reported that an increase in mean velocity in jets also leads to a deterioration of ignition performance, quantified by a reduction in ignition probability. The adverse effects of turbulent velocity fluctuation have also been found for localised forced ignition of droplet-laden mixtures [210–212].

Despite these numerical studies, the localised forced ignition of stratified mixtures for a given global mean value of equivalence ratio $\langle\phi\rangle$ but with a non-zero RMS value of equivalence ratio ϕ' has received limited attention [155, 193] in spite of its practical relevance in DI engines and LPP combustors. Although previous analyses [155, 193] revealed a number of important influences of the coupled effects of mixture and thermal inhomogeneities, a systematic analysis of the effects of ϕ' on localised ignition and the subsequent burning rate are yet to be addressed in detail. Moreover the effects of the nature of initial equivalence ratio distribution for a given set of global mean (i.e. $\langle\phi\rangle$), RMS values of equivalence ratio (i.e. ϕ') and the associated length scale of mixture inhomogeneities (i.e. l_ϕ which is taken as the Taylor micro-scale of the equivalence ratio variation (see Section 3.7)), on localised forced ignition of stratified mixtures are yet to be analysed in detail using DNS. This chapter 5 aims to address the aforementioned gap in existing literature. Here the Section 5.2 investigate the effects of mixture inhomogeneity length scale and equivalence ratio fluctuation on localised forced ignition of globally stoichiometric stratified fuel-air mixtures.

Experiment analysis by Ballal and Lefebvre group [13, 14, 16, 116] demonstrated that obtaining successful forced ignition of inhomogeneous mixtures arising from evaporation of droplets in an air stream can be dependent on critical spark energy and optimum spark duration. Initial mixture distribution is responsible for the mixture inhomogeneity, thus ignition performance and subsequent combustion in such environment will be affected. Additionally Swaminathan and Grout [193] have shown that the flame propagation statistics are strongly affected by local gradient of equivalence ratio. Recently Smirnov *et al.* [188] investigated combustion and detonation initiation in heterogeneous polydispersed mixtures using experiments with n-decane ($C_{10}H_{22}$) mixtures, where the effects of non uniformity of droplet size and spatial distribution non-uniformity on mixture ignition and flame acceleration were investigated for mild initiation of detonation by spark ignition. The experimental results from Smirnov *et al.* [188] suggests that convective combustion in dispersed mixtures could lead either to a galloping mode or to the onset of detonation. Additionally Smirnov *et al.* [188] demonstrated that the galloping combustion modes could be attained in the case of large droplets and small ignition energy. Most existing analyses [13, 14, 16, 116, 149, 188, 193] suggests that localised forced ignition and subsequent combustion depends on the initial mixture distribution. However, the effects of the nature of initial equivalence ratio distribution, for a given set of global mean and RMS values of equivalence ratio (i.e. $\langle\phi\rangle$and ϕ') and the associated length scale of mixture

inhomogeneities, on localised forced ignition of globally stoichiometric stratified mixtures are yet to be analysed in detail using 3D DNS. Here, Section 5.3 fulfills the deficit in existing literature.

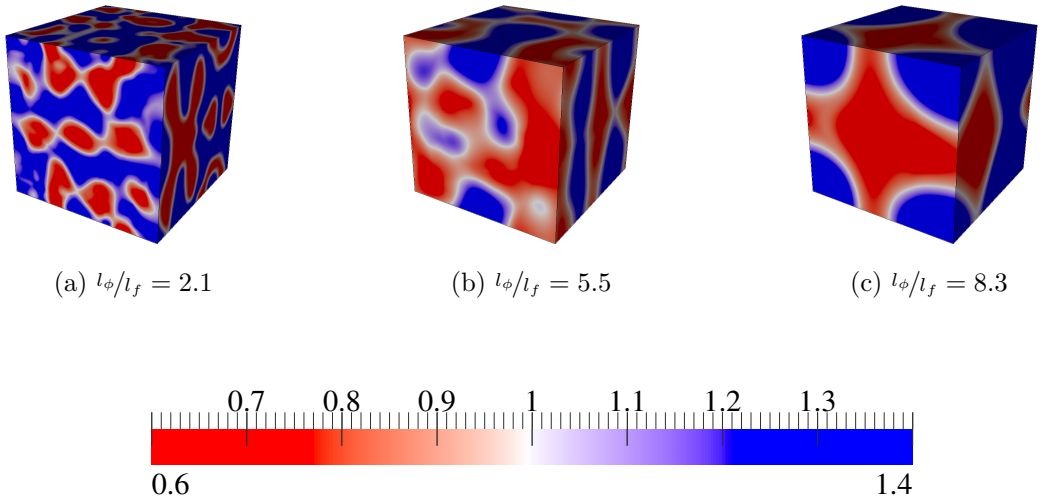

(a) $l_\phi/l_f = 2.1$ (b) $l_\phi/l_f = 5.5$ (c) $l_\phi/l_f = 8.3$

Figure 5.1: Initial computational domain showing different values of length scale of mixture inhomogeneities for $\phi' = 0.4$ in globally stoichiometric stratified mixtures for a given distribution of ϕ.

The investigation by Pera *et. al.* [156] concluded that similar to the u' effect, the integral length scale can modify the flame propagation and also affects the flame kernel shape. Additionally an experimental study from Shy *et. al.* [183] suggested that turbulent burning velocity decreases, similarly to laminar burning velocity with increasing elevated pressure in minus exponential manner when integral length scale of turbulence (hence turbulent Reynolds number) kept constant. Moreover, turbulent burning velocity increases noticeably with increasing turbulent Reynolds number at any constant elevated pressure ranging from 1-10 atm [183].

Recently DNS study by Schmitt *et. al.* [180] investigated that the decrease of kinematic viscosity resulting from the increasing pressure results in smaller turbulent length scales and higher dissipation rates. Moreover Schmitt *et. al.* [180] suggested that temperature fluctuations away from the walls decrease slightly during the first half but increase strongly during the second half of the compression stroke towards the Top Dead Center (TDC) due to heat transfer to and from the walls and turbulent

$\langle\phi\rangle = 1.0$ [S]												
	$\phi' = 0.2$ [A]			$\phi' = 0.4$ [B]			$\phi' = 0.6$ [C]					
$\frac{L_{11}}{l_f} = 3.36$	$\frac{l_\phi}{l_f} = 2.1$ [D]	$\frac{l_\phi}{l_f} = 5.5$ [E]	$\frac{l_\phi}{l_f} = 8.3$ [F]	$\frac{l_\phi}{l_f} = 2.1$ [D]	$\frac{l_\phi}{l_f} = 5.5$ [E]	$\frac{l_\phi}{l_f} = 8.3$ [F]	$\frac{l_\phi}{l_f} = 2.1$ [D]	$\frac{l_\phi}{l_f} = 5.5$ [E]	$\frac{l_\phi}{l_f} = 8.3$ [F]			
$\frac{u'}{S_{b(\phi=1)}} = 0.0$ [T0]	ST0AD	ST0AE	ST0AF	ST0BD	ST0BE	ST0BF	ST0CD	ST0CE	ST0CF			
$\frac{u'}{S_{b(\phi=1)}} = 4.0$ [T4]	ST4AD	ST4AE	ST4AF	ST4BD	ST4BE	ST4BF	ST4CD	ST4CE	ST4CF			
$\frac{u'}{S_{b(\phi=1)}} = 6.0$ [T6]	ST6AD	ST6AE	ST6AF	ST6BD	ST6BE	ST6BF	ST6CD	ST6CE	ST6CF			
Homogeneous cases ST0, ST4, ST6												

Table 5.1: List of parameters to analyse effects of $\frac{l_\phi}{l_f}$, ϕ' and $\frac{u'}{S_{b(\phi=1)}}$ in globally stoichiometric (i.e. $\langle\phi\rangle = 1.0$) stratified mixtures.

transport. The effects of turbulent integral length scale also plays a role in autoignition combustion. Recently Zhang *et al* [221] conducted DNS study on the autoignition of dimethyle ether with temperature inhomogeneities with detailed chemistry at high pressure and a constant volume relevant to homogeneous charge compression ignition (HCCI) engines. The investigation by Zhang *et al* [221] concluded that the reduction of pressure-rise rate is strongly dependent on mean initial temperature and large-amplitude pressure oscillations are possible for larger length scale. Although previous analyses [155, 193] revealed a number of important influences of integral length scale, a systematic analysis of the effects of longitudinal integral length scale L_{11} on localised forced ignition of globally stoichiometric stratified mixtures and the subsequent burning rate are yet to be addressed in detail. The analysis provided in Section 5.4 address the aforementioned gap by studying the influences of normalised turbulent integral length scale (i.e. $\frac{L_{11}}{l_f}$) on localised forced ignition of globally stoichiometric stratified mixtures.

Combustion of lean fuel-air mixtures provides an effective solution for both high restriction of engine emissions and huge demands for engine efficiency [137]. Burning lean fuel-air stratified mixtures in SI engine provides control of temperature during ignition and has been identified as one of the methods of limiting NO_X emissions and increasing engine thermal efficiency. Nitric oxide creation rate increases as the temperature in the combustion chamber rises, especially above the 1600 K [102, 112]. Recent experimental study by In *et. al.* [101] shows that stratified mixture is an effective solution for extending the fuel-air ratio of the lean limit. Additionally Park *et. al.* [148] investigated the combustion and emission characteristics of a lean-burn gasoline DI engines, and concluded that the combustion characteristics of a stratified mixture in a spray-guided-type DI system were similar to those in DI diesel engines. Moreover a thermodynamic model by Ali *et. al.* [7] considered flame propagation to predict SI engine characteristics for hydrogen-methane blends, and showed that partially charge stratification can improve engine performance by increasing mean effective pressure and decreasing specific fuel consumption.

With numerous advantages of fuel-lean stratified mixtures combustion, Masri [133] suggested that in partially premixed flames, the interaction between rich and lean mixtures leads to significant improvement in the flame's resistance to extinction by straining. Additionally in laminar stratified flames, the flux of excess heat and radicals into the lean fluid results in higher flame speeds, broader reaction zones, and extended flammability limits compared to homogeneous counterparts [133]. Despite

the advantageous applications of fuel-lean stratified mixtures, the effects of global mean of equivalence ratio $\langle\phi\rangle$ on localised forced ignition and subsequent burning process are yet to analysed in detailed using DNS. The Section 5.5 concentrates on the understanding of the influences of global mean of equivalence ratio $\langle\phi\rangle$ on localised forced ignition in stratified mixtures and subsequent burning characteristics leading from successful ignition.

5.2 Effects of Mixture Inhomogeneity Length Scale and Equivalence Ratio Fluctuation

This Section starts with brief discussion on the numerical formulation adopted for this study and then the results for effects of mixture inhomogeneity length scale and equivalence ratio fluctuation on localised forced ignition of globally stoichiometric stratified fuel-air mixtures are presented and discussed. Global behaviours of maximum values of temperature and fuel reaction rate are shown first to analyse the influences of mixture inhomogeneity length scale and equivalence ratio fluctuation on the possibility of self-sustained combustion following successful ignition. Spatial distribution of different quantities is then presented. Mode of combustion and mixing statistics are evaluated. The reaction zone structure of the flames initiated by localised ignition is examined to understand the effects of stratification on the extent of burning following successful ignition. The effects of mixture inhomogeneity length scale, equivalence ratio fluctuation and turbulence fluctuation on extent of burning are then analysed. Finally, the section investigates the effects of initial ϕ distribution on the extent of burning and ends with summary.

5.2.1 Numerical Formulation

In this current study, 3D compressible DNSs have been carried out for a range of different conditions in terms of the RMS values of velocity (i.e. u') and equivalence ratio (i.e. ϕ') and the length scale of the mixture inhomogeneity. Here, the length scale of mixture inhomogeneity is taken as the Taylor micro-scale of the equivalence ratio variation l_ϕ and is defined as [76]:

$$l_\phi = \left(\frac{6\left\langle \left[\phi - \langle\phi\rangle\right]^2 \right\rangle}{\left\langle \nabla\left[\phi - \langle\phi\rangle\right] \cdot \nabla\left[\phi - \langle\phi\rangle\right] \right\rangle} \right)^{1/2} \tag{5.1}$$

As previously described in Section 3.7, the equivalence ratio ϕ variation is initialised using a random distribution of ϕ following a Bi-modal distribution for specified values of the mean global equivalence ratio $\langle\phi\rangle$ [81, 91, 128, 130, 193]. In practice, when fuel is introduced in the liquid phase, the probability density function (PDF) of the equivalence ratio distribution is likely to be Bi-modal as a result of localised liquid fuel evaporation during the early stage of mixing. The fuel-air mixture is likely to be fuel rich close to the evaporation sites and the mixture is expected to be fuel-lean far away from the droplets. In the publications [81, 91, 128, 130, 193], it has been shown that the equivalence ratio variation approached a Gaussian distribution as the mixing is taking place and similar behaviour is observed here too. Here in this Section 5.2, globally stoichiometric (i.e. $\langle\phi\rangle = 1.0$) mixtures have been considered for $\phi' =$0.2, 0.4, 0.6 and ${}^{l_\phi}/_{l_f} = 2.1$, 5.5, 8.3, where $l_f = \frac{D_0}{S_{b(\phi=1)}}$ is the Zel'dovich flame thickness for the stoichiometric mixture, D_0 is the mass diffusivity of unburned reactants and $S_{b(\phi=1)}$ is the unstrained laminar burning velocity of the stoichiometric mixture. The initial mixture distribution for $\langle\phi\rangle = 1.0$ and $\phi' = 0.4$ with different values of ${}^{l_\phi}/_{l_f}$ are shown in Figure 5.1, which indicated that the clouds of mixture inhomogeneities increase in size with increasing ${}^{l_\phi}/_{l_f}$.

The numerical formulation remains similar to as described in Section 4.2.1 except for a few modifications. The simulation domain is taken to be a cubic with size $33l_f \times 33l_f \times 33l_f$ which in Cartesian grid size of $200 \times 200 \times 200$ with uniform grid spacing Δx. The ignition parameters are taken as: $a_{sp} = 3.60$, $b_{sp} = 0.2$ and $R = 1.10l_f$ (see Section 3.3). Simulations have been carried out for $t_{sim} \sim 8.40t_{sp} \sim 1.68\,t_f$ in all cases, and this simulation time has been found to be sufficient to determine whether or not a particular case will give rise to self-sustained combustion. Energy deposition time is taken to be proportional to the chemical time scale as: ${}^{t}/_{t_{sp}} = {}^{5t}/_{t_f}$. It is important to note here that the chosen ignition parameters guarantee the successful ignition for all cases considered here. Combustion in all the cases considered here belongs to thin reaction zones regime combustion according to the regime diagram by Peters [158].

The extensive parametric analysis of globally stoichiometric stratified mixtures (i.e. $\langle\phi\rangle = 1.0$) is summarised in Table 5.1. Additionally, simulations have been carried out for at least four different realisations of equivalence ratio distribution for each of the stratified mixture cases in order to mimic the cycle-to-cycle variation of conventional DI stratified mixture engines. Table 5.1 shows parametric variation across 27 different parameters, and thus in total 111 simulations (27×4 stratified mixture cases + 3

homogeneous mixtures) have been conducted here. The case names are chosen in such manner so that S stands for globally stoichiometric stratified mixtures; T0, T4 and T6 indicate increasing turbulent level; A, B, and C indicate increasing values of ϕ'; and D, E, and F denote increasing values of ${}^{l_\phi}/_{l_f}$ (e.g. ST4BD corresponds to a case for globally stoichiometric stratified mixtures with initial values of $\frac{u'}{S_{b(\phi=1)}} = 4.0$; $\phi' = 0.4$; ${}^{l_\phi}/_{l_f} = 2.1$).

5.2.2 Global Behaviours of Maximum Values of Temperature and Fuel Reaction Rate

The temporal evolution of the maximum values of non-dimensional temperature ($T_{\max}$) are shown in Figure 5.2 and the normalised fuel reaction rate magnitude ($(\dot{\Omega}_F)_{\max}$) are shown in Figure 5.3, where:

$$T_{\max} = \frac{\left(\hat{T}_{\max} - T_0\right)}{\left(T_{ad(\phi-1)} - T_0\right)} \tag{5.2}$$

$$\left(\dot{\Omega}_F\right)_{\max} = |\dot{w}_F|_{\max} \times \frac{l_f}{\rho_0 S_{b(\phi=1)}} \tag{5.3}$$

The $T_{\max}$ rises with time during energy deposition $0 \leq t \leq t_{sp}$ and thermal runaway appears when $T_{\max}$ attains a value close to $T_c \approx 1 - \left[\frac{1}{\beta_{(\phi=1)}}\right]$, giving rapid increases in both $T_{\max}$ and $\left(\dot{\Omega}_F\right)_{\max}$ with time until $t = t_{sp}$(see Figures 5.2 and 5.3). This ignition behavior of rapid increase in $T_{\max}$ and $\left(\dot{\Omega}_F\right)_{\max}$ is common in both homogeneous (Chapter 4) and stratified mixtures. At this point, the high thermal gradient between hot gas kernel and the surrounding unburned reactant gives rise to high rate of heat transfer from the ignition kernel. And therefore $T_{\max}$ and $\left(\dot{\Omega}_F\right)_{\max}$ decrease with time once igniter is switched off. As seen and discussed in Chapter 4, $T_{\max}$ eventually settles to the non-dimensional adiabatic flame temperature of stoichiometric mixture (i.e. $T \approx 1.0$) and $\left(\dot{\Omega}_F\right)_{\max}$ settles to much smaller non-zero value, which does not changes appreciably with time in the case of self-sustained combustion. It can be seen from Figures 5.2 and 5.3 that the conditions, which lead to achieve self-sustained flame propagation after successful ignition, depend on ϕ', l_ϕ and u'.

Almost all quiescent cases (i.e. $\frac{u'}{S_{b(\phi=1)}} = 0$) obtained self-sustained combustion following successful ignition except case ST0CE (i.e. $\frac{u'}{S_{b(\phi=1)}} = 0$; $\phi' = 0.6$; ${}^{l_\phi}/_{l_f} = 5.5$) (see Figure 5.2). It can be seen from Figure 5.2 that for all the cases from Table 5.1

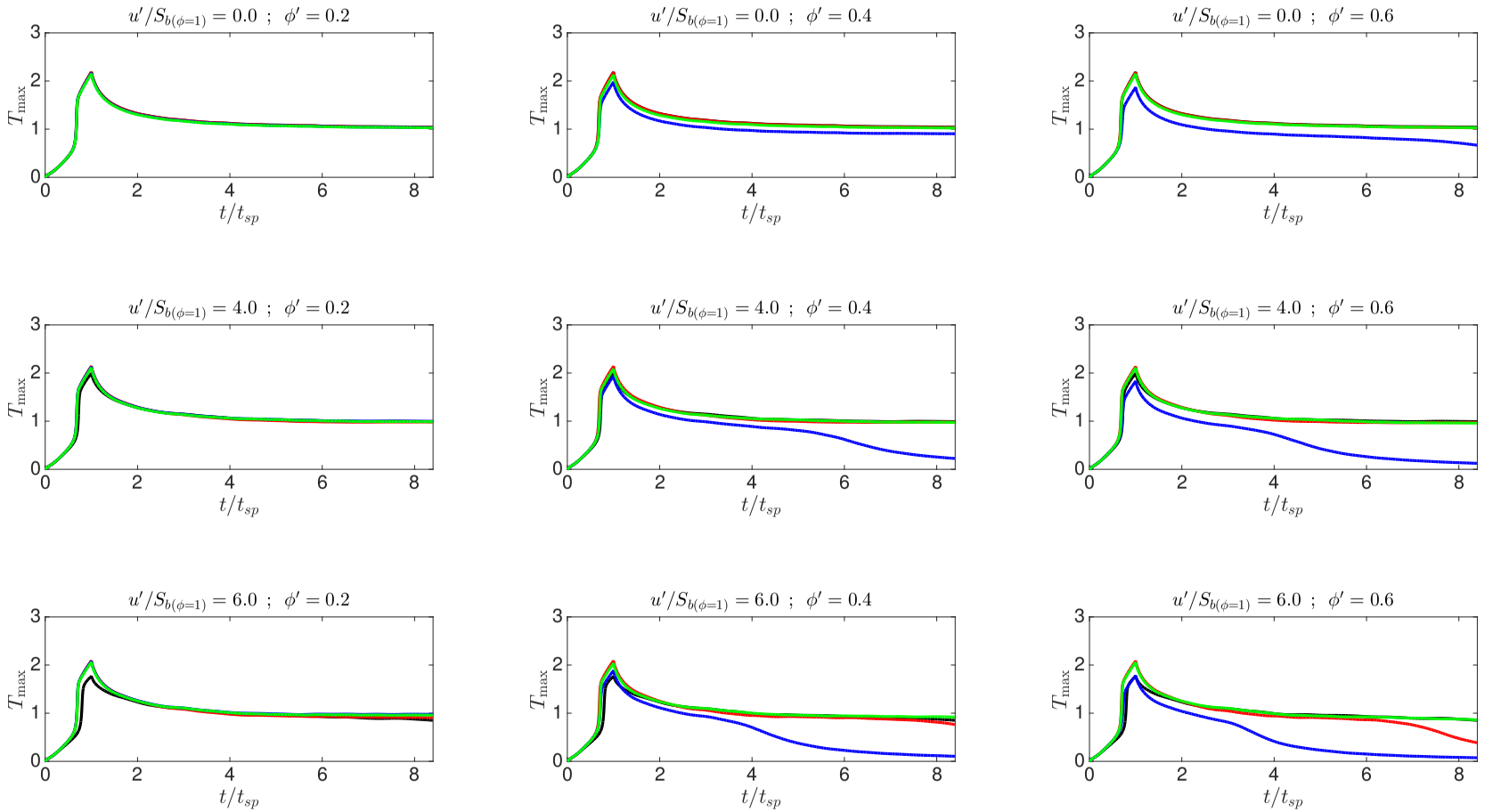

Figure 5.2: Temporal distribution of $T_{\max}$ for all the cases listed in Table 5.1.
[where ${}^{l_\phi}/_{l_f} = 2.1$; ${}^{l_\phi}/_{l_f} = 5.5$; ${}^{l_\phi}/_{l_f} = 8.3$; black like shows homogeneous case ; 1^{st} column shows $\phi' = 0.2$; 2^{nd} column shows $\phi' = 0.4$; 3^{rd} column shows $\phi' = 0.6$; additionally 1^{st} row shows $\frac{u'}{S_{b(\phi=1)}} = 0.0$; 2^{nd} row shows $\frac{u'}{S_{b(\phi=1)}} = 4.0$; 3^{rd} row shows $\frac{u'}{S_{b(\phi=1)}} = 6.0$]

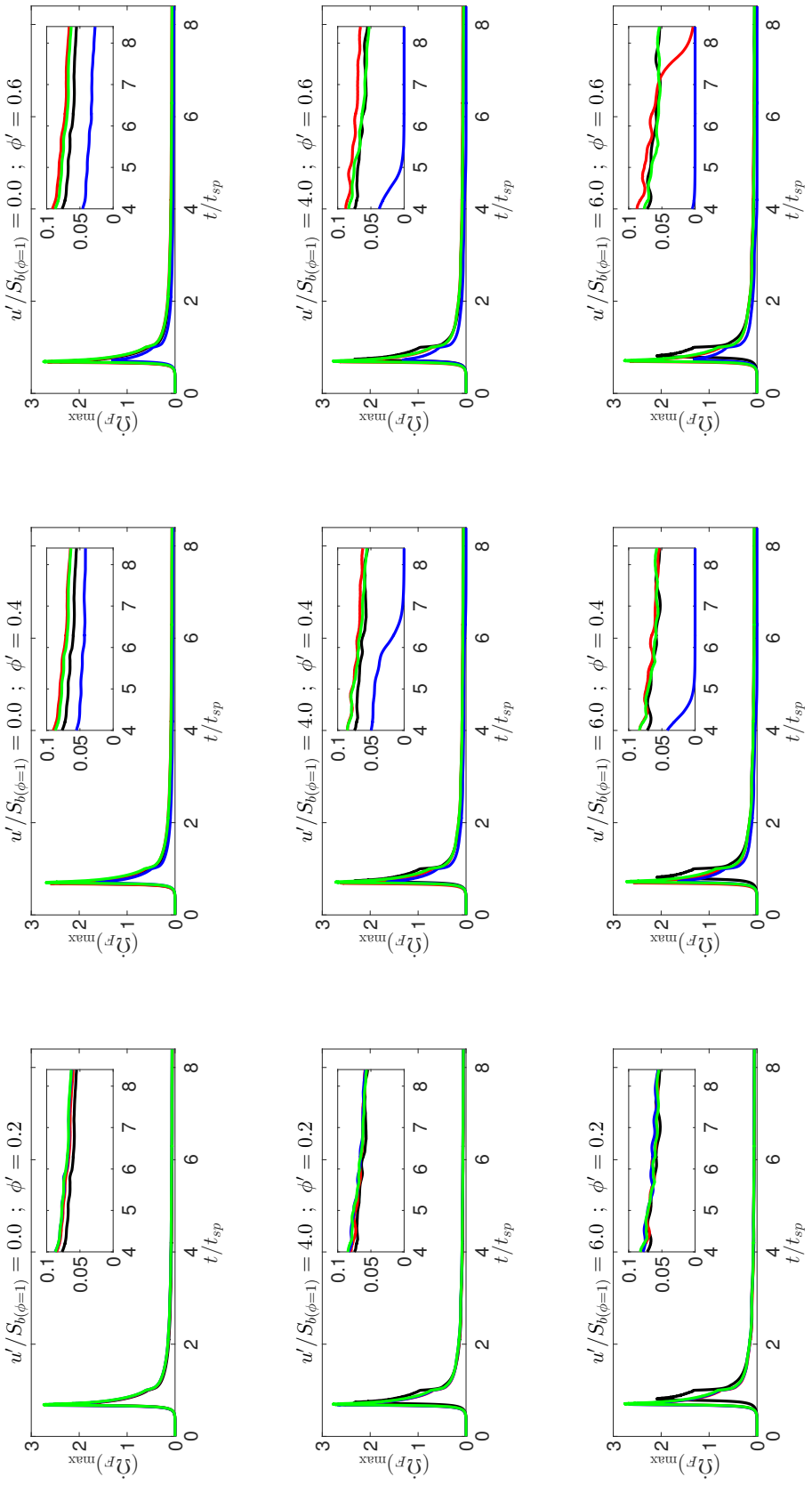

Figure 5.3: Temporal distribution of $(\dot{\Omega}_F)_{\max}$ for all the cases listed in Table 5.1.
[where $l_\phi/l_f = 2.1$; $l_\phi/l_f = 5.5$; $l_\phi/l_f = 8.3$; black like shows homogeneous case ; 1^{st} column shows $\phi' = 0.2$; 2^{nd} column shows $\phi' = 0.4$; 3^{rd} column shows $\phi' = 0.6$; additionally 1^{st} row shows $\frac{u'}{S_{b(\phi=1)}} = 0.0$; 2^{nd} row shows $\frac{u'}{S_{b(\phi=1)}} = 4.0$; 3^{rd} row shows $\frac{u'}{S_{b(\phi=1)}} = 6.0$]

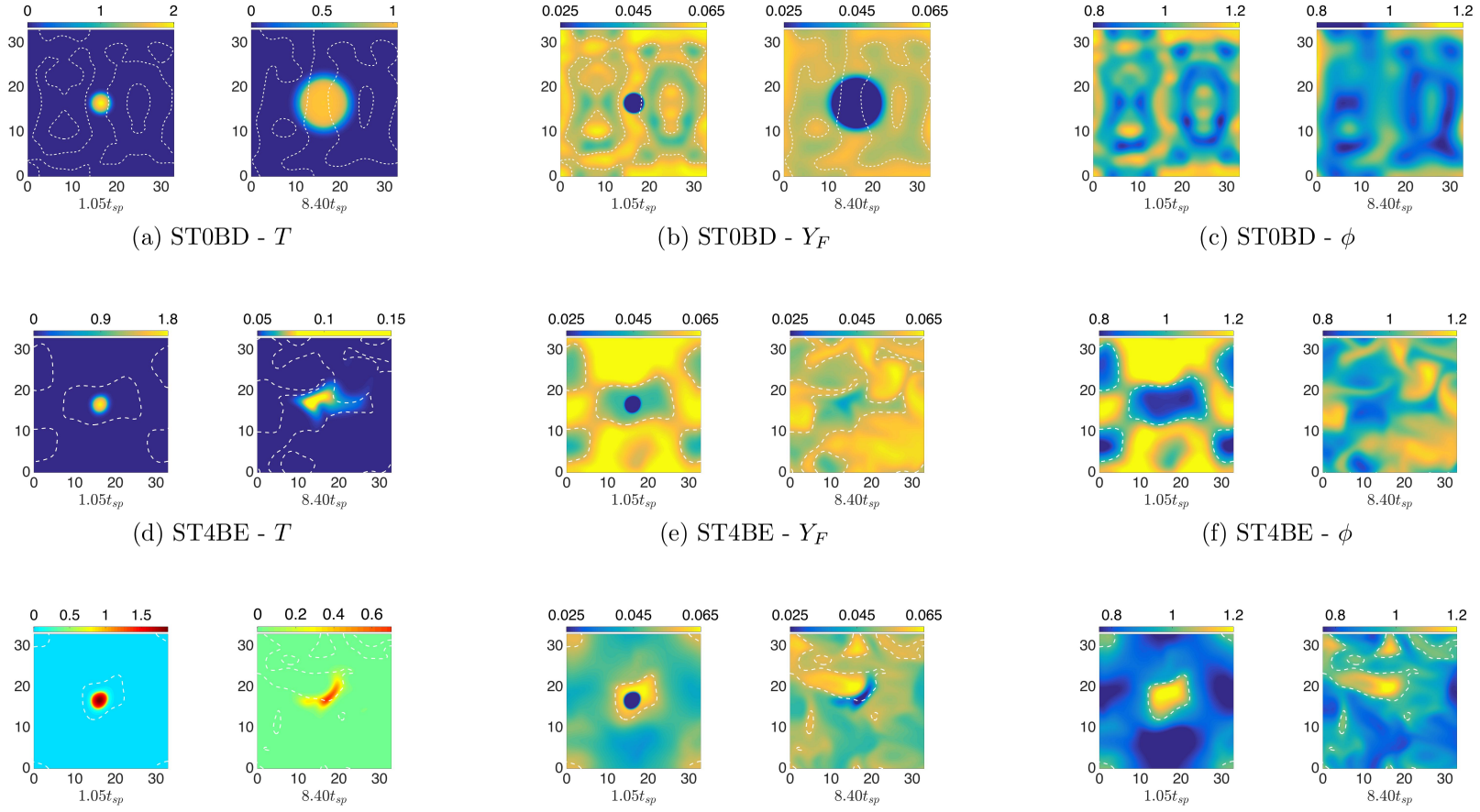

(a) ST0BD - T (b) ST0BD - Y_F (c) ST0BD - ϕ

(d) ST4BE - T (e) ST4BE - Y_F (f) ST4BE - ϕ

(g) ST6BF - T (h) ST6BF - Y_F (i) ST6BF - ϕ

Figure 5.4: Distribution of T (1^{st} & 2^{nd} columns), Y_F (3^{rd} & 4^{th} columns) and ϕ (5^{th} & 6^{th} columns) on the central $x_1 - x_2$ plane for cases ST0BD (1^{st}row), ST4BE $\left(2^{nd}\text{row}\right)$ and ST6BF $\left(3^{rd}\text{row}\right)$. The white broken like shows $\xi = \xi_{st}$.

with $\phi' = 0.2$, the $T_{\max}$ settles to a weakly time dependent value close to unity for all values of l_ϕ and u'. Although in case ST6AD (i.e. $\phi' = 0.2$; ${}^{l_\phi}/_{l_f} = 5.5$; $\frac{u'}{S_{b(\phi=1)}} = 6.0$) , $T_{\max}$ approaches a value slightly smaller than unity. In cases with initial values of $\phi' = 0.4$ and $\phi' = 0.6$, the number of cases which did not exploit self-sustained combustion following successful ignition increases in comparison to $\phi' = 0.2$ cases. For the cases with initial $\frac{u'}{S_{b(\phi=1)}} = 6.0$ and ${}^{l_\phi}/_{l_f}$ =2.1, 5.5 (i.e. cases ST6BD, ST6BE, ST6CD and ST6CE), the value of $T_{\max}$ decreases continuously for $t > t_{sp}$ but the same trend is much weaker in cases with $\frac{u'}{S_{b(\phi=1)}} = 6.0$ and ${}^{l_\phi}/_{l_f} = 8.3$ (i.e. cases ST6BF and ST6CF).

It can be seen from Figures 5.2 and 5.3 that the influence of l_ϕ shows some kind of non-monotonic trend for obtaining self-sustained flame propagation after achieving successful ignition. For example the cases ST6BD, ST6CD, ST6BE, ST6CE eventually extinguishes but the case ST6BF with same initial u' obtained self-sustained combustion following successful ignition. Additionally, Figures 5.2 and 5.3 show that $T_{\max}$ and $\left(\dot{\Omega}_F\right)_{\max}$ decrease continuously even after $t > t_{sp}$ in the cases with initial ${}^{l_\phi}/_{l_f} = 5.5$ for initial ϕ' =0.4, 0.6 (i.e. cases ST0CE, ST4BE, ST4CE, ST6BE and ST6CE), indicating failure to obtained self-sustained flame propagation, despite achieving successful ignition.

The above discussion suggests that ${}^{l_\phi}/_{l_f}$, $\frac{u'}{S_{b(\phi=1)}}$ and ϕ' have important influences on the possibility of self-sustained combustion following successful ignition. Moreover, the effects of ${}^{l_\phi}/_{l_f}$ on the success of self-sustained combustion seem to be non-monotonic, i.e. the cases with initial ${}^{l_\phi}/_{l_f} = 5.5$ are more prone to failure than the cases with initial values of ${}^{l_\phi}/_{l_f} = 2.1$ and 8.3 for the $\phi' = 0.4$ and 0.6 cases.

5.2.3 Spatial Distributions of Temperature, Fuel Mass Fraction and Equivalence Ratio

The distributions of T, Y_F and ϕ at $t = 1.05t_{sp}$ and $t = 8.40t_{sp}$ for the cases ST0BD, ST4BE, and ST6BF are shown in Figure 5.4. It can be seen from Figure 5.4 that the contour of T at $t \leq t_{sp}$ remains spherical during energy deposition and becomes wrinkled as time progresses for all turbulent cases, which is similar to localised forced ignition of homogeneous mixtures (seen and discussed in Chapter 4). Prior to ignition phase, the contours of T principally determined by the diffusion of the deposited energy, but after the ignition, the contours of T depends on the magnitude of the reaction rate at the local mixture composition and flame stretch induced by the background of

the fluid motion. Figure 5.4 also indicates that the non-uniformity of ϕ decreases as time progresses in all cases. Additionally Figure 5.4 shows that Y_F is depleted at the zones corresponds with high values of T due to chemical reaction. Similar qualitative distribution of T and Y_F have been found for other cases, but the burned gas volume was found to decrease with increasing u'.

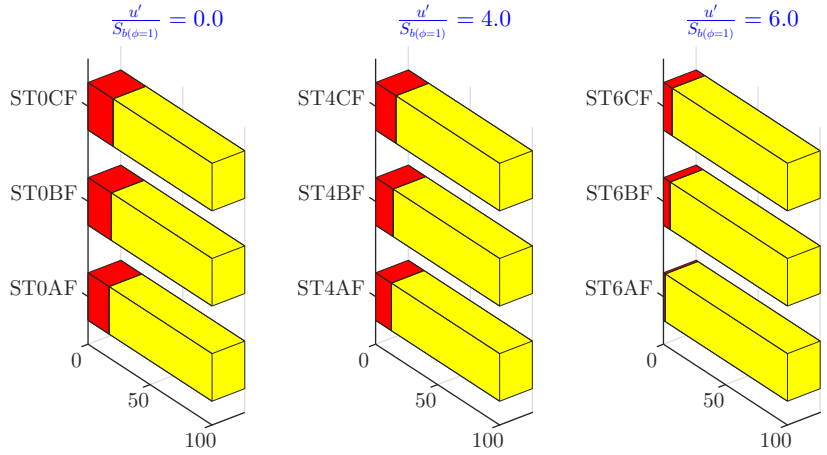

Figure 5.5: Percentage of overall heat release arising from premixed (i.e. $I_c > 0$) and non-premixed (i.e. $I_c < 0$) mode of combustion at $t = 8.40t_{sp}$ for the cases with initial ${}^{l_\phi}/_{l_f} = 8.3$.
[where premixed (i.e. $I_c > 0$) and non-premixed (i.e. $I_c < 0$) mode of combustion]

5.2.4 Mode of Combustion and Mixing Statistics

The mode of combustion in stratified mixtures can be characterised using the flame index (see Section 3.4.1.1), and according to this Equation 3.33, I_c assumes positive values for premixed and negative values for non-premixed mode of combustion [91, 130, 149, 219]. Figure 5.5 shows the percentage of overall heat release arising from both premixed and non-premixed mode of combustion for selected cases at $t = 8.40t_{sp}$ and it can be seen that reactions are taking place predominantly in premixed mode, although some regions with $I_c < 0$ indicate the possibility of finding pockets of non-premixed mode of combustion. The probability of finding non-premixed mode of combustion decreases with increasing time due to the mixing process. Additionally, it can be see from Figure 5.5 that for given ${}^{l_\phi}/_{l_f}$, the probability of finding $I_c < 0$ increases with increasing value of ϕ' because the extent of non-premixed combustion is expected to increase with increasing level of mixture inhomogeneity. On the other side, the probability of finding $I_c < 0$ decreases with increasing value of $\frac{u'}{S_{b(\phi=1)}}$ for a

given value of ${}^{l_\phi}/_{l_f}$ and ϕ' as a result of improved mixing.

The above discussion and observation from Figure 5.5 suggests that the mixing process in stratified mixture leads to finding higher probability of premixed mode of combustion. And this evolution of mixing process can further be illustrated by temporal evolution of the PDFs of ϕ are shown in Figure 5.6 (1^{st} column) . The observation of Figure 5.6 suggests that the mixing process is slower for high values of ${}^{l_\phi}/_{l_f}$ and the width of the PDFs of ϕ decreases with time (see cases ST0AF and ST4BF - the initial Bi-modal distribution of ϕ remains Bi-modal even at $t = 8.40t_{sp}$, where in the other cases the PDF of ϕ approached an approximate Gaussian profile with peak at $\phi \approx \langle\phi\rangle$ as time increases).

The scalar dissipation rate of the mixture fraction can be defined as:

$$N_\xi = D\,\nabla\xi \cdot \nabla\xi \tag{5.4}$$

Furthermore, the mean value of scalar dissipation rate of mixture fraction can be scaled as:

$$\langle N_\xi \rangle \sim \frac{D\,\langle \xi'^2 \rangle}{l_\phi^2} \tag{5.5}$$

where ξ' is the RMS of mixture fraction driven by ϕ fluctuations. The Equation 5.5 indicates that N_ξ and l_ϕ are in inverse proportional to each other, and therefore it can be seen from Figure 5.6 (1^{st} column) that the effects of mixing are stronger for smaller values of l_ϕ cases for a given u'.

The normalised scalar dissipation rate can be defined as:

$$N_\xi^+ = (D\,\nabla\xi \cdot \nabla\xi) \times \frac{t_f}{\xi_{st}^2\,(1-\xi_{st})^2} \tag{5.6}$$

The PDFs of N_ξ^+ are shown in Figure 5.6 (2^{nd} column), where it can be seen that in the cases with $\phi' = 0.6$ and ${}^{l_\phi}/_{l_f} = 2.1$ (cases ST0CD, ST4CD and ST6CD), the initial values of N_ξ^+ attains higher values. Hence, the mixing effects are stronger for cases with initial values of ${}^{l_\phi}/_{l_f} = 2.1$ in comparison to ${}^{l_\phi}/_{l_f} = 8.3$ in these cases with $\phi' = 0.6$. Additionally Figure 5.6 (2^{nd} column) shows that the probability of finding high values of N_ξ increases with decreasing values of ${}^{l_\phi}/_{l_f}$ and increasing values of u'. Therefore, small values of u' and high values of ${}^{l_\phi}/_{l_f}$ leads to slower rates of mixing process.

The temporal evolution of ϕ' are presented in Figure 5.6 (3^{rd} column), which

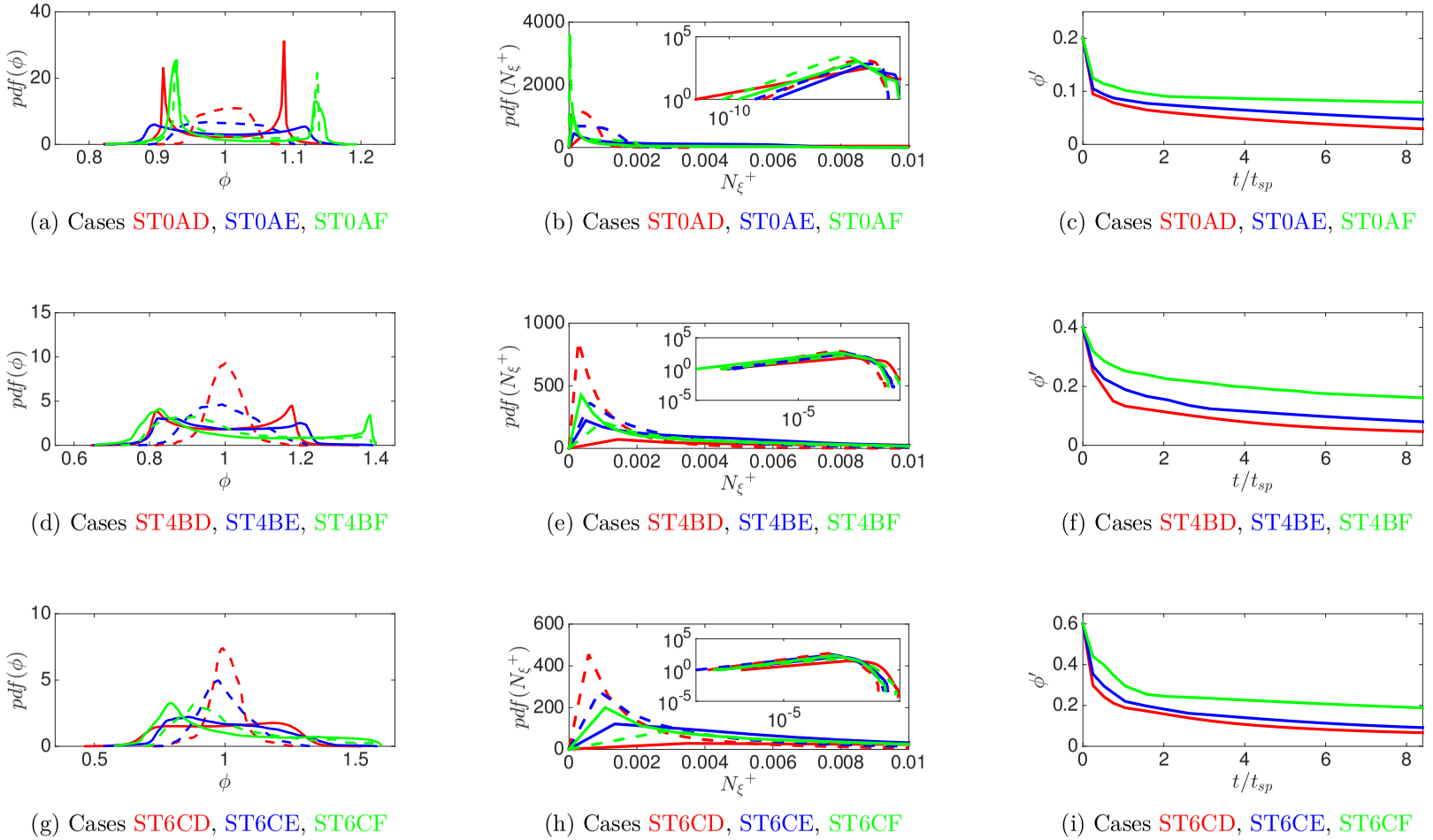

(a) Cases ST0AD, ST0AE, ST0AF (b) Cases ST0AD, ST0AE, ST0AF (c) Cases ST0AD, ST0AE, ST0AF

(d) Cases ST4BD, ST4BE, ST4BF (e) Cases ST4BD, ST4BE, ST4BF (f) Cases ST4BD, ST4BE, ST4BF

(g) Cases ST6CD, ST6CE, ST6CF (h) Cases ST6CD, ST6CE, ST6CF (i) Cases ST6CD, ST6CE, ST6CF

Figure 5.6: Temporal evolution PDF of ϕ (1^{st}column), PDF of $N_\xi^+\left(2^{nd}\text{column}\right)$ and $\phi'\left(3^{rd}\text{column}\right)$ calculated over whole computation domain for specific cases from Table 5.1. [$t = 1.05t_{sp}$(solid line) and $t = 8.40t_{sp}$(broken line)]

demonstrates that ϕ' decays more rapidly in lower value of ${}^{l_\phi}/_{l_f}$ (because of high value of N_ξ). The decreasing rate of ϕ' increases with increasing values of u', as the turbulent straining is generating a scalar gradient, which leads to increase in the N_ξ, which further leads to a greater rate of micro-mixing [130, 149]. In the cases ST0AF, ST4BF and ST6CF, the combination of small u' and high ${}^{l_\phi}/_{l_f}$ is responsible for slower rate of mixing process, whereas the mixing rate is higher for higher values of u' for same values of ${}^{l_\phi}/_{l_f}$.

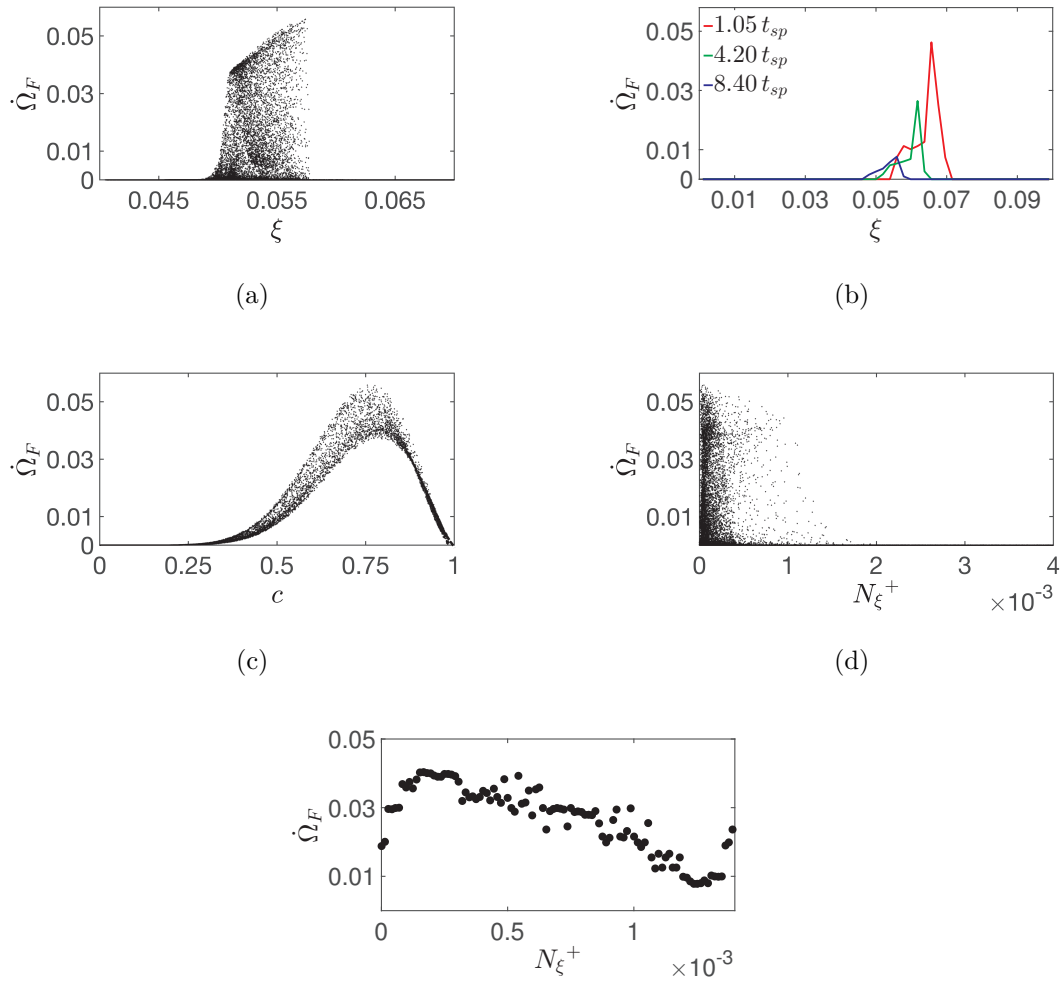

Figure 5.7: (a) Scatter of $\dot{\Omega}_F$ with ξ, (b) Variation of $\dot{\Omega}_F$ conditional on ξ for $0.01 \leq c \leq 0.99$, (c) Scatter of $\dot{\Omega}_F$ with c, (d) Scatter of $\dot{\Omega}_F$ with N_ξ^+, (e) Variation of $\dot{\Omega}_F$ conditional on N_ξ^+ for $0.7 \leq c \leq 0.9$ for case ST4BF ($\frac{u'}{S_{b(\phi=1)}} = 4$; $\phi' = 0.4$; ${}^{l_\phi}/_{l_f} = 8.3$).

5.2.5 Structure of Reaction Zone and Statistical Behaviour of Fuel Reaction Rate Magnitude ($\dot{\Omega}_F$)

In order to understand the effects of stratification on the extent of burning, it is important to analyse the reaction zone structure of the flames originated from localised forced ignition. Figure 5.7 shows analyses for a specific case ST4BF ($\frac{u'}{S_{b(\phi=1)}} = 4.0$, $\phi' = 0.4$,$^{l_\phi}/_{l_f} = 8.3$) and qualitative similar behaviour observed for all cases where self-sustained combustion is obtained. The temperature variation on the given ξ isosurface leads to scatter of $\dot{\Omega}_F$ in Figure 5.7(a), which further shows that high value of $\dot{\Omega}_F$ are observed towards the slightly rich side (i.e. $\xi \approx 0.06$ which corresponds to $\phi \approx 1.10$). At this region the unstrained planar laminar burning velocity attains its maximum value (see Figure 3.1 in Chapter 3) [128, 149, 197]. The variation of $\dot{\Omega}_F$ conditional on ξ for $0.01 \leq c \leq 0.99$ are shown in Figure 5.7(b) at different time instants, which demonstrates that the temperature distribution remains qualitatively similar for successful ignition. The scatter of $\dot{\Omega}_F$ with c at $t = 8.40t_{sp}$ is shown in Figure 5.7(c), which demonstrates that the high value of $\dot{\Omega}_F$ are corresponds to $c = 0.8$, which is in consistent agreement with previous findings [46, 48, 51]. The scatter of $\dot{\Omega}_F$ with N_ξ^+ is shown in Figure 5.7(d) which shows that the high value of $\dot{\Omega}_F$ are associated with small values of N_ξ^+. This observation are in good agreement with previous findings in the context of autoignition [99, 135] and localised forced ignition [46, 48, 51] of inhomogeneous mixtures. The variation of $\dot{\Omega}_F$ conditional on N_ξ^+ for $0.7 \leq c \leq 0.9$ are presented in Figure 5.7(e), which shows the negative correlation between $\dot{\Omega}_F$ and N_ξ^+, which further implies that the $\dot{\Omega}_F$ attains relatively high values for premixed mode of combustion.

5.2.6 Effects of l_ϕ, ϕ' and u' on the Extent of Burning

The extent of burning can be defined by the burned gas mass m_b with $c \geq 0.9$ (see Section 4.2.5). Temporal evolution of M_b (burned gas mass normalised by the mass of an unburned gas sphere with a radius l_f) for all cases from Table 5.1 are shown in Figure 5.9 and Figure 5.8 in order to demonstrate the effects of l_ϕ and ϕ' respectively. Here the Section 5.2.6 is subdivided in to three parts namely in order to explain the effects of l_ϕ, ϕ' and u' on the extent of burning.

Effects of l_ϕ on the extent of burning

Figure 5.8 shows that M_b for the quiescent cases ST0AE ($\frac{u'}{S_{b(\phi=1)}} = 0$, $\phi' = 0.2$, ${}^{l_\phi}/_{l_f} = 5.5$) and ST0AF ($\frac{u'}{S_{b(\phi=1)}} = 0$, $\phi' = 0.2$, ${}^{l_\phi}/_{l_f} = 8.3$) attains higher than the respective homogeneous case in comparison to case ST0AD ($\frac{u'}{S_{b(\phi=1)}} = 0$, $\phi' = 0.2$, ${}^{l_\phi}/_{l_f} = 2.1$) for a given realisation of ϕ. And this trend remains consistent with increasing value of u'(see Figure 5.8 - 1$^{\text{st}}$ column). Additionally Figure 5.8 demonstrates that initial values of ${}^{l_\phi}/_{l_f}$ =5.5, 8.3 shows higher M_b than ${}^{l_\phi}/_{l_f} = 2.1$ for given $\phi' = 0.2$ irrespective the values of u'. On the other side M_b attains the lowest value for ${}^{l_\phi}/_{l_f} = 5.5$ for initial $\phi' = 0.4$ and $\phi' = 0.6$ cases for all the values of u'.

Earlier, it has been shown that (see Section 5.2.4) the mixing is strongest for cases with initial ${}^{l_\phi}/_{l_f} = 2.1$ and thus this particular stratified mixture approaches to an almost homogeneous state more rapidly with predominant probability of finding $\phi = 1.0$ (see Figure 5.6). The laminar burning velocity assumes the highest value (i.e. burning rate is highest) for $\phi = 1.10$ (see Figure 3.1) and therefore mixture with $1.0 < \phi < 1.10$ can provide greater burning rate than for stoichiometric ($\phi = 1.0$) mixtures [128, 130, 149, 197]. However, for $\phi' = 0.2$, the probability of finding $1.0 < \phi < 1.10$ are greater for cases with initial values of ${}^{l_\phi}/_{l_f} = 5.5\,;\, 8.3$ than ${}^{l_\phi}/_{l_f} = 2.1$ due to less effective mixing. And this gives rise to higher burning for ${}^{l_\phi}/_{l_f} = 5.5\,;\, 8.3$ cases than ${}^{l_\phi}/_{l_f} = 2.1$ for $\phi' = 0.2$. Additionally Figure 5.7 - subfigures(d) and (e) shows that high $\dot{\Omega}_F$ are associated with small values of N_ξ^+ in the most reactive region. The turbulent cases with initial ${}^{l_\phi}/_{l_f} = 5.5$ leads to higher probability of finding $1.0 < \phi < 1.10$ in comparison to ${}^{l_\phi}/_{l_f} = 8.3$ and thus M_b attains greater values in the cases with ${}^{l_\phi}/_{l_f} = 5.5$ than ${}^{l_\phi}/_{l_f} = 8.3$ for $\phi' = 0.2$.

The clouds of mixture inhomogeneities are relatively larger for high value of ${}^{l_\phi}/_{l_f}$ (see Figure 5.1), and as a result to this, there is high probability that the igniter will encounter a large region of almost homogeneous mixture (see Figure 5.4). In addition, the cases with ${}^{l_\phi}/_{l_f} = 5.5$, there is a significant presence of non-uniform distribution clouds of fuel-air mixture near the igniter location. This gives rise to finding slow burning mixture ($\phi < 1.0$ and $\phi > 1.10$) in the reaction zone for cases with initial ${}^{l_\phi}/_{l_f} = 5.5$ when the initial $\phi' = 0.4$ and 0.6 (see Figure 5.8), thus the burning rate in case ${}^{l_\phi}/_{l_f} = 5.5$ are slower than in cases ${}^{l_\phi}/_{l_f}$ =2.1, 8.3 when $\phi' = 0.4$ and 0.6. On the other side if the igniter is located in the vicinity of a large cloud of $1.0 \leq \phi \leq 1.10$, this mixture will help in the expansion of the hot gas kernel and thus higher burning rate in cases with initial ${}^{l_\phi}/_{l_f} = 8.3$ than ${}^{l_\phi}/_{l_f} = 5.5$ when when $\phi' = 0.4$ and 0.6. High

values of N_ξ^+ are associated with cases with initial ${}^{l_\phi}/_{l_f} = 2.1$ than ${}^{l_\phi}/_{l_f} = 8.3$, thus probability of finding high $\dot{\Omega}_F$ is greater in turbulent cases with initial ${}^{l_\phi}/_{l_f} = 8.3$ than ${}^{l_\phi}/_{l_f} = 2.1$ when $\phi' = 0.4$ and 0.6 (see Figure 5.8 - 2^{nd} and 3^{rd} columns).

Effects of ϕ' on the extent of burning

Figure 5.9 shows the effects of ϕ' for all cases listed in Table 5.1. It can be seen from Figure 5.9 that an increase in ϕ' leads to reduction in the burned gas mass for all values of ${}^{l_\phi}/_{l_f}$.

The burning of the mixture with $1.0 \leq \phi \leq 1.10$ is highest (see Figure 3.1), and thus the probability of finding mixture with $\phi < 1.0$ and $\phi > 1.10$ increases with increasing values of ϕ'. The probability of finding slow burning mixture with $\phi < 1.0$ and $\phi > 1.10$ is higher in cases with ${}^{l_\phi}/_{l_f} = 5.5$ due to less efficient mixing than in cases with initial ${}^{l_\phi}/_{l_f} = 2.1$, thus M_b attains greater in initial ${}^{l_\phi}/_{l_f} = 2.1$ cases than in the cases with initial ${}^{l_\phi}/_{l_f} = 5.5$ when $\phi' = 0.4$ and 0.6 (see Figure 5.9). The observation of seeing reduction in burning rate due to mixture stratification in globally stoichiometric mixture are in consistent agreement with previous both experimental [170] and computational findings [88, 91, 104].

Effects of u' on the extent of burning

It can be seen from both Figures 5.8 and 5.9 that increase in u' leads to detrimental effects on M_b for all values of ${}^{l_\phi}/_{l_f}$ and ϕ'. The mean heat flux from the hot gas kernel can be expressed as:

$$\bar{\vec{q}} = -\bar{\rho} C_P \left(D_{mol} + D_t\right) \nabla \tilde{\hat{T}} \tag{5.7}$$

where $\bar{\rho}$ is the mean density, $\tilde{\hat{T}}$ is the density-weighted mean (Favre-mean) temperature, D_{mol} is the molecular thermal diffusivity and D_t is the eddy thermal diffusivity. The eddy thermal diffusivity can be scaled as:

$$D_t \sim u' L_{11} \tag{5.8}$$

According to Equation 5.8, an increase in u' leads to an increase in eddy thermal diffusivity for given value of L_{11} considered here, which further leads to a greater amount of heat loss from the hot gas kernel for high value of u'. In order to obtain self-sustained combustion following successful ignition, the heat release from the hot gas kernel must overcome the heat loss. The increase in u' leads to an increase in

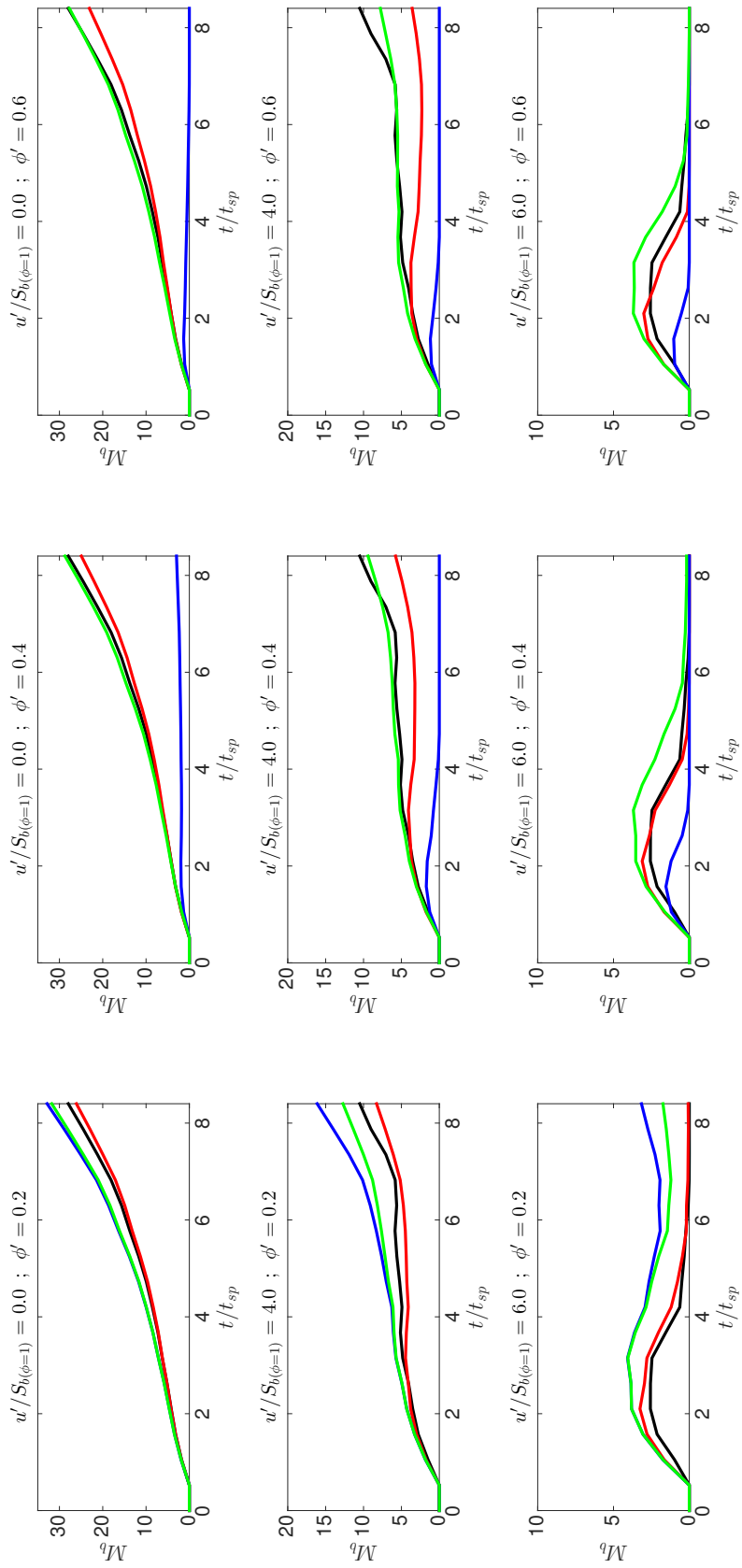

Figure 5.8: Temporal distribution of M_b for all the cases listed in Table 5.1 in order to illustrate the effects of l_ϕ/l_f. [where $l_\phi/l_f = 2.1$; $l_\phi/l_f = 5.5$; $l_\phi/l_f = 8.3$; black like shows homogeneous case ; 1^{st} column shows $\phi' = 0.2$; 2^{nd} column shows $\phi' = 0.4$; 3^{rd} column shows $\phi' = 0.6$; additionally 1^{st} row shows $\frac{u'}{S_{b(\phi=1)}} = 0.0$; 2^{nd} row shows $\frac{u'}{S_{b(\phi=1)}} = 4.0$; 3^{rd} row shows $\frac{u'}{S_{b(\phi=1)}} = 6.0$]

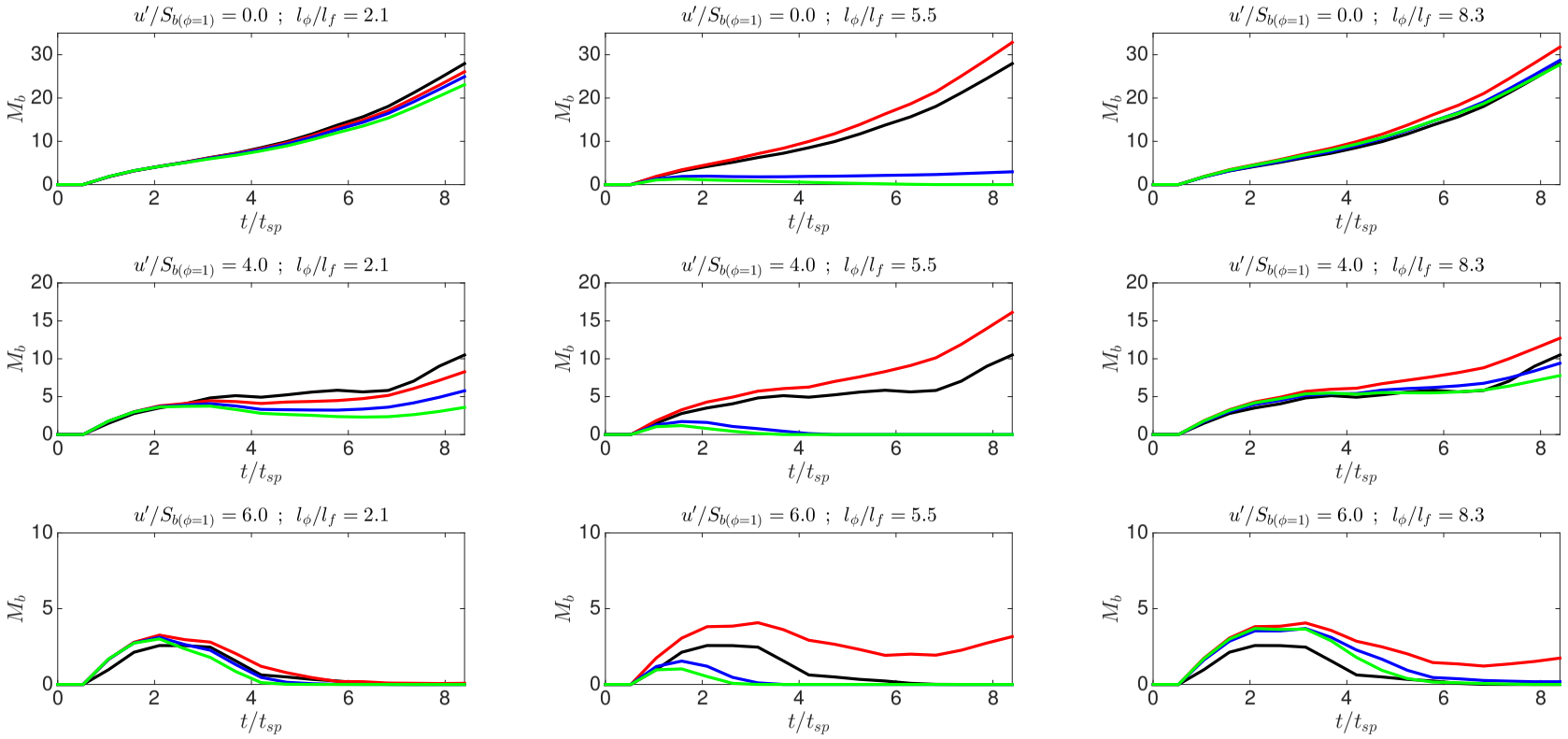

Figure 5.9: Temporal distribution of M_b for all the cases listed in Table 5.1 in order to illustrate the effects of ϕ'. [where $\phi' = 0.2$; $\phi' = 0.4$; $\phi' = 0.6$; black like shows homogeneous case ; 1^{st} column shows ${}^{l_\phi}/_{l_f} = 2.1$; 2^{nd} column shows ${}^{l_\phi}/_{l_f} = 5.5$; 3^{rd} column shows ${}^{l_\phi}/_{l_f} = 8.3$; additionally 1^{st} row shows $\frac{u'}{S_{b(\phi=1)}} = 0.0$; 2^{nd} row shows $\frac{u'}{S_{b(\phi=1)}} = 4.0$; 3^{rd} row shows $\frac{u'}{S_{b(\phi=1)}} = 6.0$]

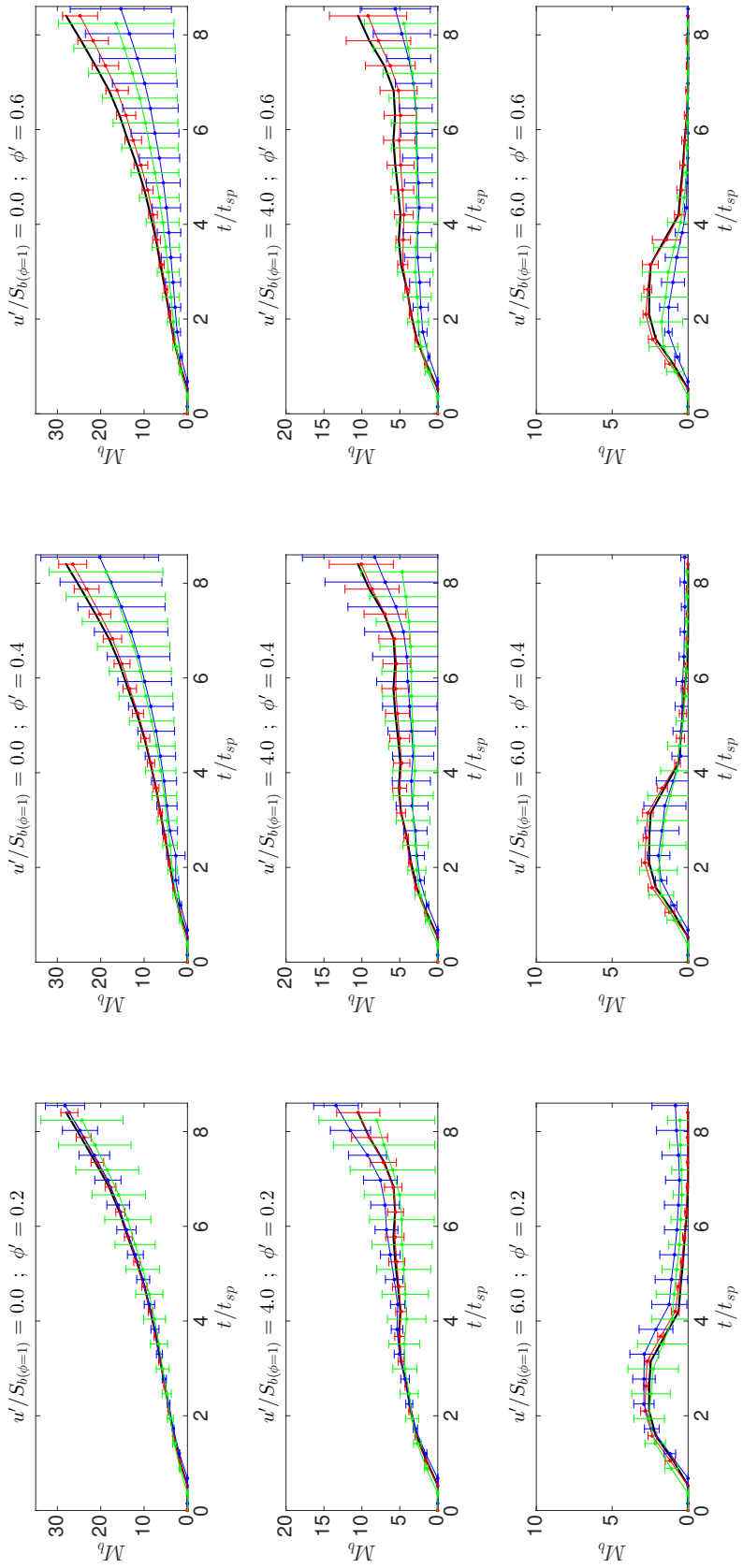

Figure 5.10: Temporal distribution of mean M_b from different realisation of ϕ for all the cases listed in Table 5.1, with standard deviation due to different realisation of initial condition are presented in form of bars.
[where $l_\phi/l_f = 2.1$; $l_\phi/l_f = 5.5$; $l_\phi/l_f = 8.3$; black like shows homogeneous case ; 1^{st} column shows $\phi' = 0.2$; 2^{nd} column shows $\phi' = 0.4$; 3^{rd} column shows $\phi' = 0.6$; additionally 1^{st} row shows $\frac{u'}{S_{b(\phi=1)}} = 0.0$; 2^{nd} row shows $\frac{u'}{S_{b(\phi=1)}} = 4.0$; 3^{rd} row shows $\frac{u'}{S_{b(\phi=1)}} = 6.0$]

heat transfer from the hot gas kernel and thus probability of finding high value of c also decreases. It can be seen from Figure 5.4 that the case ST4BE ($\frac{u'}{S_{b(\phi=1)}} = 4.0$, $\phi' = 0.4$, ${}^{l_\phi}/_{l_f} = 5.5$) fails to obtain self-sustained combustion despite the successful ignition. In this case ST4BE, the heat loss overcomes chemical heat release, and the hot gas kernel shrinks and heat release drops drastically once iso-surface of $c \approx 0.8$ disappears and therefore this case ST4BE exhibits flame extinction. It can be seen from Figures 5.8 and 5.9 that M_b varnishes at $t \gg t_{sp} (t = 8.40 t_{sp})$ for cases ST4BE ($\frac{u'}{S_{b(\phi=1)}} = 4.0$, $\phi' = 0.4$, ${}^{l_\phi}/_{l_f} = 5.5$), ST4CE ($\frac{u'}{S_{b(\phi=1)}} = 4.0$, $\phi' = 0.6$, ${}^{l_\phi}/_{l_f} = 5.5$) and for majority cases with initial $\frac{u'}{S_{b(\phi=1)}} = 6.0$ (i.e. ST6AD, ST6BD, ST6CD, ST6BE, ST6CE, ST6BF and ST6CF). This detrimental effects of u' on the extent of burning is consistent with previous both homogeneous (Chapter 4), [96, 109, 116, 159] and inhomogeneous [4, 5, 15, 48, 50, 51] mixtures studies in the context of localised forced ignition.

5.2.7 Effects of Initial ϕ Distribution on the Extent of Burning

It is well-known that the combustion succeeds only for some realisations, even when the turbulent flow statistics are the same [4, 5, 9, 28, 168]. Recently, Pera *et al.* [155] investigated the effects of residual burnt gas heterogeneity on premixed early flame propagation on cycle-to-cycle variation observed in SI engines. DNS results from Pera *et al.* [155] suggested that the effect of residual burnt gas heterogeneity on heat release fluctuation is due to fluctuations of local mixture conditions in the case of engine cycle-to-cycle variation. All the cases listed in Table 5.1 have been re-analysed for four different realisations of the initial distribution of ϕ in order to study the degree of variability on the M_b.

The temporal evolution of mean and standard deviations of M_b for all realisations are shown in Figure 5.10 to present the probabilistic nature of the localised forced ignition in stratified mixture environment. The observation from Figure 5.10 indicates that the variation of M_b between different realisations increases with increasing ${}^{l_\phi}/_{l_f}$. Additionally, Figure 5.10 shows that the adverse effects of u' remain qualitatively similar for all the realisations. For large value of ${}^{l_\phi}/_{l_f} = 8.3$, it is highly possible that the igniter will encounter highly flammable and/or weakly flammable even non-combustible mixtures clouds which leads to large variations of M_b between different realisations and this tendency strengthens further with increasing ϕ'. It can be seen

from Figure 5.10 that the variations of M_b are larger for ${}^{l_\phi}/_{l_f} = 8.3$ in comparison to ${}^{l_\phi}/_{l_f} = 2.1$ cases. It is admitted that four different realisations are not sufficient to mimic the cycle-to-cycle variation in a real IC engines, however this extensive DNS parametric analysis reveals important qualitative trends, which suggests that the variability in the extent of burning is relatively small for small values of ${}^{l_\phi}/_{l_f}$ and the degree of variability of burning increases with increasing ϕ'.

5.2.8 Summary

The effects of length scale of mixture inhomogeneity (l_ϕ) and RMS values of equivalence ratio (ϕ') in globally stoichiometric stratified mixtures (i.e. $\langle\phi\rangle = 1.0$) have been analysed in the context of localised forced ignition using 3D DNS simulations in Section 5.2. It has been found that the initial values of l_ϕ and ϕ' have significant influences for achieving self-sustained combustion following successful ignition and on the extent of burning. The flame originating from localised forced ignition shows a predominantly premixed mode of combustion, however some pockets of non-premixed combustion have been observed and the probability of non-premixed combustion pockets increases with increasing ϕ'. The results analysis demonstrates that for a given value of ${}^{l_\phi}/_{l_f}$, an increase in ϕ' leads to reduction of mass burning rate, on the other side the influences of ${}^{l_\phi}/_{l_f}$ on the extent of burning are non-monotonic and dependent on ϕ'. The adverse effects of higher values of u' shows increase in heat transfer rate from hot gas kernel, which further leads to reduction in mass burning rate irrespective values of ${}^{l_\phi}/_{l_f}$ and ϕ'. Thus self-sustained combustion may not be achieved in the cases with higher values of u'. The findings in Section 5.2 demonstrate that favorable condition in terms of u', ϕ' and l_ϕ are required in order to have self-sustained combustion subsequent to successful localised forced ignition in globally stoichiometric stratified mixtures.

The analysis carried out in Section 5.2 was for globally stoichiometric stratified mixtures in which the initial equivalence ratio distribution followed a Bi-modal probability density function. The next Section 5.3 extends the analysis to study the effects of the nature of equivalence ratio distribution on localised forced ignition of globally stoichiometric stratified mixtures.

5.3 Effects of Nature of Initial Mixture Distribution

This section starts with brief discussion on the numerical implementation adopted for this study and then the results are presented and discussed. Global behaviours of maximum value of temperature is shown first to analyse the influences of nature of initial mixture distribution on the possibility of self-sustained combustion following successful ignition. Spatial distribution of different quantities is then presented. Mode of combustion and mixing statistics is evaluated. The reaction-diffusion balance analysis of flame kernels is shown. The statistical behaviour of fuel reaction rate magnitude is examined to understand the effects of stratification on the extent of burning following successful ignition. Finally, the section investigates the effects of nature of initial mixture distribution on the extent of burning and ends with summary.

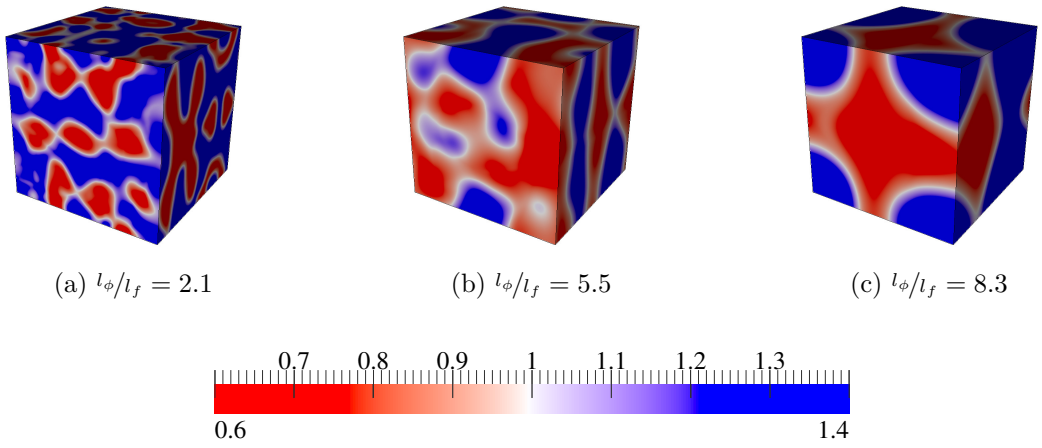

(a) $l_\phi/l_f = 2.1$ (b) $l_\phi/l_f = 5.5$ (c) $l_\phi/l_f = 8.3$

(d) $l_\phi/l_f = 2.1$ (e) $l_\phi/l_f = 5.5$ (f) $l_\phi/l_f = 8.3$

Figure 5.11: Initial computational domain showing different values of length scale of mixture inhomogeneities for $\phi' = 0.4$ in globally stoichiometric stratified mixtures for both Bi-modal (1^{st} row) and Gaussian (2^{nd} row) distribution of ϕ.

Here the numerical formulation including ignition modelling remains similar to as described in Section 5.2.1. The initial mixture inhomogeneity field is initiated following Gaussian distribution [81] and Bi-modal distribution [76] for a given set of values of ϕ' and l_ϕ for given $\langle\phi\rangle$ (Section 3.7). The Figure 5.11 illustrates the different initial length scale of mixture inhomogeneities values for given ϕ' in a computational domain for both Bi-modal and Gaussian distribution of ϕ. It can be seen from Figure 5.11 that in Bi-modal distribution of ϕ, the fuel rich and fuel lean regions are segregated from each other, whereas in Gaussian distribution of ϕ, some level of mixing is already observed. Table 5.2 shows a parametric variation, and thus total 219 simulations (54×4 stratified mixture cases + 3 homogeneous mixtures) have been conducted here. The case names are chosen in such manner so that S stands for globally stoichiometric stratified mixtures; G and Bi stands for initial Gaussian and Bi-modal distribution of ϕ; T0, T4 and T6 indicate increasing turbulent level; A, B, and C indicate increasing values of ϕ'; and D, E, and F denote increasing values of ${}^{l_\phi}/_{l_f}$ (e.g. GST6AF corresponds to a case for initial Gaussian distribution of globally stoichiometric stratified mixtures with values of $\frac{u'}{S_{b(\phi=1)}} = 6.0$; $\phi' = 0.2$; ${}^{l_\phi}/_{l_f} = 8.3$).

	Gaussian [G] Bi-modal [Bi]		
	$\langle\phi\rangle = 1.0$ [S]		
$\frac{L_{11}}{l_f} = 3.36$	$\frac{l_\phi}{l_f} = 2.1$ [D]	$\frac{l_\phi}{l_f} = 5.5$ [E]	$\frac{l_\phi}{l_f} = 8.3$ [F]
$\frac{u'}{S_{b(\phi=1)}} = 0.0$ [T0]	GST0AD BiST0AD	GST0AE BiST0AE	GST0AF BiST0AF
$\frac{u'}{S_{b(\phi=1)}} = 4.0$ [T4]	GST4AD BiST4AD	GST4AE BiST4AE	GST4AF BiST4AF
$\frac{u'}{S_{b(\phi=1)}} = 6.0$ [T6]	GST6AD BiST6AD	GST6AE BiST6AE	GST6AF BiST6AF
Homogeneous cases			
ST0, ST4, ST6			

Table 5.2: List of parameters to analyse effects of initial distribution (i.e. Gaussian and Bi-modal) in globally stoichiometric (i.e. $\langle\phi\rangle = 1.0$) stratified mixtures. Replace [A] with [B] and [C] for $\phi' = 0.2$ and $\phi' = 0.4$ cases.

5.3.1 Global Behaviours of Maximum Value of Temperature

The non-dimensional maximum temperature $T_{\max}$ (see Equation 5.2) for all the cases listed in Table 5.2 are shown in Figures 5.12, 5.13 and 5.14 for $\phi' = 0.2$, $\phi' = 0.4$ and $\phi' = 0.6$, respectively. The general behaviour of $T_{\max}$ remains unchanged in the cases of self-sustained combustion following successful ignition (as seen in Section 5.2.2). The general trend of normalised fuel reaction rate magnitude $\left(\dot{\Omega}_F\right)_{\max}$ remains qualitatively similar as observed in Section 5.2.2 (and thus not shown here). A comparison between Figures 5.13 and 5.14 shows that self-sustained combustion has been obtained for all Gaussian distribution cases with $\frac{u'}{S_{b(\phi=1)}}$ =0.0 and 4.0, whereas some cases with initial Bi-modal distribution (e.g. BiST4BE and BiST4CE) fail to achieve self-sustained combustion for $\frac{u'}{S_{b(\phi=1)}} = 4.0$.

It is found that the initial Bi-modal distribution cases with ${}^{l_\phi}/_{l_f} = 5.5$ for ϕ' =0.4 and 0.6 are more prone to flame extinction at $t > t_{sp}$ than the initial ${}^{l_\phi}/_{l_f}$ =2.1 and 8.3 cases but no such trend is observed for the corresponding cases with initial Gaussian equivalence ratio distribution. By contrast, some cases with initial Bi-modal distribution show more resistance to flame extinction at $t > t_{sp}$ for initial $\frac{u'}{S_{b(\phi=1)}} =$ 6.0 (e.g. the initial Bi-modal distribution cases BiST6AD, BiST6AE, BiST6AF and BiST6BF exhibit self-sustained combustion) than the corresponding cases with initial Gaussian distribution (all cases with initial Gaussian distribution fails to achieve self-sustained combustion for $\frac{u'}{S_{b(\phi=1)}} = 6.0$). In general, the probability of flame extinction at $t > t_{sp}$ (i.e. without any external addition of energy) increases with increasing $\frac{u'}{S_{b(\phi=1)}}$ for both initial Bi-modal and Gaussian distribution cases. For example the cases BiST4BE, BiST6BE in Figure 5.13 ; cases BiST0CCE, BiST4CE, BiST6CE in Figure 5.14 and all cases with $\frac{u'}{S_{b(\phi=1)}} = 6.0$ for initial Gaussian distribution may requires an additional external energy after $t = t_{sp}$ in able to achieve self-sustained combustion.

The observations made from Figures 5.12, 5.13 and 5.14 indicate that the nature of initial mixture distribution, $\frac{u'}{S_{b(\phi=1)}}$, ϕ' and l_ϕ have important influences on the possibility of obtaining self-sustained combustion following successful ignition in stratified mixtures.

5.3.2 Spatial Distributions of Temperature, Fuel Mass Fraction, Fuel Reaction Rate Magnitude and Equivalence Ratio

The distribution of non-dimensional temperature (T), fuel mass fraction (Y_F), normalised fuel reaction rate magnitude ($\dot{\Omega}_F$) and equivalence ratio (ϕ) at the central $x_1 - x_2$ plane at both $t = 1.05t_{sp}$ and $t = 8.40t_{sp}$ for the cases GST4BD (Gaussian distribution with $\langle\phi\rangle = 1.0$, $\frac{u'}{S_{b(\phi=1)}} = 4$, $\phi' = 0.4$, ${}^{l_\phi}/_{l_f} = 2.1$) and BiST4BD (Bi-modal distribution with $\langle\phi\rangle = 1.0$, $\frac{u'}{S_{b(\phi=1)}} = 4$, $\phi' = 0.4$, ${}^{l_\phi}/_{l_f} = 2.1$) are shown in Figure 5.15. Similar qualitative behaviour has been observed for other cases but the burned gas volume has been found to decrease with increasing $\frac{u'}{S_{b(\phi=1)}}$ irrespective of the nature of the initial mixture distribution. In both cases of initial distribution the contours of T shows approximate spherical shape during the period of energy deposition, as seen in Section 5.2.3.

After the igniter has been switched off, the T evolution of isotherms heavily depends on the magnitude of reaction rate at the given local mixture composition and the flame stretch induced by the background fluid motion. The flame stretch rate dependences on local flame propagation and these observation are qualitatively similar to earlier reported literature by Malkeson and Chakraborty [129]. In Figure 5.15, the non-uniformity of ϕ decreases as time increases in all cases (compare Figure 5.15 for $t = 1.05t_{sp}$ and $t = 8.40t_{sp}$). The observation from Figure 5.15 suggests that the local mixture composition and their mixing decay rate are affecting the flame propagation once the flame is generated (in the case of successful ignition) for a given set of $\frac{u'}{S_{b(\phi=1)}}$, ${}^{l_\phi}/_{l_f}$ and ϕ'. Therefore it is important to analyse the progress of mixing in the cases with different initial mixture distribution which is discussed in the following section.

5.3.3 Mode of Combustion and Mixing Statistics

It is vital to understand the flame structure originating from localised forced ignition to explain the observed burning behaviour for different nature of initial mixture distributions. The percentage of overall heat release arising from premixed (i.e. $I_c > 0$) and non-premixed (i.e. $I_c < 0$) modes of combustion at $t = 8.40t_{sp}$ are shown in Figures 5.16 and 5.17. Additionally Figure 5.16 shows the effects of ${}^{l_\phi}/_{l_f}$ and Figure 5.17 shows the effects of ϕ', $\frac{u'}{S_{b(\phi=1)}}$ comparing different nature of initial mixture distributions on mode of combustion.

It is clear from Figures 5.16 and 5.17 that chemical reaction takes place mostly

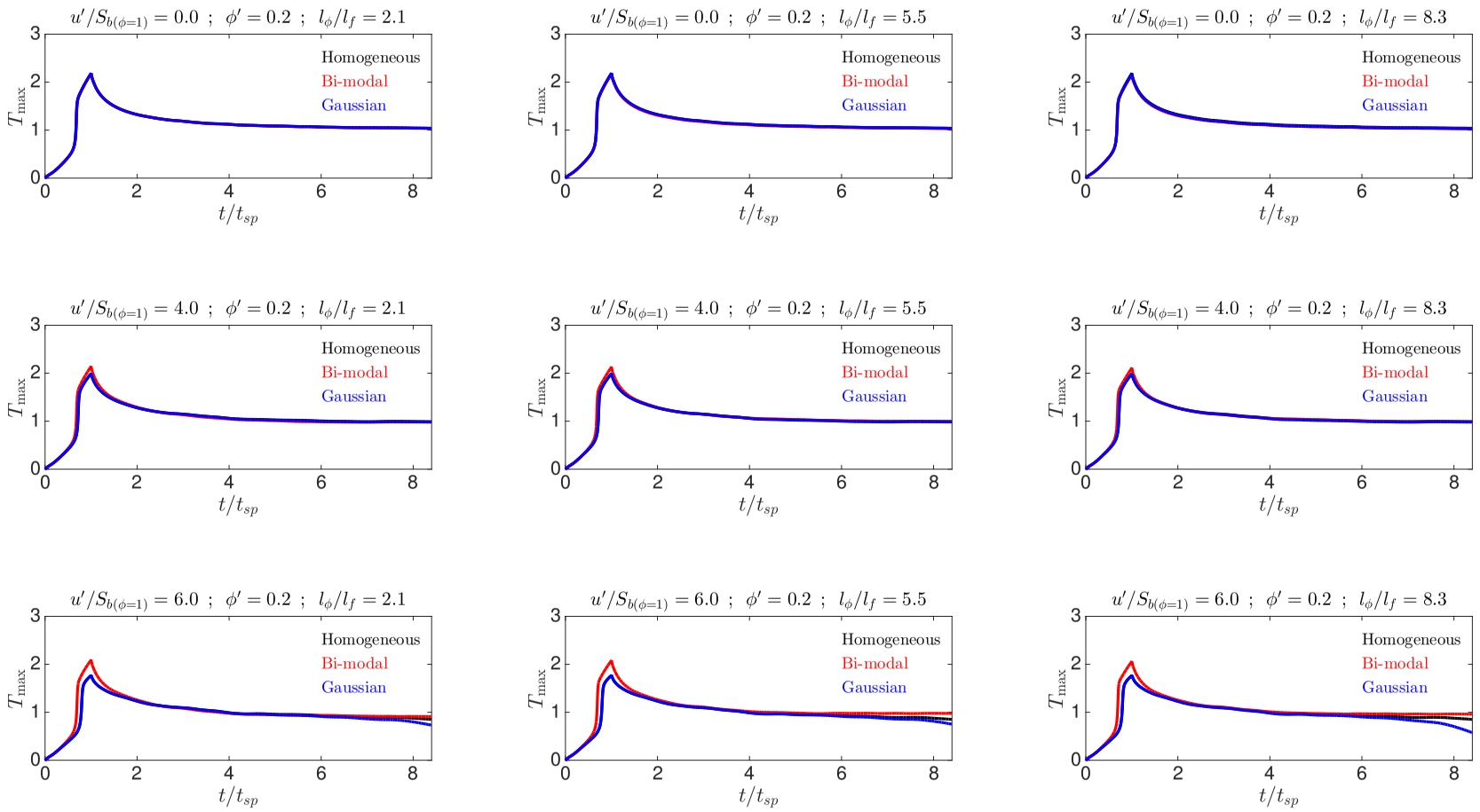

Figure 5.12: Temporal distribution of $T_{\max}$ for all the cases with $\phi' = 0.2$ listed in Table 5.2. [where 1^{st} column shows ${}^{l_\phi}/_{l_f} = 2.1$; 2^{nd} column shows ${}^{l_\phi}/_{l_f} = 5.5$; 3^{rd} column shows ${}^{l_\phi}/_{l_f} = 8.3$; additionally 1^{st} row shows $\frac{u'}{S_{b(\phi=1)}} = 0.0$; 2^{nd} row shows $\frac{u'}{S_{b(\phi=1)}} = 4.0$; 3^{rd} row shows $\frac{u'}{S_{b(\phi=1)}} = 6.0$]

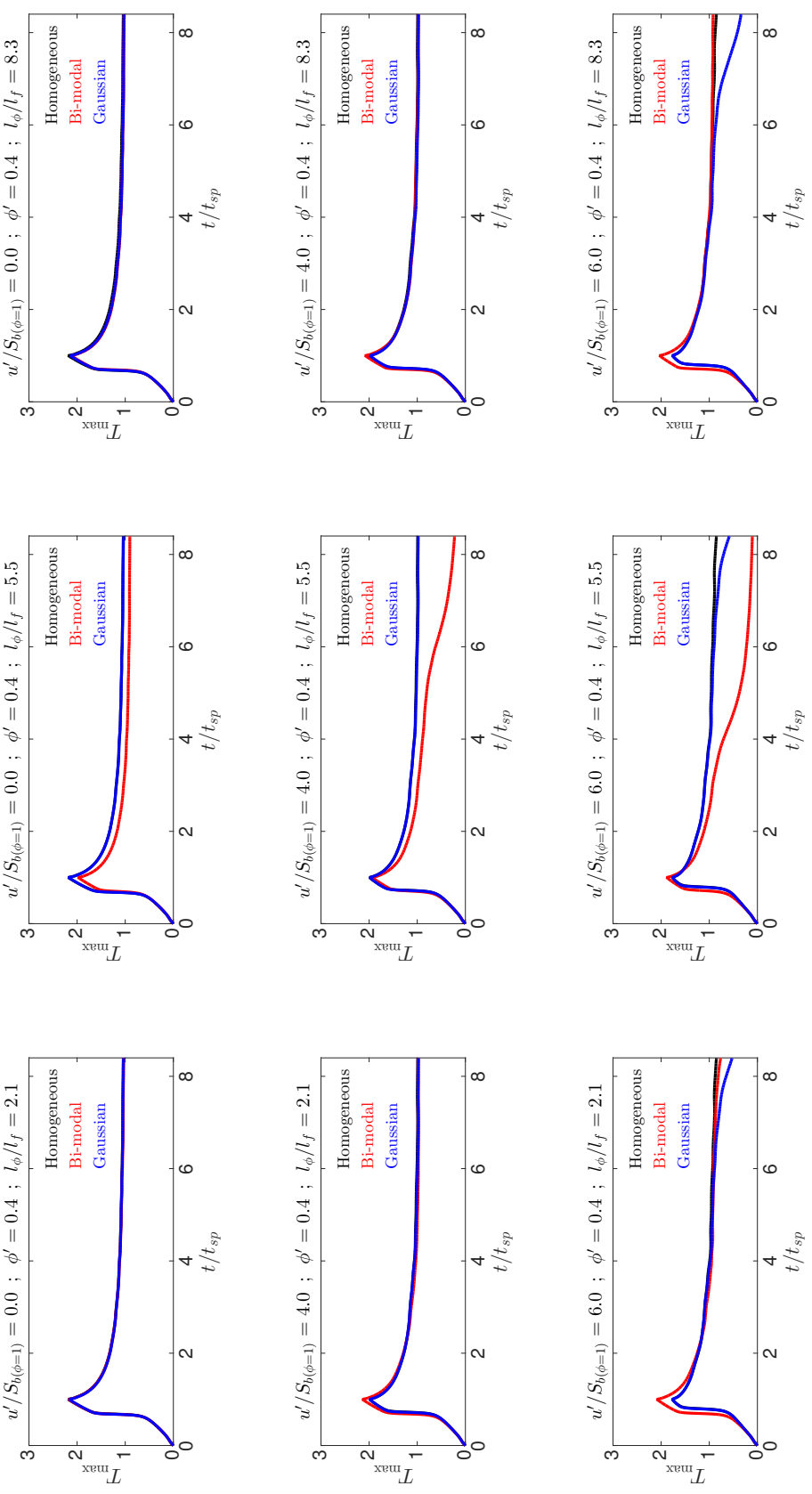

Figure 5.13: Temporal distribution of $T_{\max}$ for all the cases with $\phi' = 0.4$ listed in Table 5.2.
[where 1^{st} column shows $l_\phi/l_f = 2.1$; 2^{nd} column shows $l_\phi/l_f = 5.5$; 3^{rd} column shows $l_\phi/l_f = 8.3$; additionally 1^{st} row shows $\frac{u'}{S_{b(\phi=1)}} = 0.0$; 2^{nd} row shows $\frac{u'}{S_{b(\phi=1)}} = 4.0$; 3^{rd} row shows $\frac{u'}{S_{b(\phi=1)}} = 6.0$]

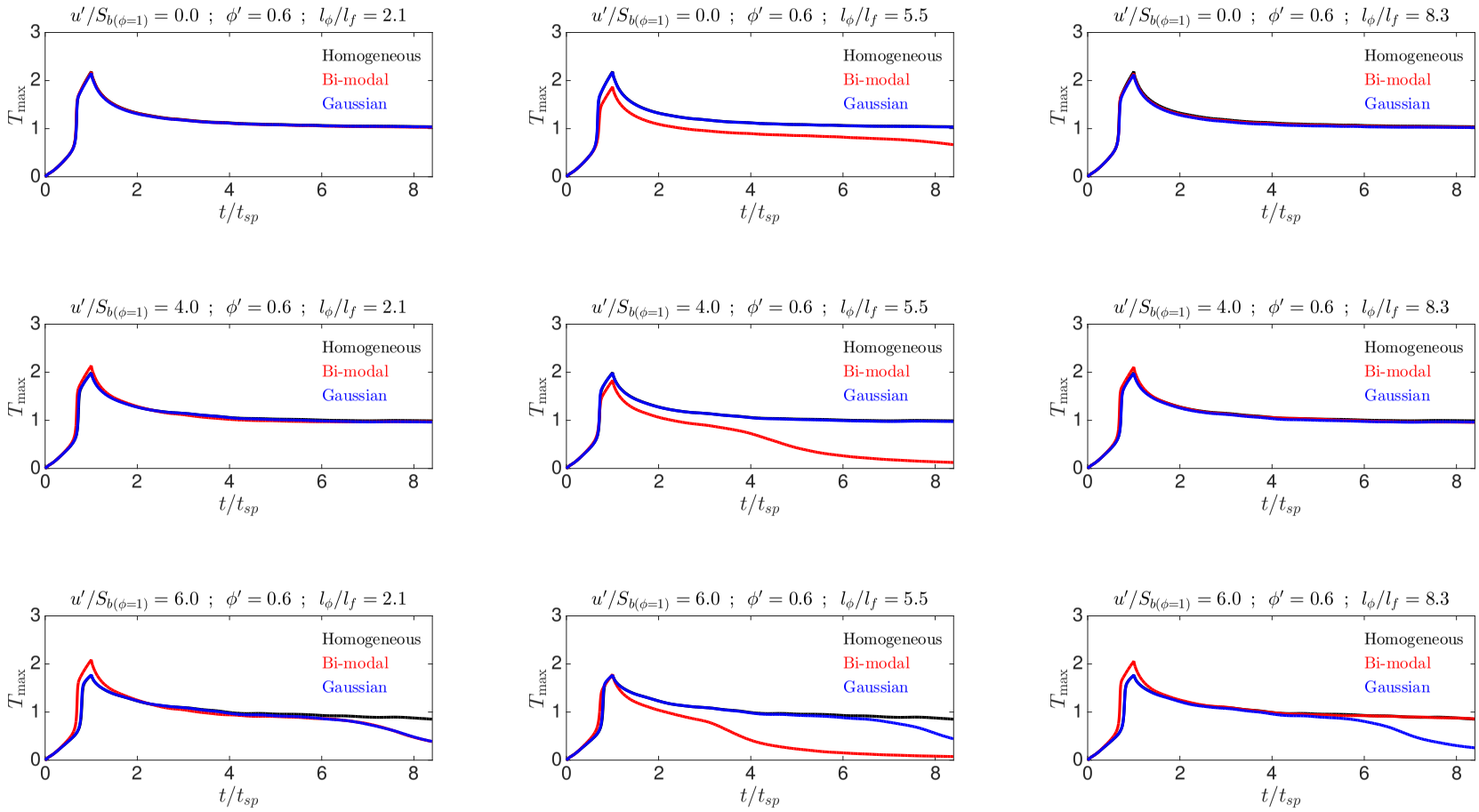

Figure 5.14: Temporal distribution of $T_{\max}$ for all the cases with $\phi' = 0.6$ listed in Table 5.2. [where 1^{st} column shows $l_\phi/l_f = 2.1$; 2^{nd} column shows $l_\phi/l_f = 5.5$; 3^{rd} column shows $l_\phi/l_f = 8.3$; additionally 1^{st} row shows $\frac{u'}{S_{b(\phi=1)}} = 0.0$; 2^{nd} row shows $\frac{u'}{S_{b(\phi=1)}} = 4.0$; 3^{rd} row shows $\frac{u'}{S_{b(\phi=1)}} = 6.0$]

in premixed mode of combustion despite the nature of initial mixture distributions, but non-premixed combustion can also be found in some pockets. Moreover, Figure 5.16 shows that the percentage of heat release from the premixed mode of combustion is greater in the initial Gaussian mixture distribution cases in comparison to the initial Bi-modal distribution case. The percentage of heat release arising from the non-premixed mode of combustion increases with increasing ϕ' for both types of initial mixture distribution, but this effect is more prominent in the initial Bi-modal distribution cases in comparison to the initial Gaussian distribution cases. Furthermore, the percentage of heat release arising from non-premixed combustion (i.e. $I_c < 0$) decreases with decreasing (increasing) values of ${}^{l_\phi}/_{l_f}$ (ϕ'), as a result of improved mixing due to high magnitudes of N_ξ, and this effect is more prominent in the initial Bi-modal distribution cases than in the initial Gaussian distribution cases (see Figures 5.7 and 5.22).

The evolution of mixing process can be illustrated from analysing the temporal evolution of PDF(ϕ) and ϕ', which are shown in Figures 5.18, 5.19 and 5.20 demonstrating effects of ${}^{l_\phi}/_{l_f}$, ϕ' and $\frac{u'}{S_{b(\phi=1)}}$ respectively. It can be clearly seen from Figure 5.11 that the initial Gaussian distribution cases, there is a very high probability of finding $\phi \approx \langle\phi\rangle = 1.0$ in comparison with the corresponding initial Bi-modal distribution cases. The equivalence ratio PDFs for the initial Gaussian distribution cases show peak values at $\phi \approx \langle\phi\rangle = 1.0$, whereas the cases with initial Bi-modal distribution show higher probabilities of finding $\phi < \langle\phi\rangle$ and $\phi > \langle\phi\rangle$ than the initial Gaussian distribution cases. Figures 5.18, 5.19 and 5.20 indicate that the PDF(ϕ) for the initial Bi-modal distribution cases approaches an approximate Gaussian distribution as time progresses due to mixing, whereas the width of PDF(ϕ) decreases, and the peak values of PDF(ϕ) at $\phi \approx \langle\phi\rangle = 1.0$ increases with time in the initial Gaussian distribution cases.

It can be demonstrated from Figure 5.18 that the ϕ' decay rate is faster (slower) for lower (higher) values of ${}^{l_\phi}/_{l_f}$. This ϕ' decay rate is more prominent in initial Gaussian distribution than in initial Bi-modal distribution. As previously demonstrated in Section 5.2.4 the mean scalar dissipation rate of mixture fraction N_ξ is likely assume higher magnitudes for the smaller values of ${}^{l_\phi}/_{l_f}$ for a given value of ξ'.

This can be confirmed from the temporal evolution of ϕ'(see Figure 5.18), where high (low) rate of mixing (i.e. faster (slower) decay rate of ϕ') is associated with smaller (bigger) values of ${}^{l_\phi}/_{l_f}$. Furthermore Figure 5.19 shows that mixing is quicker for lower values of ϕ'. An observation from Figure 5.19 suggests that the comparison

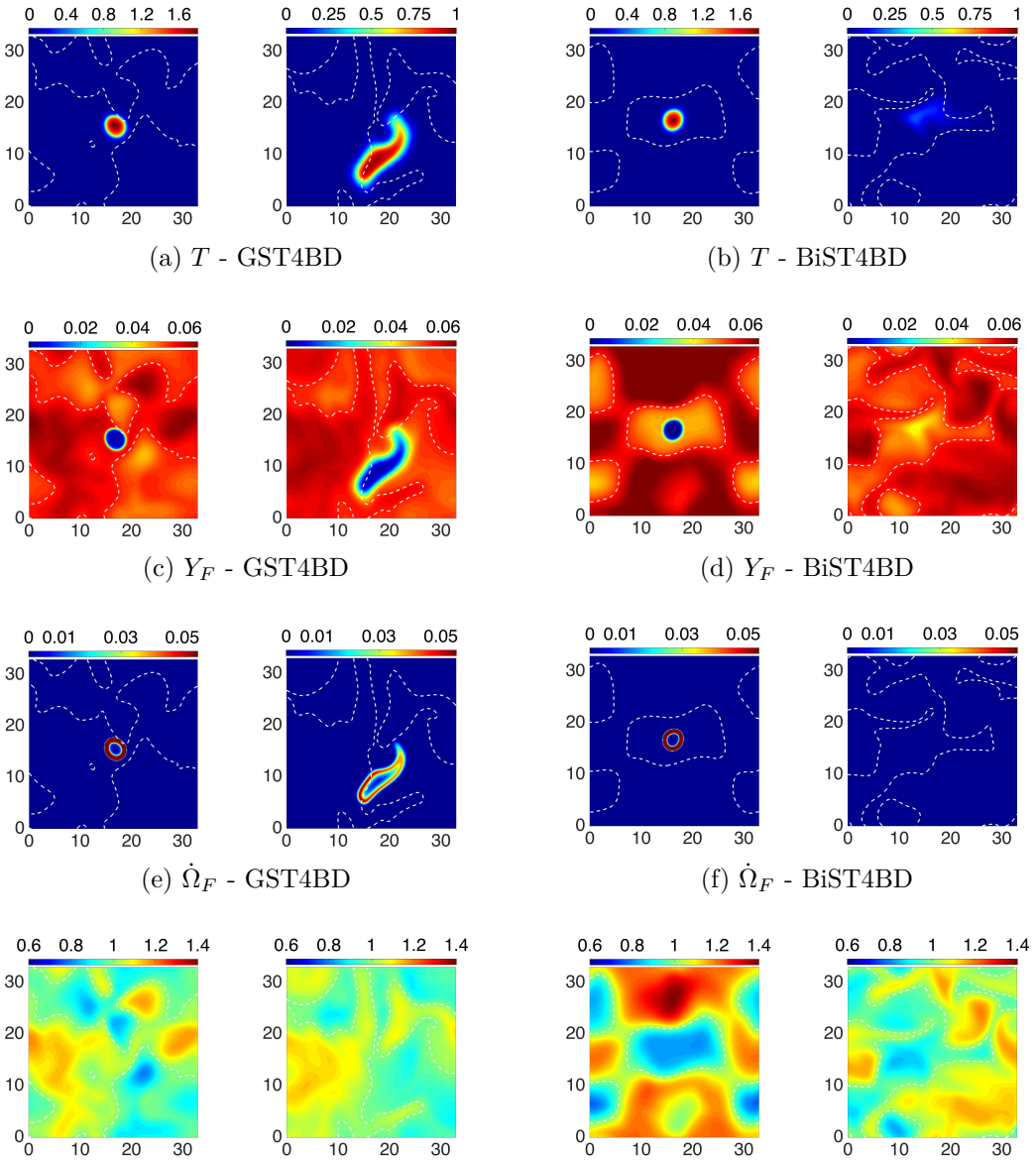

(a) T - GST4BD (b) T - BiST4BD

(c) Y_F - GST4BD (d) Y_F - BiST4BD

(e) $\dot{\Omega}_F$ - GST4BD (f) $\dot{\Omega}_F$ - BiST4BD

(g) ϕ - GST4BD (h) ϕ - BiST4BD

Figure 5.15: Distribution of T (1^{st} row), Y_F (2^{nd} row), $\dot{\Omega}_F$ (3^{rd} row) and ϕ (4^{th} row) on the central $x_1 - x_2$ plane for the cases GST4BD (1^{st} and 2^{nd} column) and BiST4BD (1^{st} and 2^{nd} column). The white broken like shows $\xi = \xi_{st}$. Additionally 1^{st}& 3^{rd} column showing $t = 1.05t_{sp}$, 2^{nd}& 4^{th} column showing $t = 8.40t_{sp}$.

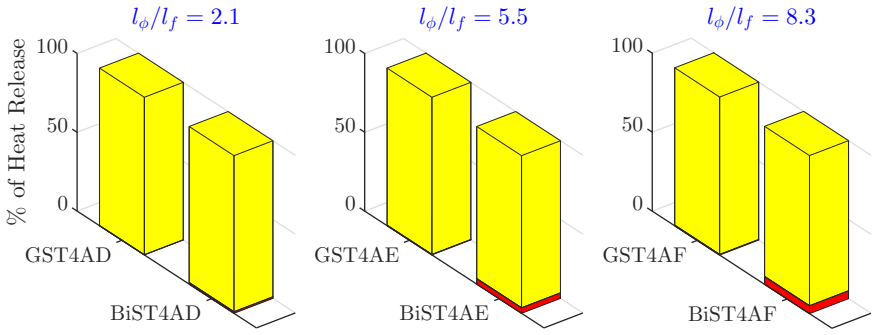

Figure 5.16: Percentage of overall heat release arising from premixed and non-premixed mode of combustion at $t = 8.40t_{sp}$ for the selected cases with $\phi' = 0.2$ and ${}^{u'}/_{S_{b(\phi=1)}} = 4.0$ from Table 5.2 demonstrating effects of ${}^{l_\phi}/_{l_f}$ on the mode of combustion.
[where premixed (i.e. $I_c > 0$) and non-premixed (i.e. $I_c < 0$) mode of combustion]

between initial Gaussian and Bi-modal distribution the probability of finding $\phi \approx 1.0$ ($\phi \neq 1.0$) is greater for the cases with initial Gaussian (Bi-modal) distribution then those with initial bi-modal (Gaussian) distribution for a given set of values of ${}^{l_\phi}/_{l_f}$ and $\frac{u'}{S_{b(\phi=1)}}$.

The probability of finding high value of N_ξ increases with increasing $\frac{u'}{S_{b(\phi=1)}}$, because the turbulent straining acts to generate the scalar gradient, which further increasing the rate of micro-mixing [128, 130]. This findings are consistent with high ϕ' decay rate as associated with high values of $\frac{u'}{S_{b(\phi=1)}}$ (see Figure 5.20).

5.3.4 Reaction-Diffusion Balance Analysis of the Flame Kernels

It is important that heat release due to chemical reaction should overcome the heat transfer from the hot gas kernel in order to obtain self-sustained combustion following successful ignition. Although Figure 5.13 provides clear indication of the possibility of obtaining self-sustained or failed combustion at $t \gg t_{sp}$, it is important to understand the physical processes which lead to self-sustained combustion in some cases and flame extinction in some other conditions. In that respect, related terms to explain reaction-diffusion balance analysis are already been defined in Sections 3.4.2.1 and 4.3.4. Figure 5.21 demonstrates the evolution of $T_{\max}$ for both initial Gaussian and

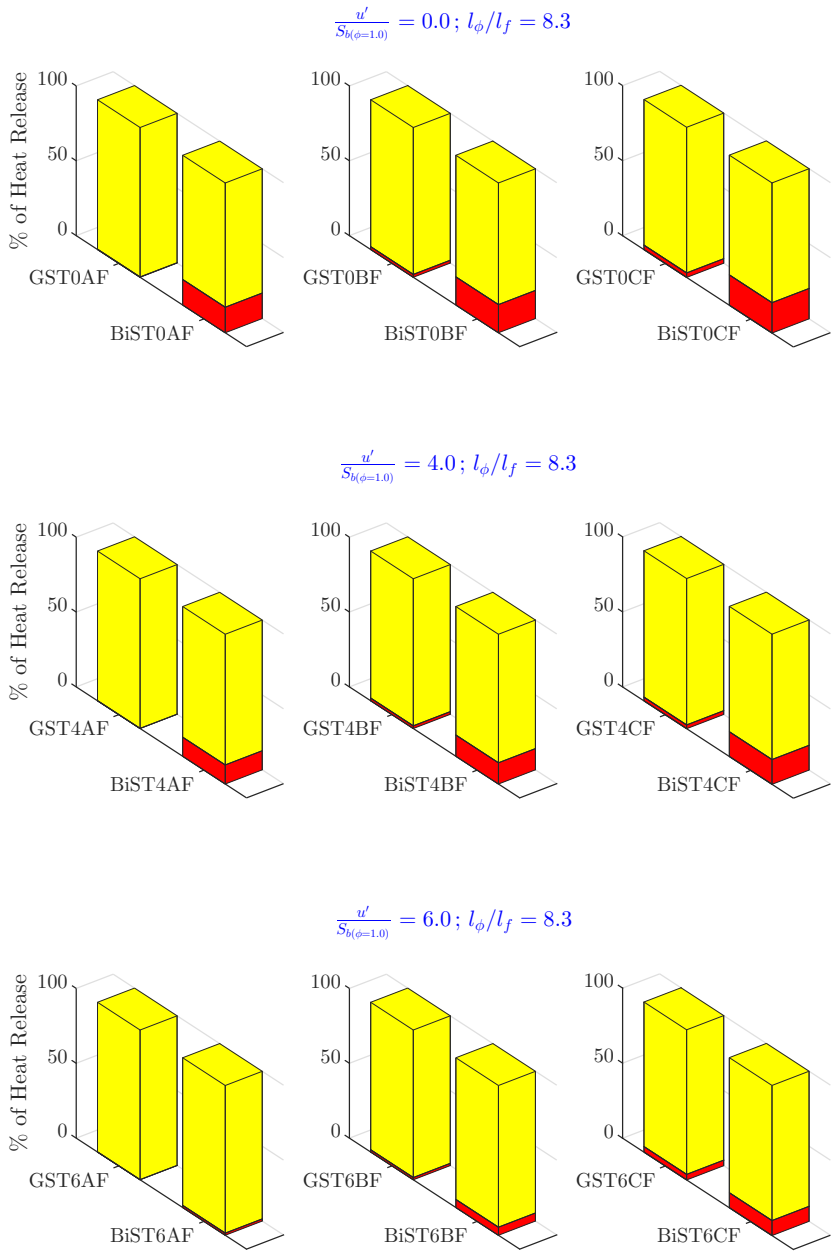

Figure 5.17: Percentage of overall heat release arising from premixed and non-premixed mode of combustion at $t = 8.40t_{sp}$ for the selected cases with $l_\phi/l_f = 8.3$ from Table 5.2 demonstrating effects of ϕ' and $\frac{u'}{S_{b(\phi=1)}}$ on the mode of combustion.
[where premixed (i.e. $I_c > 0$) and non-premixed (i.e. $I_c < 0$) mode of combustion]

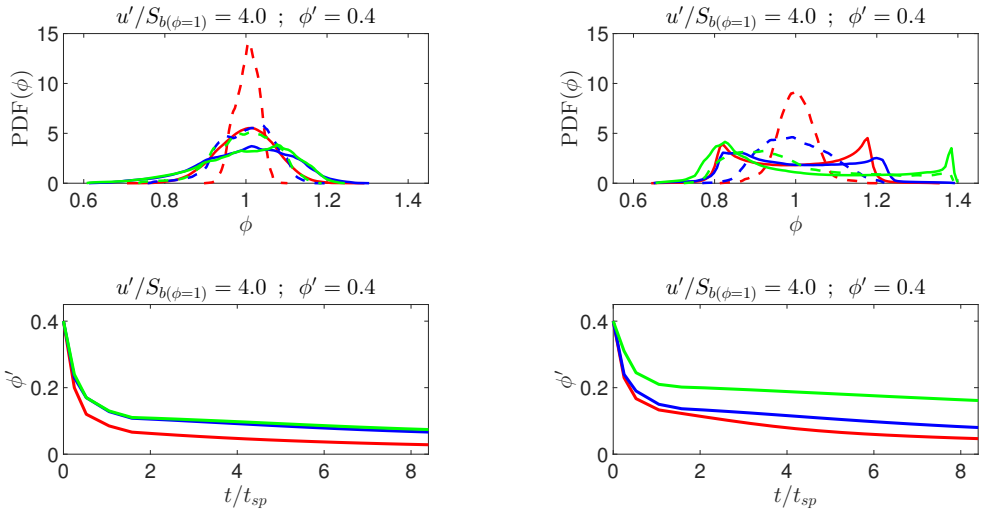

Figure 5.18: Temporal evolution of the PDF of ϕ at $t = 1.05t_{sp}$ (solid line) and $t = 8.40t_{sp}$ (broken line) and temporal evolution of ϕ' evaluated over the entire domain for the selected cases with $\phi' = 0.4$ and $\frac{u'}{S_{b(\phi=1)}} = 4.0$ (1^{st} column showing Gaussian distribution and 2^{nd} column showing Bi-modal distribution)from listed in Table 5.2.
[where ${}^{l_\phi}/_{l_f} = 2.1$; ${}^{l_\phi}/_{l_f} = 5.5$; ${}^{l_\phi}/_{l_f} = 8.3$ demonstrating effects of ${}^{l_\phi}/_{l_f}$ on mixing process].

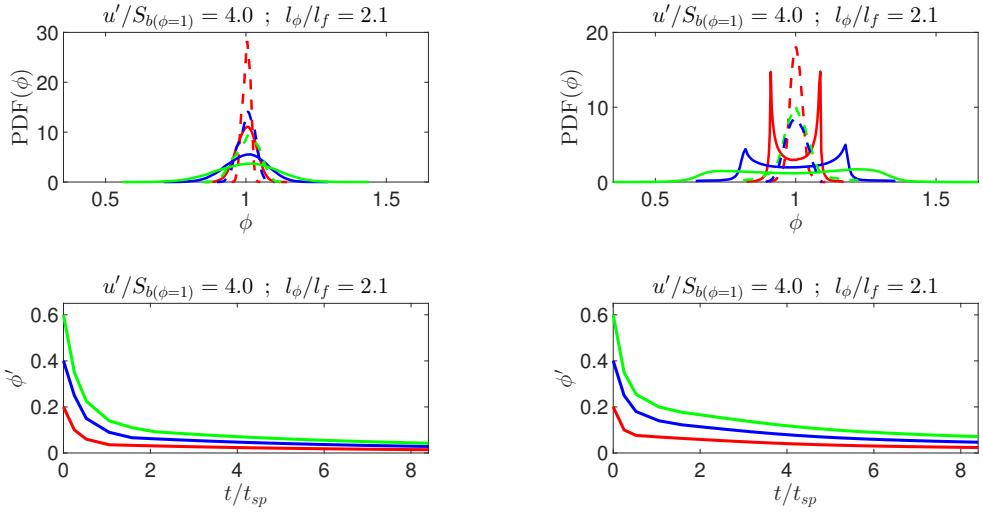

Figure 5.19: Temporal evolution of the PDF of ϕ at $t = 1.05t_{sp}$ (solid line) and $t = 8.40t_{sp}$ (broken line) and temporal evolution of ϕ' evaluated over the entire domain for the selected cases with ${}^{l_\phi}/_{l_f} = 2.1$ and $\frac{u'}{S_{b(\phi=1)}} = 4.0$ (1^{st} column showing Gaussian distribution and 2^{nd} column showing Bi-modal distribution)from listed in Table 5.2.
[where $\phi' = 0.2$; $\phi' = 0.4$; $\phi' = 0.6$ demonstrating effects of ϕ' on mixing process].

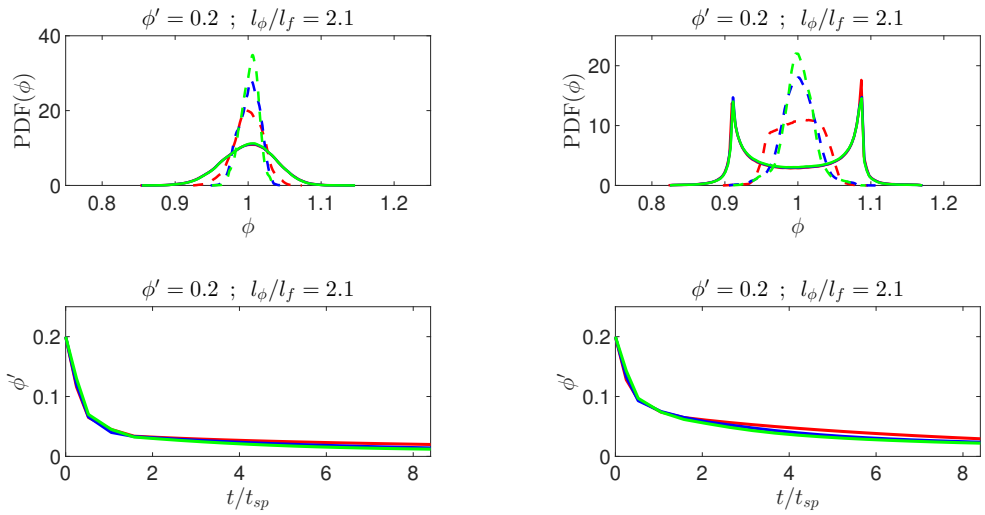

Figure 5.20: Temporal evolution of the PDF of ϕ at $t = 1.05t_{sp}$ (solid line) and $t = 8.40t_{sp}$ (broken line) and temporal evolution of ϕ' evaluated over the entire domain for the selected cases with $\phi' = 0.2$ and ${}^{l_\phi}/_{l_f} = 2.1$ (1^{st} column showing Gaussian distribution and 2^{nd} column showing Bi-modal distribution)from listed in Table 5.2. [where $\frac{u'}{S_{b(\phi=1)}} = 0.0$; $\frac{u'}{S_{b(\phi=1)}} = 4.0$; $\frac{u'}{S_{b(\phi=1)}} = 6.0$ demonstrating effects of $\frac{u'}{S_{b(\phi=1)}}$ on mixing process].

Bi-modal distribution for case with $\phi' = 0.4$; ${}^{l_\phi}/_{l_f} = 5.5$; $\frac{u'}{S_{b(\phi=1)}} = 4.0$ along with the mean variation of different terms of reaction progress variable (i.e. c) at different time instances.

It can be seen from Figure 5.21 that for a given case ($\phi' = 0.4$; ${}^{l_\phi}/_{l_f} = 5.5$; $\frac{u'}{S_{b(\phi=1)}} = 4.0$) with initial Gaussian mixture distribution exhibits successful self-sustained combustion, whereas the same case with initial Bi-modal mixture distribution leads to flame extinction at $t > t_{sp}$. Recently, Hesse *et al.* [93] and Malkeson and Chakraborty [129] studied statistics of density-weighted displacement speed of reaction progress variable isosurfaces for stratified mixture combustion arising from localised forced ignition of turbulent planar coflowing jet using DNS. Additionally Hesse *et al.* [93] and Malkeson and Chakraborty [129] concluded that contribution of term (A_H [ ]) arising due to mixture inhomogeneity remains small in magnitude in comparison to the magnitudes of reaction term ($\dot{w}_c$ [ ]) and molecular diffusion term ($\nabla\cdot(\rho D\nabla c)$ [ ]) throughout the flame brush at all stages of flame evolution. The results shown in Figure 5.21 confirms these findings, and also consistent with previous experimental findings [64, 176].

Moreover, it can be seen from Figure 5.21 that the reaction rate term $\dot{w}_c$ [ ]

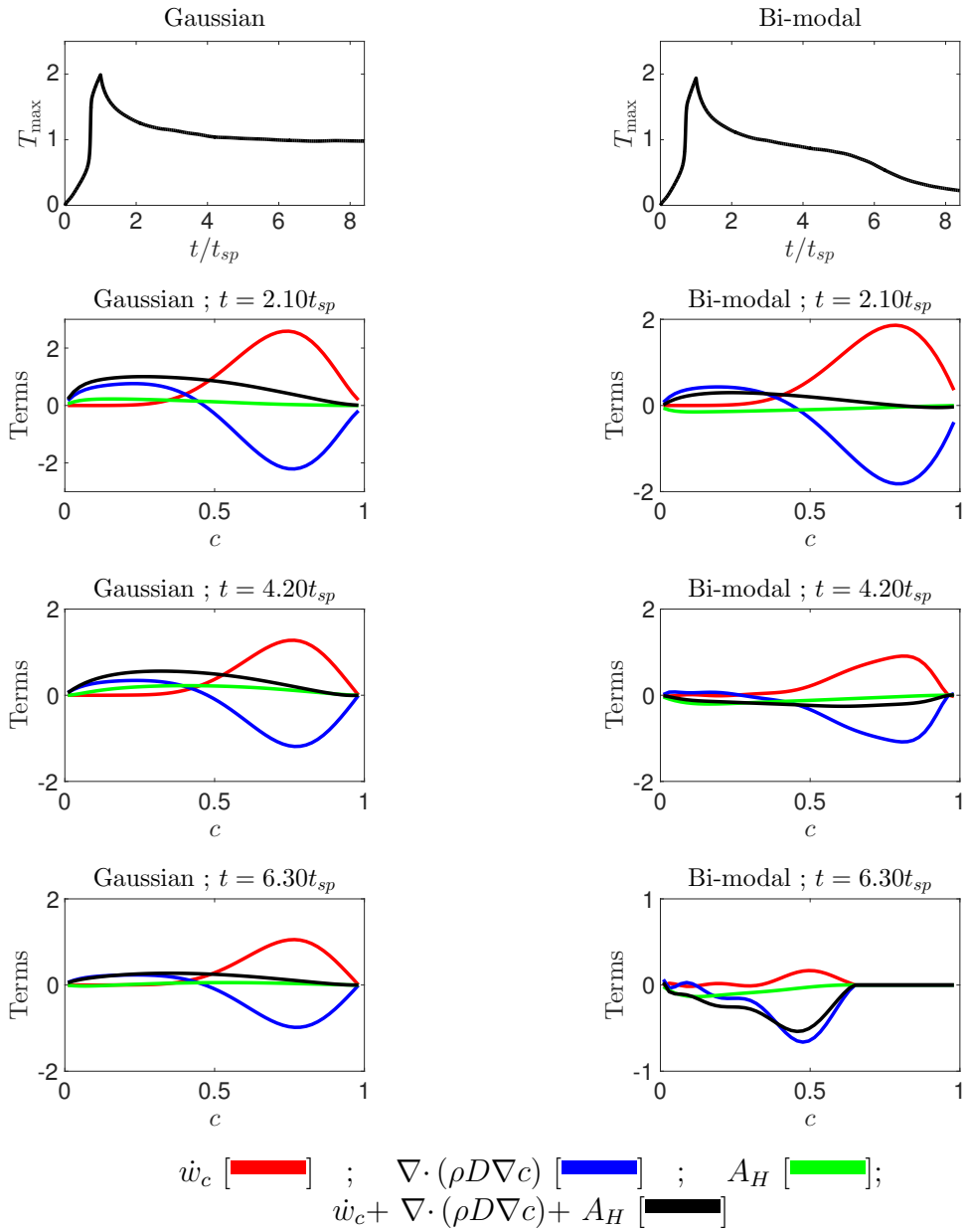

Figure 5.21: Temporal evolution of $T_{\max}$ along with the mean variation of different terms with reaction progress variable (i.e. c) at different time instances for cases with $\phi' = 0.4$; ${}^{l_\phi}/_{l_f} = 5.5$; $\frac{u'}{S_{b(\phi=1)}} = 4.0$.

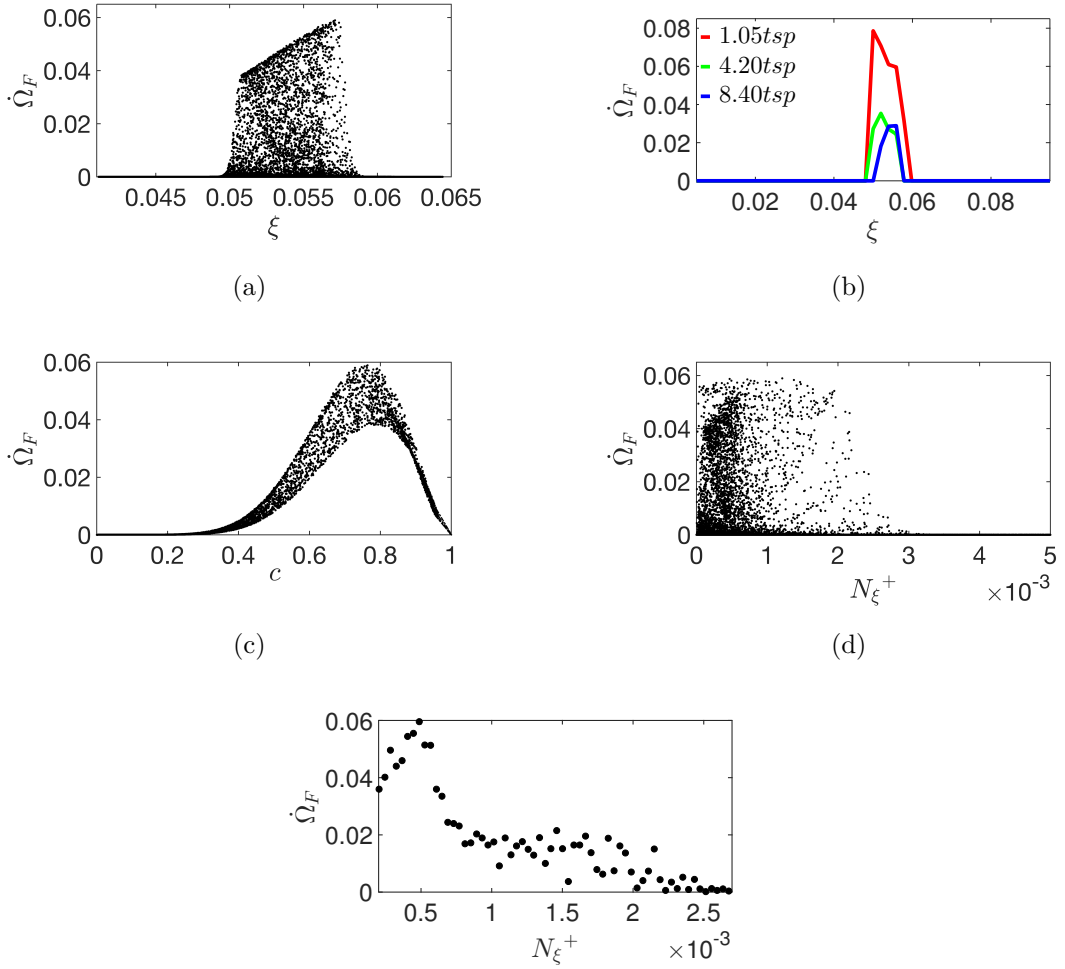

Figure 5.22: (a) Scatter of $\dot{\Omega}_F$ with ξ, (b) Variation of $\dot{\Omega}_F$ conditional on ξ for $0.01 \leq c \leq 0.99$, (c) Scatter of $\dot{\Omega}_F$ with c, (d) Scatter of $\dot{\Omega}_F$ with N_ξ^+, (e) Variation of $\dot{\Omega}_F$ conditional on N_ξ^+ for $0.7 \leq c \leq 0.9$ for case GST4BF (initial Gaussian distribution; $\langle\phi\rangle = 1.0$; $\frac{u'}{S_{b(\phi=1)}} = 4$; $\phi' = 0.4$; $l_\phi/l_f = 8.3$).

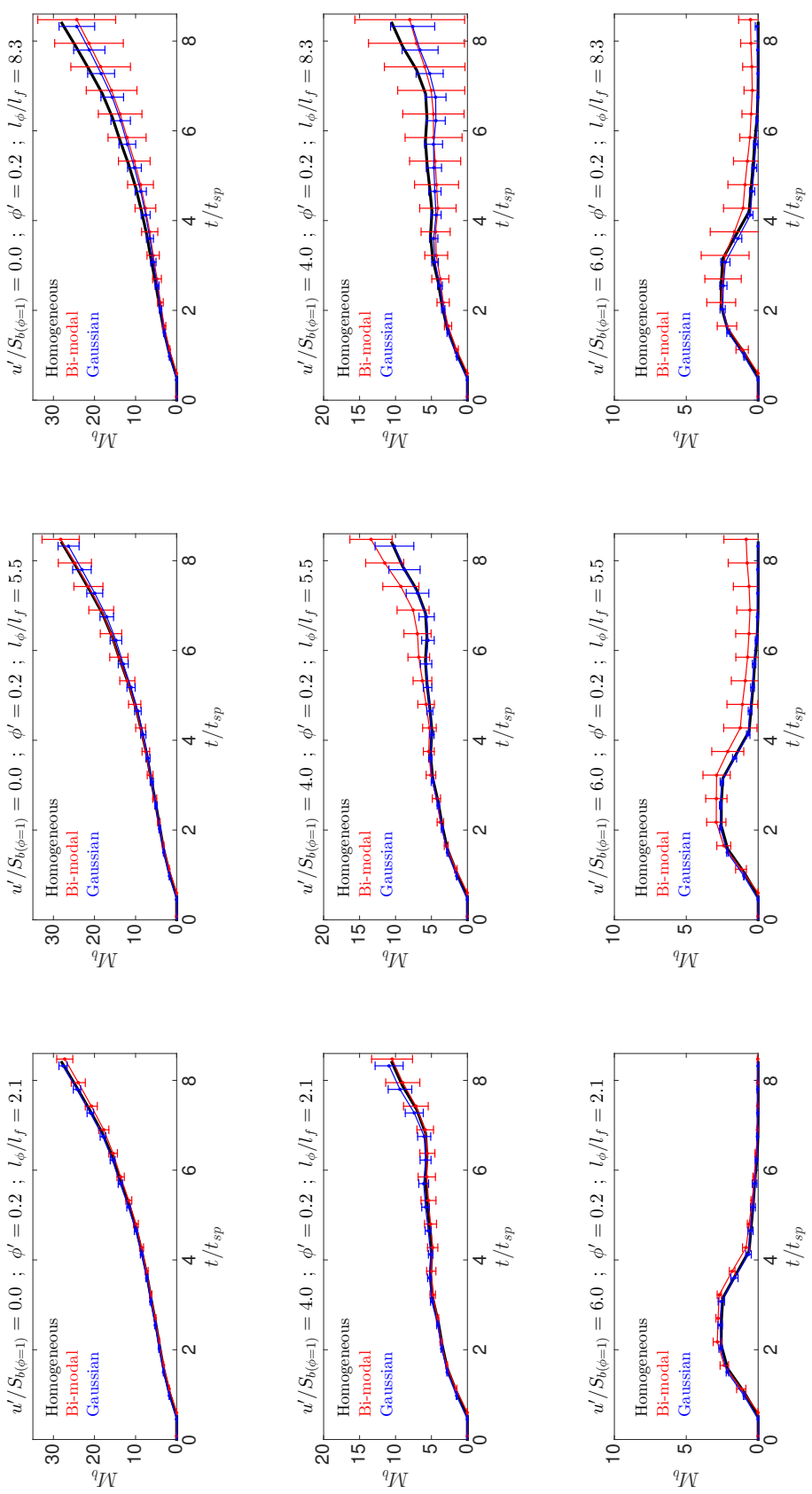

Figure 5.23: Temporal evolution of the mean and standard deviation of M_b for all the cases with $\phi' = 0.2$ listed in Table 5.2. [where 1st column shows $l_\phi/l_f = 2.1$; 2nd column shows $l_\phi/l_f = 5.5$; 3rd column shows $l_\phi/l_f = 8.3$; additionally 1st row shows $\frac{u'}{S_{b(\phi=1)}} = 0.0$; 2nd row shows $\frac{u'}{S_{b(\phi=1)}} = 4.0$; 3rd row shows $\frac{u'}{S_{b(\phi=1)}} = 6.0$]

remains negligible in unburned side and increases sharply towards the burned side before decreasing to zero in the fully burned products. The magnitude of the reaction rate term $\dot{w}_c$ [▬] decreases with time, once the igniter is switched off, which is principally due to the decrease in fuel reaction rate magnitude with time. It can be seen from Figure 5.21 that the magnitudes of $\dot{w}_c$ [▬] and $\nabla\cdot(\rho D\nabla c)$ [▬] decreases with time. However, the magnitude of $\nabla\cdot(\rho D\nabla c)$ [▬] becomes greater than $\dot{w}_c$ [▬] for $t \geq 4.20t_{sp}$ for Bi-modal distribution case but the opposite remains true for the Gaussian distribution case.

Moreover, one needs to have a positive mean value of $\dot{w}_c + \nabla\cdot(\rho D\nabla c) + A_H$ [▬] to ensure a situation where chemical reaction overcomes molecular diffusion, which is essential for self-sustained flame propagation. By contrast, a negative mean value of $\dot{w}_c + \nabla\cdot(\rho D\nabla c) + A_H$ [▬] indicates molecular diffusion overcoming chemical process which makes the flame to retreat and eventually quench. It can be seen from Figure 5.21 that the mean $\dot{w}_c + \nabla\cdot(\rho D\nabla c) + A_H$ [▬] becomes negative for $t \geq 4.20t_{sp}$ which eventually leads to flame extinction for initial Bi-modal distribution case considered here. By contrast, the mean value of $\dot{w}_c + \nabla\cdot(\rho D\nabla c) + A_H$ [▬] remains positive for initial Gaussian distribution case and thus ensures self-sustained combustion.

5.3.5 Statistical Behaviour of Fuel Reaction Rate Magnitude ($\dot{\Omega}_F$)

In order to analyse the effects of mixture stratification on the burned gas mass once the successful ignition taken place, the reaction zone structure of the flames initiated by the localised forced ignition needs to be known. The specific cases (i.e. $\langle\phi\rangle = 1.0$, $\frac{u'}{S_{b(\phi=1)}} = 4$, $\phi' = 0.4$, $l_\phi/l_f = 8.3$) have been chosen to compare this analysis for different nature of initial mixture distributions. Figure 5.22 shows analyses for case GST4BF with initial Gaussian mixture distribution whereas Figure 5.7 (Section 5.2.5) shows analyses for case BiST4BF with initial Bi-modal mixture distribution. Here, the statistical behaviour of fuel reaction rate magnitude for both initial mixture distribution (i.e. Bi-modal and Gaussian) cases is qualitatively similar (compare analyses for a case GST4BF in Figure 5.22 with the same analyses for a case BiST4BF in Figure 5.7). Therefore, the discussion has not been repeated here for the sake of brevity.

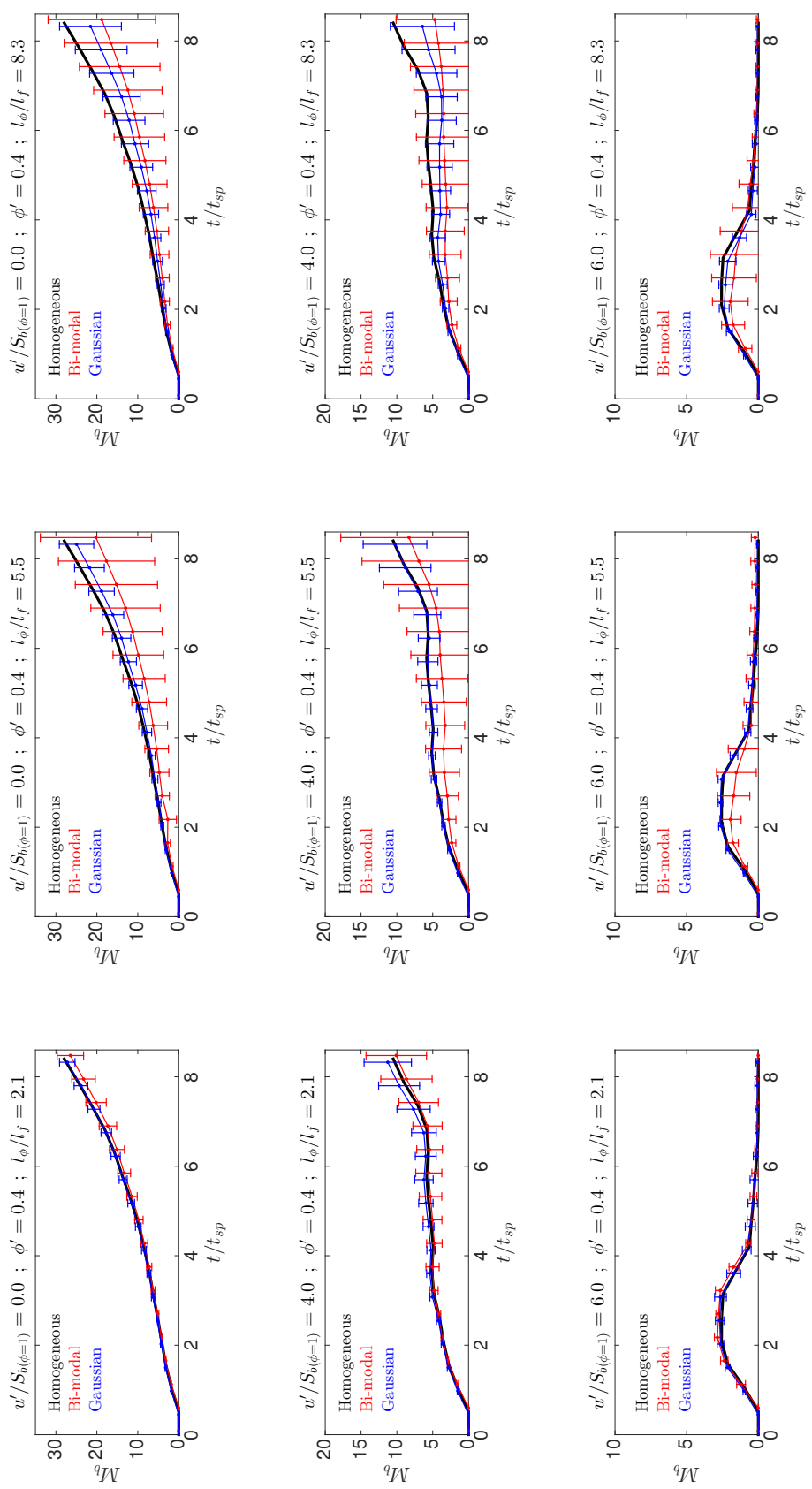

Figure 5.24: Temporal evolution of the mean and standard deviation of M_b for all the cases with $\phi' = 0.4$ listed in Table 5.2. [where 1st column shows $l_\phi/l_f = 2.1$; 2nd column shows $l_\phi/l_f = 5.5$; 3rd column shows $l_\phi/l_f = 8.3$; additionally 1st row shows $\frac{u'}{S_{b(\phi=1)}} = 0.0$; 2nd row shows $\frac{u'}{S_{b(\phi=1)}} = 4.0$; 3rd row shows $\frac{u'}{S_{b(\phi=1)}} = 6.0$]

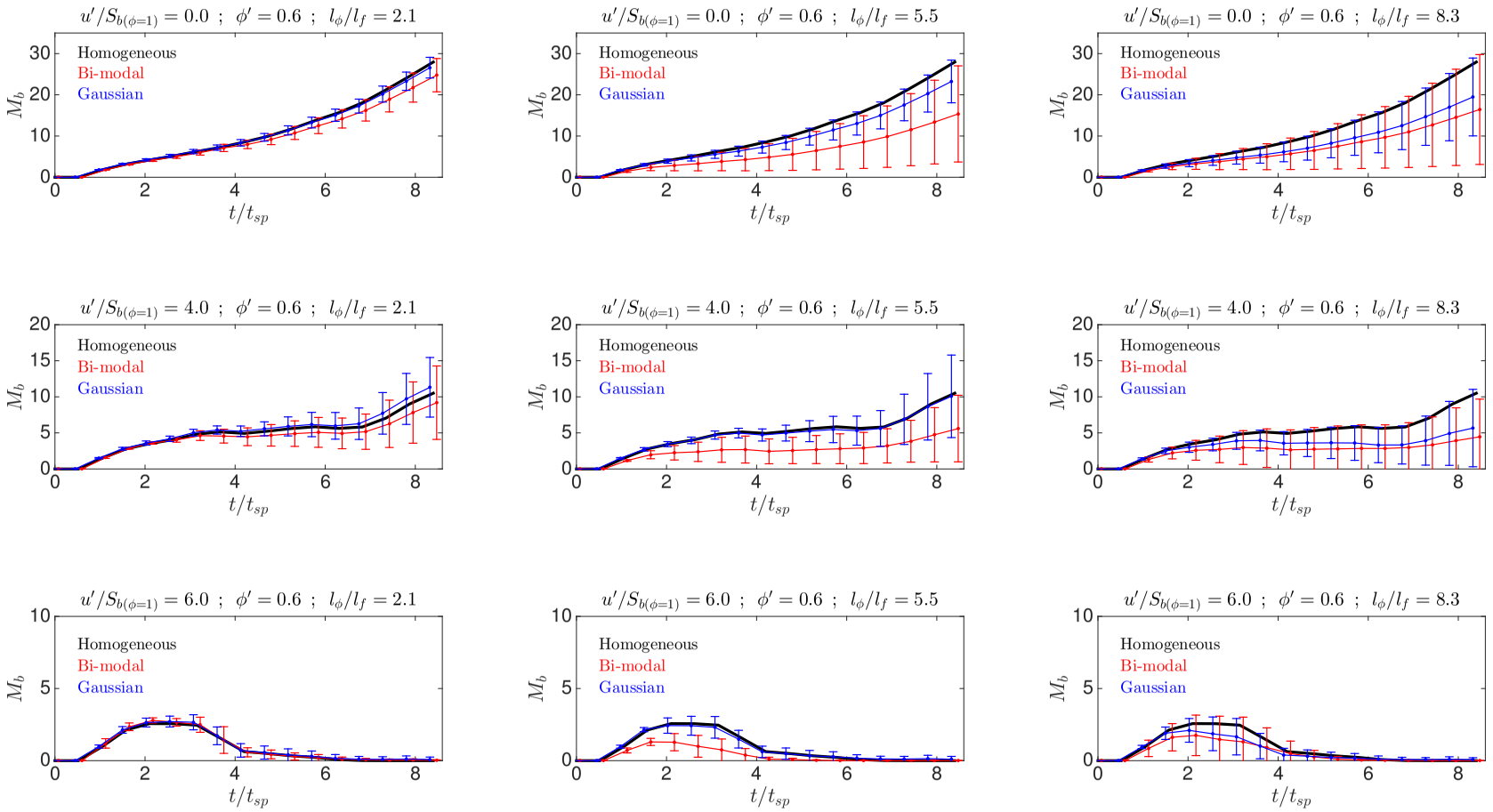

Figure 5.25: Temporal evolution of the mean and standard deviation of M_b for all the cases with $\phi' = 0.6$ listed in Table 5.2. [where 1$^{\text{st}}$ column shows $^{l_\phi}/_{l_f} = 2.1$; 2$^{\text{nd}}$ column shows $^{l_\phi}/_{l_f} = 5.5$; 3$^{\text{rd}}$ column shows $^{l_\phi}/_{l_f} = 8.3$; additionally 1$^{\text{st}}$ row shows $\frac{u'}{S_{b(\phi=1)}} = 0.0$; 2$^{\text{nd}}$ row shows $\frac{u'}{S_{b(\phi=1)}} = 4.0$; 3$^{\text{rd}}$ row shows $\frac{u'}{S_{b(\phi=1)}} = 6.0$]

5.3.6 Extent of Burning

As previously described the extent of burning can be characterised by the burned gas mass M_b (see Section 4.2.5). The temporal evolution of the mean and standard deviation of M_b for all the cases from Table 5.2 are shown in Figures 5.23, 5.24 and 5.25 for $\phi' = 0.2$, $\phi' = 0.4$ and $\phi' = 0.6$ cases respectively. The comprehensive discussion and observed physical explanation for effects of u' and ϕ' are previously presented in Section 5.2.6 for initial Bi-modal mixture distribution. The effects of u' and ϕ' on the extent of burning remains qualitatively similar in the cases with initial Gaussian mixture distribution, and thus have not been repeated. However effects of l_ϕ/l_f on the extent of burning has been found different for different initial mixture distributions. Therefore the results and discussion presented here only focuses on explaining the effects of different mixture distribution on the extent of burning.

It is evident from Figure 5.23 that the mean values of M_b remains comparable for the all quiescent cases for all values of l_ϕ/l_f in both Gaussian and Bi-modal mixture distributions. A comparison between Figures 5.23, 5.24 and 5.25 reveals that the initial Gaussian distribution with initial $u'/s_{b(\phi)} = 6.0$ fails to sustain combustion once the ignitor is switched off irrespective of the initial values of ϕ' and l_ϕ/l_f, on the other side the initial Bi-modal distribution with initial $\phi' = 0.2$ and $l_\phi/l_f = 5.5$; $l_\phi/l_f = 8.3$ exhibit self-sustained combustion for $u'/s_{b(\phi)} = 6.0$. As previously seen in Figure 5.18 that Bi-modal distribution shows higher probability of finding $1.0 \leq \phi \leq 1.10$ than in the Gaussian distribution case for $l_\phi/l_f > 2.1$. Therefore the heat release due to combustion for the initial Bi-modal distribution cases with initial $\phi' = 0.2$ and $l_\phi/l_f = 5.5$; $l_\phi/l_f = 8.3$ is greater than that in the corresponding Gaussian distribution cases and thus initial Bi-modal distribution cases show self-sustained combustion whereas flame extinction takes place for the initial Gaussian distribution cases at $t \gg t_{sp}$.

Additionally, in the initial Bi-modal distribution with $\phi' = 0.2$, the mean M_b attains lower (higher) magnitudes for $l_\phi/l_f = 2.1$ ($l_\phi/l_f = 5.5$). But on the opposite side the mean M_b attains lower (higher) magnitudes for $l_\phi/l_f = 5.5$ ($l_\phi/l_f = 8.3$) for $\phi' = 0.4$; $\phi' = 0.6$ cases with initial Bi-modal distribution. However for the initial Gaussian distribution cases the the mean M_b increases with decreasing values of l_ϕ/l_f irrespective values of ϕ'. The highly reactive $1.0 \leq \phi \leq 1.10$ mixtures are more likely to be available with decreasing value of l_ϕ/l_f due to more efficient mixing for smaller l_ϕ/l_f(see Figure 5.18).

For the $l_\phi/l_f = 8.3$ cases the clouds of mixture inhomogeneity are relatively big as seen from Figure 5.11 and this leads to high probability of encountering almost

homogeneous mixture in the vicinity of the centre of igniter, which leads to large variation of M_b between different realisations. Although these variation of M_b between different realisations are lower in Gaussian distribution cases than those in Bi-modal distributions. In the initial Bi-modal distribution the PDF peaks of fuel lean and fuel rich mixtures are segregated from each other and situated away from the $\langle\phi\rangle = 1.0$ (see Figures 3.3 and 5.11), and the mixing take place in the presence of turbulent and combustion process (i.e. the probability of finding reactive region $1.10 \geq \phi \geq 1.0$ are relatively low than initial Bi-modal distribution). On the other side in initial Gaussian distribution the probability of finding homogeneous mixture with $\phi \approx 1.0$ is high.

The effects of nature of initial mixture distributions for different values of $\frac{u'}{S_{b(\phi=1)}}$, ϕ' and ${}^{l_\phi}/_{l_f}$ on the outcome of the localised forced ignition is summarised in Table 5.3. The observation from Table 5.3 reveals that the initial Bi-modal mixture distribution cases offer higher probability of obtaining self-sustained combustion in comparison to the cases with initial Gaussian mixture distribution for $\phi' = 0.2$ and $\frac{u'}{S_{b(\phi=1)}} = 6.0$. It is evident from Figures 5.23, 5.24 and 5.25 that both initial Gaussian and Bi-modal distribution cases with smaller ϕ' and ${}^{l_\phi}/_{l_f}$ behave similar to homogeneous mixtures due to rapid mixing process, where the sharp decay rate of ϕ' has been observed (see Figures 5.18 and 5.19). Importantly, Figures 5.23, 5.24 and 5.25 reveals that it is possible to achieve M_b value higher than the corresponding homogeneous mixture case for a given realisation for both initial Gaussian and Bi-modal distributions. Although this propensity is higher in the initial Bi-modal distribution cases than in the Gaussian cases (see Table 5.3). The variation of M_b for different realisations increases with increasing values of ϕ' and ${}^{l_\phi}/_{l_f}$ for both initial Gaussian and Bi-modal distributions.

The variability of burned gas mass is routinely obtained in the cylinder of IC engines due to cycle-to-cycle variations [155]. The findings from Figures 5.23, 5.24, 5.25 and Table 5.3 reveal that the degree of variability of burning depends not only on ϕ' and l_ϕ but also on the nature of mixture distribution, which can be manipulated by careful design of the nozzle and fuel injection systems in IC engines. Moreover, in-cylinder turbulence together with injection characteristics can influence the values of u', ϕ' and l_ϕ and thus the effective control of mixing characteristics in IC engine combustion chamber can potentially play a pivotal role in ensuring successful ignition and reducing the variability associated with the ignition event. Furthermore, the minimum ignition energy for ensuring self-sustained combustion subsequent to successful ignition in turbulent stratified mixtures is not only dependent on u', ϕ' and l_ϕ but also on the nature of mixture distribution. This suggests that the success or failure of

$\langle\phi\rangle = 1.0$ [S]												
Gaussian [G] Bi-modal [B]												
	$\phi' = 0.2$			$\phi' = 0.4$				$\phi' = 0.6$				
	$\frac{l_\phi}{l_f} = 2.1$	$\frac{l_\phi}{l_f} = 5.5$	$\frac{l_\phi}{l_f} = 8.3$	$\frac{l_\phi}{l_f} = 2.1$	$\frac{l_\phi}{l_f} = 5.5$	$\frac{l_\phi}{l_f} = 8.3$		$\frac{l_\phi}{l_f} = 2.1$	$\frac{l_\phi}{l_f} = 5.5$	$\frac{l_\phi}{l_f} = 8.3$	
$\frac{u'}{S_{b(\phi=1)}} = 0.0$	G:[✓][↓] B:[✓][↓]	G:[✓][↓] B:[✓][↑]	G:[✓][↓] B:[✓][↓]	G:[✓][↓] B:[✓][↓]	G:[✓][↓] B:[✓][↓]	G:[✓][↓] B:[✓][↓]		G:[✓][↓] B:[✓][↓]	G:[✓][↓] B:[✓][↓]	G:[✓][↓] B:[✓][↓]	
$\frac{u'}{S_{b(\phi=1)}} = 4.0$	G:[✓][↑] B:[✓][↓]	G:[✓][↓] B:[✓][↑]	G:[✓][↓] B:[✓][↓]	G:[✓][↑] B:[✓][↓]	G:[✓✓][↓] B:[✗]	G:[✓][↓] B:[✓][↓]		G:[✓][↑] B:[✓][↓]	G:[✓][↓] B:[✗]	G:[✓][↓] B:[✓][↓]	
$\frac{u'}{S_{b(\phi=1)}} = 6.0$	G:[✗] B:[✓][↑]	G:[✗] B:[✓][↑]	G:[✗] B:[✓][↑]	G:[✗] B:[✗]	G:[✗] B:[✗]	G:[✗] B:[✓][↑]		G:[✗] B:[✗]	G:[✗] B:[✗]	G:[✗] B:[✗]	
Homogeneous cases ST0 [✓], ST4 [✓], ST6 [✗]											

Table 5.3: Summary of outcomes for the self-sustained combustion for all cases.

[✓]: self-sustained combustion has been obtained,
[✗]: self-sustained combustion has not been obtained,
[↑]: mean value of M_b is higher than homogeneous case,
[↓]: mean value of M_b is lower than homogeneous case

the ignition of stratified mixtures is a highly random event and that a small change in mixture distribution has the potential to alter the outcome.

5.3.7 Summary

Here the Section 5.3 investigates the effects of initial mixture distribution on early stages of combustion following localised forced ignition of globally stoichiometric (i.e. $\langle\phi\rangle = 1.0$) stratified mixtures using 3D DNS simulations. The cases with initial Gaussian mixture distribution provides lower probability of finding non-premixed pockets in comparison to initial Bi-modal distribution where the probability of finding $I_c < 0$ are higher. In both initial distribution for given ${}^{l_\phi}/_{l_f}$, increasing ϕ' leads to decreasing burning rate. However, the influence of ${}^{l_\phi}/_{l_f}$ on the extent of burning is shows non-monotonic behaviour and dependent of ϕ' for initial Bi-modal distribution. By contrast, for initial Gaussian distribution cases, the decreasing values of ${}^{l_\phi}/_{l_f}$ leads to an increase in extent of burning for all initial values of ϕ' considered here. Moreover the detrimental effects of high values of $\frac{u'}{S_{b(\phi=1)}}$ on the extent of burning remains unchanged irrespective of ϕ' , ${}^{l_\phi}/_{l_f}$ and the nature of initial mixture distribution. The findings discussed in Sections 5.3 demonstrate that the effects of $\frac{u'}{S_{b(\phi=1)}}$, ϕ' and ${}^{l_\phi}/_{l_f}$ on the early stages of combustion following successful forced ignition of globally stoichiometric stratified mixtures are dependent on the nature of initial equivalence ratio distribution.

5.4 Effects of Turbulent Integral Length Scale

This section focuses on understanding the influence of normalised turbulent integral length scale (i.e. ${}^{L_{11}}/_{l_f}$) on localised forced ignition of globally stoichiometric stratified mixture. This section starts with introducing the parametric analysis and brief discussion on turbulence decay profile. Modification adopted in ignition parameters for this investigation are then introduced. The results on mixing statistics and extent of burning are presented and discussed to highlight the effects of turbulent integral length scale. Finally, the section ends with short summary.

Here the turbulent integral length scale is taken to be [24, 41]:

$$L_{11} = \frac{1}{\sqrt{2\pi}}\left(\frac{1}{\kappa_0}\right) \tag{5.9}$$

where L_{11} is the longitudinal integral length scale, κ_0 is the wavenumber corre-

sponding to the peak turbulent kinetic energy. Table 5.4 shows parametric variation across different parameters, and thus 169 simulations (162 stratified mixture cases + 7 homogeneous mixtures) have been conducted here. The case names are chosen in such manner so that S stands for globally stoichiometric stratified mixtures; G and Bi stands for initial Gaussian and Bi-modal distribution of ϕ; T0, T4 and T6 indicate increasing turbulent level; A, B, and C indicate increasing values of ϕ'; D, E, and F denote increasing values of ${}^{l_\phi}/_{l_f}$; and X, Y and Z denote increasing values of ${}^{L_{11}}/_{l_f}$ (e.g. GST0ADX corresponds to a case for initial Gaussian distribution of globally stoichiometric stratified mixtures with values of $\frac{u'}{S_{b(\phi=1)}} = 0.0$; $\phi' = 0.2$; ${}^{l_\phi}/_{l_f} = 2.1$; ${}^{L_{11}}/_{l_f} = 2.52$).

	$\langle\phi\rangle = 1.0$ [S]		
	Gaussian [G] Bi-modal [Bi]		
	${}^{L_{11}}/_{l_f} = 2.52$ [X]		
	$\phi' = 0.2$ [A]		
	$\frac{l_\phi}{l_f} = 2.1$ [D]	$\frac{l_\phi}{l_f} = 5.5$ [E]	$\frac{l_\phi}{l_f} = 8.3$ [F]
$\frac{u'}{S_{b(\phi=1)}} = 0.0$ [T0]	GST0ADX	GST0AEX	GST0AFX
$\frac{u'}{S_{b(\phi=1)}} = 4.0$ [T4]	GST4ADX	GST4AEX	GST4AFX
$\frac{u'}{S_{b(\phi=1)}} = 6.0$ [T6]	GST6ADX	GST6AEX	GST6AFX
Homogeneous cases ST0, ST4X, ST6X, ST4Y, ST6Y, ST4Z, ST6Z			

Table 5.4: List of parameters to analyse effects of ${}^{L_{11}}/_{l_f}$ in globally stoichiometric (i.e. $\langle\phi\rangle = 1.0$) stratified mixtures. (Replace [G] with [Bi] for initial Bi-modal mixture distribution, Replace [A] with [B] and [C] for $\phi' = 0.4$ and $\phi' = 0.6$, Replace [X] with [Y] and [Z] for ${}^{L_{11}}/_{l_f} = 3.36$ and ${}^{L_{11}}/_{l_f} = 4.20$)

The numerical formulation remains similar to as described in Section 5.2 except for ignition parameters modification. The findings from Chapter 4 (Section 4.2) suggests that the judicious choice of R (characteristic width of ignition energy deposition profile) and a_{sp} (ignition energy) can lead to obtaining self-sustained combustion for given flow and mixture conditions. In order to obtain self-sustained combustion following successful ignition for all the cases in Table 5.4, the ignition parameters has been taken as: $a_{sp} = 9.20$, $b_{sp} = 0.2$ and $R = 1.55 l_f$ (see Section 3.3). For the sake of brevity, only the mixing statistics and extent of burning results are presented and

discussed here in order to demonstrate the effects of $^{L_{11}}/_{l_f}$.

Figure 5.26 shows turbulence decay profile for all turbulence homogeneous cases listed in Table 5.4. It can be seen from Figure 5.26 that for a given value of u', a decrease in L_{11} leads to more decay of u'.

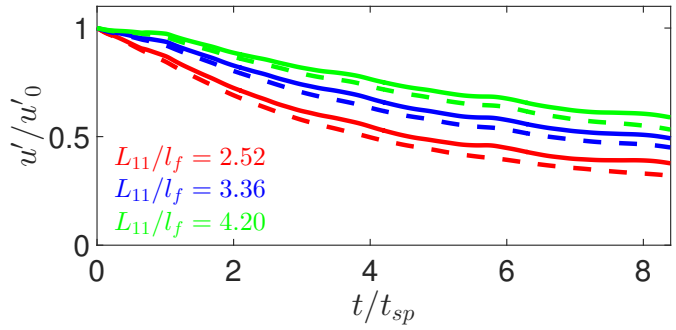

(where $\frac{u'}{S_{b(\phi=1)}} = 4.0$ [——] and $\frac{u'}{S_{b(\phi=1)}} = 6.0$ [– – – –])

Figure 5.26: Turbulence decay profile showing all turbulence homogeneous cases listed in Table 5.4.

5.4.1 Mixing Statistics

It has already been observed in Section 5.2 that the decreasing rate of ϕ' increases with increasing values of u', as the turbulent straining is generating a scalar gradient, which leads to increase in the N_ξ, which further leads to a greater rate of micro-mixing [130, 149]. These effectively leads to two opposing Mixing Effects for L_{11}:

MEff-1: For a given value of u', a decrease in L_{11} leading to strengthening of turbulent straining which acts to increase the magnitude of N_ξ. The increase in scalar dissipation rate with decreasing L_{11} acts to augment micro-mixing rate which eventually leads to more rapid decay in ϕ'.

MEff-2: A smaller value of L_{11} gives rise to higher values of dissipation rate of kinetic energy $\left(\epsilon \sim \frac{u'^3}{L_{11}}\right)$ and thus u' decays more rapidly for small values of L_{11}, which in turn gives rise to small values of eddy diffusivity as $D_t \sim u' L_{11}$ and acts to reduce the rate of mixing.

The effects of initial mixture distribution (i.e. Gaussian and Bi-modal distribution), ϕ', $^{l_\phi}/_{l_f}$ and u' on evolution of mixing during combustion process has already been discussed before in previous Sections 5.2.4 and 5.3.3. Therefore this section 5.4.1

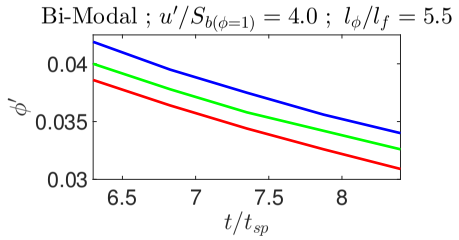

(a) BiST4AEX, BiST4AEY, BiST4AEZ

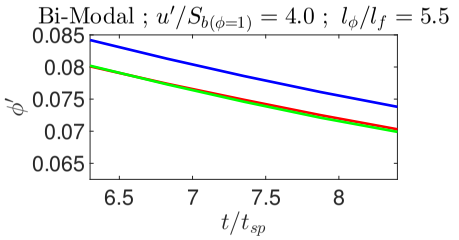

(b) BiST4BEX, BiST4BEY, BiST4BEZ

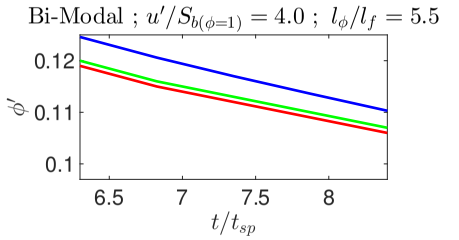

(c) BiST4CEX, BiST4CEY, BiST4CEZ

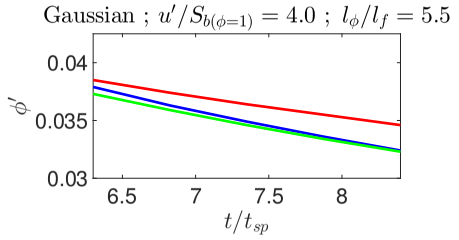

(d) GST4AEX, GST4AEY, GST4AEZ

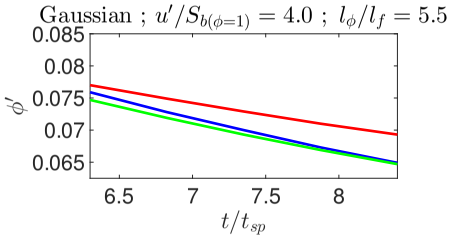

(e) GST4BEX, GST4BEY, GST4BEZ

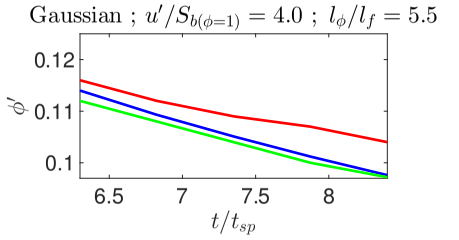

(f) GST4CEX, GST4CEY, GST4CEZ

Figure 5.27: Temporal evolution of ϕ' evaluated over the entire domain for selected cases with ${}^{l_\phi}/_{l_f} = 5.5$ and $\frac{u'}{S_{b(\phi=1)}} = 4.0$ from the Table 5.4.
($^{L_{11}}/_{l_f} = 2.52$; $^{L_{11}}/_{l_f} = 3.36$; $^{L_{11}}/_{l_f} = 4.20$; 1^{st} column showing $\phi' = 0.2$; 2^{nd} column showing $\phi' = 0.4$ and 3^{rd} column showing $\phi' = 0.6$)

only concentrate on effects of $^{L_{11}}/_{l_f}$ on the mixing process. Figures 5.27 and 5.28 demonstrates the temporal evolution of ϕ' evaluated over entire domain for selected cases from Table 5.4. It is worth nothing that both Figures 5.27 and 5.28 show the ϕ' decay rate with limited range of $^{t}/_{t_{sp}}$ in order to distinguish the effects of $^{L_{11}}/_{l_f}$. It can be seen from Figure 5.27 that, for a given case (initial Bi-modal distribution, $^{u'}/_{S_{b(\phi)}} = 4.0$, $^{l_\phi}/_{l_f} = 5.5$, $\phi' = 0.2$), when $^{L_{11}}/_{l_f}$ reduces from $3.36l_f$ to $2.52l_f$, the MEff-1 effect dominates the MEff-2 effect. However for the same case, when $^{L_{11}}/_{l_f}$ reduces from $4.20l_f$ to $3.36l_f$, MEff-2 effect takes place. Furthermore Figure 5.27 shows that MEff-2 effect is stronger in cases with initial Gaussian distribution with $^{u'}/_{S_{b(\phi)}} = 4.0$, $^{l_\phi}/_{l_f} = 5.5$, $\phi' = 0.2$. Moreover, Figure 5.27 shows that mixing is quicker for lower values of ϕ' (consistent with the results in Section 5.3). For a given value of $\phi' = 0.2$ and $\frac{u'}{S_{b(\phi=1)}} = 4.0$, effects of $^{L_{11}}/_{l_f}$ is more noticeable in initial Bi-modal distribution case than Gaussian case (see and compare first column of Figure 5.28).

5.4.2 Extent of Burning

It is important to study the effects of $^{L_{11}}/_{l_f}$ on the burning rate once successful ignition has taken place. The temporal evolution of M_b for all the cases from Table 5.4 are shown in Figures 5.29 and 5.30 for $\phi' = 0.2$ and $\phi' = 0.6$ cases. Here the cases with initial $\phi' = 0.4$ are not explicitly shown because the temporal evolution of M_b for these cases are mostly qualitatively similar to that of the initial $\phi' = 0.6$ cases.

In previous Section 5.3.3, it has already been concluded that the probability of finding high value of N_ξ increases with increasing $^{u'}/_{S_{b(\phi)}}$ [128, 130]. Furthermore, an increase in L_{11} decreases the dissipation rate of kinetic energy ($\epsilon \sim \frac{u'^3}{L_{11}}$, see Section 2.5.1) and thus reduces the decay rate of u' (see Figure 5.26). These effectively gives rise to two opposing Burning Effects:

BEff-1: The flame kernel gets increasingly wrinkled with increasing values of u' which increases flame surface area and overall burning rate.

BEff-2: An increase in u' value due to weak decay of turbulence for large L_{11} increases the eddy diffusivity ($D_t \sim u'L_{11}$), which acts to increase heat loss from the hot gas kernel and reduces the kernel size, which further reduces the burned gas mass.

For ease of understanding, the Section 5.4.2 is subdivided in to three parts namely in order to explain the effects of L_{11} for a given set of parameter values on the extent of burning.

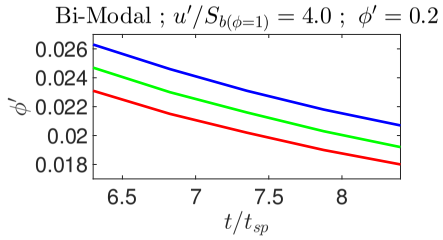

(a) BiST4ADX, BiST4ADY, BiST4ADZ

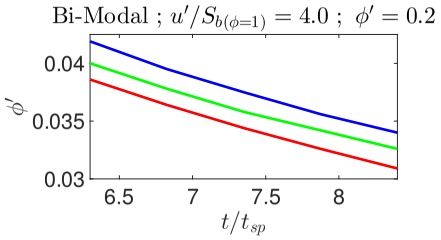

(b) BiST4AEX, BiST4AEY, BiST4AEZ

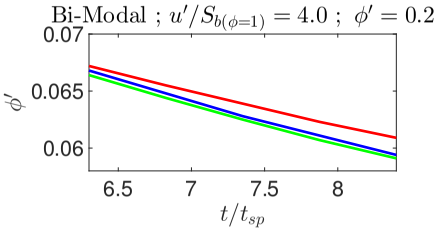

(c) BiST4AFX, BiST4AFY, BiST4AFZ

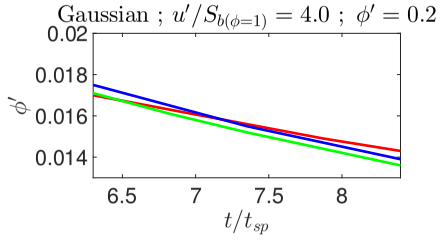

(d) GST4ADX, GST4ADY, GST4ADZ

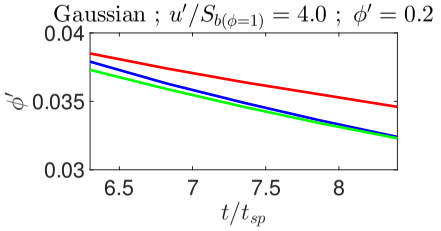

(e) GST4AEX, GST4AEY, GST4AEZ

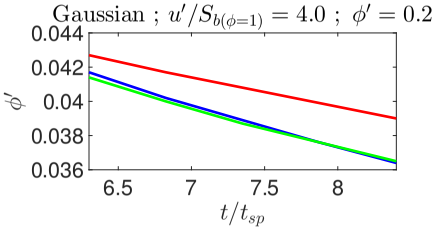

(f) GST4AFX, GST4AFY, GST4AFZ

Figure 5.28: Temporal evolution of ϕ' evaluated over the entire domain for selected cases with $\phi' = 0.2$ and $\frac{u'}{S_{b(\phi=1)}} = 4.0$ from the Table 5.4.
($L_{11}/l_f = 2.52$; $L_{11}/l_f = 3.36$; $L_{11}/l_f = 4.20$; 1^{st} column showing $l_\phi/l_f = 2.1$; 2^{nd} column showing $l_\phi/l_f = 5.5$ and 3^{rd} column showing $l_\phi/l_f = 8.3$)

Effects of L_{11} on different values of ${}^{l_\phi}/_{l_f}$

Figure 5.29 shows that M_b for majority cases with ${}^{L_{11}}/_{l_f} = 3.36$ attains higher values in comparison to cases with ${}^{L_{11}}/_{l_f} = 2.52$ and ${}^{L_{11}}/_{l_f} = 4.20$ for a given $\phi' = 0.2$ and ${}^{l_\phi}/_{l_f} = 2.1$. And, this effect remains consistent for even higher values of ${}^{l_\phi}/_{l_f}$. When L_{11} increases from $2.52l_f$ to $3.36l_f$, the BEff-1 effect overcomes the BEff-2 effect, which shows higher burning rate associated with ${}^{L_{11}}/_{l_f} = 3.36$ for a given set of values (i.e. $\phi' = 0.2$, all values of ${}^{l_\phi}/_{l_f}$ and despite the initial mixture distribution). However, when L_{11} increases from $3.36l_f$ to $4.20l_f$, the BEff-2 effect overcomes the BEff-1 effect. The effects of ${}^{l_\phi}/_{l_f}$ on extent of burning remains similar as observed in Section 5.3.6. Moreover, Figure 5.30 demonstrate that the case with initial values ${}^{l_\phi}/_{l_f} = 5.5$ are attaining lower burned gas mass than the cases with initial value ${}^{l_\phi}/_{l_f}$ =2.1, 8.3 for $\phi' = 0.6$ in initial Bi-modal distribution irrespective values of ${}^{L_{11}}/_{l_f}$. Furthermore, for initial Bi-modal distribution the higher values of M_b has been found for ${}^{l_\phi}/_{l_f} = 5.5$,$\phi' = 0.2$, $\frac{u'}{S_{b(\phi=1)}} = 6.0$ and ${}^{l_\phi}/_{l_f} = 8.3$, $\phi' = 0.6$, $\frac{u'}{S_{b(\phi=1)}} = 6.0$ cases with ${}^{L_{11}}/_{l_f} = 3.36$ (see Figures 5.29 and 5.30), in comparison to initial Gaussian distribution.

Effects of L_{11} on different values of ϕ'

It can be seen from Figures 5.29 and 5.30 that an increase in ϕ' leads to reduction in burned gas mass for all values of ${}^{l_\phi}/_{l_f}$ (consistent with Section 5.2.6). Furthermore, for both values of $\phi' = 0.4$, 0.6 , cases with ${}^{L_{11}}/_{l_f} = 2.52$ shows higher burning rate in comparison to ${}^{L_{11}}/_{l_f} = 3.36$ for a given set of values ${}^{l_\phi}/_{l_f} = 2.1$; $\frac{u'}{S_{b(\phi=1)}} = 6.0$; initial Bi-modal distribution. Moreover, cases with a given set of values ${}^{l_\phi}/_{l_f} = 5.5$; $\frac{u'}{S_{b(\phi=1)}} = 6.0$; initial Bi-modal distribution, increasing value of ϕ' leads to reduction in burned gas mass irrespective values of ${}^{L_{11}}/_{l_f}$ (see Figures 5.29 and 5.30).

Effects of L_{11} on different nature of initial mixture distribution

Figure 5.29 (first column) shows that highest extent of burning has been found for initial Gaussian distribution for $\phi' = 0.2$; ${}^{l_\phi}/_{l_f} = 2.1$; ${}^{L_{11}}/_{l_f} = 3.36$; for all values of u'. However, initial Bi-modal distribution exhibits higher extent of burning with increasing value of ${}^{l_\phi}/_{l_f}$ for $\phi' = 0.2$; ${}^{L_{11}}/_{l_f} = 3.36$; for all values of u' in comparison to initial Gaussian distribution. For higher values of $\phi' = 0.6$ (Figure 5.30), the initial Gaussian distribution suggests higher burning rate in comparison to initial Bi-modal distribution for ${}^{l_\phi}/_{l_f} = 5.5$; all values of u' irrespective values of ${}^{L_{11}}/_{l_f}$.

It is worth nothing that the results shown in Sections 5.4.1 and 5.4.2 represent

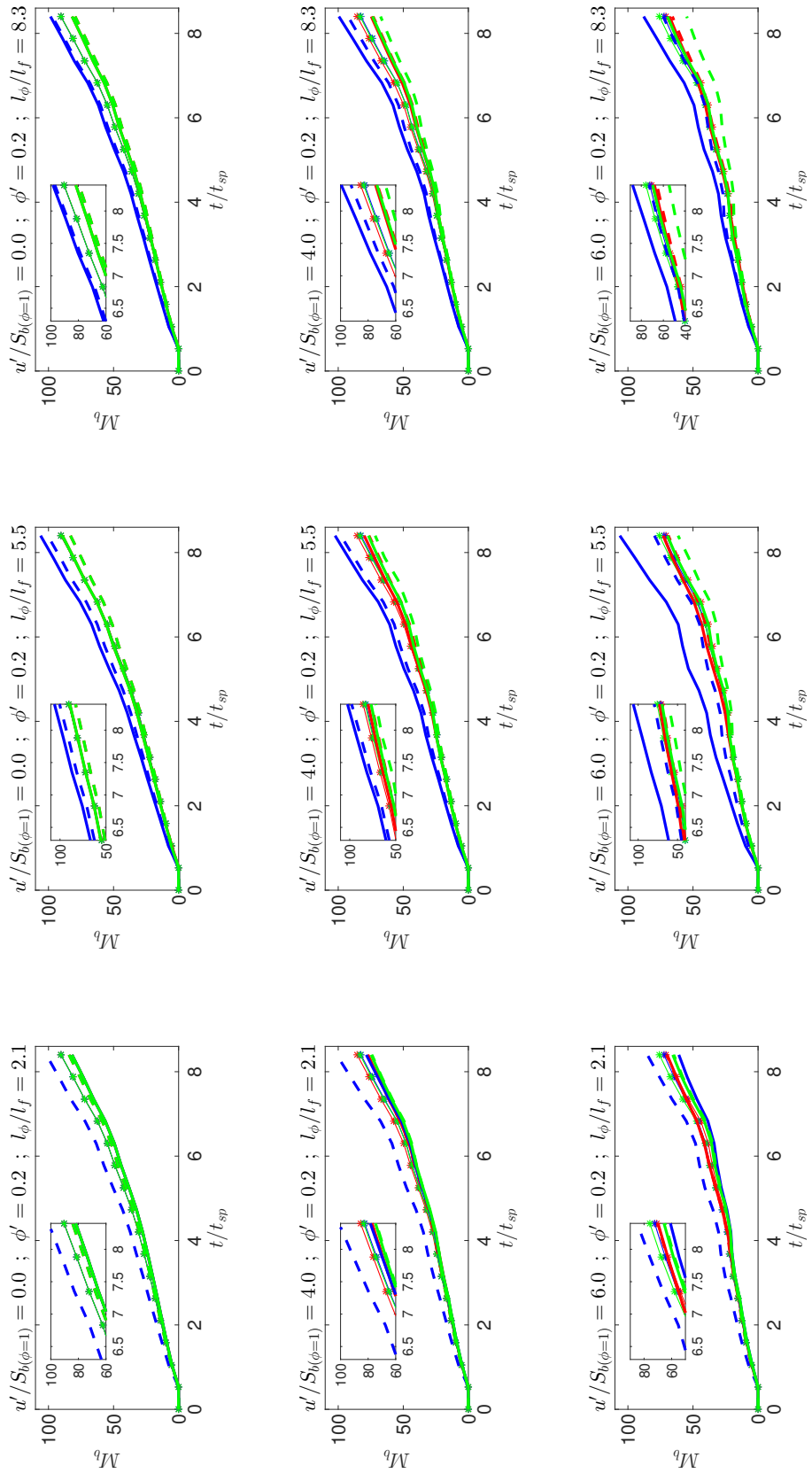

Figure 5.29: Temporal evolution of the M_b for all the cases with $\phi' = 0.2$ listed in Table 5.4. [where $L_{11}/l_f = 2.52$; $L_{11}/l_f = 3.36$; $L_{11}/l_f = 4.20$; 1^{st} column shows $l_\phi/l_f = 2.1$; 2^{nd} column shows $l_\phi/l_f = 5.5$; 3^{rd} column shows $l_\phi/l_f = 8.3$; additionally 1^{st} row shows $\frac{u'}{S_{b(\phi=1)}} = 0.0$; 2^{nd} row shows $\frac{u'}{S_{b(\phi=1)}} = 4.0$; 3^{rd} row shows $\frac{u'}{S_{b(\phi=1)}} = 6.0$, additionally the respected homogeneous cases are shown with marker [—*—] and Gaussian: [- - - - -] and Bi-modal: [———];]

for only a given realisation of the initial distribution of ϕ. Therefore, further analysis with different realisations of the initial distribution of ϕ is needed to conclude rigorous effects of ${}^{L_{11}}/_{l_f}$ on mixing and extent of burning. Furthermore, the observed results suggest that the Mixing effects (i.e. MEff-1 and MEff-2) are multifying each other and so as the Burning effects (i.e. BEff-1 and BEff-2).

5.4.3 Summary

Here the Section 5.4.2 investigates the effects of normalised turbulent integral length scale on localised forced ignition of globally stoichiometric stratified mixture using 3D DNS simulations. The effects of ${}^{l_\phi}/_{l_f}$ on burnt gas mass showing non-monotonic trends and dependent of ϕ' for initial Bi-modal distribution. However the initial Gaussian mixture distribution, the lower values of ${}^{l_\phi}/_{l_f}$ leads to better mixing and thus increases the extent of burning rate for given values of ϕ'. The initial value of ${}^{L_{11}}/_{l_f} = 3.36$ exhibits better choice for obtaining higher values of M_b out of three different values considered here. The better mixing process associated with increasing (decreasing) values of $u'(l_\phi$ and $\phi')$ for given L_{11} despite the nature of initial mixture distribution. However decreasing values of L_{11} leads to increase in the mixing process for a given initial Bi-modal mixture distributions, suggesting effects of L_{11} are dependent on initial mixture distributions and initial values of ϕ'. The adverse effects of $\frac{u'}{S_{b(\phi=1)}}$ on extent of burning can be seen in all the cases irrespective of ${}^{L_{11}}/_{l_f}$, ${}^{l_\phi}/_{l_f}$, ϕ' and profile of initial mixture distribution. Once the igniter is switched off the hot gas kernel is in the vicinity of local mixture gradient which is seriously affected by initial values of ${}^{L_{11}}/_{l_f}$, ${}^{l_\phi}/_{l_f}$, ϕ', $\frac{u'}{S_{b(\phi=1)}}$ and initial mixture distribution profile. Therefore judicious control on ${}^{L_{11}}/_{l_f}$, ${}^{l_\phi}/_{l_f}$, ϕ', $\frac{u'}{S_{b(\phi=1)}}$ and monitoring initial mixture distribution can support achieving better quality of burning for a given combustion cycle.

So far, DNS study presented in Sections 5.2, 5.3 and 5.3 were restricted to only globally stoichiometric (i.e. $\langle\phi\rangle = 1.0$) stratified mixtures. Numerous advantages of fuel-lean stratified mixtures combustion have been highlighted in the literature [101, 133, 137, 148]. Despite the advantageous applications of fuel-lean stratified mixtures, the effects of global mean of equivalence ratio $\langle\phi\rangle$ on localised forced ignition and subsequent burning process are yet to analysed in detailed using 3D DNS. The following Section 5.5 extends the DNS analysis to investigate such effects.

Figure 5.30: Temporal evolution of the M_b for all the cases with $\phi' = 0.6$ listed in Table 5.4. [where $L_{11}/l_f = 2.52$; $L_{11}/l_f = 3.36$; $L_{11}/l_f = 4.20$; 1^{st} column shows $l_\phi/l_f = 2.1$; 2^{nd} column shows $l_\phi/l_f = 5.5$; 3^{rd} column shows $l_\phi/l_f = 8.3$; additionally 1^{st} row shows $\frac{u'}{S_{b(\phi=1)}} = 0.0$; 2^{nd} row shows $\frac{u'}{S_{b(\phi=1)}} = 4.0$; 3^{rd} row shows $\frac{u'}{S_{b(\phi=1)}} = 6.0$, additionally the respected homogeneous cases are shown with marker [—✳—] and Gaussian: [- - - - -] and Bi-modal: [———];]

	$\langle\phi\rangle = 0.8$ [L]		
	Gaussian [G] Bi-modal [Bi]		
	$\phi' = 0.2$ [A]		
$L_{11}/l_f = 3.36$	$\frac{l_\phi}{l_f} = 2.1$ [D]	$\frac{l_\phi}{l_f} = 5.5$ [E]	$\frac{l_\phi}{l_f} = 8.3$ [F]
$\frac{u'}{S_{b(\phi=1)}} = 0.0$ [T0]	GLT0AD BiLT0AD	GLT0AE BiLT0AE	GLT0AF BiLT0AF
$\frac{u'}{S_{b(\phi=1)}} = 4.0$ [T4]	GLT4AD BiLT4AD	GLT4AE BiLT4AE	GLT4AF BiLT4AF
$\frac{u'}{S_{b(\phi=1)}} = 6.0$ [T6]	GLT6AD BiLT6AD	GLT6AE BiLT6AE	GLT6AF BiLT6AF
Homogeneous cases LT0, LT4, LT6, ST0, ST4, ST6			

Table 5.5: List of parameters to analyse effects of $\langle\phi\rangle$ in stratified mixtures. (Replace [L] with [S] for globally stoichiometric mixtures $\langle\phi\rangle = 1.0$, Replace [A] with [B] and [C] for $\phi' = 0.4$ and $\phi' = 0.6$)

5.5 Effects of Global Mean Equivalence Ratio

This section starts with brief discussion on ignition modification adopted to accommodate globally fuel-lean stratified mixtures, which ensures successful ignition for all the cases studies here. Then the results for effects of global mean of equivalence ratio $\langle\phi\rangle$ on localised forced ignition are presented and discussed. Global behaviours of maximum value of temperature is shown first to analyse the influence of $\langle\phi\rangle$ on the possibility of self-sustained combustion following successful ignition. Spatial distribution of different quantities is then presented. Mode of combustion and mixing statistics are not presented here for the sake of brevity, as the findings remains mostly qualitatively similar in globally fuel-lean stratified mixture cases to those found in globally stoichiometric stratified mixture cases (see previous Sections 5.2, 5.3 and 5.3). The effects of $\langle\phi\rangle$ including effects of initial ϕ distribution on the extent of burning is then analysed. Finally, the section ends with summary.

Figure 5.31: Temporal distribution of $T_{\max}$ for all the cases with $\langle\phi\rangle = 0.8$ and $\phi' = 0.2$ listed in Table 5.5. [where 1^{st} column shows $l_\phi/l_f = 2.1$; 2^{nd} column shows $l_\phi/l_f = 5.5$; 3^{rd} column shows $l_\phi/l_f = 8.3$; additionally 1^{st} row shows $\frac{u'}{S_{b(\phi=1)}} = 0.0$; 2^{nd} row shows $\frac{u'}{S_{b(\phi=1)}} = 4.0$; 3^{rd} row shows $\frac{u'}{S_{b(\phi=1)}} = 6.0$]

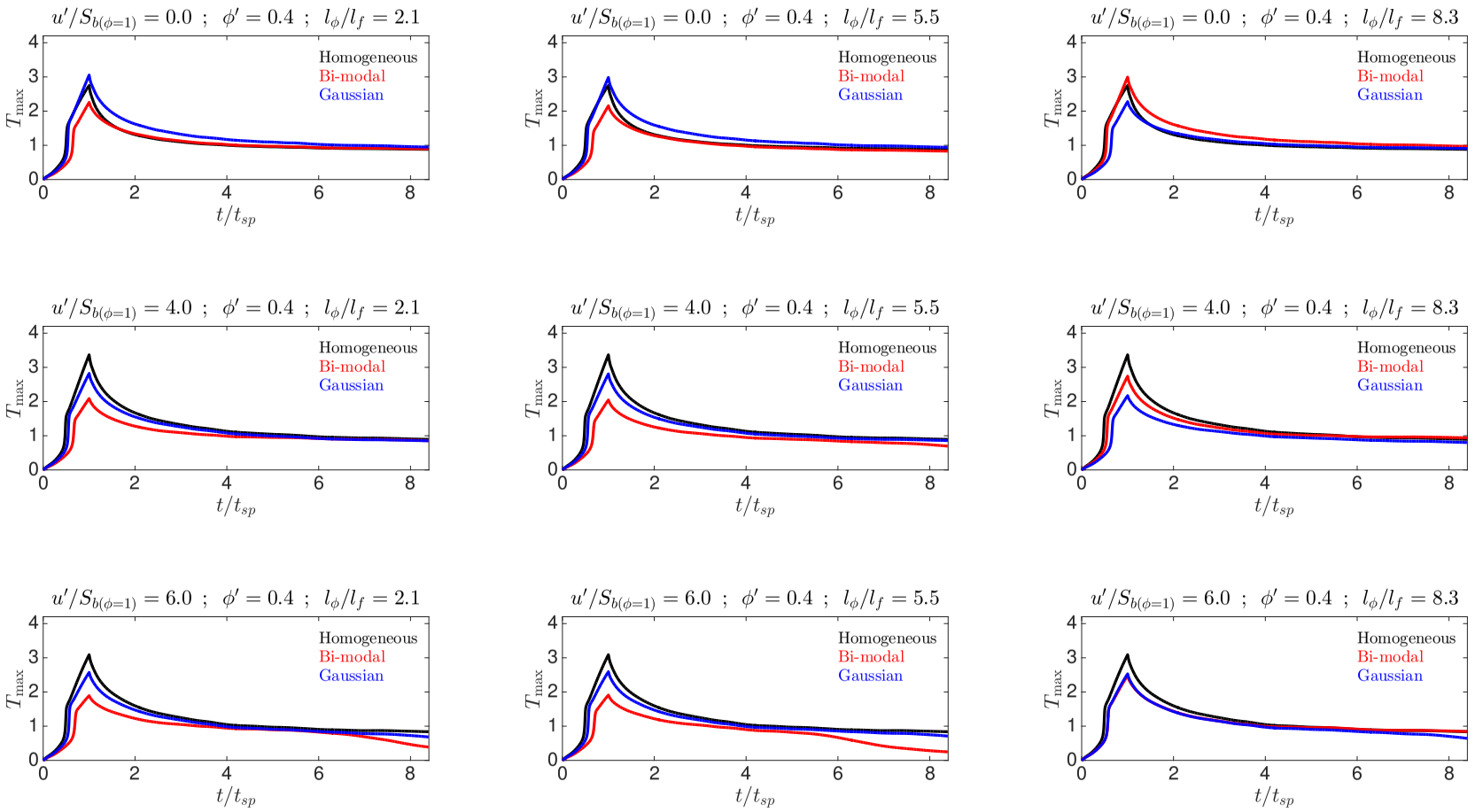

Figure 5.32: Temporal distribution of $T_{\max}$ for all the cases with $\langle\phi\rangle = 0.8$ and $\phi' = 0.4$ listed in Table 5.5. [where 1^{st} column shows $l_\phi/l_f = 2.1$; 2^{nd} column shows $l_\phi/l_f = 5.5$; 3^{rd} column shows $l_\phi/l_f = 8.3$; additionally 1^{st} row shows $\frac{u'}{S_{b(\phi=1)}} = 0.0$; 2^{nd} row shows $\frac{u'}{S_{b(\phi=1)}} = 4.0$; 3^{rd} row shows $\frac{u'}{S_{b(\phi=1)}} = 6.0$]

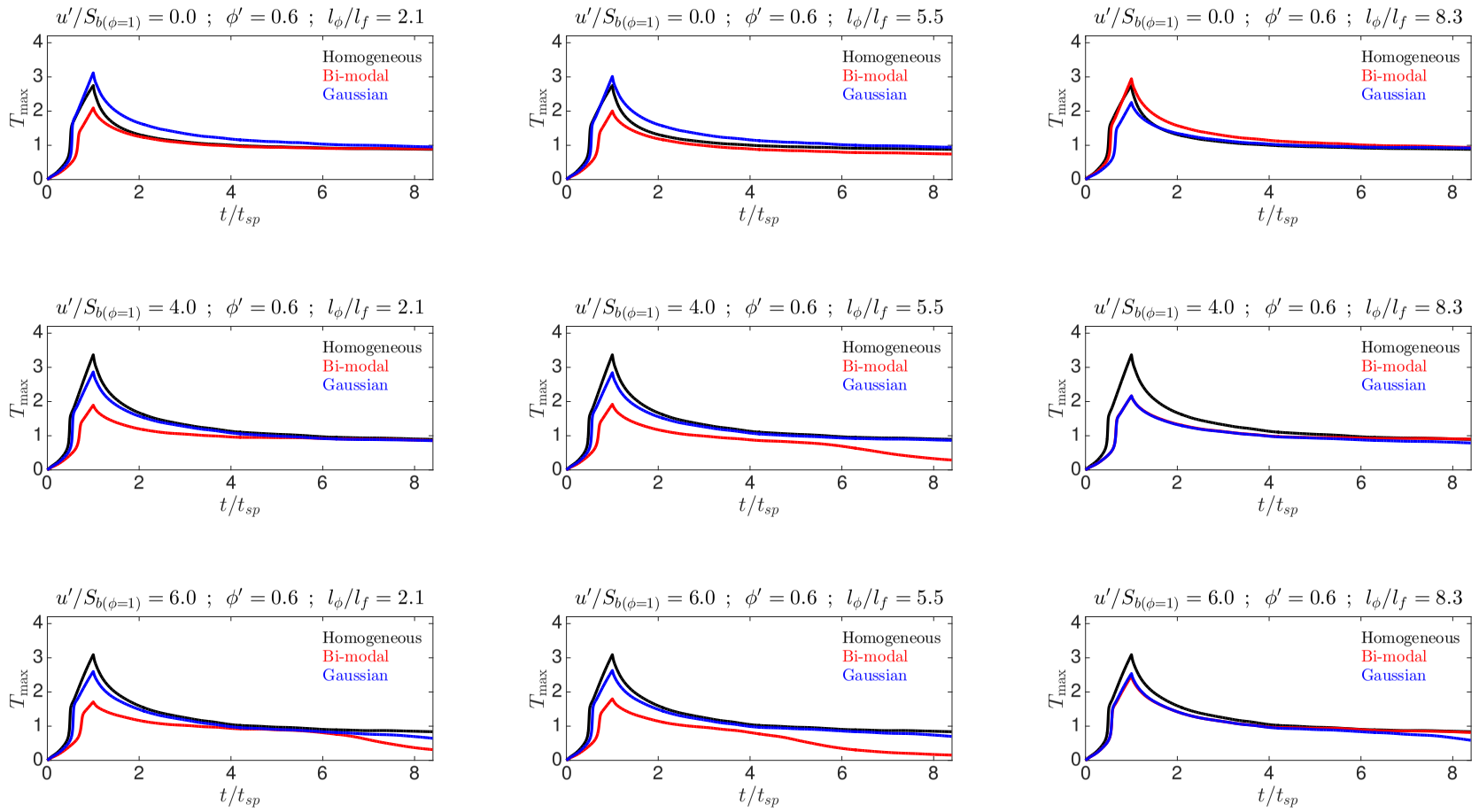

Figure 5.33: Temporal distribution of $T_{\max}$ for all the cases with $\langle\phi\rangle = 0.8$ and $\phi' = 0.6$ listed in Table 5.5. [where 1^{st} column shows ${}^{l_\phi}/_{l_f} = 2.1$; 2^{nd} column shows ${}^{l_\phi}/_{l_f} = 5.5$; 3^{rd} column shows ${}^{l_\phi}/_{l_f} = 8.3$; additionally 1^{st} row shows $\frac{u'}{S_{b(\phi=1)}} = 0.0$; 2^{nd} row shows $\frac{u'}{S_{b(\phi=1)}} = 4.0$; 3^{rd} row shows $\frac{u'}{S_{b(\phi=1)}} = 6.0$]

5.5.1 Numerical Modification to Accommodate $\langle\phi\rangle = 0.8$ Cases

As concluded in the Chapter 4 the energy deposition characteristics (i.e. ignition energy [characterised by a_{sp}], characteristic width of ignition energy deposition profile [characterised by R] and duration of ignition energy deposition [characterised by b_{sp}]) in localised forced ignition plays predominant role in obtaining MIE and subsequent early stages of flame development. Furthermore the MIE requirement is higher in order to obtain self-sustained combustion in fuel-lean cases than in stoichiometric cases (see Section 4.4).

The judicious choice of R and a_{sp} can lead to obtaining self-sustained combustion for given flow and mixture conditions. The ignition parameters have been modified here due to the higher MIE requirements for fuel-lean mixtures (see Section 4.4). Here numerical configuration remains unaltered as previously described in Section 5.2.1, except the ignition parameters. The ignition parameters is taken as : $R = 1.55l_f$, $a_{sp} = 9.20$, $b_{sp} = 0.2$, which ensure successful ignition for all the cases listed in Table 5.5. These ignition parameters provide self-sustained combustion following successful ignition for all the cases with $\langle\phi\rangle = 1.0$, whereas self-sustained combustion is obtained only for some cases with $\langle\phi\rangle = 0.8$. Table 5.5 shows parametric variation across different parameters, and thus 438 simulations (108×4 stratified mixture cases + 6 homogeneous mixtures) have been conducted here. The case names are chosen in such manner so that L stands for $\langle\phi\rangle = 0.8$; S stands for $\langle\phi\rangle = 1.0$; G and Bi stands for initial Gaussian and Bi-modal distribution of ϕ; T0, T4 and T6 indicate increasing turbulent level; A, B, and C indicate increasing values of ϕ'; D, E, and F denote increasing values of ${}^{l_\phi}/_{l_f}$ (e.g. GLT6AE corresponds to a case for initial Gaussian distribution of globally fuel-lean (i.e. $\langle\phi\rangle = 0.8$) stratified mixtures with values of $\frac{u'}{S_{b(\phi=1)}} = 6.0$; $\phi' = 0.2$; ${}^{l_\phi}/_{l_f} = 5.5$).

5.5.2 Global Behaviours of Maximum Value of Temperature

The temporal evolution of the non-dimensional maximum temperature $T_{\max}$ profiles for all the cases from Table 5.5 are shown in Figures 5.31-5.33. It is important to note that all cases with $\langle\phi\rangle = 1.0$ from Table 5.5 exhibited self-sustained combustion following successful ignition and therefore are not shown here. The non-dimensional temperature $T_{\max}$ is defined as $T_{\max} = (\hat{T}_{\max} - T_0)/(T_{ad(\phi=0.8)} - T_0)$ for $\langle\phi\rangle = 0.8$ cases.

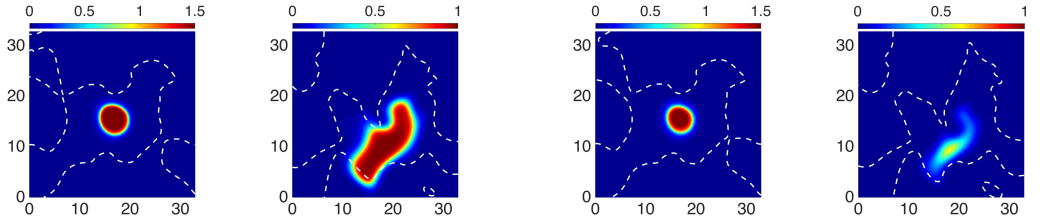

(a) T - BiST4BE (b) T - BiLT4BE

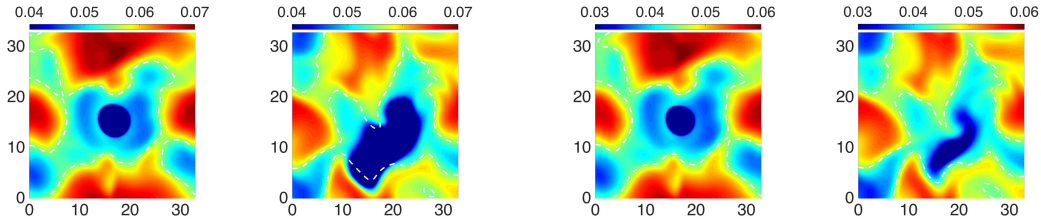

(c) Y_F - BiST4BE (d) Y_F - BiLT4BE

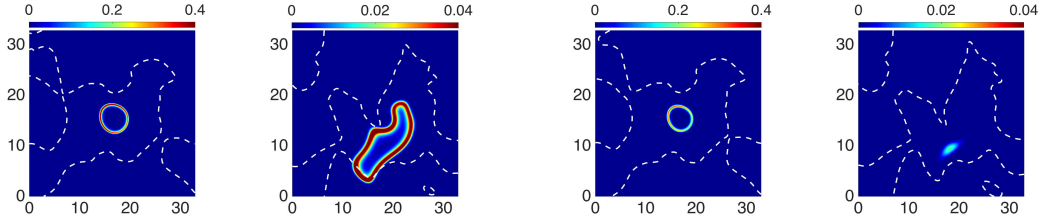

(e) $\dot{\Omega}_F$ - BiST4BE (f) $\dot{\Omega}_F$ - BiLT4BE

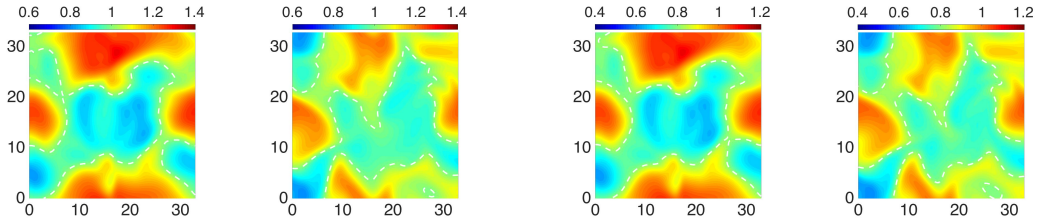

(g) ϕ - BiST4BE (h) ϕ - BiLT4BE

Figure 5.34: Distribution of T (1^{st} row), Y_F (2^{nd} row), $\dot{\Omega}_F$ (3^{rd} row) and ϕ (4^{th} row) on the central $x_1 - x_2$ plane for the cases BiST4BE (1^{st} and 2^{nd} column) and BiLT4BE (1^{st} and 2^{nd} column). The white broken like shows $\xi = \xi_{st}$. Additionally 1^{st}& 3^{rd} column showing $t = 1.05t_{sp}$, 2^{nd}& 4^{th} column showing $t = 8.40t_{sp}$.

The general characteristics of $T_{\max}$ during and after energy deposition time is remain unchanged for all the cases (as seen and discussed in Sections 5.2.2 and 5.3.1).

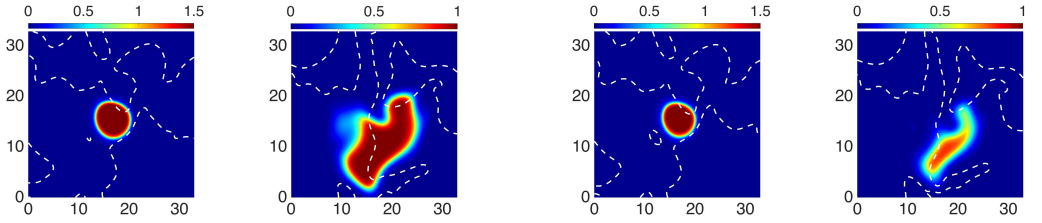

(a) T - GST4BE

(b) T - GLT4BE

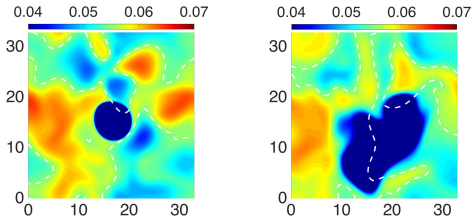

(c) Y_F - GST4BE

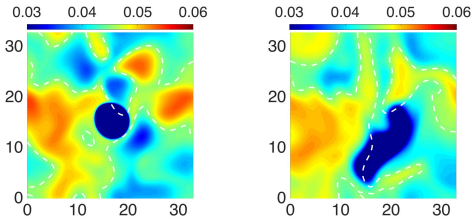

(d) Y_F - GLT4BE

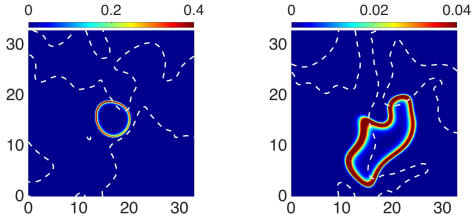

(e) $\dot{\Omega}_F$ - GST4BE

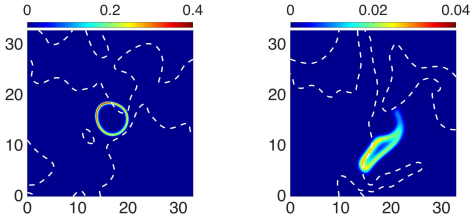

(f) $\dot{\Omega}_F$ - GLT4BE

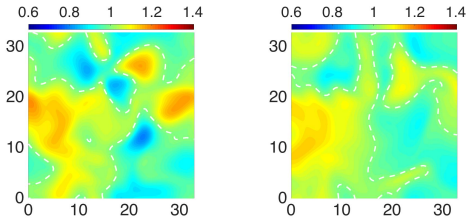

(g) ϕ - GST4BE

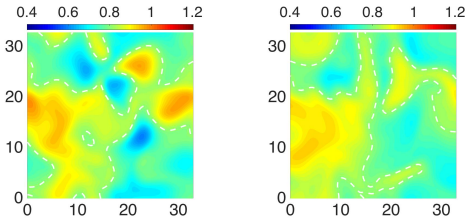

(h) ϕ - GLT4BE

Figure 5.35: Distribution of T (1^{st} row), Y_F (2^{nd} row), $\dot{\Omega}_F$ (3^{rd} row) and ϕ (4^{th} row) on the central $x_1 - x_2$ plane for the cases GST4BE (1^{st} and 2^{nd} column) and GLT4BE (1^{st} and 2^{nd} column). The white broken like shows $\xi = \xi_{st}$. Additionally 1^{st}& 3^{rd} column showing $t = 1.05t_{sp}$, 2^{nd}& 4^{th} column showing $t = 8.40t_{sp}$.

Furthermore a comparison of Figures 5.31, 5.32 and 5.33 indicate that all the quiescent (i.e. $\frac{u'}{S_{b(\phi=1)}} = 0.0$) cases show self-sustained combustion after successful

ignition. Moreover all the $\frac{u'}{S_{b(\phi=1)}} = 4.0$ cases also exhibit self-sustained combustion except for BiLT4BE (Bi-modal distribution, $\langle\phi\rangle = 0.8$, $\frac{u'}{S_{b(\phi=1)}} = 4.0$, $\phi' = 0.4$, ${}^{l_\phi}/_{l_f} = 5.5$) and BiLT4CE (Bi-modal distribution, $\langle\phi\rangle = 0.8$, $\frac{u'}{S_{b(\phi=1)}} = 4.0$, $\phi' = 0.6$, ${}^{l_\phi}/_{l_f} = 5.5$) cases. A large number of cases with $\frac{u'}{S_{b(\phi=1)}} = 6.0$ exhibit eventual flame extinction at $t \gg t_{sp}$, despite the successful ignition was achieved (see cases BiLT6AD, BiLT6BD, BiLT6BE, GLT6BF, BiLT6CD, BiLT6CE, GLT6BF and GLT6CF). Moreover Figures 5.31, 5.32 and 5.33 demonstrate that the globally fuel-lean stratified mixtures (i.e. $\langle\phi\rangle = 0.8$) with $\phi' = 0.2$ and $\frac{u'}{S_{b(\phi=1)}} = 4.0$ are more favorable to sustain combustion following successful ignition irrespective of ${}^{l_\phi}/_{l_f}$ and initial mixture distributions. On the other side cases with initial Bi-modal mixture distribution, ${}^{l_\phi}/_{l_f} = 5.5$ for $\phi' = 0.4$ and $\phi' = 0.6$ are more prone to flame extinction once the igniter is switched off at $t \gg t_{sp}$ for all turbulent cases considered here. The initial Gaussian mixture distribution cases provide more favorable conditions than the initial Bi-modal mixture distribution cases where self-sustained combustion has been obtained except for three cases (GLT6BD, GLT6BF and GLT6CF) in globally fuel-lean $\langle\phi\rangle = 0.8$ stratified mixtures. Additionally, it can be seen from Figures 5.31, 5.32 and 5.33 that, in many cases smaller values of $T_{\max}$ have been obtained at $t = t_{sp}$ than the corresponding homogeneous cases. This suggests that high values of temperature during ignition can be avoided, which ultimately reduces thermal NO_X emission.

Figures 5.31, 5.32 and 5.33 suggest that the influence of initial mixture inhomogeneity distribution, $\frac{u'}{S_{b(\phi=1)}}$, ϕ' and ${}^{l_\phi}/_{l_f}$ have important influences on the possibility of obtaining self-sustained combustion following successful ignition in stratified mixtures.

5.5.3 Spatial Distributions of Temperature, Fuel Mass Fraction, Fuel Reaction Rate Magnitude and Equivalence Ratio

The distribution of non-dimensional temperature (T), fuel mass fraction (Y_F), fuel reaction rate magnitude ($\dot{\Omega}_F$) and equivalence ratio (ϕ) at the central $x_1 - x_2$ plane at both $t = 1.05t_{sp}$ and $t = 8.40t_{sp}$ are presented here. Figure 5.34 demonstrates the initial Bi-modal mixture distribution cases with $\frac{u'}{S_{b(\phi=1)}} = 4$, $\phi' = 0.4$, ${}^{l_\phi}/_{l_f} = 5.5$ for both $\langle\phi\rangle = 1.0$ (BiST4BE) and $\langle\phi\rangle = 0.8$ (BiLT4BE) stratified mixtures. Additionally Figure 5.35 demonstrates the initial Gaussian mixture distribution cases with $\frac{u'}{S_{b(\phi=1)}} = 4$, $\phi' = 0.4$, ${}^{l_\phi}/_{l_f} = 5.5$ for both $\langle\phi\rangle = 1.0$ (GST4BE) and $\langle\phi\rangle = 0.8$ (GLT4BE) stratified mixtrures. The presented cases are chosen for the purpose of

highlighting the effects of $\langle\phi\rangle$ and nature of initial mixture distribution. Other cases from Table 5.5 also shows similar qualitative behaviour, but the volume of burned gas decreases with increasing values of $\frac{u'}{S_{b(\phi=1)}}$ irrespective of $\langle\phi\rangle$ values and/or nature of initial mixture distribution.

It can be seen from Figures 5.34 and 5.35 that during the ignition energy deposition ($t = t_{sp}$), the contour of T remains comparable for both globally stoichiometric ($\langle\phi\rangle = 1.0$) and fuel-lean ($\langle\phi\rangle = 0.8$) stratified mixtures. A comparison between Figures 5.34 and 5.35 reveals that initial Bi-modal mixture distribution case (BiLT4BE) shows flame extinction at $t \gg t_{sp}$, whereas the corresponding case with initial Gaussian mixture distribution (GLT4BE) shows successful flame propagation even at $t \gg t_{sp}$. In all cases the non-uniformity of ϕ decreases as combustion progresses (compare Figures 5.34 and 5.35 for $t = 1.05t_{sp}$ and $t = 8.40t_{sp}$).

Furthermore Figures 5.34 and 5.35 suggest that it is possible to achieve both successful ignition and self-sustained combustion for globally fuel lean $\langle\phi\rangle = 0.8$ stratified cases for correct choice of initial mixture distribution, ${}^{l_\phi}/_{l_f}$, ϕ' and $\frac{u'}{S_{b(\phi=1)}}$. Additionally a comparison between Figures 5.34 and 5.35 demonstrates that, in the case of self-sustained combustion the volume of flame kernel at $t = 8.40t_{sp}$ is larger for $\langle\phi\rangle = 1.0$ cases than that for $\langle\phi\rangle = 0.8$ case (compare case GST4BE and GLT4BE), as $\langle\phi\rangle = 1.0$ provides more presence of highly reactive mixture in the vicinity of igniter in comparison to the corresponding $\langle\phi\rangle = 0.8$ cases. The observations from Figures 5.34 and 5.35 indicate that the nature of initial mixture distribution and subsequent mixing process influence the flame propagation in $\langle\phi\rangle = 0.8$ cases.

5.5.4 Extent of Burning

The temporal evolution of the mean and standard deviation of M_b for all the cases from Table 5.5 are shown and discussed here. The temporal evolution of the mean and standard deviation of M_b characteristics for all the cases from Table 5.5 are sub divided in to different figures based on individual $\langle\phi\rangle$ and ϕ' for ease of comparison. Figures 5.36, 5.37 and 5.38 shows the mean and standard deviation of M_b profile for $\phi' = 0.2$,$\phi' = 0.4$ and $\phi' = 0.6$ respectively, for all the cases with $\langle\phi\rangle = 0.8$ from Table 5.5. Additionally, Figures 5.39, 5.40 and 5.41 demonstrating mean and standard deviation of M_b profile for $\phi' = 0.2$,$\phi' = 0.4$ and $\phi' = 0.6$ respectively, for all the cases with $\langle\phi\rangle = 1.0$ from Table 5.5.

It is evident from Figures 5.36-5.41 that M_b decreases for increasing values of $\frac{u'}{S_{b(\phi=1)}}$ for both initial (Bi-modal and Gaussian) mixture distribution of ϕ. In addition to

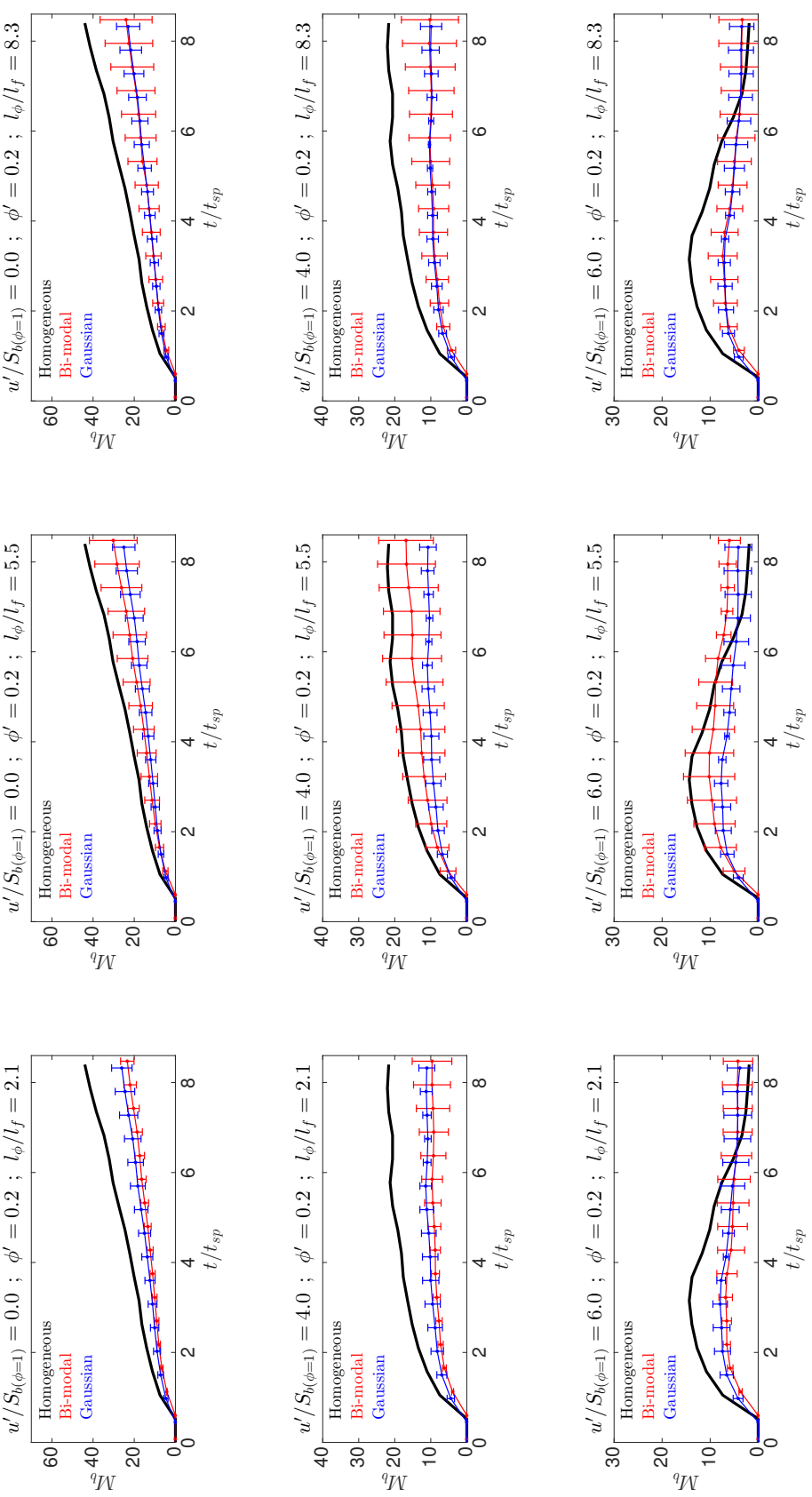

Figure 5.36: Temporal evolution of the mean and standard deviation of M_b for all the cases with $\langle\phi\rangle = 0.8$ and $\phi' = 0.2$ listed in Table 5.5.
[where 1^{st} column shows $^{l_\phi}/_{l_f} = 2.1$; 2^{nd} column shows $^{l_\phi}/_{l_f} = 5.5$; 3^{rd} column shows $^{l_\phi}/_{l_f} = 8.3$; additionally 1^{st} row shows $\frac{u'}{S_{b(\phi=1)}} = 0.0$; 2^{nd} row shows $\frac{u'}{S_{b(\phi=1)}} = 4.0$; 3^{rd} row shows $\frac{u'}{S_{b(\phi=1)}} = 6.0$]

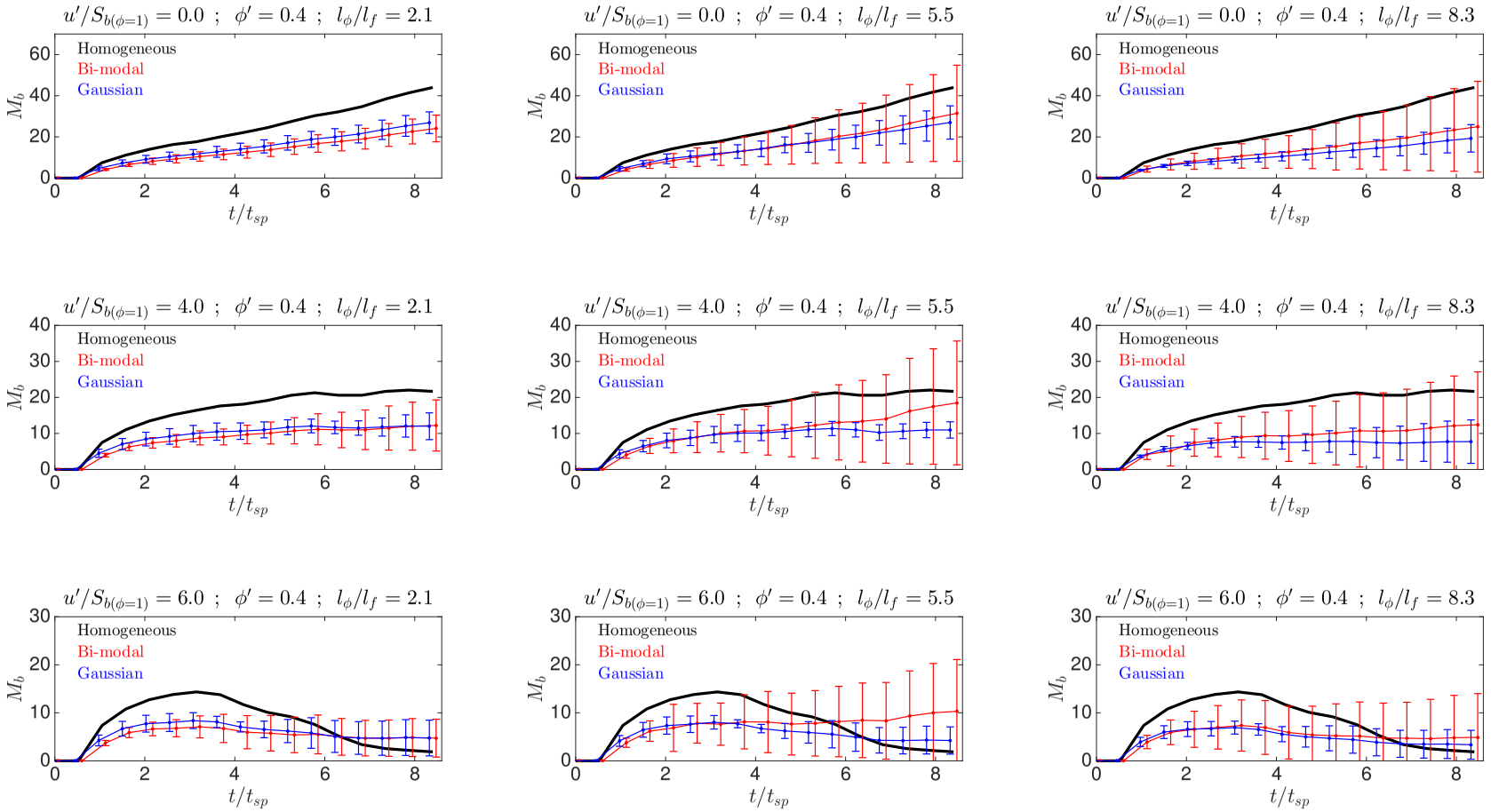

Figure 5.37: Temporal evolution of the mean and standard deviation of M_b for all the cases with $\langle\phi\rangle = 0.8$ and $\phi' = 0.4$ listed in Table 5.5.
[where 1^{st} column shows ${}^{l_\phi}/_{l_f} = 2.1$; 2^{nd} column shows ${}^{l_\phi}/_{l_f} = 5.5$; 3^{rd} column shows ${}^{l_\phi}/_{l_f} = 8.3$; additionally 1^{st} row shows $\frac{u'}{S_{b(\phi=1)}} = 0.0$; 2^{nd} row shows $\frac{u'}{S_{b(\phi=1)}} = 4.0$; 3^{rd} row shows $\frac{u'}{S_{b(\phi=1)}} = 6.0$]

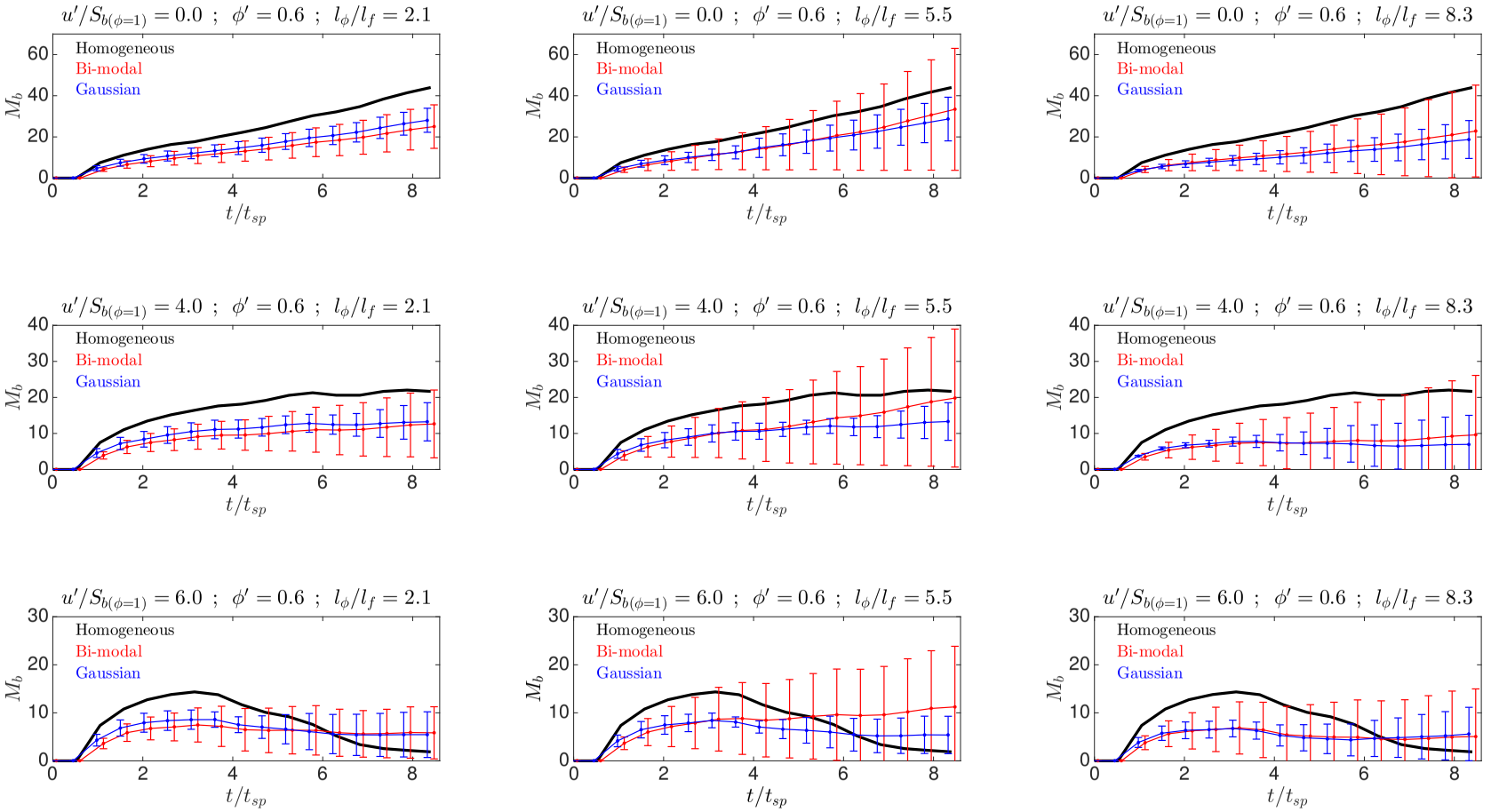

Figure 5.38: Temporal evolution of the mean and standard deviation of M_b for all the cases with $\langle\phi\rangle = 0.8$ and $\phi' = 0.6$ listed in Table 5.5.
[where 1^{st} column shows ${}^{l_\phi}/_{l_f} = 2.1$; 2^{nd} column shows ${}^{l_\phi}/_{l_f} = 5.5$; 3^{rd} column shows ${}^{l_\phi}/_{l_f} = 8.3$; additionally 1^{st} row shows $\frac{u'}{S_{b(\phi=1)}} = 0.0$; 2^{nd} row shows $\frac{u'}{S_{b(\phi=1)}} = 4.0$; 3^{rd} row shows $\frac{u'}{S_{b(\phi=1)}} = 6.0$]

that the detrimental effects of larger values of $\frac{u'}{S_{b(\phi=1)}}$ on M_b are more in $\langle\phi\rangle = 0.8$ cases in comparison to $\langle\phi\rangle = 1.0$ cases (compare Figures 5.36 and 5.39 for $\phi' = 0.2$, Figures 5.37 and 5.40 for $\phi' = 0.4$, Figures 5.38 and 5.41 for $\phi' = 0.6$). An increase in u' leads to an increase in eddy thermal diffusivity for given L_{11} (see Equation 5.8), which further leads to greater amount of heat loss from hot gas kernel for high values of $\frac{u'}{S_{b(\phi=1)}}$. These detrimental effects of $\frac{u'}{S_{b(\phi=1)}}$ on M_b are in good agreement with previous findings (see Section 5.2.6 and 5.3.6) and previous experimental results [116, 184]. However, it is possible to exhibit higher mean values of M_b in the case of globally fuel-lean stratified mixtures than homogeneous mixtures for high values of $\frac{u'}{S_{b(\phi=1)}}$= 6.0 (compare Figures 5.36, 5.37 and 5.38 for all ${}^{l_\phi}/_{l_f}$ cases).

Additionally, Figures 5.36-5.41 demonstrate that an increase in ϕ' leads to decrease in M_b for all cases considered here irrespective of initial mixture distributions and the values of $\langle\phi\rangle$. The laminar burning velocity $S_{b(\phi=1)}$ of mixture with $\phi < 1.0$ and $\phi > 1.10$ is smaller than that in the mixture with $1.0 \leq \phi \leq 1.10$ (see Figure 3.1 in Chapter 3). The probability of finding $1.0 \leq \phi \leq 1.10$ decreases with increase in ϕ' and this leads to reduction in the burning rate for higher values of ϕ'. The probability of finding highly reactive mixture corresponding to $1.0 \leq \phi \leq 1.10$ is greater in the cases with $\langle\phi\rangle = 1.0$ in comparison to those with $\langle\phi\rangle = 0.8$, and therefore the M_b attains higher values for $\langle\phi\rangle = 1.0$ cases than in the $\langle\phi\rangle = 0.8$ cases (compare Figures 5.36 and 5.39 for $\phi' = 0.2$, Figures 5.37 and 5.40 for $\phi' = 0.4$, Figures 5.38 and 5.41 for $\phi' = 0.6$).

Furthermore the mean values of M_b remains comparable for the quiescent cases with $\phi' = 0.2$ for all values of ${}^{l_\phi}/_{l_f}$ irrespective the initial mixture distributions. The figure 5.39 suggests that the initial Gaussian mixture distribution for all $\phi' = 0.2$ and $\langle\phi\rangle = 1.0$ cases, the mean M_b values attains higher values in comparison to initial Bi-modal mixture distribution for all values of ${}^{l_\phi}/_{l_f}$ and $\frac{u'}{S_{b(\phi=1)}}$. The initial Gaussian mixture distribution cases show an increase in burned gas mass with decreasing values of ${}^{l_\phi}/_{l_f}$ irrespective of ϕ', as the probability of finding $1.0 \leq \phi \leq 1.10$ ($0.8 \leq \phi \leq 1.10$) mixtures in the $\langle\phi\rangle = 1.0$ ($\langle\phi\rangle = 0.8$) cases increases with decreasing values of ${}^{l_\phi}/_{l_f}$ due to more efficient mixing for smaller values of ${}^{l_\phi}/_{l_f}$. Moreover the probability of finding mixture corresponding to $1.0 \leq \phi \leq 1.10$ ($0.8 \leq \phi \leq 1.10$) is greater in $\langle\phi\rangle = 1.0$ ($\langle\phi\rangle = 0.8$) cases for ${}^{l_\phi}/_{l_f} = 5.5$ and ${}^{l_\phi}/_{l_f} = 8.3$ in comparison to ${}^{l_\phi}/_{l_f} = 2.1$ cases due to less efficient mixing for the initial Bi-modal distribution with $\phi' = 0.2$ cases, which leads to greater rate of mass burning.

For initial ${}^{l_\phi}/_{l_f} = 8.3$ in Bi-modal cases the clouds of mixture inhomogeneities are

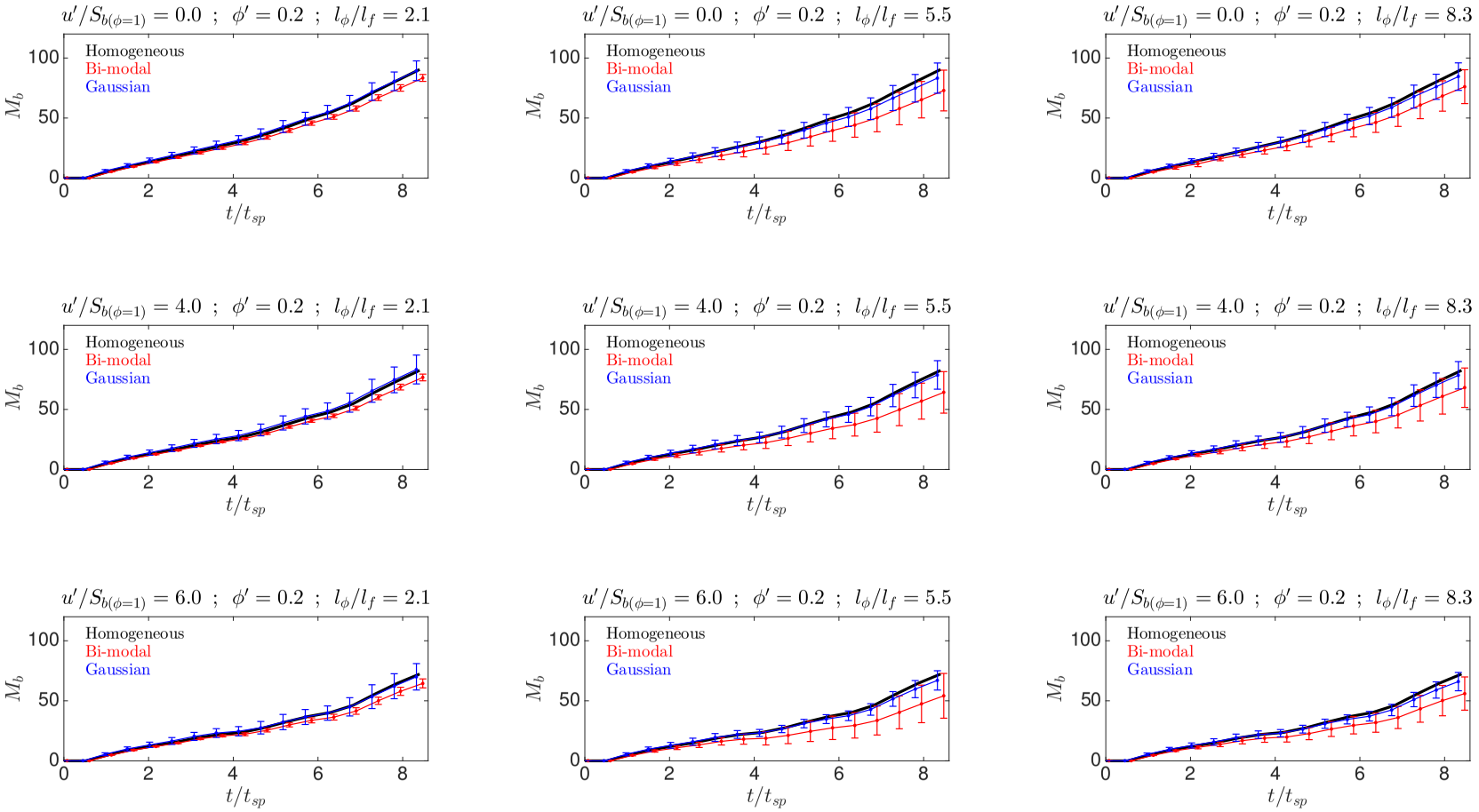

Figure 5.39: Temporal evolution of the mean and standard deviation of M_b for all the cases with $\langle\phi\rangle = 1.0$ and $\phi' = 0.2$ listed in Table 5.5.
[where 1^{st} column shows ${}^{l_\phi}/_{l_f} = 2.1$; 2^{nd} column shows ${}^{l_\phi}/_{l_f} = 5.5$; 3^{rd} column shows ${}^{l_\phi}/_{l_f} = 8.3$; additionally 1^{st} row shows $\frac{u'}{S_{b(\phi=1)}} = 0.0$; 2^{nd} row shows $\frac{u'}{S_{b(\phi=1)}} = 4.0$; 3^{rd} row shows $\frac{u'}{S_{b(\phi=1)}} = 6.0$]

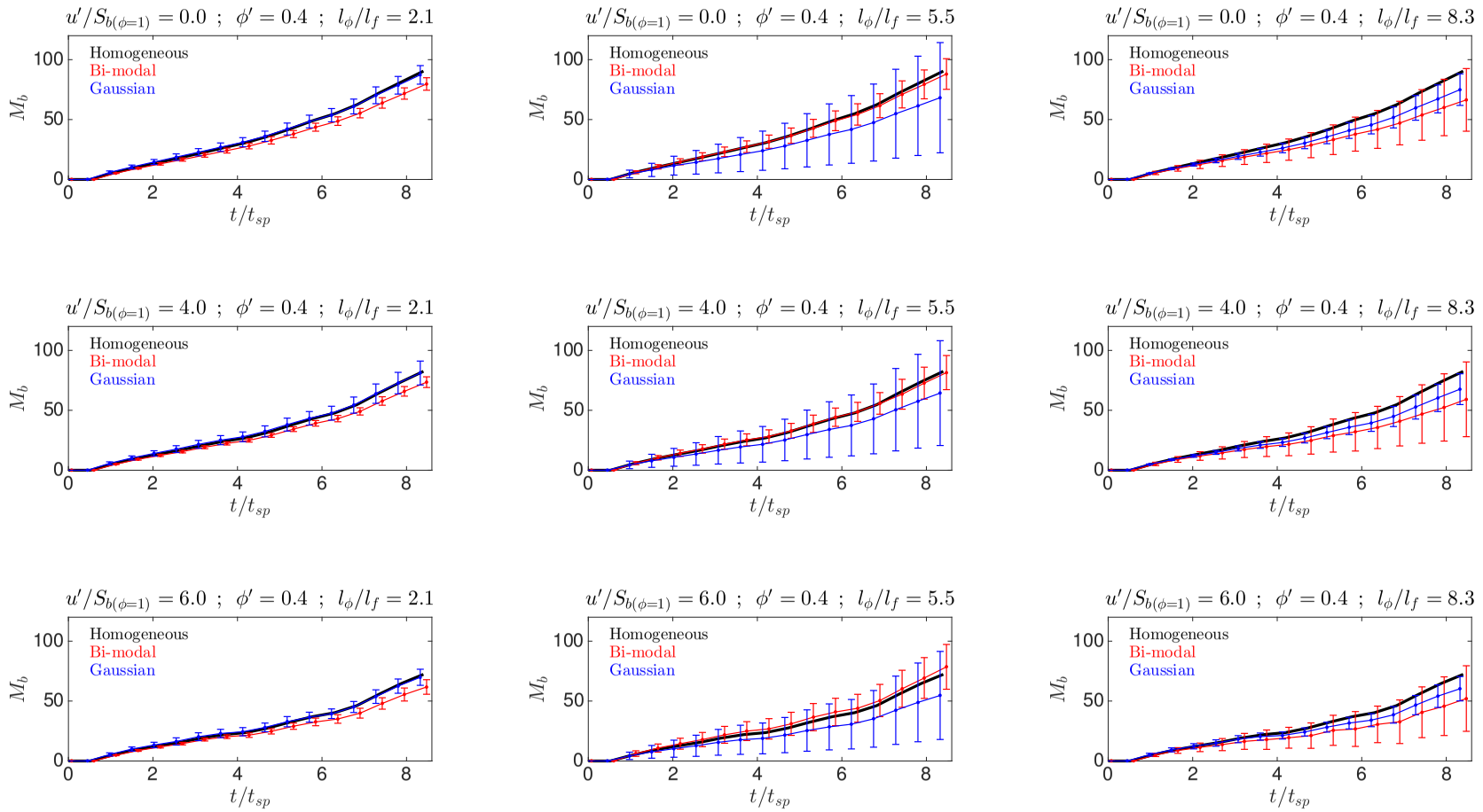

Figure 5.40: Temporal evolution of the mean and standard deviation of M_b for all the cases with $\langle\phi\rangle = 1.0$ and $\phi' = 0.4$ listed in Table 5.5.
[where 1^{st} column shows ${}^{l_\phi}/_{l_f} = 2.1$; 2^{nd} column shows ${}^{l_\phi}/_{l_f} = 5.5$; 3^{rd} column shows ${}^{l_\phi}/_{l_f} = 8.3$; additionally 1^{st} row shows $\frac{u'}{S_{b(\phi=1)}} = 0.0$; 2^{nd} row shows $\frac{u'}{S_{b(\phi=1)}} = 4.0$; 3^{rd} row shows $\frac{u'}{S_{b(\phi=1)}} = 6.0$]

relatively big (see Figure 5.11), and as a result to this there is a high probability of obtaining a large region of almost homogeneous mixture at the centre of igniter. If the igniter centre is located in the vicinity of a large cloud of $1.0 \leq \phi \leq 1.10$ ($0.8 \leq \phi \leq 1.10$) in the $\langle\phi\rangle = 1.0$ ($\langle\phi\rangle = 0.8$)case, the slow burning rate in $1.0 < \phi$ ($0.8 < \phi$) and $\phi > 1.10$ encountered during hot gas kernel expansion is mostly compensated by the high burning rate in the $1.0 \leq \phi \leq 1.10$ ($0.8 \leq \phi \leq 1.10$) mixtures. This leads to greater burned gas mass in the ${}^{l_\phi}/_{l_f} = 8.3$ cases than the ${}^{l_\phi}/_{l_f} = 2.1$ cases when initial $\phi' = 0.4$ or $\phi' = 0.6$ for initial Bi-modal mixture distribution. These effects of ${}^{l_\phi}/_{l_f}$ and ϕ' on the mean values of M_b are in good agreement with previously presented findings (see Section 5.2.6 and 5.3.6).

5.5.5 Summary

This Section 5.5 investigates the effects of ${}^{l_\phi}/_{l_f}$, ϕ', $\frac{u'}{S_{b(\phi=1)}}$ on localised forced ignition of both globally fuel-lean ($\langle\phi\rangle = 0.8$) and stoichiometric ($\langle\phi\rangle = 1.0$) stratified mixtures for different initial (i.e. Bi-modal and Gaussian) mixture distributions of ϕ. The results discussed here demonstrate that for a given value of ${}^{l_\phi}/_{l_f}$, an increase in ϕ' leads to reduction of burned gas mass irrespective of the nature of initial mixture distributions. The influence of ${}^{l_\phi}/_{l_f}$ on the extent of burning has been found to be non-monotonic and dependent on ϕ' for the initial Bi-modal distribution irrespective values of $\langle\phi\rangle$. In the cases with initial Gaussian mixture distributions, the mean values of M_b increases with decreasing values of ${}^{l_\phi}/_{l_f}$ irrespective of ϕ' and $\langle\phi\rangle$ considered here. The increase in heat transfer rate from hot gas kernel with increasing $\frac{u'}{S_{b(\phi=1)}}$ leads to detrimental effects on the extent of burning. It is possible to exhibit higher mean values of M_b in the case of globally fuel-lean stratified mixtures than homogeneous mixtures for high values of $\frac{u'}{S_{b(\phi=1)}} = 6.0$ for both initial mixture distributions.

5.6 Main Findings

Localised forced ignition and subsequent burning process of stratified mixtures have been investigated using 3D DNS simulations to study the parameters effecting mixture inhomogeneity (i.e. nature of initial mixture distribution, mixture inhomogeneity length scale (${}^{l_\phi}/_{l_f}$), equivalence ratio fluctuation (ϕ'), turbulent integral length scale (${}^{L_{11}}/_{l_f}$) and global mean equivalence ratio ($\langle\phi\rangle$)). The main findings can be summarised as follows:

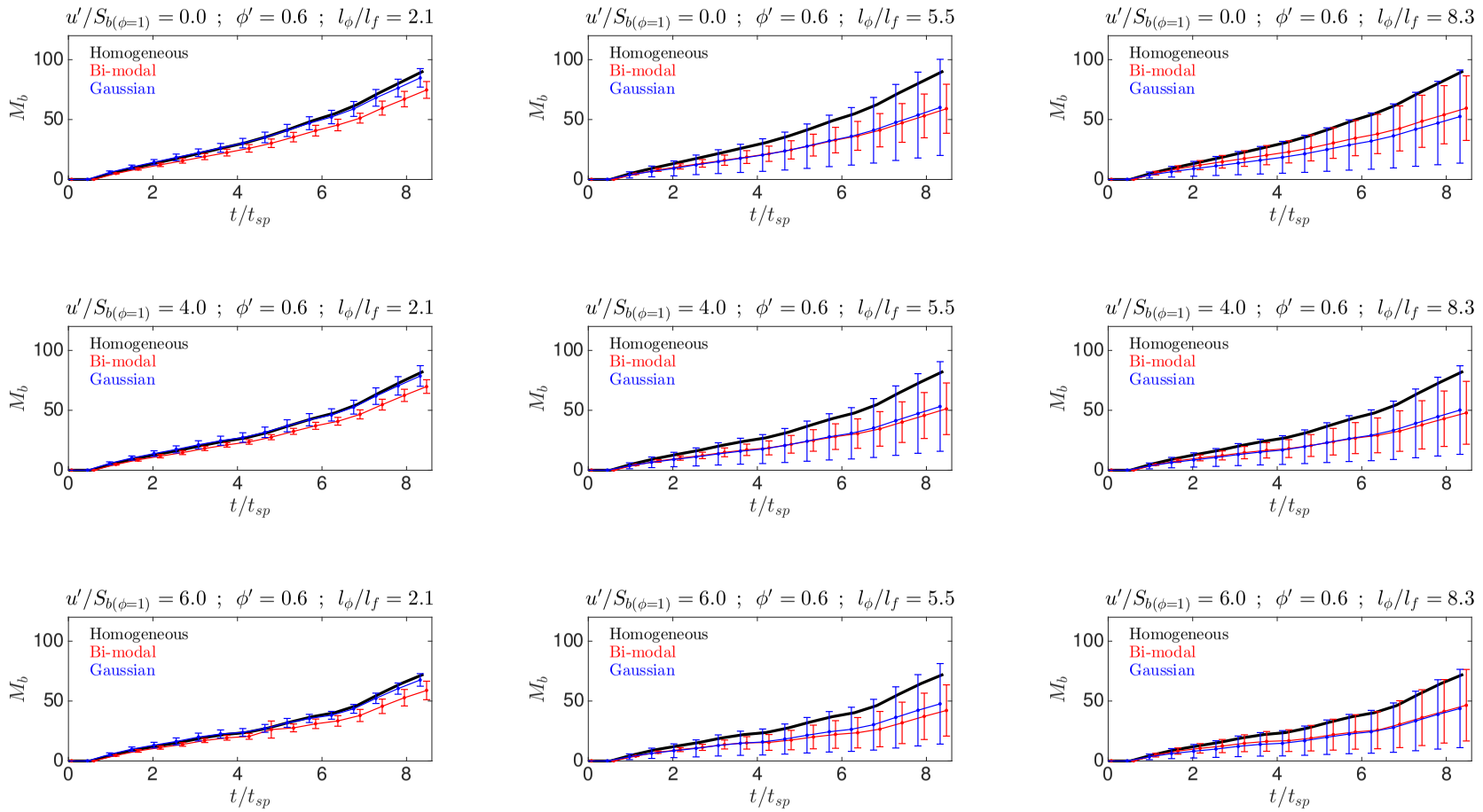

Figure 5.41: Temporal evolution of the mean and standard deviation of M_b for all the cases with $\langle\phi\rangle = 1.0$ and $\phi' = 0.6$ listed in Table 5.5.
[where 1^{st} column shows ${}^{l_\phi}/_{l_f} = 2.1$; 2^{nd} column shows ${}^{l_\phi}/_{l_f} = 5.5$; 3^{rd} column shows ${}^{l_\phi}/_{l_f} = 8.3$; additionally 1^{st} row shows $\frac{u'}{S_{b(\phi=1)}} = 0.0$; 2^{nd} row shows $\frac{u'}{S_{b(\phi=1)}} = 4.0$; 3^{rd} row shows $\frac{u'}{S_{b(\phi=1)}} = 6.0$]

- The flame originating from localised forced ignition shows a predominantly premixed mode of combustion, however with higher values of ϕ' some areas of non-premixed combustion have been observed.

- For given value of ${}^{l_\phi}/_{l_f}$, an increase in ϕ' leads to reduction of the burned gas mass for both initial Gaussian and Bi-modal mixture distribution. By contrast, the influences of ${}^{l_\phi}/_{l_f}$ on the extent of burning have been found to be non-monotonic and dependent of ϕ' for initial Bi-modal mixture distributions, whereas initial Gaussian mixture distribution shows an increase in burned gas mass with decreasing values of ${}^{l_\phi}/_{l_f}$ for all initial values of ϕ' considered here.

- The self-sustained combustion may not be achieved in the cases with high values of $\frac{u'}{S_{b(\phi=1)}}$ and globally fuel-lean stratified mixtures (i.e. $\langle\phi\rangle = 0.8$), although with judicious choices of ignition parameters self-sustained combustion can be achieved in such environments. Moreover, choice of such parameters can avoid unnecessary high temperature during ignition and thus reduces thermal NO_X emission. The adverse effects of higher values of $\frac{u'}{S_{b(\phi=1)}}$ show an increase in heat transfer rate from hot gas kernel, which further leads to a reduction in the burned gas mass irrespective values of $\langle\phi\rangle$, ${}^{l_\phi}/_{l_f}$, ϕ' and nature of initial mixture distribution.

- The initial value of ${}^{L_{11}}/_{l_f} = 3.36$ exhibits better choice for obtaining higher values of M_b out of three different values considered here (i.e. ${}^{L_{11}}/_{l_f} = 2.52$, 3.36 and 4.20). The better mixing process associated with increasing (decreasing) values of $u'(l_\phi$ and $\phi')$ for given L_{11} despite the nature of initial mixture distribution. However decreasing values of L_{11} leads to increase in the mixing process for a given initial Bi-modal mixture distributions, suggesting effects of L_{11} are dependent on initial mixture distributions and initial values of ϕ'.

- It is well known that combustion succeeds only for some realisations and this aspect is particularly prevalent in the cylinder of IC engines due to cycle-to-cycle variations. It is possible to obtain large clouds of both highly flammable and weakly flammable (or non-combustible) mixtures at the igniter location for large values of ${}^{l_\phi}/_{l_f}$, which leads to large variation of M_b between different realisations irrespective of nature of initial mixture distribution.

- It is admitted that four realisations may not be sufficient to mimic cycle-to-cycle variations in a real IC engine. However, as a step forward 800+ DNS

simulations have been conducted here to draw the conclusions. This analysis reveals an important qualitative trend, which suggests that variability in the extent of burning is relatively small for small values ${}^{l_\phi}/_{l_f}$, and the degree of variability of burning increases with increasing ϕ'.

- The variability of burned gas mass is routinely obtained in the cylinder of IC engines due to cycle-to-cycle variation. The findings reveal that the degree of variability of burning depends not only on u', ϕ' and ${}^{l_\phi}/_{l_f}$ but also on the nature of initial mixture distribution, which can be manipulated by careful design of the nozzle and fuel injection systems in IC engines. The success or failure of the ignition of stratified mixtures is a highly random event and that a small change in mixture distribution has the potential to alter the outcome. Moreover, in-cylinder turbulence along with injection characteristics can influence the values of u', ϕ' and ${}^{l_\phi}/_{l_f}$, and thus the effective control of mixing characteristics in IC engine combustion chamber can potentially play a pivotal role to ensure successful ignition and reduce the variability associated with the ignition event.

The effects of energy deposition characteristics and the effects of combustion regimes on localised forced ignition of turbulent homogeneous mixtures have been studied in Chapter 4. Furthermore Chapter 5 investigated the parameters affecting mixture inhomogeneity on localised forced ignition of stratified mixtures. There has been considerable recent interest in fuel-flexible combustion systems [11] and especially the automotive industry faces a context of fuel diversification [36]. The use of different fuels has an impact on the performance of ignition and subsequent combustion, as the efficiency of SI engines is a function of the combustion speed, i.e. the speed at which the fresh fuel-air mixture is getting consumed by the flame front. The effects of fuel Lewis number (Le_F) on localised forced ignition of both homogeneous mixtures and stratified mixtures have been investigated in the following Chapter 6.

Chapter 6

Effects of Fuel Lewis Number on Localised Forced Ignition

This Chapter 6 starts with an introduction about the existing literature and the purpose of this study. The first half of this chapter (Section 6.2) investigates the effects of fuel Lewis number on localised forced ignition of turbulent homogeneous mixtures. And the second half of this chapter (Section 6.3) deals with the effects of fuel Lewis number on localised forced ignition of globally stoichiometric stratified mixtures. The results are presented and discussed. This Chapter ends with main findings.

6.1 Introduction

Combustion chemistry of large practical fuels involves hundreds to thousands of species and even higher number of reactions [126]. Flame-turbulence interaction is generally characterised by a strong coupling between the heat release rate and flow motions. Recent papers by Lipatnikov and Chomiak [123] and Driscoll [69] discuss about the influences of flame on turbulence and turbulent scalar transport as well as wrinkling and quenching due to flame stretching by the flow. This latter phenomenon results from strain, curvature and propagation mechanisms, which depend on flame and turbulent structures properties [60]. The impact of fuel composition on combustion is a crucial importance when localised forced ignition is concern and subsequent burning characteristics for a given flow conditions. The response of a laminar premixed flame to stretch depends strongly on the overall Lewis number of the reactant mixture [43]. The Lewis number (Le) has been defined in Equation 3.26 (Chapter 3). For $Le \simeq 1.0$, heat and mass transfer are in balance. The flame is initiated as a spherical kernel

from the localised forced ignition (as seen in Chapters 4 and 5), for $Le > 1.0$, heat conduction is greater than mass diffusion, and a flame that is curved convex toward the reactants will tend to slow down due to its thermal influence on the reactant mixture. By contrast, for $Le < 1.0$, heat conduction is slower than mass diffusion, and a flame that is curved convex toward the reactants will tend to accumulate heat in the products adjacent to the curved portion. This acts to accelerate the flame locally and to accentuate the convex curvature. Lewis number also affects the susceptibility of the flame to straining [43]. Lewis numbers for most hydrocarbon-air mixtures are generally close to unity and are not strongly affected by the stoichiometry mixtures. By contrast, Lewis numbers of lean hydrogen-air mixtures can be significantly less than unity, resulting in strongly unstable flames [43, 143].

Localised forced ignition (e.g. spark or laser) of homogeneous mixtures plays a pivotal role in the design and smooth functioning of efficient and reliable SI and DI engines. However, relatively few studies concentrated on localised forced ignition of homogeneous mixtures with non-unity fuel Lewis number ($Le_F \neq 1.0$) [48, 80, 90, 116, 186]. Moreover, Chapter 4, Section 4.2 summarised the effects of energy deposition characteristics on localised forced ignition of homogeneous mixtures. A number of previous analyses both numerical [48, 90, 186] and experimental [48, 80, 90, 116, 186] have demonstrated that the fuel Lewis number (Le_F) has significant influences on localised forced ignition of both homogeneous and inhomogeneous gaseous mixtures. It has been reported that the MIE for homogeneous mixtures is affected by the differential diffusion [80, 116, 186]. Analytical experimental study by Subulkin and Siskind [186] concluded that MIE for quiescent homogeneous mixtures decreases with increasing D_i for a given value of thermal diffusivity (i.e. decreasing global Lewis number).

Recently Wu *et al.* [217] conducted an experimental investigation of the propagation and associated propagation speeds of expanding C_4 to C_8 $n-$alkane flames in isotropic turbulence at different pressure. Experimental results from Wu *et al.* [217] show that the turbulent flame speeds of lean mixtures, whose Lewis number is greater than unity, exhibit strong propensity of local extinction, ostensibly caused by local stretch through the $Le_F > 1.0$ mixture. Additionally Wu *et al.* [217] also concluded that at lean conditions, the turbulent flame speeds decrease with the molecular weight of fuel. Moreover, the heterogeneous combustion and the combined heterohomogeneous combustion of mixtures with $Le_F > 1.0$ investigated analytically and numerically by Zheng and Mantzaras [222] in different geometrical configuration. The results from Zheng and Mantzaras [222] suggested that the $Le_F > 1.0$ led to the un-

		$\phi = 1.0$ [S] ; $\phi = 0.8$ [L]		
		$Le_F = 0.8$ [Le08]		
	$\frac{L_{11}}{l_f} = 3.36$	$\frac{u'}{S_{b(\phi=1)}} = 0$ [T0]	$\frac{u'}{S_{b(\phi=1)}} = 4$ [T4]	$\frac{u'}{S_{b(\phi=1)}} = 6$ [T6]
$b_{sp} = 0.2$ $a_{sp} = 3.5$	$R = 0.93l_f$ [A]	Le08ST0A Le08LT0A	Le08ST4A Le08LT4A	Le08ST6A Le08LT6A
	$R = 1.10l_f$ [B]	Le08ST0B Le08LT0B	Le08ST4B Le08LT4B	Le08ST6B Le08LT6B
	$R = 1.41l_f$ [C]	Le08ST0C Le08LT0C	Le08ST4C Le08LT4C	Le08ST6C Le08LT6C
$R = 1.10l_f$ $a_{sp} = 3.5$	$b_{sp} = 0.1$ [D]	Le08ST0D Le08LT0D	Le08ST4D Le08LT4D	Le08ST6D Le08LT6D
	$b_{sp} = 0.2$ [E]	Le08ST0E Le08LT0E	Le08ST4E Le08LT4E	Le08ST6E Le08LT6E
	$b_{sp} = 0.3$ [F]	Le08ST0F Le08LT0F	Le08ST4F Le08LT4F	Le08ST6F Le08LT6F
$R = 1.10l_f$ $b_{sp} = 0.2$	$a_{sp} = 2.7$ [G]	Le08ST0G Le08LT0G	Le08ST4G Le08LT4G	Le08ST6G Le08LT6G
	$a_{sp} = 3.5$ [H]	Le08ST0H Le08LT0H	Le08ST4H Le08LT4H	Le08ST6H Le08LT6H
	$a_{sp} = 4.3$ [I]	Le08ST0I Le08LT0I	Le08ST4I Le08LT4I	Le08ST6I Le08LT6I

Table 6.1: Initial values of the simulation parameters to investigate the effects of fuel Lewis number
(replace [Le08] with [Le10] for $Le_F = 1.0$ and [Le12] for $Le_F = 1.2$ cases)

deradiabatic surface temperatures, which in turn gave rise to gas-phase regions with local energy excess, and the gas-phase superadiabaticity led to peak prompt NO_X values 30% higher than those achieved by a diffusionally neutral deficient reactant ($Le = 1.0$).

From the discussion above it becomes evident that Le_F is also likely to play key roles on the localised forced ignition of homogeneous mixtures but these effects coupled with energy deposition characteristics in localised forced ignition are yet to be analysed in detail using DNS. In this section 6.2, 3D compressible DNS simulations have been carried out in order to investigate the influences of Le_F and energy deposition characteristics on the localised forced ignition of homogeneous stoichiometric and fuel-lean mixtures for different RMS value of turbulence velocity u'.

Several modern internal combustion devices operate in an intermediate regime in

which reactants are imperfectly mixed. In this case, the flame propagates through spatial variations of equivalence ratio, altering both the global behaviour of the combustion system, and the local properties of the reaction zone [209]. Premixed regimes are desired in combustion chambers to control flame temperatures and reduce pollutant emissions such as nitrogen oxides (NO_X). In practice, as fuel and oxidizer are often introduced separately in the combustion chamber, perfect mixing is extremely difficult to achieve and stratified mixtures are often observed [138]. The flame then propagates in inhomogeneous mixtures, where characteristic spatial scales of equivalence ratio variations are of the order of the reaction zone thickness [59]. Moreover, in automotive applications, fuels such as hydrogen may play an increasingly important role due to zero tailpipe emissions of CO_2, particulates and unburned hydrocarbons. Experimental evidence suggests that hydrogen can be used as a primary fuel for HCCI engines, albeit in a very lean mixture ($0.1 < \phi < 0.3$) due to hydrogen's fast burning characteristics and rapid heat release due to its very high mass diffusivity [29].

In combustion devices, it is desirable to increase efficiency and decrease harmful emissions, combustion among different hydrocarbon fuels may be a promising solution to achieve these goals. Localised forced ignition of inhomogeneous mixtures plays pivotal roles in smooth functioning of Direct Injection (DI) engines and high altitude relight in aero-gas turbines. Therefore improved understanding is needed to identify the conditions which lead to successful ignition and self-sustained combustion among different hydrocarbon fuels for automotive applications. The experimental data of Ahmed and Mastorakos [3, 5] and Ahmed *et al.* [4] showed that an increase in mean velocity leads to a deterioration of ignition performance, quantified by a reduction in ignition probability. Most existing studies on localised forced ignition of inhomogeneous mixtures [4, 5, 48, 50, 51] have been carried out for a mixture distribution, which is characterised by a mean variation of equivalence ratio ϕ. Moreover, results from previous Chapter 5 (Section 5.2) demonstrate that the RMS value of equivalence ratio fluctuation ϕ' and the Taylor micro-scale l_ϕ of equivalence ratio ϕ variation, in addition to the RMS values of turbulent velocity u', have significant effects on the extent of burning and the possibility of attaining self-sustained combustion following successful ignition.

A number of previous analyses [48, 80, 90, 186, 191] have demonstrated that the Lewis number of the fuel, in addition to the mixture composition and background turbulence, has significant influences on localised forced ignition of both homogeneous and inhomogeneous gaseous mixtures. Furthermore, He [90] analytically demonstrated

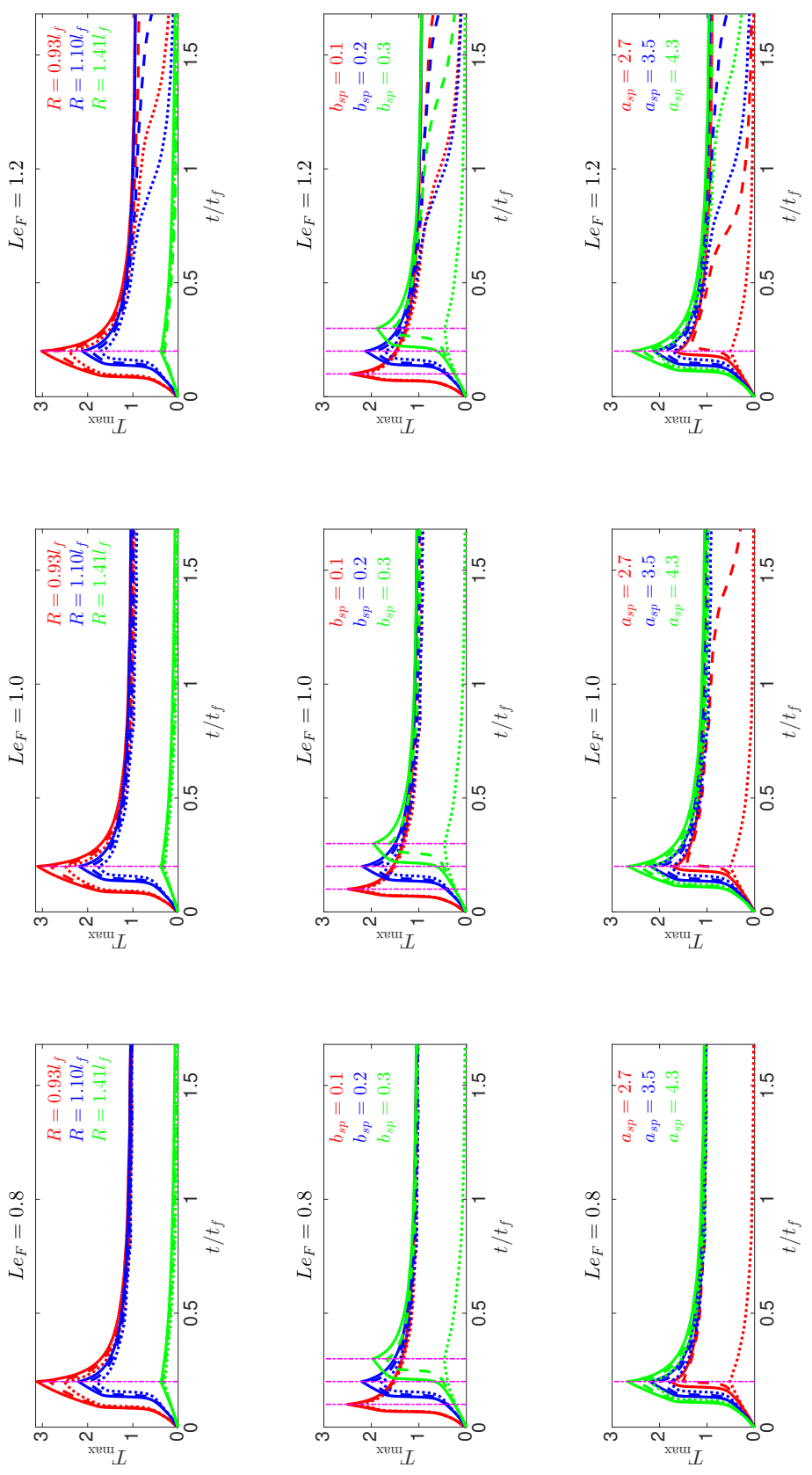

Figure 6.1: Temporal distribution of $T_{\max}$ for all the cases with $\phi = 1.0$ listed in Table 6.1.
(where 1^{st} column shows $Le_F = 0.8$; 2^{nd} column shows $Le_F = 1.0$; 3^{rd} column shows $Le_F = 1.2$; magenta vertical dashed-broken line shows $t = t_{sp}$; additionally $\frac{u'}{S_{b(\phi=1)}} = 0.0$ [——]; $\frac{u'}{S_{b(\phi=1)}} = 4.0$ [– – – –]; $\frac{u'}{S_{b(\phi=1)}} = 6.0$ [. . . . . .])

that localised ignition of quiescent homogeneous mixtures with global Lewis number $Le > 1.0$ can be unstable. This is indeed demonstrated by Chakraborty *et al.* [48] that it is easier to ignite mixing layers and obtain self-sustained combustion for small values of global Lewis number and this tendency is particularly prevalent for cases with $Le_F < 1.0$. From the above discussion, it becomes evident that Le_F is also likely to play key roles on the localised forced ignition of stratified mixtures but these effects are yet to be analysed in detail using DNS. This deficit in the existing literature has been addressed in this section 6.3 by carrying out 3D compressible DNS for a range of different initial mixture distribution and difference values of Le_F, $\frac{u'}{S_{b(\phi=1)}}$, ϕ' and ${}^{l_\phi}/_{l_f}$.

6.2 Effects of Le_F on Localised Forced Ignition of Turbulent Homogeneous Mixtures

This section starts with brief discussion of the numerical formulation and then results for effects of Le_F on localised forced ignition of turbulent homogeneous mixtures are presented and discussed. Temporal evolution of maximum temperature is shown first, followed by the spatial distribution of different quantities is presented. Reaction-diffusion balance analysis of flame kernels is then presented. The temporal evolution of the burned gas mass has been analysed for cases where self-sustained combustion following successful ignition was achieved. Ignition parameters have been modified to achieve self-sustained combustion for fuel-lean mixtures with $Le_F > 1.0$. Finally, this section ends with implication analysis in the context of MIE and summary is provided.

The numerical formulation remains similar to as described in Section 4.2.1 except for one modification, the fuel Lewis number is ranging from 0.8 to 1.2 here. The fuel Lewis number Le_F, initial values of normalised turbulent velocity fluctuation $\frac{u'}{S_{b(\phi=1)}}$ and the parametric variation of energy deposition characteristics for all homogeneous stoichiometric and fuel-lean mixtures are listed in Table 6.1. The case names in Table 6.1 are chosen in such a manner that Le08, Le10, Le12 indicate Le_F values 0.8, 1.0 and 1.2 respectively; and T0, T4, T6 indicate the initial values of normalised rms turbulent velocity values $\frac{u'}{S_{b(\phi=1)}} = 0.0$, $\frac{u'}{S_{b(\phi=1)}} = 4.0$ and $\frac{u'}{S_{b(\phi=1)}} = 6.0$ respectively. In Table 6.1, S indicates the stoichiometric homogeneous mixture where L indicates the fuel-lean mixture with $\phi = 0.8$. For example, the case name Le10LT4 corresponds to a case with $Le_F = 1.0$, $\phi = 0.8$ and $\frac{u'}{S_{b(\phi=1)}} = 4.0$.

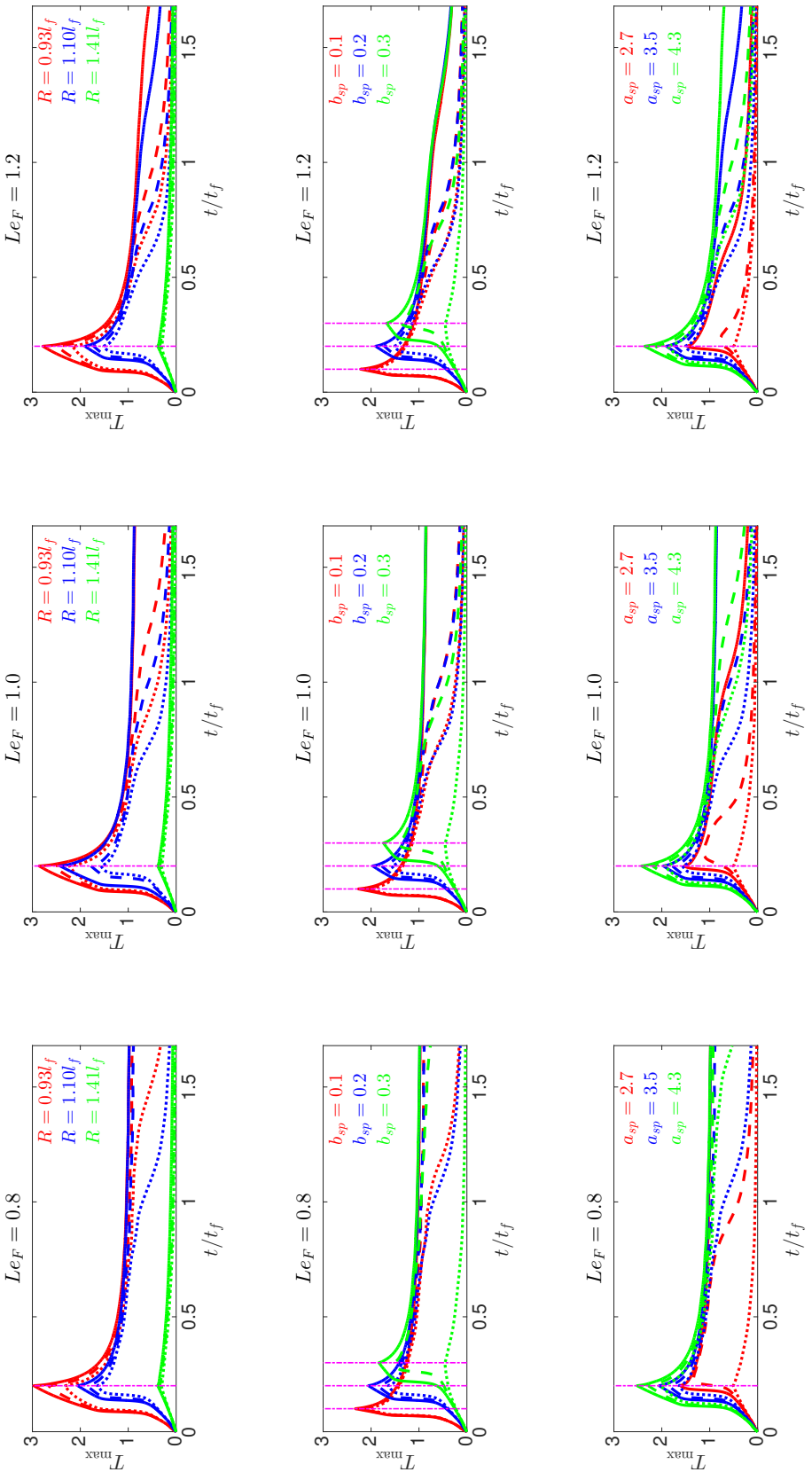

Figure 6.2: Temporal distribution of $T_{\max}$ for all the cases with $\phi = 0.8$ listed in Table 6.1. (where 1^{st} column shows $Le_F = 0.8$; 2^{nd} column shows $Le_F = 1.0$; 3^{rd} column shows $Le_F = 1.2$; magenta vertical dashed-broken line shows $t = t_{sp}$; additionally $\frac{u'}{S_{b(\phi=1)}} = 0.0$ [——]; $\frac{u'}{S_{b(\phi=1)}} = 4.0$ [– – – –]; $\frac{u'}{S_{b(\phi=1)}} = 6.0$ [· · · · · · · ·])

6.2.1 Temporal Evolution of Maximum Temperature

The temporal evolution of the maximum values of non-dimensional temperature ($T_{\max}$) for all cases listed in Table 6.1 are shown in Figures 6.1 and 6.2 for stoichiometric ($\phi = 1.0$) and fuel-lean ($\phi = 0.8$) mixtures respectively. The profile of $T_{\max}$ shown in Figures (6.1 and 6.2) are good indicators for successful ignition and subsequent self-sustained combustion. The global behaviour of $T_{\max}$ until energy deposition time ($t = t_{sp}$) remain unchanged from what has been observed and discussed in previous Chapter 4. Once the energy deposition is switched off ($t \geq t_{sp}$), the thermal gradient between the hot gas kernel and the surrounding unburned gas gives rise to high rate of heat transfer from the hot gas kernel. This, in turn, leads to decrease in $T_{\max}$ with time immediately after $t = t_{sp}$ but $T_{\max}$ approaches the non-dimensional adiabatic flame temperature (i.e. $T \approx 1.0$) at $t \gg t_{sp}$ for the cases where the self-sustained combustion is obtained.

Figure 6.1 demonstrates that self-sustained combustion has achieved following successful ignition for all the stoichiometric cases with $Le_F = 0.8$ except for cases with $R = 1.41l_f$, $b_{sp} = 0.2$ (Le08ST0C, Le08ST4C, Le08ST6C) and cases with higher $\frac{u'}{S_{b(\phi=1)}} = 6.0$ and $b_{sp} = 0.3$ (Le08ST6F) and case with smaller $a_{sp} = 2.7$ (Le08ST6G). A similar qualitative trend has been observed for the $Le_F = 1.0$ stoichiometric cases, additionally cases with $a_{sp} = 2.7$ and $\frac{u'}{S_{b(\phi=1)}} = 4.0$, 6.0 fails to exhibit self-sustained combustion (self-sustained combustion has not been achieved for cases Le10ST0C, Le10ST4C, Le10ST6C, Le10ST6F, Le10ST4G and Le10ST6G). The detrimental effects of $\frac{u'}{S_{b(\phi=1)}} = 6.0$ can be easily seen for all $Le_F = 1.2$ stoichiometric cases. The initial $\frac{u'}{S_{b(\phi=1)}} = 4.0$ stoichiometric cases with $Le_F = 1.2$ show self-sustained combustion only for the combinations of $R = 0.93l_f$, $a_{sp} = 3.5$ and $b_{sp} = 0.2$, and $R = 1.10l_f$, $a_{sp} = 4.3$ and $b_{sp} = 0.2$, whereas all the quiescent cases exhibit self-sustained combustion expect for $R = 1.41l_f$ (e.g. self-sustained combustion is obtained for Le12ST0A, Le12ST4A, Le12ST0B, Le12ST0D, Le12ST0E, Le10ST0F, Le12ST0G, Le12ST0H, Le12ST0I, Le12ST4I cases).

A comparison between Figures 6.1 and 6.2 reveals that the cases with $\phi = 0.8$ are more susceptible to flame extinction than the $\phi = 1.0$ cases (for example, compare cases Le08ST6A, Le08LT6A, Le08ST6B, Le08LT6B, Le10ST6D, Le10LT6D, Le12ST0B, Le12LT0B) as the rate of chemical reaction is smaller in the $\phi = 0.8$ cases than in the $\phi = 1.0$ cases. The fuel-lean cases with $R = 1.41l_f$ show misfire for $a_{sp} = 3.5$ and $b_{sp} = 0.2$. All the $Le_F = 1.2$ cases with fuel-lean mixtures listed in Table 6.1 ultimately give rise to failed self-sustained combustion even for the cases with successful

(a) T - Le08ST4B (b) T- Le10ST4B (c) T - Le12ST4B

(d) $\dot{\Omega}_F$ - Le08ST4B (e) $\dot{\Omega}_F$ - Le10ST4B (f) $\dot{\Omega}_F$ - Le12ST4B

(g) Y_F - Le08ST4B (h) Y_F - Le10ST4B (i) Y_F - Le12ST4B

Figure 6.3: Distribution of T (1^{st} row), $\dot{\Omega}_F$ (2^{nd} row) and Y_F (3^{rd} row) on central $x_1 - x_2$ plane with domain size $33l_f \times 33l_f \times 33l_f$ for cases with $\phi = 1.0$, $R = 1.10l_f$, $b_{sp} = 0.2$, $a_{sp} = 3.5$, $u'/s_{b(\phi=1.0)} = 4.0$ from Table 6.1 in order to illustrate the effects of Le_F.
(where 1^{st} & 2^{nd} columns showing $Le_F = 0.8$ case; 3^{rd} & 4^{th} columns showing $Le_F = 1.0$ case ; 5^{th} & 6^{th} columns showing $Le_F = 1.2$ case, additionally $1^{st}, 3^{rd}, 5^{th}$ columns showing $t = 0.2t_f$ and $2^{nd}, 4^{th}, 6^{th}$ columns showing $t = 1.68t_f$)

ignition. For the complete review and effects of energy deposition characteristics on localised forced ignition for both stoichiometric and fuel-lean mixtures please refer to Chapter 4 Section 4.2. All the quiescent fuel-lean $\phi = 0.8$ cases exhibit self-sustained combustion. The turbulent fuel-lean $\phi = 0.8$ cases with initial $\frac{u'}{S_{b(\phi=1)}} = 6.0$ fail to exhibit self-sustained combustion, and the flame extinction also takes place for initial $\frac{u'}{S_{b(\phi=1)}} = 4.0$ cases with the combinations of $a_{sp} = 2.7$ and $b_{sp} = 0.2$, and $a_{sp} = 3.5$ and $b_{sp} = 0.3$.

The observation made from Figure 6.1 and 6.2 indicates that Le_F, R, a_{sp}, b_{sp} and $\frac{u'}{S_{b(\phi=1)}}$ have important influences on the possibility of self-sustained combustion following successful ignition. The above discussion indicates that the self-sustained combustion has been obtained for majority cases with $Le_F = 0.8$, whereas only some cases with $Le_F = 1.0$ and $Le_F = 1.2$ manage to show self-sustained combustion. Furthermore Figure 6.1 demonstrates that the possibility of obtaining self-sustained combustion increases with decreasing Le_F (compare the cases Le08ST4G, Le10ST4G and Le12ST4G in Figure 6.1). The fuel diffuses into the reaction zone at a higher rate than the rate of heat conduction out of the reaction layer for the cases with $Le_F < 1.0$. This gives rise to simultaneous presence of high fuel concentration and high temperature in the $Le_F = 0.8$ cases, which increases the rate of heat release and flame propagation, and thus improves the chance of obtaining self-sustained combustion following successful ignition. By contrast, in the $Le_F = 1.2$ cases heat diffuses at a faster rate from the reaction zone than the rate at which the fuel diffuses into it and thus the rate of heat transfer is more likely to dominate over the chemical heat release rate in these cases and the flame eventually extinguishes when the heat transfer from the hot gas kernel overcomes the heat release rate (see cases Le12ST6A, Le12ST6B, Le12ST4D, Le12ST6D, Le12ST6E etc. in Figure 6.1). The difficulty in igniting homogeneous mixture with $Le_F > 1.0$ is consistent with previous findings [48, 90, 205].

6.2.2 Spatial Distribution of Temperature, Reaction Rate Magnitude and Fuel Mass Fraction

The distribution of non-dimensional temperature (T), magnitude of fuel consumption rate ($\dot{\Omega}_F$) and the fuel mass fraction (Y_F) at the central $x_1 - x_2$ plane for cases with $\phi = 1.0$, $R = 1.10 l_f$, $b_{sp} = 0.2$, $a_{sp} = 3.5$, $\frac{u'}{S_{b(\phi=1)}} = 4.0$ (cases Le08ST4B, Le10ST4B and Le12ST4B) from Table 6.1 in order to illustrate the effects of Le_F are shown in

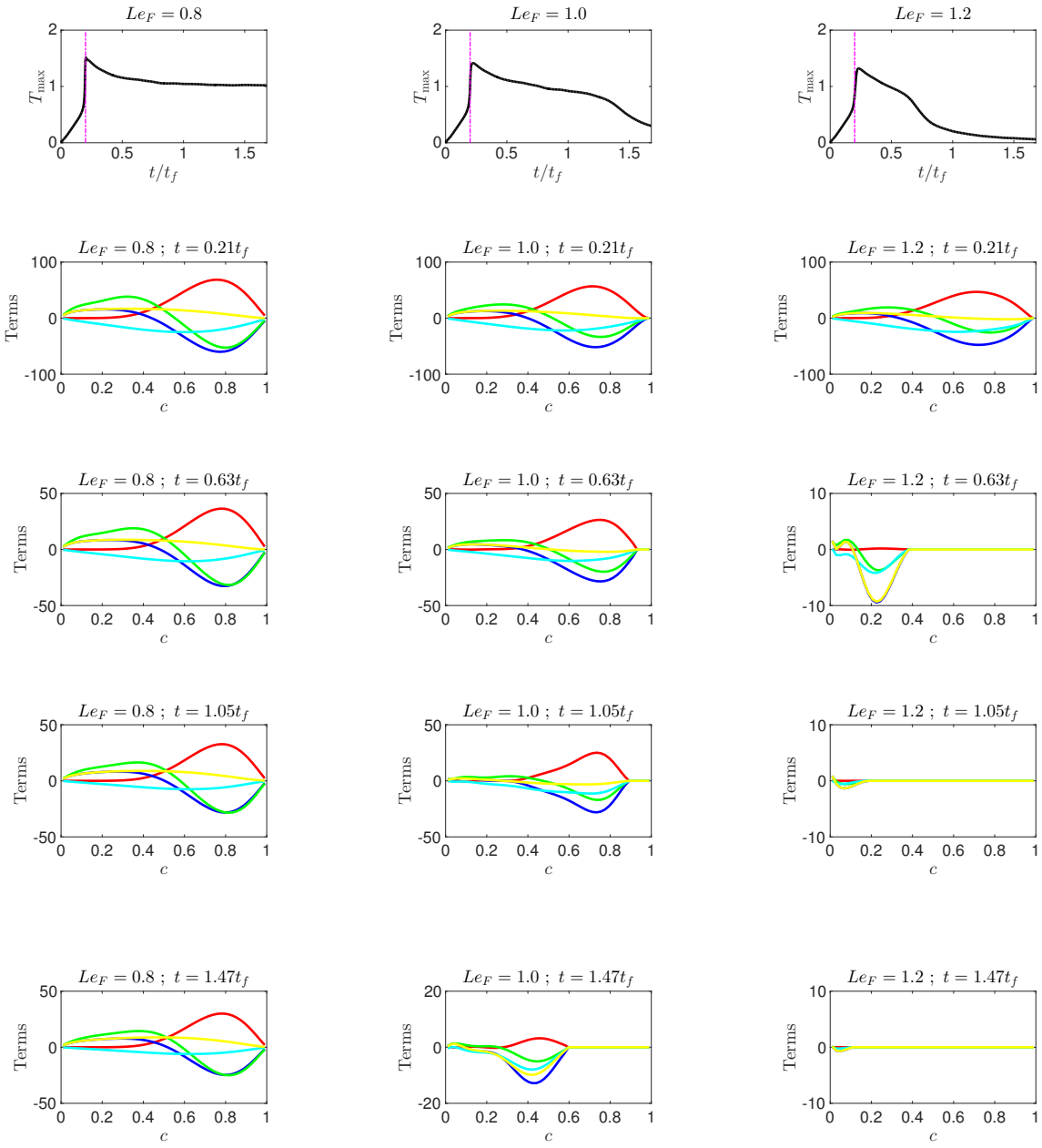

Figure 6.4: Temporal evolution of $T_{\max}$ along with the mean variation of different terms with reaction progress variable (i.e. c) at different time instances for case with $R = 1.10l_f$, $b_{sp} = 0.2$, $a_{sp} = 2.7$, ${}^{u'}/_{S_{b(\phi=1)}} = 4.0$ where magenta dashed-broken line shows $t = t_{sp}$.
[1^{st} column showing $Le_F = 0.8$ case and 2^{nd} column showing $Le_F = 1.0$ case and 3^{rd} column showing $Le_F = 1.2$ case]

Figure 6.3 at times $t = 0.2t_f$ and $t = 1.68t_f$. As previously seen in Chapter 4, the temperature contours remain spherical during the period of energy deposition but they become increasingly distorted as time progresses. The evolution of temperature field for $t \leq t_{sp}$ is principally determined by the diffusion of deposited energy, whereas after ignition, the evolution of temperature field anad the flame propagation depends on the local reaction-diffusion balance, which is affected by local flame stretching mechanism. Moreover Figure 6.3 shows that Y_F is depleted at the areas associated with high values of T due to consumption of fuel as a result of chemical reaction. A comparison between different Le_F cases reveals that the volume of high temperature region and the extent of flame wrinkling decreases with increasing Le_F. For the cases with $Le_F < 1.0$, fuel diffuses faster into reaction zone than the rate at which heat of conducted out, whereas the opposite mechanism remains prevalent for $Le_F > 1.0$ cases. As a result to this, simultaneous presence of high concentration of fuel and high temperature leads to higher rate of burning and greater extent of flame wrinkling (because larger surface area of flame kernel) in the $Le_F < 1.0$ cases than in the corresponding $Le_F = 1.0$ cases. By contrast, $Le_F > 1.0$ cases encounter low concentration of fuel and relatively low temperature leading to smaller rate of burning (compare cases Le08ST4B and Le12ST4B in Figure 6.3).

6.2.3 Reaction-Diffusion Balance Analysis of the Flame Kernels

Figure 6.4 (1^{st} row) shows the temporal evolution of $T_{\max}$ for cases with $R = 1.10l_f$, $b_{sp} = 0.2$, $a_{sp} = 2.7$, $\frac{u'}{S_{b(\phi=1)}} = 4.0$ for different fuel Lewis numbers $Le_F = 0.8$ (1^{st} column), $Le_F = 1.0$ (2^{nd} column) and $Le_F = 1.2$ (3^{rd} column). Additionally Figure 6.4 demonstrates the behaviour of different terms at different time instances for cases Le08ST4G, Le10ST4G and Le12ST4G. The qualitative nature of flame normal diffusion rate term ($\vec{N}\cdot\nabla\left(\rho D\vec{N}\cdot\nabla c\right)$ [ ]) and tangential diffusion rate term ($-\rho D\nabla\cdot\vec{N}\,|\nabla c|$ [ ]) remains similar as described in Chapter 4 Section 4.3.4, and therefore not discussed in this section. Here the effects of fuel Lewis number Le_F has major implication on molecular diffusion term ($\nabla\cdot(\rho D\nabla c)$ [ ]).

It can be seen from Figure 6.4 that self-sustained combustion has been achieved for case Le08ST4G (see Figure 6.4, 1^{st} row, 1^{st} column), whereas case Le10ST4G fails to attain adiabatic flame temperature after $t = 1.0t_f$ and case Le12ST4G only provided successful ignition and then exhibited flame extinction at $t > 0.5t_f$. Moreover, Figure

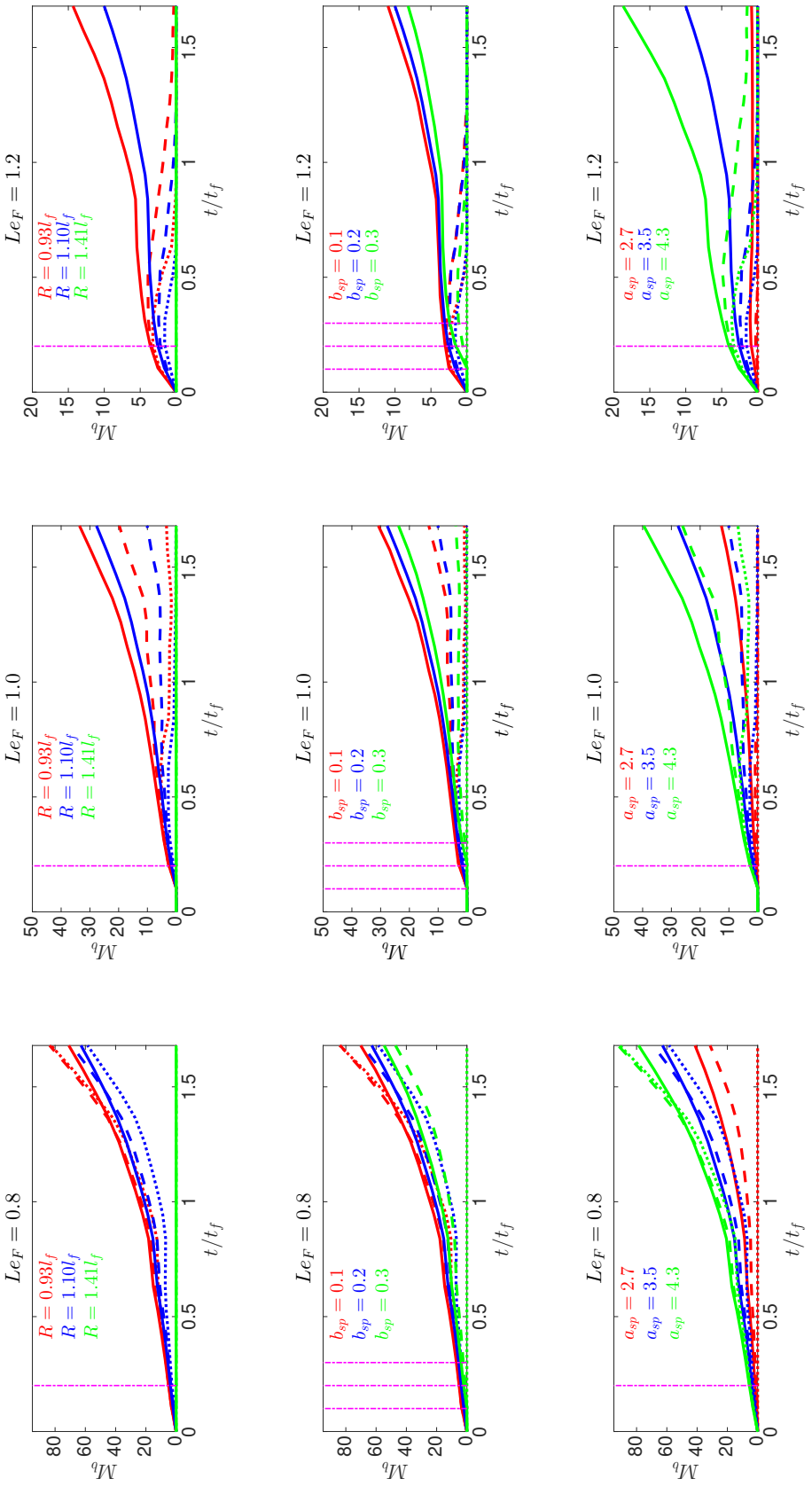

Figure 6.5: Temporal distribution of M_b for all the cases with $\phi = 1.0$ listed in Table 6.1. (where 1^{st} column shows $Le_F = 0.8$; 2^{nd} column shows $Le_F = 1.0$; 3^{rd} column shows $Le_F = 1.2$; magenta vertical dashed-broken line shows $t = t_{sp}$; additionally $\frac{u'}{S_{b(\phi=1)}} = 0.0$ [——]; $\frac{u'}{S_{b(\phi=1)}} = 4.0$ [– – – –]; $\frac{u'}{S_{b(\phi=1)}} = 6.0$ [. . . . .])

6.4 suggests that the term $\dot{w}_c$ [■] remains negligible in unburned side and increases sharply towards the burned side before decreasing to zero in the fully burned products. The magnitude of the term $\dot{w}_c$ [■] decreases with time, once the igniter is switched off, which is principally due to the decrease in fuel reaction rate magnitude with time. Fuel Lewis number lower (greater) than unity provides faster mass (thermal) diffusion influencing flame propagation. The molecular diffusion term ($\nabla\cdot(\rho D\nabla c)$ [■]) remains positive in unburnt reactants (between $c = 0$ and $c \leq 0.4$) whereas becomes negative for burned products (between $c > 0.4$ and $c = 1.0$). At time $t = 0.21t_f$ in Figure 6.4 (2^{nd} row) all fuel Lewis number cases shows both positive and negative values for molecular diffusion term ($\nabla\cdot(\rho D\nabla c)$ [■]), with higher positive values for $Le_F = 0.8$ case in compare to $Le_F = 1.2$ case, suggesting fuel diffusing faster in Le08ST4G case adding more fuel to reaction zone and supporting freely flame propagation for a given condition. On the other side case Le12ST4G shows less positive values (in comparison to Le08ST4G) of molecular diffusion term ($\nabla\cdot(\rho D\nabla c)$ [■]) suggesting slower mass diffusion and faster thermal diffusion, leading more heat transfer from hot gas kernel and flame leading to extinction in a given condition. Additionally the positive value of the term $\dot{w}_c + \nabla\cdot(\rho D\nabla c)$ [■] suggesting a self-sustained propagation of the flame kernel. The term $\dot{w}_c + \nabla\cdot(\rho D\nabla c)$ [■] remains positive throughout the simulation time for Le08ST4G case, suggesting self-sustained combustion (healthy flame kernel growth). The negative values of the term $\dot{w}_c + \nabla\cdot(\rho D\nabla c)$ [■] suggesting flame propagating to inward direction leading to flame quenching and eventually extinguishing (see Figure 6.4 for $Le_F = 1.0$ and $Le_F = 1.2$ cases).

6.2.4 Temporal Evolution of the Burned Gas Mass

The temporal evolution of M_b for all cases listed in Table 6.1 are shown in Figures 6.5 and 6.6 for stoichiometric ($\phi = 1.0$) and fuel-lean ($\phi = 0.8$) mixtures respectively. For the ease of understanding, this section 6.2.4 is further divided in two parts in order to illustrate the effects of $\frac{u'}{S_{b(\phi=1)}}$ coupled with Le_F in the first part, and the effects of energy deposition characteristics with different Le_F in the second part.

Effects of $\frac{u'}{S_{b(\phi=1)}}$ and Le_F

It can be seen from Figure 6.5 that M_b assumes the highest value for the quiescent condition ($\frac{u'}{S_{b(\phi=1)}} = 0.0$) for all the cases with $Le_F = 1.0$ and $Le_F = 1.2$. The

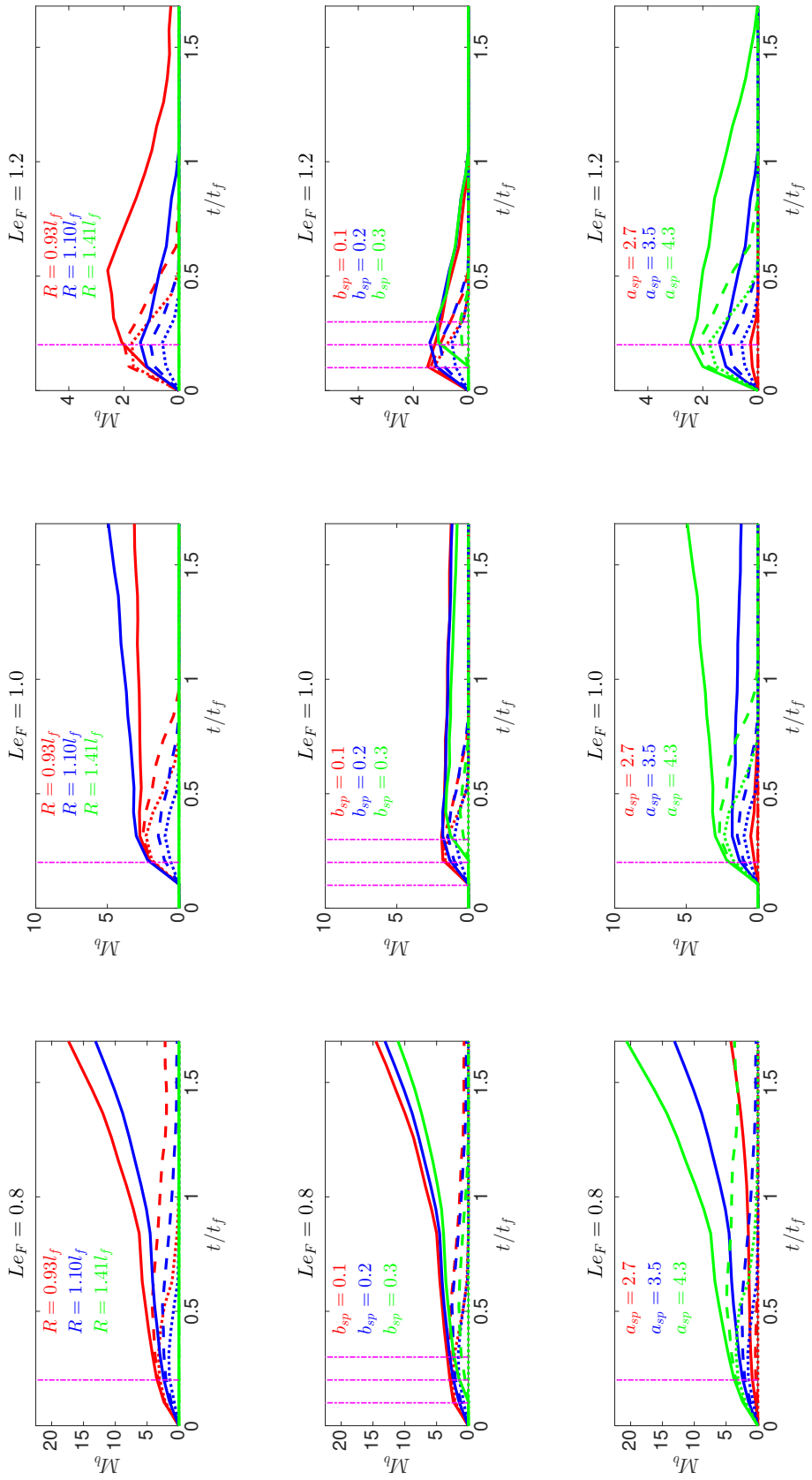

Figure 6.6: Temporal distribution of M_b for all the cases with $\phi = 0.8$ listed in Table 6.1. (where 1^{st} column shows $Le_F = 0.8$; 2^{nd} column shows $Le_F = 1.0$; 3^{rd} column shows $Le_F = 1.2$; magenta vertical dashed-broken line shows $t = t_{sp}$; additionally $\frac{u'}{S_{b(\phi=1)}} = 0.0$ [——]; $\frac{u'}{S_{b(\phi=1)}} = 4.0$ [– – – –]; $\frac{u'}{S_{b(\phi=1)}} = 6.0$ [. . . . .])

eddy thermal diffusivity D_t (see Equation 5.8) increases with increasing $\frac{u'}{S_{b(\phi=1)}}$ for a given value of $^{L_{11}}/_{l_f}$, which acts to increase the heat transfer rate from the hot gas kernel. However, an increase in $\frac{u'}{S_{b(\phi=1)}}$ also increases the extent of flame wrinkling, which acts to increase the overall burning rate in turbulent flames. The heat release due to combustion must overcome the heat loss in order to have the growth of the hot gas kernel and self-sustained flame propagation following successful ignition. The augmentation of heat transfer rate due to turbulence overcomes the enhancement of burning rate in the $Le_F = 1.0$ and $Le_F = 1.2$ cases for all values of R, b_{sp} and a_{sp}, and thus the extent of burning decreases with increasing $\frac{u'}{S_{b(\phi=1)}}$ and for high values of $\frac{u'}{S_{b(\phi=1)}}$ heat transfer from the kernel dominates over the rate of heat release and flame may eventually extinguish for large values of $\frac{u'}{S_{b(\phi=1)}}$. The probability of finding high values of reaction progress variable c decreases with increasing $\frac{u'}{S_{b(\phi=1)}}$ due to enhanced heat transfer rate from hot gas kernel for $Le_F = 1.0$ and $Le_F = 1.2$ cases. This phenomena reflected in the smaller values of M_b for higher values of $\frac{u'}{S_{b(\phi=1)}}$ for $Le_F = 1.0$ and $Le_F = 1.2$ cases. Moreover in majority turbulent cases the flame kernel eventually extinguishes for $Le_F = 1.2$ with $\phi = 1.0$ (see Figure 6.5-3^{rd} column). The flame kernel eventually extinguishes for all $Le_F = 1.2$ turbulent cases with fuel-lean mixtures $\phi = 0.8$ (see Figure 6.6-3^{rd} column).

The favorable effects of $\frac{u'}{S_{b(\phi=1)}}$ can be observed in the extent of burning for $Le_F = 0.8$ with $\phi = 1.0$ cases (see Figure 6.5-1^{st} column). The generation of flame surface area is particularly strong in the turbulent $Le_F = 0.8$ with $\phi = 1.0$ cases due to high rate of flame propagation and burning rate. As discussed in Section 6.2.3 and observed from Figure 6.4, molecular diffusion is strongest and thermal diffusion is slowest for $Le_F = 0.8$ cases in compare to $Le_F = 1.0$ and $Le_F = 1.2$ cases. The burning rate augmentation due to increased flame area generation in the turbulent $Le_F = 0.8$ cases with initial $\frac{u'}{S_{b(\phi=1)}} = 4.0$ overcomes the augmented heat transfer from the hot gas kernel. This gives rise to greater extent of burning for $Le_F = 0.8$ cases with initial $\frac{u'}{S_{b(\phi=1)}} = 4.0$ than the corresponding quiescent case with $Le_F = 0.8$. The generation of flame surface area is particularly strong in the turbulent $Le_F = 0.8$ cases with $\phi = 1.0$ due to the high rate of flame propagation and burning rate as a result of the combination of strong focusing of fuel and weak defocusing of conductive heat fluxes for the flame surfaces which are convex towards the reactants and the probability of finding the flame elements which are convex towards the reactants is high in this configuration as the flames are initiated as spherical kernels. As the higher extent of flame area generation and burning rate for turbulent $Le_F = 0.8$ cases with $\phi = 1.0$

		$\phi = 1.0$ [S] ; $\phi = 0.8$ [L]		
		$Le_F = 0.8$ [Le08] ; $Le_F = 1.0$ [Le10] ; $Le_F = 1.2$ [Le12]		
$\frac{L_{11}}{l_f} = 3.36$		$\frac{u'}{S_{b(\phi=1)}} = 0.0$ [T0]	$\frac{u'}{S_{b(\phi=1)}} = 4.0$ [T4]	$\frac{u'}{S_{b(\phi=1)}} = 6.0$ [T6]
$a_{sp} = 5.5$ $R = 1.10l_f$ $b_{sp} = 0.2t_f$	[M]	Le08ST0M Le08LT0M	Le08ST4M Le08LT4M	Le08ST6M Le08LT6M
$a_{sp} = 13.0$ $R = 1.55l_f$ $b_{sp} = 0.2t_f$	[N]	Le08ST0N Le08LT0N	Le08ST4N Le08LT4N	Le08ST6N Le08LT6N

Table 6.2: List of parameters that provides self-sustained combustion for some fuel-lean mixtures cases.
(replace [Le08] with [Le10] for $Le_F = 1.0$ and [Le12] for $Le_F = 1.2$ cases.)

eclipses the enhanced heat transfer rate from the hot gas kernel, which, in turn, gives rise to an increase in $M_b(c \geq 0.9)$ with increasing $\frac{u'}{S_{b(\phi=1)}}$ (see Figure 6.5 for case Le08ST4A, Le08ST6A, Le08ST4B, Le08ST4G, Le08ST6G, Le08ST4H).

The presence of high fuel concentration in the high temperature reaction zone in the $Le_F = 0.8$ cases gives rise to higher extent of burning than the corresponding $Le_F = 1.0$ cases. By contrast, heat diffuses faster than the rate at which fuel diffuses into the reaction zone in the cases with $Le_F = 1.2$ and thus a combination of fuel depletion due to slow diffusion and low temperature due to high thermal diffusion rate in these cases gives rise to smaller extent of burning than the corresponding $Le_F = 1.0$ cases (see Figures 6.5 and 6.6). Moreover it can be seen from Figure 6.5 that the $Le_F = 1.2$ cases eventually extinguish for initial value of $\frac{u'}{S_{b(\phi=1)}} = 4.0$ and $\frac{u'}{S_{b(\phi=1)}} = 6.0$, whereas all the $Le_F = 0.8$ cases with same initial $\frac{u'}{S_{b(\phi=1)}}$ exhibit self-sustained combustion. Moreover the comparison of Figure 6.5 and Figure 6.6 reveals that the extent of burning is greater in stoichiometric ($\phi = 1.0$) mixtures than in fuel-lean ($\phi = 0.8$) cases for a given set of values of Le_F, R, b_{sp}, a_{sp} and $\frac{u'}{S_{b(\phi=1)}}$ due to higher rate of chemical reaction and heat release in the stoichiometric mixtures.

Effects of energy deposition characteristics with different Le_F

A detailed discussion on the effects of energy deposition characteristics has been already provided in Chapter 4. Here the focus is to demonstrate the effects of energy deposition characteristics for different values of Le_F. Figures 6.5 and 6.6 show that all cases with $R = 1.41l_f$ fail to ignite irrespective of the values of Le_F and ϕ, whereas a

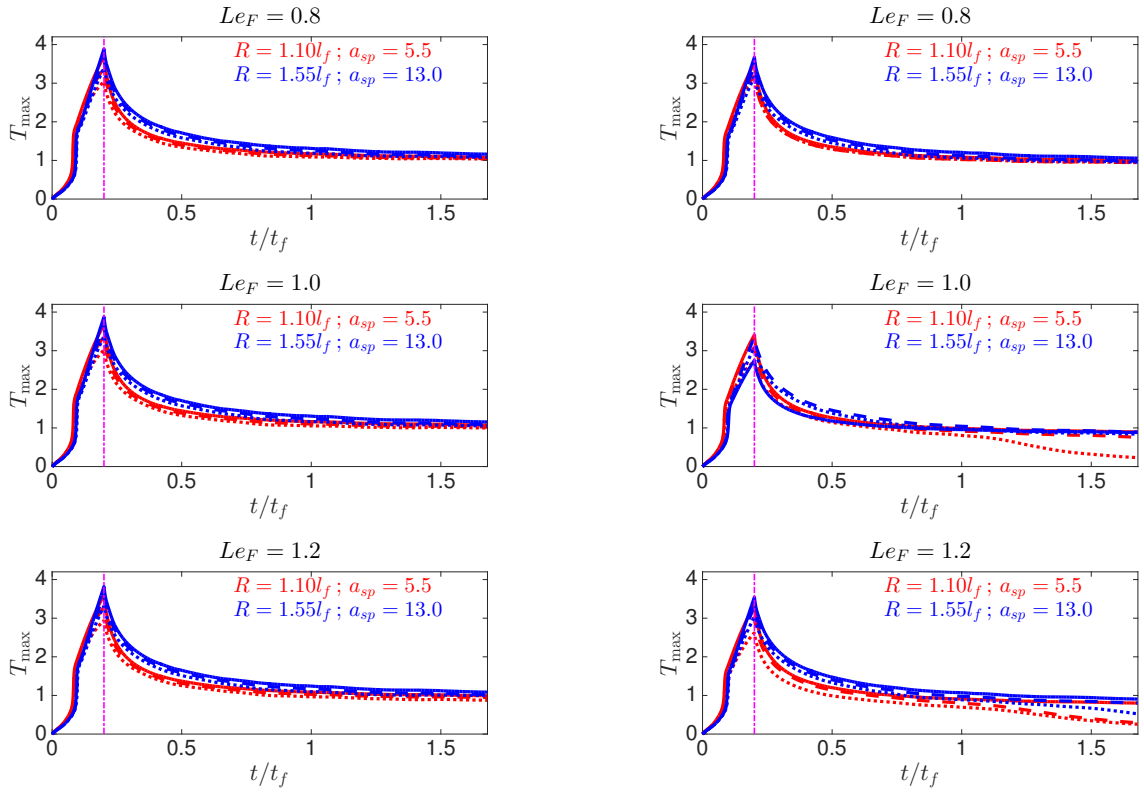

Figure 6.7: Temporal distribution of $T_{\max}$ for all the cases listed in Table 6.2. (where 1^{st} row shows $Le_F = 0.8$; 2^{nd} row shows $Le_F = 1.0$; 3^{rd} row shows $Le_F = 1.2$; magenta vertical dashed-broken line shows $t = t_{sp}$; 1^{st} column shows $\phi = 1.0$ cases and 2^{nd} column shows $\phi = 0.8$ cases; additionally $\frac{u'}{S_{b(\phi=1)}} = 0.0$ [——]; $\frac{u'}{S_{b(\phi=1)}} = 4.0$ [– – – –]; $\frac{u'}{S_{b(\phi=1)}} = 6.0$ [· · · · · · · · ·])

reduction in R gives rise to successful ignition and increases the burning rate and this event is strongest for $Le_F = 0.8$ cases. Moreover an increase in R for a given set values of b_{sp} and a_{sp} leads to deposition of energy over a larger volume of mixture, which leads to reduction in the probability of finding high temperature to support chemical reaction. This in turn reduces the overall rate of fuel consumption and heat release within the flame kernel for high values of R, and flame eventually extinguishes when the heat transfer from hot gas kernel overcomes the chemical release.

Additionally Figures 6.5 and 6.6 show that the effects of b_{sp} on the extent of burning in both stoichiometric and fuel-lean mixtures are qualitatively similar irrespective values of Le_F. An increase in b_{sp} gives rise to a reduction in ignition power for a given set of values of a_{sp} and R. This, in turn, reduces the the probability of finding high magnitude of $\dot{\Omega}_F$ and thus chemical heat release decreases with increasing b_{sp}, which leads to a reduction in the extent of burning and the flames are more prone to extinction for high values of b_{sp} especially for fuel-lean cases (this detrimental effect is particularly prevalent in the $Le_F = 1.2$ cases, see Figure 6.6-3^{rd} column).

It can further be seen from Figures 6.5 and 6.6 that an increase in a_{sp} for a given set of value of Le_F, R, b_{sp} and $\frac{u'}{S_{b(\phi=1)}}$ increases the probability of finding high temperature and $\dot{\Omega}_F$ values. This in turn leads to a higher extent of burning with increasing a_{sp} and improve the chances of successful ignition and self-sustained combustion, which is especially critical for the fuel-lean cases and for the $Le_F > 1.0$ cases. It can be concluded from the Figures 6.5 and 6.6 that high (small) values of a_{sp} (Le_F, R, b_{sp}) provide favourable condition in order to achieve self- sustained combustion following successful ignition of homogeneous mixtures. Furthermore, the choice of R, b_{sp} and a_{sp}, which leads to successful self-sustained combustion, depends on turbulence intensity $\frac{u'}{S_{b(\phi=1)}}$ and fuel Lewis number Le_F.

6.2.5 Ignition and Self-Sustained Combustion for Fuel-Lean Mixtures

The requirement of MIE increases with decreasing ϕ [116, 134]. The turbulent fuel-lean cases shown in Figures 6.2 and 6.6 do not exhibit self-sustained combustion but it is possible to obtain self-sustained combustion for turbulent fuel-lean cases for judicious choice of R, b_{sp} and a_{sp} (discussed n Section 4.2.6). The judicious choice of R, b_{sp} and a_{sp} can be favorable for $Le_F > 1.0$ and $\phi = 0.8$ turbulent cases in order to achieve self-sustained combustion. In order to demonstrate this, the cases summarised in Table 6.2

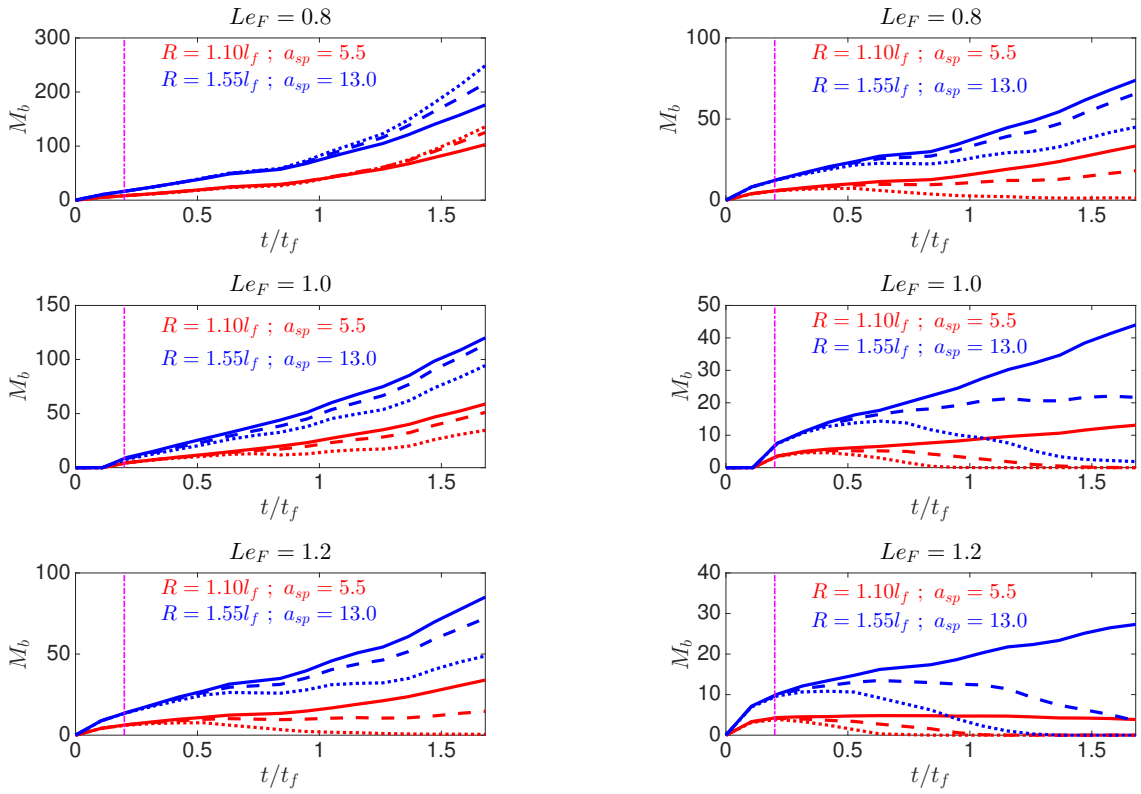

Figure 6.8: Temporal distribution of M_b for all the cases listed in Table 6.2. (where 1^{st} row shows $Le_F = 0.8$; 2^{nd} row shows $Le_F = 1.0$; 3^{rd} row shows $Le_F = 1.2$; magenta vertical dashed-broken line shows $t = t_{sp}$; 1^{st} column shows $\phi = 1.0$ cases and 2^{nd} column shows $\phi = 0.8$ cases; additionally $\frac{u'}{S_{b(\phi=1)}} = 0.0$ [——]; $\frac{u'}{S_{b(\phi=1)}} = 4.0$ [– – – –]; $\frac{u'}{S_{b(\phi=1)}} = 6.0$ [· · · · · · · · ·])

have been considered here. The temporal evolution of $T_{\max}$ and M_b for cases in Table 6.2 are shown in Figures 6.7 and 6.8 respectively. The observation from Figure 6.7 reveals that $T_{\max}$ settles to the adiabatic flame temperature ($T \approx 1.0$) for $t \gg t_{sp}$ for all Le_F values in stoichiometric mixture cases. On the other hand the fuel lean mixture with $Le_F \geq 1.0$ cases with initial $\frac{u'}{S_{b(\phi=1)}} = 6.0$ for the combination of $a_{sp} = 13.0$ and $R = 1.55l_f$ (Le10LT6N and Le12LT6N) do not exhibit self-sustained combustion despite obtaining successful ignition. Additionally fuel-lean $Le_F = 1.2$ cases with initial $\frac{u'}{S_{b(\phi=1)}} = 4.0$ and $\frac{u'}{S_{b(\phi=1)}} = 6.0$ for the combination of $a_{sp} = 5.5$ and $R = 1.10l_f$ (Le12LT4M and Le12LT6M) also failed to obtain self-sustained combustion. However, successful self-sustained combustion has been obtained for same level of $\frac{u'}{S_{b(\phi=1)}}$ for all stoichiometric cases (cases Le10ST6N, Le12ST4M, Le12ST6M and Le12ST6N in Figure 6.7).

Despite that $T_{\max}$ approaches to adiabatic flame temperature for $t \gg t_{sp}$ for some

cases (Le08LT6M, Le10LT4M, Le12LT4M for the combination of $a_{sp} = 5.5$ and $R = 1.10l_f$) the burned gas mass M_b decreases with time suggesting that these cases may eventually extinguish with time. Moreover Figure 6.8 shows that the choice of $R = 1.55l_f$ and $a_{sp} = 13.0$ yields self-sustained combustion following successful ignition for all stoichiometric cases for all values of $\frac{u'}{S_{b(\phi=1)}}$ irrespective of the values of Le_F considered in this study. However, the values of M_b continues to increase with time for fuel-lean Le10LT0N, Le10LT4N cases (see Figure 6.8 - 2^{nd} row - 2^{nd} column), but M_b decreases with time $t \gg t_{sp}$ for the Le10LT6N, Le12LT4N, Le12LT6N cases with $Le_F \geq 1.0$ for the combination of $R = 1.55l_f$ and $a_{sp} = 13.0$.

The findings based on Figure 6.8 indicate that it is possible to obtain self-sustained combustion and successful ignition even for fuel-lean cases with $Le_F > 1.0$ for proper choices of R, b_{sp} and a_{sp}. A combination of R, b_{sp} and a_{sp}, which leads to self-sustained combustion for fuel-lean mixtures, is likely to yield self-sustained combustion for the corresponding stoichiometric cases following successful ignition. Similarly, the combination of R, b_{sp} and a_{sp}, which gives rise to self-sustained combustion for mixtures with $Le_F \geq 1.0$ are also likely to yield successful ignition and self- sustained combustion for the corresponding with $Le_F < 1.0$ cases. The ignition parameters R, b_{sp} and a_{sp} can be altered independently of each other in case of laser ignition. The recent experimental [63, 141, 198] findings suggest that laser ignition can be effective in igniting fuel-lean mixtures by altering the laser beam radius (i.e. equivalent to the variation of R), laser power (i.e. equivalent to the variation of a_{sp}) and laser pulse duration (i.e. equivalent to the variation of b_{sp}), which is consistent with current findings. However the present results indicate that the optimum values of R, b_{sp} and a_{sp} depend on background turbulence intensity $\frac{u'}{S_{b(\phi=1)}}$, equivalence ratio of the homogeneous mixture ϕ and fuel Lewis number Le_F.

6.2.6 Implication in the Context of MIE

The detailed comparison for effects of energy deposition characteristic parameters with experimental results are already presented in Chapter 4 (Section 4.2.7). Here, the Section 6.2.6 discuss the effects of Le_F in the context of MIE. The MIE ($E_{\min}$) can be extimated by the energy required to heat the mass of unburned gas with diameter d_q to its adiabatic flame temperature (see Equation 4.11) [16]. This Equation 4.11 and the discussion of Section 4.2.7 signifies that high values of a_{sp} are needed for successful ignition and self-sustained flame for fuel-lean mixture than for the stoichiometric mixture, which is in good agreement with findings shown in Figures 6.1, 6.2, 6.5 and 6.6

for the cases listed in Table 6.1 (also refer to Figures 6.7 and 6.8 for the cases listed in Table 6.2). The detrimental effects of u' on localised forced ignition are more critical for fuel-lean mixtures as the demand for $E_{\min}$ increases sharply with decreasing ϕ. This implies that a_{sp} needs to be increased for high (small) values of $u'(\phi)$ in order to obtain successful ignition and self-sustained flame combustion. For example, it was not possible to ignite both stoichiometric and fuel-lean mixtures for $a_{sp} = 2.7$, $R = 1.10l_f$ and $b_{sp} = 0.2$ for initial $\frac{u'}{S_{b(\phi=1)}} = 6.0$ but it was possible to obtain self-sustained combustion for the quiescent ($\frac{u'}{S_{b(\phi=1)}} = 0.0$) and initial $\frac{u'}{S_{b(\phi=1)}} = 4.0$ conditions for stoichiometric mixtures with $Le_F = 0.8$ and $Le_F = 1.0$. However, it is possible to obtain self-sustained combustion for $a_{sp} = 3.5$ and $a_{sp} = 4.3$ (with $R = 1.10l_f$ and $b_{sp} = 0.2$) in the case of the stoichiometric mixture with $Le_F = 0.8$ and $Le_F = 1.0$ for initial $\frac{u'}{S_{b(\phi=1)}} = 6.0$, whereas these ignition parameters lead to successful ignition of turbulent $\phi = 0.8$ mixtures but self-sustained combustion is not achieved.

Although Equation 4.11 provide information about the MIE for successful ignition and subsequent flame propagation, it does not provide any information about the effects of energy distribution on the success of ignition and subsequent flame propagation. For example, the stoichiometric cases with $Le_F = 0.8$ and $Le_F = 1.0$ exhibit self-sustained combustion for $R = 0.93l_f$ and $R = 1.10l_f$ when $a_{sp} = 3.5$ is used but the corresponding case with $R = 1.41l_f$ in Table 6.1 did not even ignite (see Figure 6.1).

A comparison between ignition power Equation 3.30 with the total energy deposited by the igniter in Equation 4.11 reveals that the value of a_{sp} corresponding to $E_{\min}$ is greater for the fuel-lean mixture than the stoichiometric mixture. For example, a combination $a_{sp} = 5.5$, $R = 1.10l_f$ and $b_{sp} = 0.2$ gives rise to self-sustained combustion in turbulent $Le_F = 0.8$ cases for the quiescent ($\frac{u'}{S_{b(\phi=1)}} = 0.0$) and initial $\frac{u'}{S_{b(\phi=1)}} = 4.0$ conditions in the case of $\phi = 0.8$ but the combination $a_{sp} = 3.5$, $R = 1.10l_f$ and $b_{sp} = 0.2$ leads to failed self-sustained combustion.

However, a direct quantitative comparison between the experimentally obtained empirical relations with present computational results is not attempted here because the experimentally obtained minimum ignition energy accounts for heat loss through the electrode which is not addressed in the simplified ignition model used in the current DNS study. Furthermore, different analyses [15, 116, 206] suggested different values/expressions of parameters A, B and S_T so the quantitative prediction of $E_{\min}$ is not entirely unambiguous, and the existing models (e.g. Equation 4.11) do not account for energy deposition and non-unity fuel Lewis number Le_F effects. The present

numerical findings suggest that the parameters A and B in Equation 4.11 are likely to be functions of fuel Lewis number Le_F such that their magnitudes increase with increasing Le_F (see Figures 6.1, 6.2, 6.5, 6.6 and 6.7, 6.8 to find that it is more difficult to obtain self-sustained combustion for $Le_F = 1.2$ cases than in the corresponding $Le_F = 0.8$ cases for same input ignition energy).

Moreover, Klein *et al.* [109] indicated that the critical diameter d_q for the limiting condition for quenching scales as:

$$d_q \propto \frac{u' L_{11}}{S_{b(\phi)} \Psi} \tag{6.1}$$

where Ψ is a parameter which increases with increasing flame wrinkling. As the extent of flame wrinkling increases with decreasing Le_F, the critical diameter d_q and the minimum ignition energy $\rho_0 C_P \left(T_{ad(\phi)} - T_0\right) \times {}^{\pi d_q^3}/_6$ are expected to decrease with decreasing fuel Lewis number Le_F .

The time scale for the diffusion of deposited energy over a distance R in the absence of mean flow, can be estimated as (see Chapter 4 - Section 4.2.7.3):

$$t_{diff} \sim \frac{R^2}{D_{ref} + D_t} \tag{6.2}$$

The eddy thermal diffusivity in turbulent flows scales as $D_t \sim u' L_{11}$, which gives rise to:

$$t_{diff} \sim \left[\frac{R}{l_f}\right]^2 t_f \left[\frac{1}{1 + a\left(\frac{u'}{S_L}\right)\left(\frac{L_{11}}{l_f}\right)}\right] \tag{6.3}$$

Experimental findings by Ballal and Lefebvre suggests that, the constant parameter $a \sim 0.16$ [16]:

$$t_{diff} \sim \frac{a_e^2 \, t_f}{\left(\frac{l_f}{L_{11}}\right)^2 + 0.2\left(\frac{t_f}{t_e}\right)} \tag{6.4}$$

where $t_e = {}^{L_{11}}/_{\sqrt{\kappa_0}}$ is the eddy turn over time and $a_e = {}^{R}/_{L_{11}}$, which is equal to 0.27, 0.22 and 0.42 for $R = 0.93 l_f$, $R = 1.10 l_f$ and $R = 1.41 l_f$, respectively. Equation 6.4 suggests that the diffusion timescale t_{diff} decreases in comparison to t_f with increasing u' with constant ${}^{L_{11}}/_{l_f}$ and therefore ${}^{t_e}/_{t_f}$ decreases with increasing u'. Thus, a decrease in b_{sp} makes more rapid energy deposition than the rate of diffusion of heat, which in turn increases the temperature of hot gas kernel and the increase in the extent of

burning with decreasing b_{sp} (or t_{sp}). For example, higher value of $T_{\max}$ and M_b are obtained in the case Le08ST0D than the case Le08ST0F (see Figures 6.1, 6.2, 6.5, 6.6 and refer to Table 6.1). Although an increase in R (or a_e in Equation 6.4) acts to increase t_{diff} , this advantage is eclipsed by the decrease in temperature in the ignition kernel as the energy is deposited over a larger mass of gas. This leads to failed ignition for $R = 1.41l_f$ in Table 6.1 (see Figures 6.1, 6.2, 6.5, 6.6). However, the detrimental effects of large values of R can be eclipsed by increasing a_{sp} , which can be substantiated by the successful self-sustained combustion for the cases Le08ST0N, Le08ST4N, Le08ST6N, Le10ST0N, Le10ST4N and Le12ST0N in Table 6.2 (see Figures 6.7 and 6.8). A similar observation has been made by Wandel [211] in the context of droplet-laden mixtures, which indicated that a large region of hot gas with small equivalence ratio variation can be advantageous from the point of ignition provided sufficient ignition energy is supplied.

6.2.7 Summary

The Section 6.2 investigates the influences of fuel Lewis number Le_F (ranging from 0.8 to 1.2) on the energy deposition characteristics on the localised forced ignition of both stoichiometric ($\phi = 1.0$) and fuel-lean ($\phi = 0.8$) homogeneous mixtures using simplified chemistry 3D compressible DNS for different values of u'. The extent of burning M_b has been found to increase with decreasing values of Le_F for a given set of values of R, b_{sp}, a_{sp} and $\frac{u'}{S_{b(\phi=1)}}$. Higher rate of fuel diffusion into the reaction zone than the rate of thermal diffusion out of this region in the $Le_F = 0.8$ cases gives rise to simultaneous presence of high values of fuel concentration and temperature within the reaction layer, which in turn leads to greater magnitude of fuel reaction rate than in the corresponding $Le_F = 1.0$ cases. By contrast, the combination of the depletion of fuel due to slow fuel diffusion and rapid thermal diffusion rate from the reaction zone leads to weaker burning for the $Le_F = 1.2$ cases than in the corresponding $Le_F = 1.0$ cases. It has been found that higher amount of ignition energy is necessary to obtain self-sustained combustion in fuel-lean cases than in the stoichiometric cases, which is consistent findings from Chapter 4. Moreover, the MIE for self-sustained combustion decreases with decreasing Le_F. Moreover, an increase in turbulent velocity fluctuation decreases the extent of burning and may lead to misfire for large values of $\frac{u'}{S_{b(\phi=1)}}$ when the augmentation of heat transfer due to turbulence dominates over the enhanced burning rate in turbulent flames. This is prevalent in the $Le_F \geq 1.0$ cases

and the detrimental effects of $\frac{u'}{S_{b(\phi=1)}}$ are more critical in fuel-lean mixture than in the stoichiometric mixture due to its weaker heat release effects in the fuel-lean mixtures. However, the enhanced rate of burning due to flame wrinkling may dominate over the augmented heat transfer rate in the $Le_F < 1.0$ cases under some conditions, which may give rise to an increase in the burned gas mass M_b with increasing $\frac{u'}{S_{b(\phi=1)}}$. An increase in energy deposition width (R) and duration of energy deposition (b_{sp}) for a given amount of input ignition energy (a_{sp}) has been found to have detrimental effects on the extent of burning and these effects can be critical for ignition of fuel-lean mixtures and also for the mixtures with $Le_F > 1.0$.

6.3 Effects of Le_F on Localised Forced Ignition of Globally Stoichiometric Stratified Mixtures

This Section 6.3 starts with brief overview on the numerical formulation and then the results for effects of Le_F on localised forced ignition of globally stoichiometric stratified mixtures are presented and discussed. Global behaviours of maximum values of temperature is shown first to analyse the influences of Le_F on the possibility of self-sustained combustion following successful ignition. Spatial distribution of different quantities is then presented. Mode of combustion and mixing statistics is evaluated. The reaction-diffusion balance analysis of flame kernels is shown. The statistical behaviour of fuel reaction rate magnitude is examined to understand the effects of Le_F on the extent of burning following successful ignition. Finally, this section investigate the effects of Le_F on the extent of burning and ends with summary.

The numerical formulation remains similar to as described in Section 5.2.1 except for one modification, the fuel Lewis number is ranging from 0.8 to 1.2 here. Moreover, the length scale of mixture inhomogeneity is taken as the Taylor micro-scale of the equivalence ratio variation l_ϕ and is already defined in Equation 5.1 (Section 5.2). The initial mixture inhomogeneity field is initiated following Gaussian distribution [81] and Bi-modal distribution [76] for a given set of values of ϕ' and l_ϕ for $\langle\phi\rangle$ (Section 3.7). The ignition parameters is taken as: $a_{sp} = 3.60$, $b_{sp} = 0.2$ and $R = 1.10l_f$ (see Section 3.3). Simulations have been carried out for $t_{sim} \sim 8.40t_{sp}$ in all cases. Table 6.3 shows parametric variation across different parameters, and thus in total 657 simulations (162 $\times$ 4 stratified mixture cases + 9 homogeneous mixtures) have been conducted here. The case names are chosen in such manner so that Le08, Le10, Le12

	$Le_F = 0.8$ [Le08]		
	$\langle\phi\rangle = 1.0$ [S]		
	Gaussian [G]; Bi-modal [Bi]		
	$\phi' = 0.2$ [A]		
$L_{11}/l_f = 3.36$	$\frac{l_\phi}{l_f} = 2.1$ [D]	$\frac{l_\phi}{l_f} = 5.5$ [E]	$\frac{l_\phi}{l_f} = 8.3$ [F]
$\frac{u'}{S_{b(\phi=1)}} = 0.0$ [T0]	Le08GST0AD Le08BiST0AD	Le08GST0AE Le08BiST0AE	Le08GST0AF Le08BiST0AF
$\frac{u'}{S_{b(\phi=1)}} = 4.0$ [T4]	Le08GST4AD Le08BiST4AD	Le08GST4AE Le08BiST4AE	Le08GST4AF Le08BiST4AF
$\frac{u'}{S_{b(\phi=1)}} = 6.0$ [T6]	Le08GST6AD Le08BiST6AD	Le08GST6AE Le08BiST6AE	Le08GST6AF Le08BiST6AF
Homogeneous cases Le08T0, Le08T4, Le08T6			

Table 6.3: List of parameters to analyse effects of Le_F with different initial distribution (i.e. Gaussian and Bi-modal) in globally stoichiometric (i.e. $\langle\phi\rangle = 1.0$) stratified mixtures. (Replace [Le08] with [Le10] and [Le12] for $Le_F = 1.0$ and $Le_F = 1.2$ cases; Replace [A] with [B] and [C] for $\phi' = 0.4$ and $\phi' = 0.6$ cases.)

indicate Le_F values 0.8, 1.0 and 1.2 respectively; S stands for globally stoichiometric ($\langle\phi\rangle = 1.0$) stratified mixtures; G and Bi stands for initial Gaussian and Bi-modal distribution of ϕ; T0, T4 and T6 indicate increasing turbulent level; A, B, and C indicate increasing values of ϕ'; and D, E, and F denote increasing values of l_ϕ/l_f (e.g. Le08GST0AD corresponds to a case for initial Gaussian distribution of globally stoichiometric ($\langle\phi\rangle = 1.0$) stratified mixtures with values of $Le_F = 0.8$; $\frac{u'}{S_{b(\phi=1)}} = 0.0$; $\phi' = 0.2$; $l_\phi/l_f = 2.1$).

6.3.1 Global Behaviours of Maximum Values of Temperature

The temporal evolution of the maximum values of non-dimensional temperature are shown in Figure 6.9, 6.10 and 6.11 for $\phi' = 0.2$, $\phi' = 0.4$ and $\phi' = 0.6$ cases respectively from Table 6.3. The global behaviour of increasing $T_{\max}$ during $0 \leq t \leq t_{sp}$ are similar as seen in Chapter 5. Moreover the trend of $T_{\max}$ in Figures 6.9, 6.10 and 6.11 provides an indication for achieving self-sustained combustion and for flame extinction. It can be seen from Figures 6.9, 6.10 and 6.11 that self-sustained combustion has been obtained for all cases with $Le_F = 0.8$, whereas only some cases with $Le_F = 1.0$ and $Le_F = 1.2$ exhibit self-sustained combustion. The conditions, which led to self-sustained flame propagation originated from successful ignition, depend on the

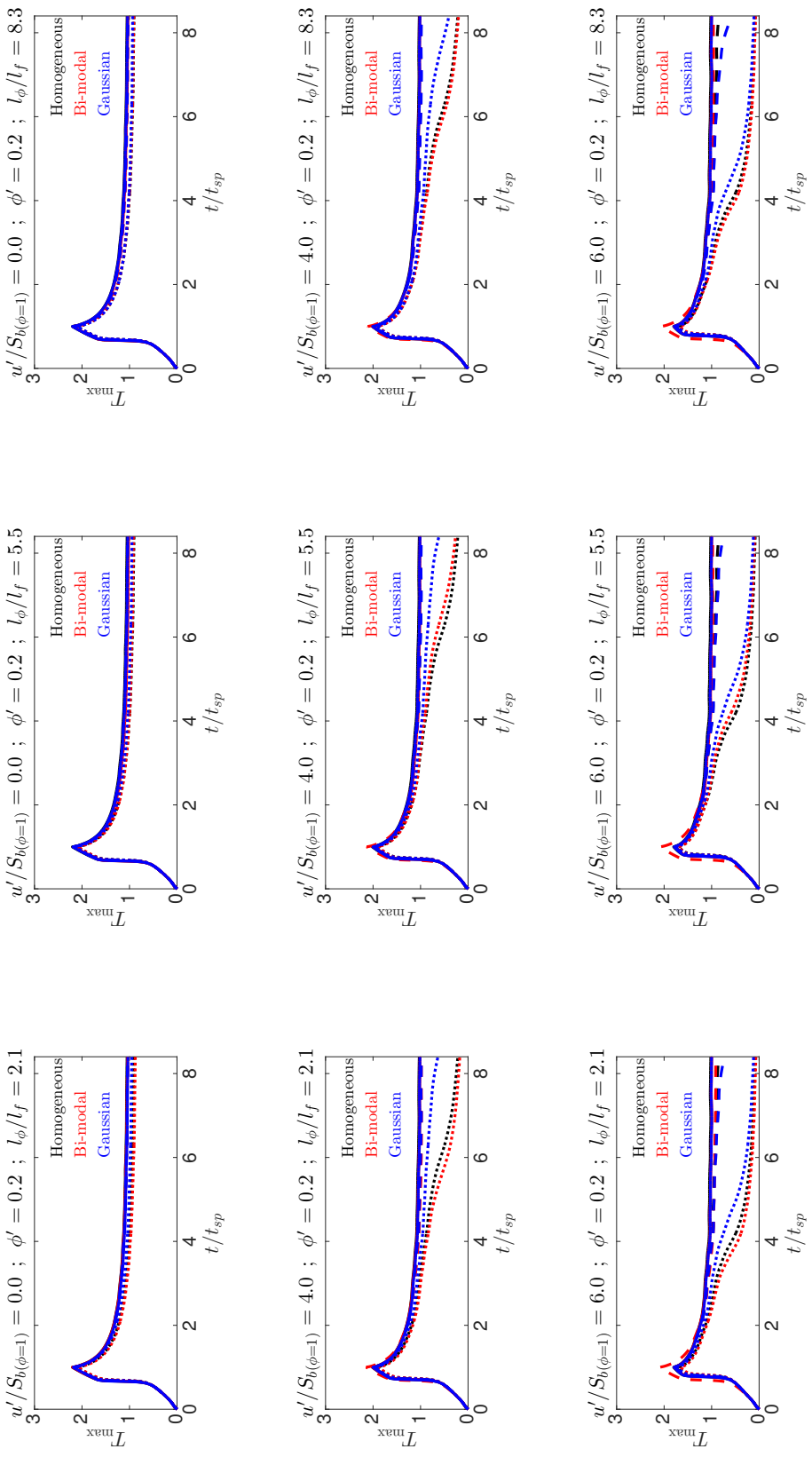

Figure 6.9: Temporal distribution of $T_{\max}$ for all the cases with $\phi' = 0.2$ listed in Table 6.3. [where 1^{st} column shows $l_\phi/l_f = 2.1$; 2^{nd} column shows $l_\phi/l_f = 5.5$; 3^{rd} column shows $l_\phi/l_f = 8.3$; additionally 1^{st} row shows $\frac{u'}{S_{b(\phi=1)}} = 0.0$; 2^{nd} row shows $\frac{u'}{S_{b(\phi=1)}} = 4.0$; 3^{rd} row shows $\frac{u'}{S_{b(\phi=1)}} = 6.0$, moreover $Le_F = 0.8$(——), $Le_F = 1.0$ (— — —) and $Le_F = 1.2$ (·····)]

nature of initial mixture distribution, Le_F, $\frac{u'}{S_{b(\phi=1)}}$, ϕ' and ${}^{l_\phi}/_{l_f}$. It has been found that self-sustained flame propagation has been obtained for all the quiescent cases except for the Le12BiST0BE, Le12BiST0CD, Le10BiST0CE and Le12BiST0CE cases. This suggests that the initial Gaussian mixture distribution in quiescent ($\frac{u'}{S_{b(\phi=1)}} = 0.0$) cases are more favorable choice for obtaining self-sustained combustion in comparison to initial Bi-modal mixture distribution. Additionally, for the initial Bi-modal mixture distribution the temporal evolution of $T_{\max}$ for $\phi' = 0.4$ cases are mostly qualitatively similar to that of the initial $\phi' = 0.6$ cases except for the quiescent $Le_F = 1.0$ and $Le_F = 1.2$ cases with initial ${}^{l_\phi}/_{l_f} = 5.5$, which exhibit self-sustained combustion for initial $\phi' = 0.4$ whereas the flames extinguish after successful ignition for initial $\phi' = 0.6$.

There are cases where the initial mixture distribution play pivotal role for obtaining self-sustained combustion. For example, compare cases Le10BiST6BF and Le10GST6BF in Figure 6.10, shows initial Bi-modal mixture distribution are more favorable for obtaining self-sustained combustion following successful ignition in cases with $Le_F = 1.0$, $\phi' = 0.4$, $\frac{u'}{S_{b(\phi=1)}} = 6.0$ and ${}^{l_\phi}/_{l_f} = 8.3$ over initial Gaussian mixture distribution for a given realisation of ϕ. On the other side, compare cases Le10BiST4BE and Le10GST4BE in Figure 6.10, demonstrated the initial Gaussian mixture distribution are provides favorable condition for obtaining self-sustained combustion following successful ignition in cases with $Le_F = 1.0$, $\phi' = 0.4$, $\frac{u'}{S_{b(\phi=1)}} = 4.0$ and ${}^{l_\phi}/_{l_f} = 5.5$ over initial Bi-modal mixture distribution for a given realisation of ϕ. This dependency on the nature of initial mixture distribution for achieving self-sustained combustion is consistent for higher values of $\phi' = 0.6$ (compare cases Le10BiST6CF with Le10GST6CF and Le10BiST4CE with Le10GST4CE in Figure 6.11).

The maximum temperature value $T_{\max}$ decreases continuously with time for $t > t_{sp}$ in all the turbulent cases with $Le_F = 1.2$ despite the nature of initial mixture distribution considered here, indicating failure to obtain self-sustained combustion in these cases and flame extinguishes at an earlier time for higher values of u'. This is consistent with analytical results by He [90] who demonstrated that it is more difficult to ignite and sustain combustion for $Le_F > 1.0$.

Additionally, Figure 6.11 demonstrate that $T_{\max}$ decreases continuously with time for $t > t_{sp}$ in the high turbulent cases ($\frac{u'}{S_{b(\phi=1)}} = 6.0$) with $Le_F = 1.0$ and $Le_F = 1.2$ for initial values of ${}^{l_\phi}/_{l_f} = 5.5$, whereas self-sustained combustion is obtained for all the turbulent cases with initial values of ${}^{l_\phi}/_{l_f} = 5.5$ for $Le_F = 0.8$ despite the nature of initial mixture distributions (see 2^{nd}column - 3^{rd}rows of Figure 6.11). The observation

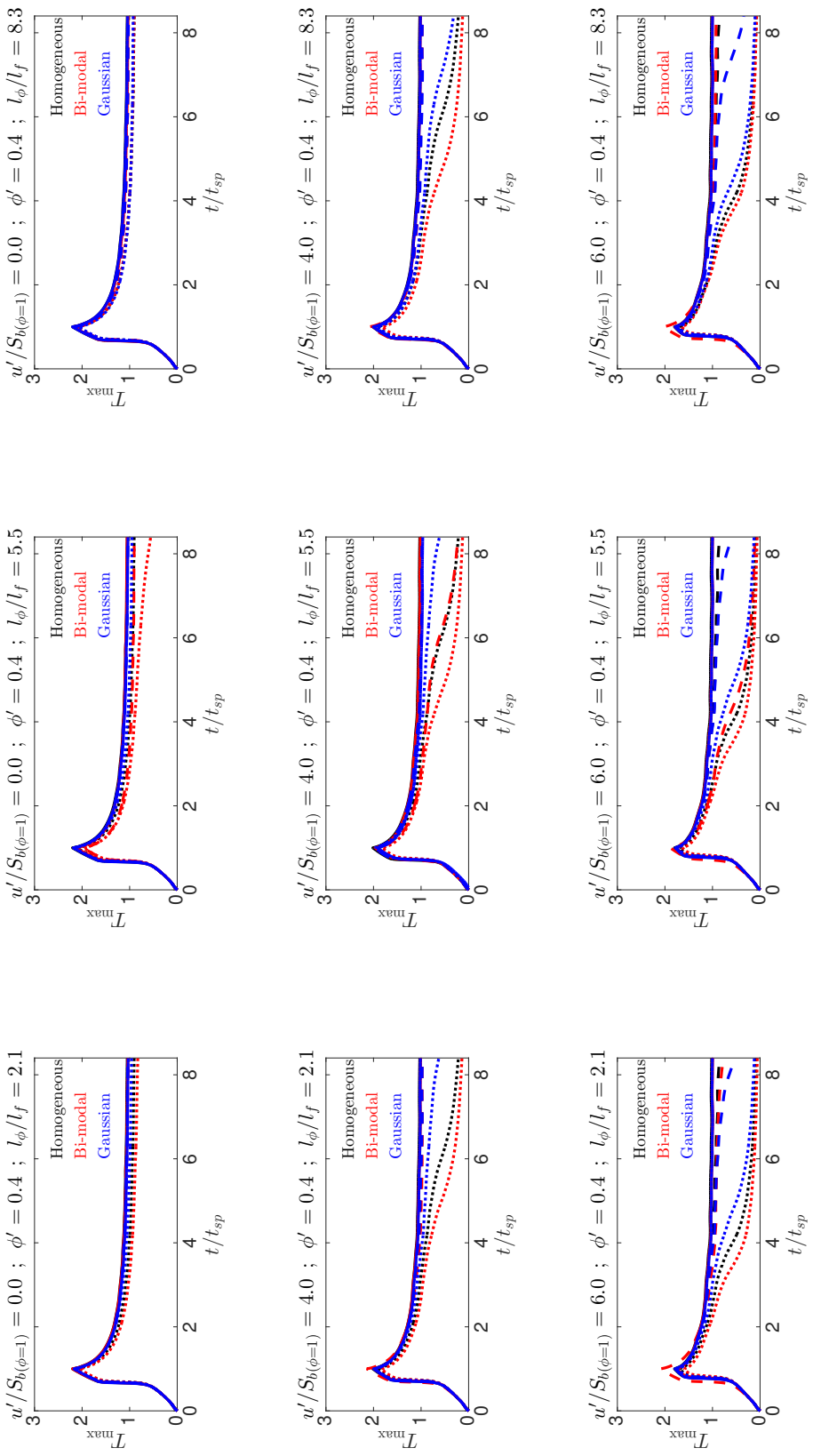

Figure 6.10: Temporal distribution of T_{max} for all the cases with $\phi' = 0.4$ listed in Table 6.3. [where 1^{st} column shows $l_\phi/l_f = 2.1$; 2^{nd} column shows $l_\phi/l_f = 5.5$; 3^{rd} column shows $l_\phi/l_f = 8.3$; additionally 1^{st} row shows $\frac{u'}{S_{b(\phi=1)}} = 0.0$; 2^{nd} row shows $\frac{u'}{S_{b(\phi=1)}} = 4.0$; 3^{rd} row shows $\frac{u'}{S_{b(\phi=1)}} = 6.0$, moreover $Le_F = 0.8$(——), $Le_F = 1.0$ (— — —) and $Le_F = 1.2$ (·····)]

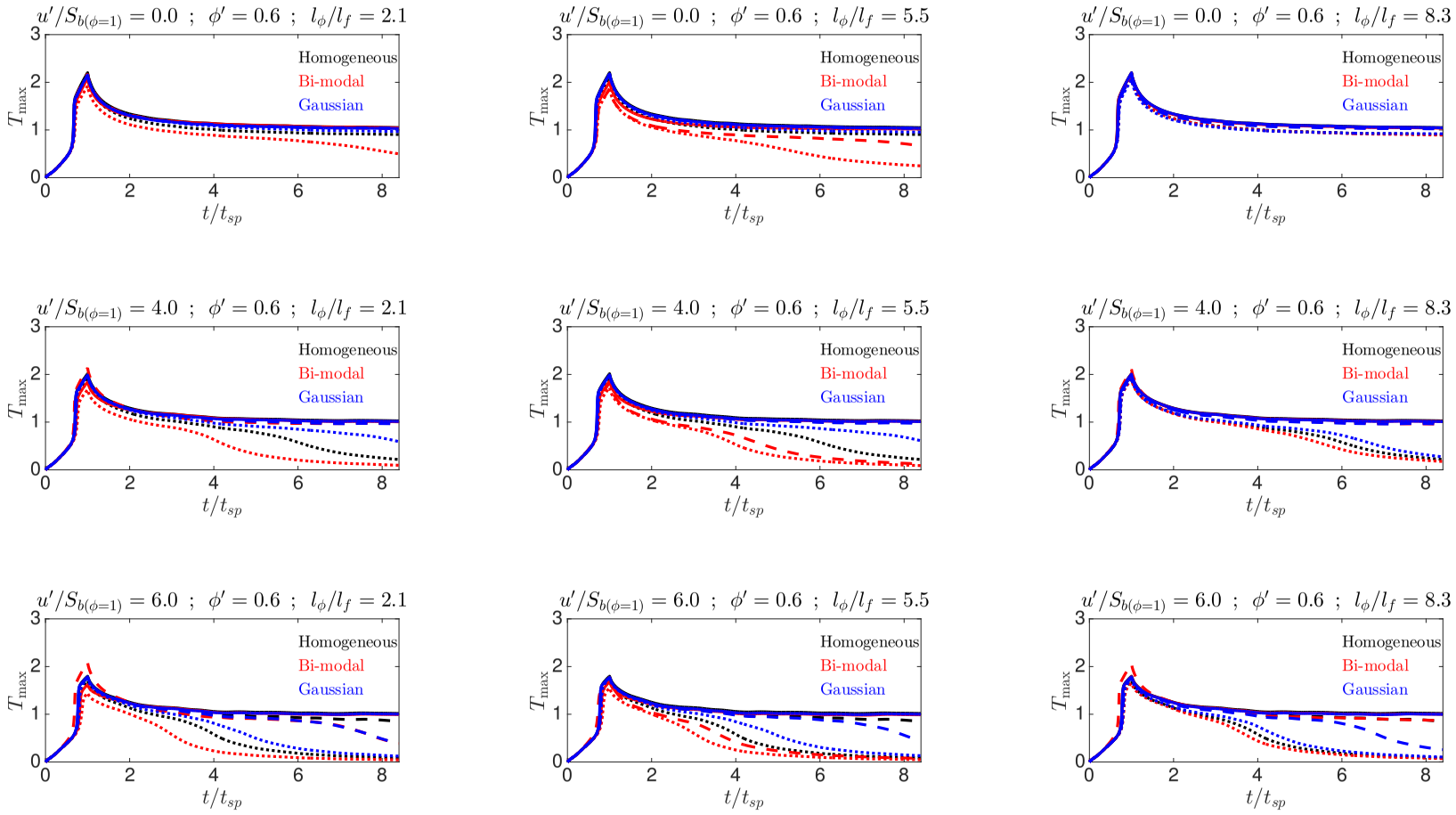

Figure 6.11: Temporal distribution of $T_{\max}$ for all the cases with $\phi' = 0.6$ listed in Table 6.3. [where 1^{st} column shows ${}^{l_\phi}/_{l_f} = 2.1$; 2^{nd} column shows ${}^{l_\phi}/_{l_f} = 5.5$; 3^{rd} column shows ${}^{l_\phi}/_{l_f} = 8.3$; additionally 1^{st} row shows $\frac{u'}{S_{b(\phi=1)}} = 0.0$; 2^{nd} row shows $\frac{u'}{S_{b(\phi=1)}} = 4.0$; 3^{rd} row shows $\frac{u'}{S_{b(\phi=1)}} = 6.0$, moreover $Le_F = 0.8$(——), $Le_F = 1.0$ (— — — —) and $Le_F = 1.2$ (·····)]

made from Figures 6.9, 6.10 and 6.11 indicate that initial mixture distribution profile, Le_F, $\frac{u'}{S_{b(\phi=1)}}$, ϕ' and ${}^{l_\phi}/_{l_f}$ have important influences on the possibility of self-sustained combustion following successful ignition. Moreover, the effects of ${}^{l_\phi}/_{l_f}$ on the success of self-sustained combustion seem to be non-monotonic for initial Bi-modal mixture distribution (e.g. the cases with initial ${}^{l_\phi}/_{l_f} = 5.5$ are more prone to flame extinction than the cases with initial values of ${}^{l_\phi}/_{l_f} = 2.1$ and ${}^{l_\phi}/_{l_f} = 8.3$ for $\phi' = 0.6$ with initial Bi-modal mixture distribution) in the cases of unity fuel Lewis number.

6.3.2 Spatial Distribution of Temperature, Fuel Mass Fraction, Reaction Rate Magnitude and Equivalence Ratio

The distribution of non-dimensional temperature (i.e. T), fuel mass fraction (i.e. Y_F), normalised fuel reaction rate magnitude (i.e. $\dot{\Omega}_F$) and equivalence ratio (i.e. ϕ) at $t = 1.05t_{sp}$ and $t = 8.40t_{sp}$ in the central x_1-x_2 plane for the cases with $\phi' = 0.4$, ${}^{l_\phi}/_{l_f} = 8.3$ and $\frac{u'}{S_{b(\phi=1)}} = 4$ are shown in Figure 6.12 for initial Bi-modal distribution and Figure 6.13 for initial Gaussian distribution of ϕ. Similar qualitative behaviour has been observed for other cases but the burned gas volume for the stratified mixture cases has been found to decrease with increasing ${}^{u'}/_{S_{b(\phi=1)}}$ for given set values of Le_F, ϕ' and ${}^{l_\phi}/_{l_f}$. It can be seen from Figures 6.12 and 6.13 that the contours of T remain approximately spherical during the period of energy deposition but they become increasingly wrinkled as time progresses for all turbulent cases. Additionally observation from Figures 6.12 and 6.13 reveals that fuel mass diffuses faster in $Le_F = 0.8$ cases in compare to $Le_F = 1.2$ cases, providing more fuel diffuses into the reaction zone leading to high flame kernel growth for $Le_F = 0.8$ cases.

Moreover, it can be seen from Figures 6.12 and 6.13 that the level of non-uniformity in ϕ distribution decreases as time progresses in all cases. A comparison between different Le_F cases reveals that the volume of high temperature region and the extent of flame wrinkling decrease with increasing Le_F. For the cases with $Le_F < 1.0$, fuel diffuses rapidly into the reaction zone than the rate at which heat is conducted out, whereas the opposite mechanism remains prevalent for the $Le_F > 1.0$ cases. As a result of rapid mass diffusion for $Le_F < 1.0$ provided high concentration of fuel and high temperature leads higher rate of burning and greater extent of flame wrinkling than in the corresponding $Le_F = 1.0$ and $Le_F = 1.2$ cases. The above observation of Figures 6.12 and 6.13 are consistent for both initial mixture distributions of ϕ (i.e. Gaussian and Bi-modal).

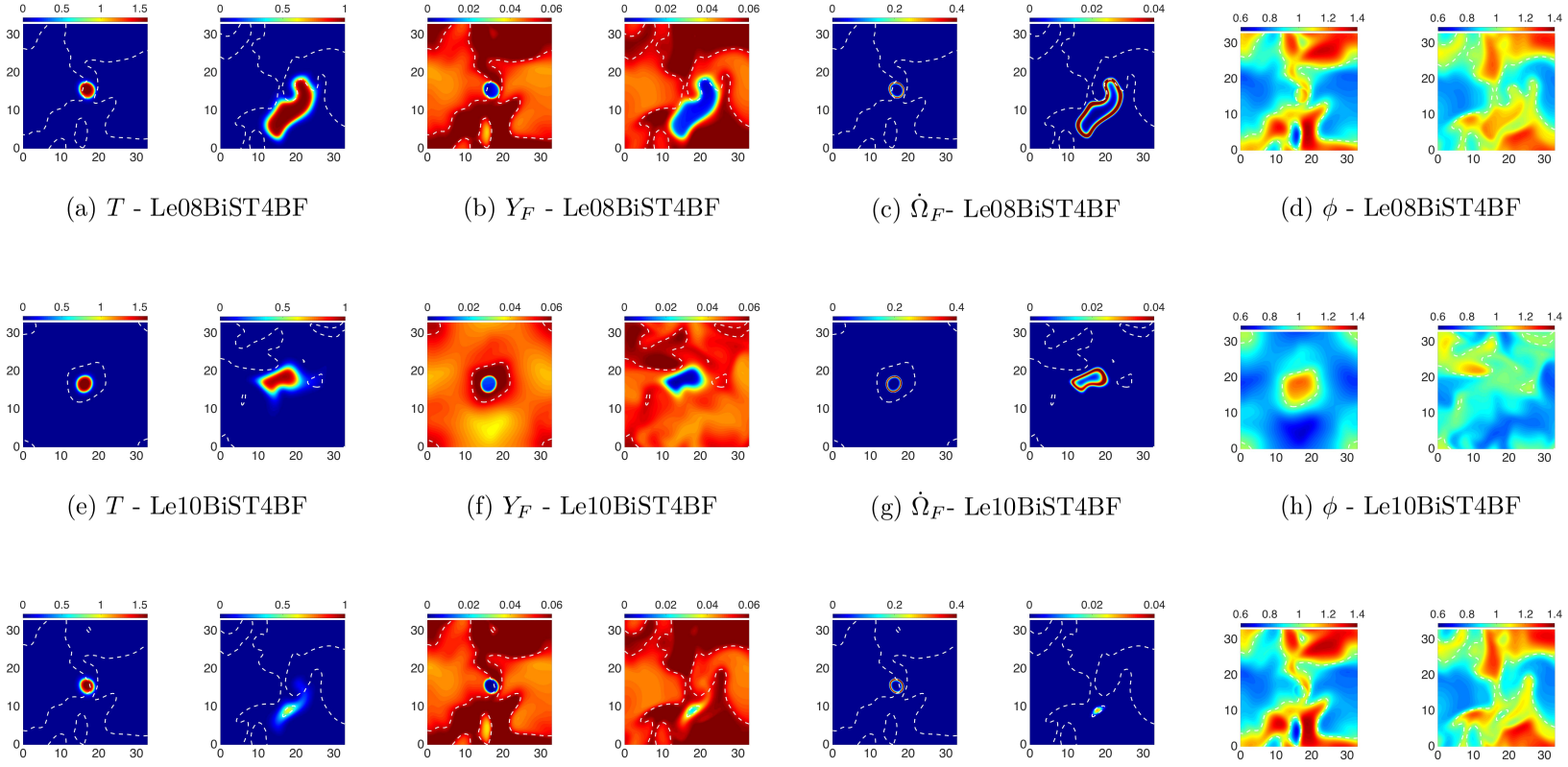

(a) T - Le08BiST4BF (b) Y_F - Le08BiST4BF (c) $\dot{\Omega}_F$- Le08BiST4BF (d) ϕ - Le08BiST4BF

(e) T - Le10BiST4BF (f) Y_F - Le10BiST4BF (g) $\dot{\Omega}_F$- Le10BiST4BF (h) ϕ - Le10BiST4BF

(i) T - Le12BiST4BF (j) Y_F - Le12BiST4BF (k) $\dot{\Omega}_F$- Le12BiST4BF (l) ϕ - Le12BiST4BF

Figure 6.12: Distribution of T (1^{st} & 2^{nd} columns), Y_F (3^{rd} & 4^{th} columns), $\dot{\Omega}_F$ (5^{th} & 6^{th} columns) and ϕ (7^{th} & 8^{th} columns) on the central $x_1 - x_2$ plane for the cases with $\phi' = 0.4$, ${}^{l_\phi}/_{l_f} = 8.3$ and $\frac{u'}{S_{b(\phi=1)}} = 4$. The white broken like shows $\xi = \xi_{st}$. Additionally 1^{st}, 3^{rd}, 5^{th}, 7^{th} columns showing $t = 1.05t_{sp}$, 2^{nd}, 4^{th}, 6^{th}, 8^{th} columns showing $t = 8.40t_{sp}$, moreover $Le_F = 0.8$ (1^{st} row), $Le_F = 1.0$ (2^{nd} row), $Le_F = 1.2$ (3^{rd} row) for initial Bi-modal mixture distribution.

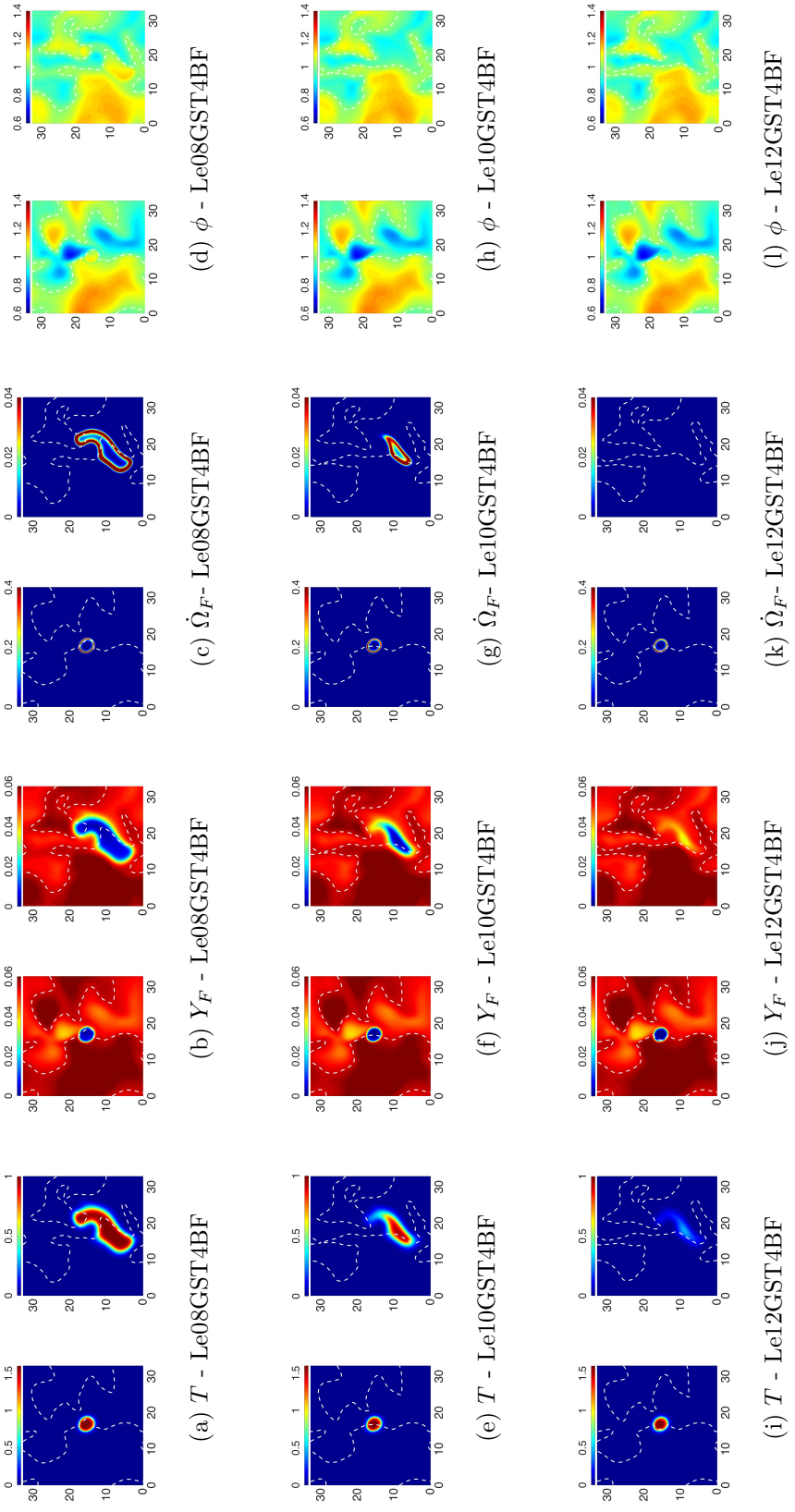

(a) T - Le08GST4BF (b) Y_F - Le08GST4BF (c) $\dot{\Omega}_F$- Le08GST4BF (d) ϕ - Le08GST4BF

(e) T - Le10GST4BF (f) Y_F - Le10GST4BF (g) $\dot{\Omega}_F$- Le10GST4BF (h) ϕ - Le10GST4BF

(i) T - Le12GST4BF (j) Y_F - Le12GST4BF (k) $\dot{\Omega}_F$- Le12GST4BF (l) ϕ - Le12GST4BF

Figure 6.13: Distribution of T (1^{st} & 2^{nd} columns), Y_F (3^{rd} & 4^{th} columns), $\dot{\Omega}_F$ (5^{th} & 6^{th} columns) and ϕ (7^{th} & 8^{th} columns) on the central $x_1 - x_2$ plane for the cases with $\phi' = 0.4$, $l_\phi/l_f = 8.3$ and $\frac{u'}{S_{b(\phi=1)}} = 4$. The white broken like shows $\xi = \xi_{st}$. Additionally 1^{st}, 3^{rd}, 5^{th}, 7^{th} columns showing $t = 1.05t_{sp}$ and 2^{nd}, 4^{th}, 6^{th}, 8^{th} columns showing $t = 8.40t_{sp}$, moreover $Le_F = 0.8$ (1^{st} row), $Le_F = 1.0$ (2^{nd} row), $Le_F = 1.2$ (3^{rd} row) for initial Gaussian mixture distribution.

6.3.3 Mode of Combustion and Mixing Statistics

In the environment of stratified mixtures the mode of combustion can be either premixed or non-premixed. It is important to understand the flame structure originating from localised forced ignition to explain the observed burning behaviour of the cases considered here. The percentage of overall heat release arising from premixed (i.e. $I_c > 0$) and non-premixed (i.e. $I_c < 0$) modes of combustion at $t = 8.40t_{sp}$ are shown in Figure 6.14 for selected cases from Table 6.3 in order to highlight effects of Le_F (Figure 6.14-(a)), effects of ${}^{l_\phi}/_{l_f}$ (Figure 6.14-(b)), effects of ϕ' (Figure 6.14-(c)), and effects of $\frac{u'}{S_{b(\phi=1)}}$ (Figure 6.14-(d)).

It is evident from Figure 6.14 that the chemical reaction takes place predominantly in premixed mode but some pockets of non-premixed combustion are also found in these cases. However, the probability of finding $I_c < 0$ decreases with increasing time due to mixing process (not shown here for the sake of brevity). It can be seen from Figure 6.14-(a) that the percentage of heat release from the premixed (i.e. $I_c > 0$) mode of combustion decreases with increasing Le_F. Higher fuel diffusivity for small values of Le_F augments the mixing rate and thus strengthens the contribution of premixed combustion to overall heat release. Moreover, the proportion of heat release originating from non-premixed combustion (i.e. $I_c < 0$) increases with increasing ϕ' for a given value of ${}^{l_\phi}/_{l_f}$ because the extent of non-premixed combustion is expected to increase with increasing extent of mixture inhomogeneity (see Figure 6.14-(c)).

Furthermore, the percentage of heat release arising from non-premixed mode of combustion decreases with decreasing values of ${}^{l_\phi}/_{l_f}$ and increasing values of $\frac{u'}{S_{b(\phi=1)}}$ for a given values of ϕ' as a result of improved mixing for small values of ${}^{l_\phi}/_{l_f}$ and high values of $\frac{u'}{S_{b(\phi=1)}}$. The mean scalar dissipation rate of mixture fraction can be defined as [151]:

$$\langle N_\xi \rangle = \langle D_\xi \nabla\xi \cdot \nabla\xi \rangle \tag{6.5}$$

which can further be scaled as [149]:

$$\langle N_\xi \rangle \sim \frac{D \langle \xi'^2 \rangle}{l_\phi^2} \tag{6.6}$$

where ξ' is the RMS of mixture fraction driven by ϕ fluctuations. It has been demonstrated in Chapter 5 that an decrease in ${}^{l_\phi}/_{l_f}$ and increase in $\frac{u'}{S_{b(\phi=1)}}$ augments the rate of mixing for $Le_F = 1.0$ cases and thus same qualitative behaviour has been

Figure 6.14: Percentage of overall heat release arising from premixed and non-premixed mode of combustion at $t = 8.40t_{sp}$ for the selected cases from Table 6.3.
[where premixed (i.e. $I_c > 0$) and non-premixed (i.e. $I_c < 0$) mode of combustion]

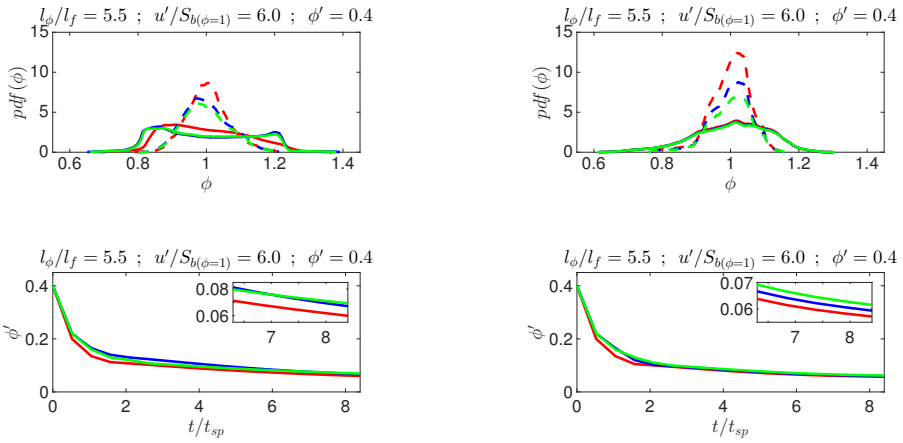

[$Le_F = 0.8$; $Le_F = 1.0$; $Le_F = 1.2$]

Figure 6.15: Temporal evolution of the PDF of ϕ (1^{st} row) at $t = 1.05t_{sp}$ (solid line) and $t = 8.40t_{sp}$ (broken line) and temporal evolution of ϕ' (2^{nd} row) evaluated over the entire domain for the selected cases in order to demonstrate effects of Le_F on mixing process(1^{st} column showing initial Bi-modal mixture distribution and 2^{nd} column showing initial Gaussian distribution) from listed in Table 6.3.

observed for $Le_F = 0.8$ and $Le_F = 1.2$ cases.

Moreover Figure 6.14 shows that the percentage of heat release from premixed mode of combustion is greater in the initial Gaussian mixture distribution cases in comparison to the initial Bi-modal distribution cases. This is consistent with higher probability of finding $\phi \approx \langle\phi\rangle$ in the initial Gaussian distribution cases than in the cases with initial Bi-modal distribution. It can be seen from Figure 6.14 that increasing value of ϕ' provides increasing in finding non-premixed mode of combustion, this is true for both initial Gaussian and Bi-modal mixture distribution. This effect can be seen easily in the initial Bi-modal distribution cases in comparison to the initial Gaussian distribution.

The evolution of mixing process can be illustrated by the temporal evolution of the PDF(ϕ) and rms value of equivalence ratio (i.e. ϕ') evaluated over the whole computational domain. The temporal evolution of the PDF(ϕ) and temporal evolution of ϕ' for the selected cases from Table 6.3 are shown in Figures 6.15, 6.16, 6.17 and 6.18 in order to demonstrate the effects of Le_F, ${}^{l_\phi}/_{l_f}$, ϕ' and $\frac{u'}{S_{b(\phi=1)}}$, respectively. Furthermore, Figures 6.15, 6.16, 6.17 and 6.18 demonstrate that both initial mixture distribution (i.e. Bi-modal and Gaussian) approaches an approximate Gaussian distribution with peak value at $\phi \approx \langle\phi\rangle = 1.0$, as time progresses. It can be seen from Figure 6.15

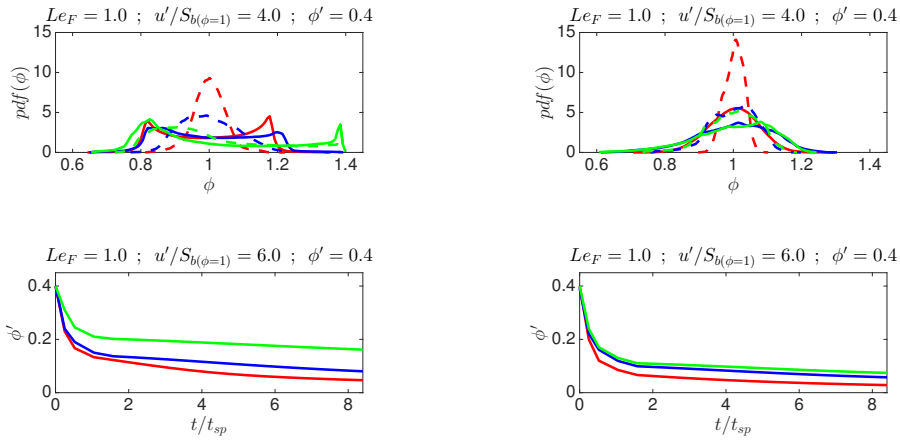

$[\frac{l_\phi}{l_f} = 2.1; \frac{l_\phi}{l_f} = 5.5; \frac{l_\phi}{l_f} = 8.3\ ]$

Figure 6.16: Temporal evolution of the PDF of ϕ (1^{st} row) at $t = 1.05t_{sp}$ (solid line) and $t = 8.40t_{sp}$ (broken line) and temporal evolution of ϕ' (2^{nd} row) evaluated over the entire domain for the selected cases in order to demonstrate effects of l_ϕ/l_f on mixing process(1^{st} column showing initial Bi-modal mixture distribution and 2^{nd} column showing initial Gaussian distribution) from listed in Table 6.3.

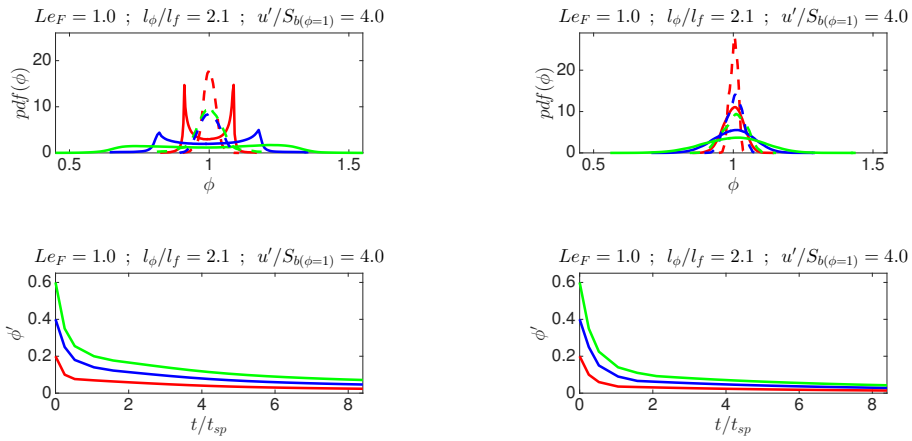

$[\phi' = 0.2\ ;\ \phi' = 0.4\ ;\ \phi' = 0.6\ ]$

Figure 6.17: Temporal evolution of the PDF of ϕ (1^{st} row) at $t = 1.05t_{sp}$ (solid line) and $t = 8.40t_{sp}$ (broken line) and temporal evolution of ϕ' (2^{nd} row) evaluated over the entire domain for the selected cases in order to demonstrate effects of ϕ' on mixing process(1^{st} column showing initial Bi-modal mixture distribution and 2^{nd} column showing initial Gaussian distribution) from listed in Table 6.3.

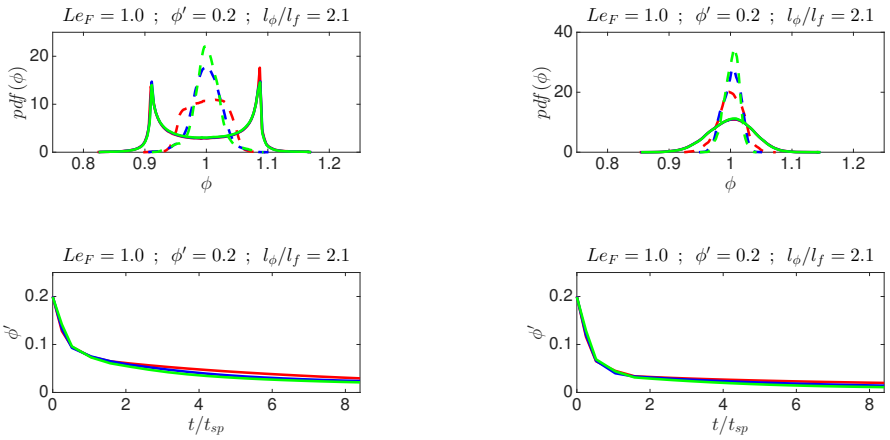

$$[\frac{u'}{S_{b(\phi=1)}} = 0.0 \; ; \; \frac{u'}{S_{b(\phi=1)}} = 4.0 \; ; \; \frac{u'}{S_{b(\phi=1)}} = 6.0 \;]$$

Figure 6.18: Temporal evolution of the PDF of ϕ (1^{st} row) at $t = 1.05t_{sp}$ (solid line) and $t = 8.40t_{sp}$ (broken line) and temporal evolution of ϕ' (2^{nd} row) evaluated over the entire domain for the selected cases in order to demonstrate effects of $\frac{u'}{S_{b(\phi=1)}}$ on mixing process(1^{st} column showing initial Bi-modal mixture distribution and 2^{nd} column showing initial Gaussian distribution) from listed in Table 6.3.

that the decay rate of ϕ' is faster for decreasing values of Le_F. Additionally, Figure 6.15 demonstrates that the PDF(ϕ) attains its maximum value for $Le_F = 0.8$ with initial Gaussian mixture distribution in comparison to the corresponding Bi-modal distribution.

Moreover, it can be seen from Figure 6.18 that the decay rate of ϕ' increases with increasing $\frac{u'}{S_{b(\phi=1)}}$ as turbulent straining acts to increase scalar dissipation rate, which in turn increases the greater rate of micro-mixing [129, 149]. The effects of initial mixture distribution, $\frac{u'}{S_{b(\phi=1)}}$, ϕ' and $^{l_\phi}/_{l_f}$ are already analysed and explained in Chapter 5 (Sections 5.2.4 and 5.3.3) and thus not repeated here.

6.3.4 Reaction-Diffusion Balance Analysis of the Flame Kernels

Figure 6.19 (6.20) demonstrates the evolution of $T_{\max}$ for initial Bi-modal (Gaussian) distribution for cases with $\phi' = 0.4$; $^{l_\phi}/_{l_f} = 5.5$; $\frac{u'}{S_{b(\phi=1)}} = 4.0$ along with the mean variation of different terms with reaction progress variable (i.e. c) at different time instances. It can be seen from Figures 6.19 and 6.20 that self-sustained combustion has (has not) been attained for $Le_F = 0.8$ ($Le_F = 1.2$) cases despite the nature of initial

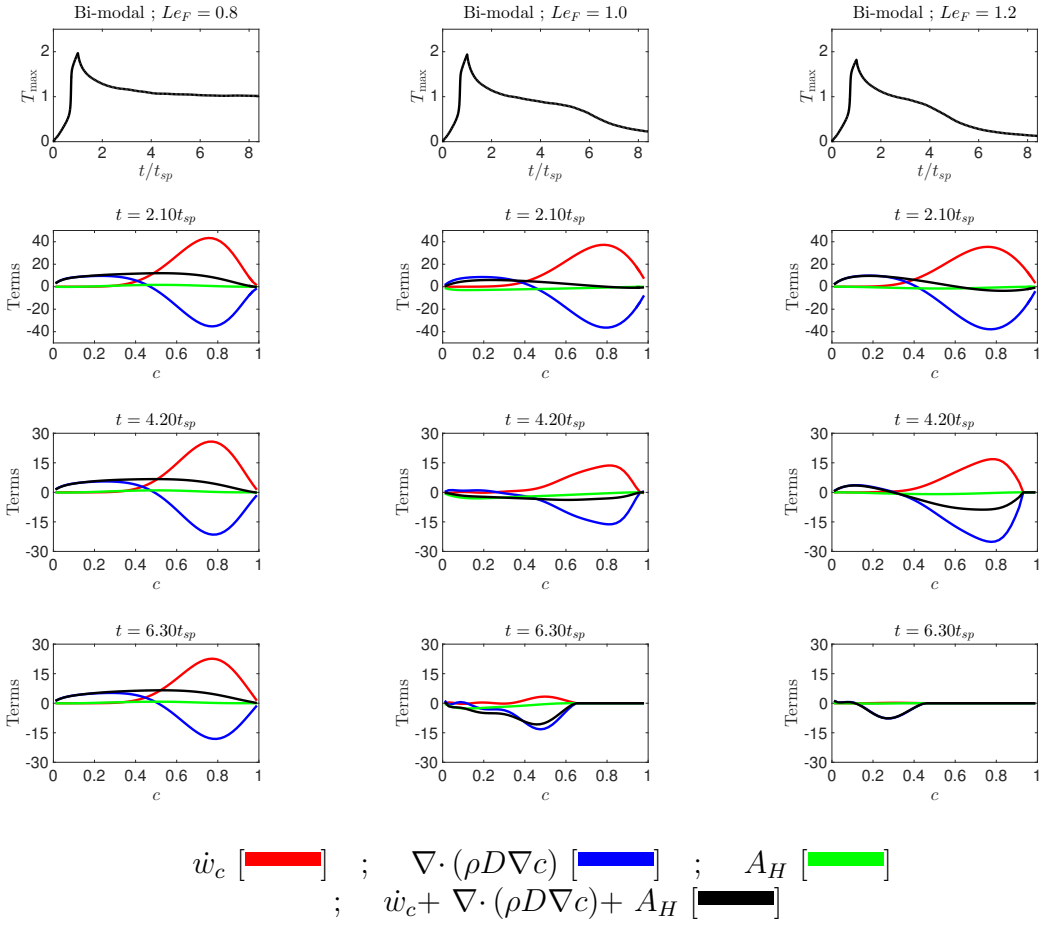

Figure 6.19: Temporal evolution of $T_{\max}$ along with the mean variation of different terms with reaction progress variable (i.e. c) at different time instances for cases with initial Bi-modal mixture distribution and $\phi' = 0.4$; ${}^{l_\phi}/_{l_f} = 5.5$; $\frac{u'}{S_{b(\phi=1)}} = 4.0$. (1^{st}, 2^{nd} and 3^{rd} column representing Le_F =0.8, 1.0 and 1.2, respectively)

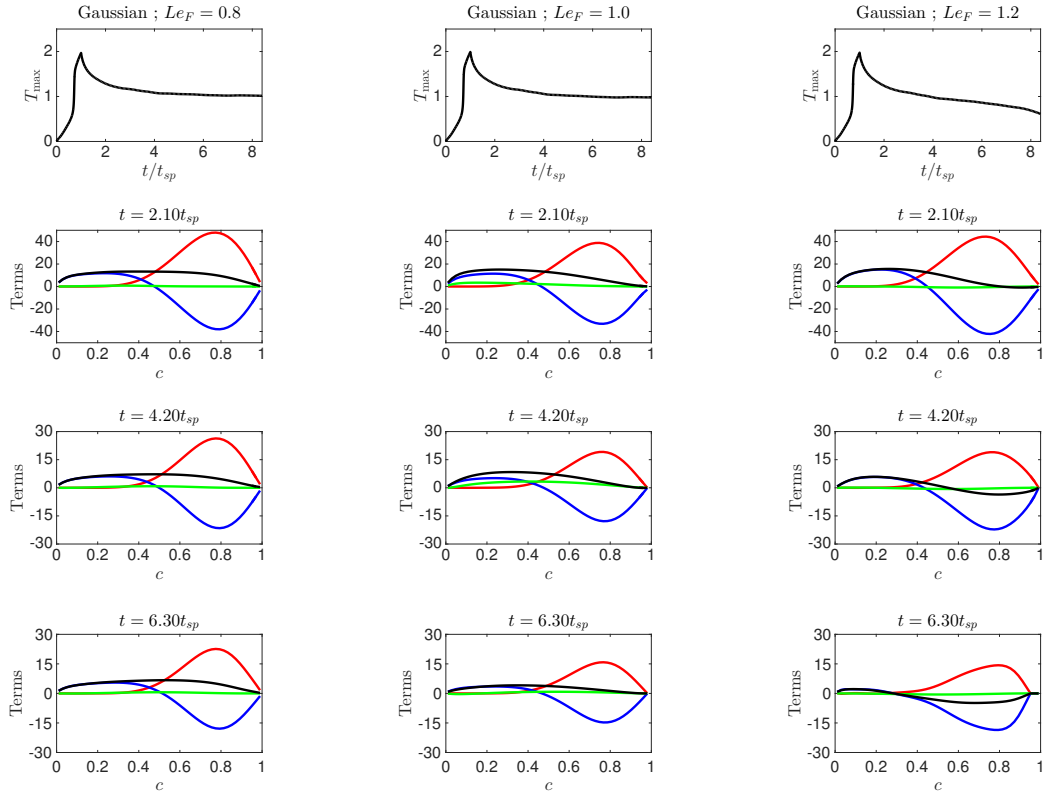

Figure 6.20: Temporal evolution of $T_{\max}$ along with the mean variation of different terms with reaction progress variable (i.e. c) at different time instances for cases with initial Gaussian mixture distribution and $\phi' = 0.4$; ${}^{l_\phi}/_{l_f} = 5.5$; $\frac{u'}{S_{b(\phi=1)}} = 4.0$. (1^{st}, 2^{nd} and 3^{rd} column representing Le_F =0.8, 1.0 and 1.2, respectively)

mixture distribution. However, for $Le_F = 1.0$ case with initial Gaussian distribution achieved self-sustained combustion and with initial Bi-modal mixture distribution exhibited flame extinction at $t \gg t_{sp}$.

It has been demonstrated in Chapter 5 (Section 5.3.4) and existing literature [93, 129] that contribution of the term (A_H [ ]) arising due to mixture inhomogeneity remains small in magnitude in comparison to the magnitudes of reaction term ($\dot{w}_c$ [ ]) and molecular diffusion term ($\nabla\cdot(\rho D\nabla c)$ [ ]) throughout the flame brush at all stages of flame evolution, where the stratified mixture combustion arising from localised forced ignition. Moreover, it can be seen from Figures 6.19 and 6.20 that the term $\dot{w}_c$ [ ] remains negligible in unburned side and increases sharply towards the burned side before decreasing to zero in the fully burned products. The magnitude of the term $\dot{w}_c$ [ ] decreases with time, once the igniter is switched off, which is principally due to the decrease in fuel reaction rate magnitude with time. Additionally, the weaker molecular diffusion process for $Le_F = 1.2$ cases provides less fuel diffuses into the reaction zone and high heat transfer (due to greater thermal diffusivity for $Le_F > 1.0$) leading to flame kernel extinction. Additionally, it can be seen from Figures 6.19 and 6.20 that the positive value of the net sum of terms $\dot{w}_c + \nabla\cdot(\rho D\nabla c) + A_H$ [ ] suggesting a self-sustained propagation of the flame kernel for $Le_F = 0.8$. Moreover negative value of $\dot{w}_c + \nabla\cdot(\rho D\nabla c) + A_H$ [ ] suggesting flame extinction for $Le_F = 1.2$ cases at $t \gg t_{sp}$ for both initial mixture distributions (i.e. Bi-modal and Gaussian). The effects of nature of initial mixture distribution with $Le_F = 1.0$; $\phi' = 0.4$; ${}^{l_\phi}/_{l_f} = 5.5$; $\frac{u'}{S_{b(\phi=1)}} = 4.0$ case has already been discussed previously in Section 5.3.4.

6.3.5 Statistical Behaviour of $\dot{\Omega}_F$

In order to understand the effects of Le_F coupled with stratification on extent of burning following successful ignition, it is important to analyse the reaction zone structure of the flames initiated by the localised forced ignition. The scatter of $\dot{\Omega}_F$ with reaction progress variable c (Figure 6.21), with ξ (Figure 6.22) and with conditional on ξ for $0.01 \leq c \leq 0.99$ (Figure 6.23) is presented at $t = 8.40t_{sp}$ for the selected cases with $\phi' = 0.4$, ${}^{l_\phi}/_{l_f} = 8.3$ and $\frac{u'}{S_{b(\phi=1)}} = 6.0$ from Table 6.3.

Figure 6.21 shows that the high values of $\dot{\Omega}_F$ are obtained close to $c = 0.8$, which is consistent with previous analyses [48, 50, 51, 149]. Additionally, the high scatter values of $\dot{\Omega}_F$ are presented in $Le_F = 0.8$ cases in compare to $Le_F = 1.2$ cases. Figure

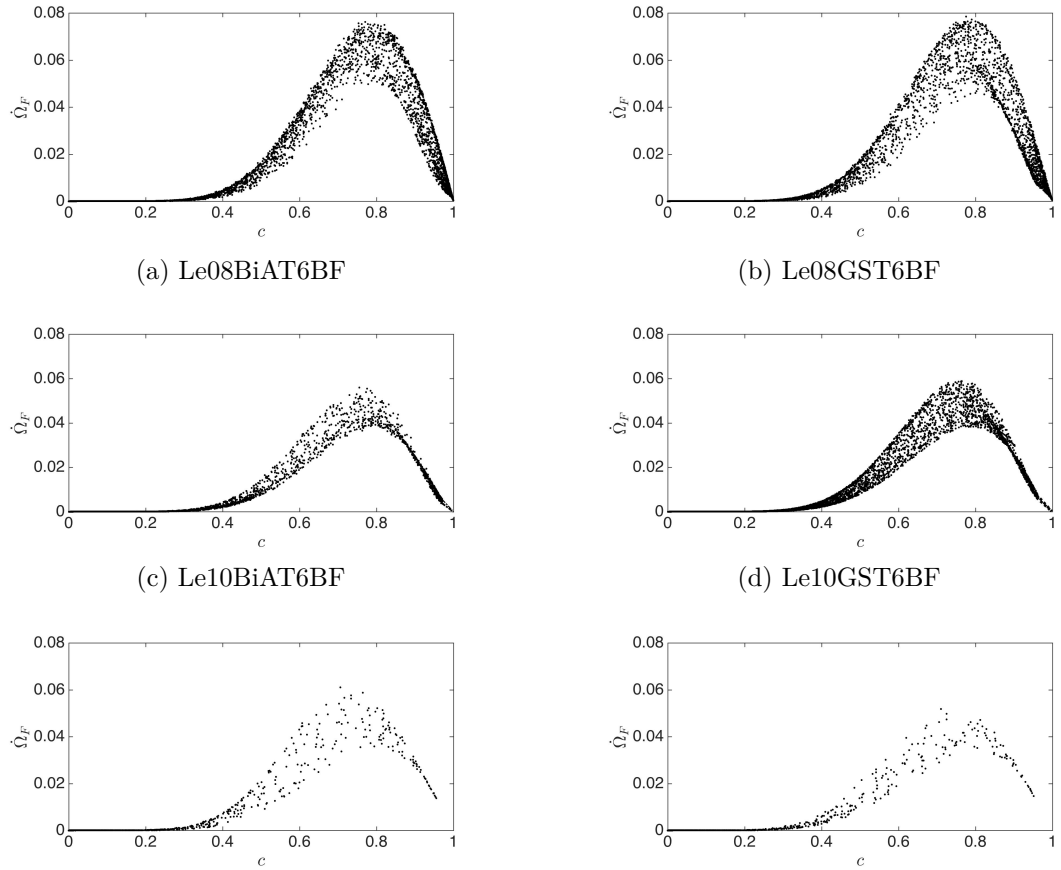

(a) Le08BiAT6BF

(b) Le08GST6BF

(c) Le10BiAT6BF

(d) Le10GST6BF

(e) Le12BiAT6BF

(f) Le12GST6BF

Figure 6.21: Scatter of $\dot{\Omega}_F$ with c for selected cases with $\phi' = 0.4$, ${}^{l_\phi}/_{l_f} = 8.3$ and $\frac{u'}{S_{b(\phi=1)}} = 6.0$ at $t = 8.40 t_{sp}$ from Table 6.3, moreover $Le_F = 0.8$ (1^{st} row), $Le_F = 1.0$ (2^{nd} row), $Le_F = 1.2$ (3^{rd} row), initial Bi-modal mixture distribution (left column) and initial Gaussian mixture distribution (right column).

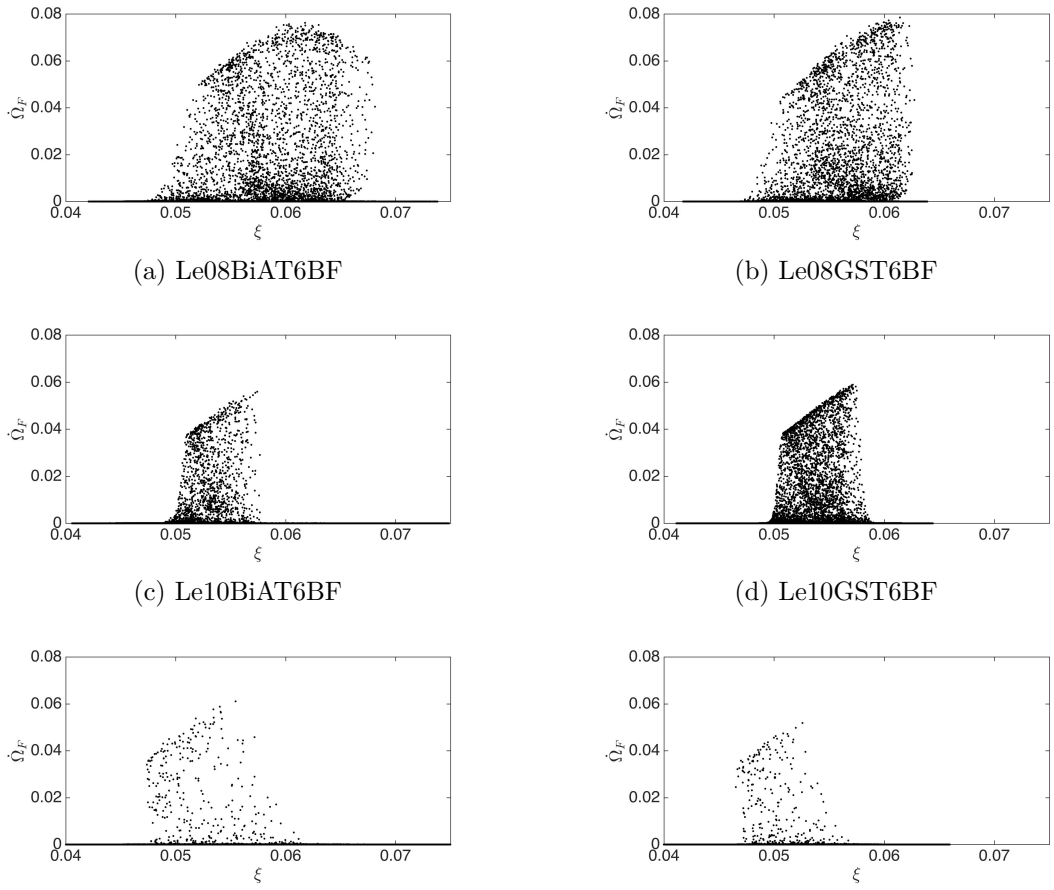

(a) Le08BiAT6BF

(b) Le08GST6BF

(c) Le10BiAT6BF

(d) Le10GST6BF

(e) Le12BiAT6BF

(f) Le12GST6BF

Figure 6.22: Scatter of $\dot{\Omega}_F$ with ξ for selected cases with $\phi' = 0.4$, ${}^{l_\phi}/_{l_f} = 8.3$ and $\frac{u'}{S_{b(\phi=1)}} = 6.0$ at $t = 8.40 t_{sp}$ from Table 6.3, moreover $Le_F = 0.8$ (1^{st} row), $Le_F = 1.0$ (2^{nd} row), $Le_F = 1.2$ (3^{rd} row), initial Bi-modal mixture distribution (left column) and initial Gaussian mixture distribution (right column).

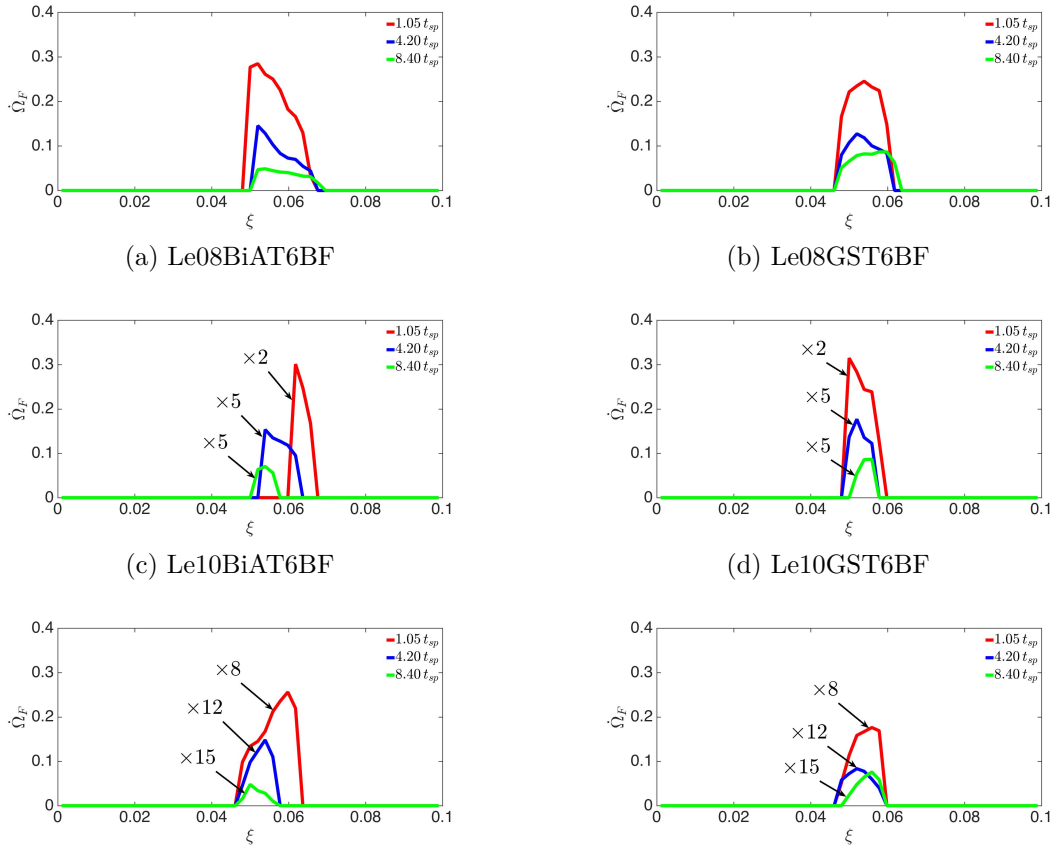

(a) Le08BiAT6BF

(b) Le08GST6BF

(c) Le10BiAT6BF

(d) Le10GST6BF

(e) Le12BiAT6BF

(f) Le12GST6BF

Figure 6.23: Scatter of $\dot{\Omega}_F$ with conditional on ξ for $0.01 \leq c \leq 0.99$ for selected cases with $\phi' = 0.4$, ${}^{l_\phi}/_{l_f} = 8.3$ and $\frac{u'}{S_{b(\phi=1)}} = 6.0$ at $t = 8.40 t_{sp}$ from Table 6.3, moreover $Le_F = 0.8$ (1^{st} row), $Le_F = 1.0$ (2^{nd} row), $Le_F = 1.2$ (3^{rd} row), initial Bi-modal mixture distribution (left column) and initial Gaussian mixture distribution (right column).

6.22 shows a considerable amount of scatter, and the same qualitative behaviour is observed for other cases. The large variation of non-dimensional temperature T on a given ξ isosurfrace (because of both unburned and burned contributions) leads to a large extent of scatter of $\dot{\Omega}_F$. Additionally Figure 6.22 shows that the high values of $\dot{\Omega}_F$ are obtained towards the slightly rich side (i.e. $\xi = 0.06 \Rightarrow \phi = 1.10$), where the unstrained planar laminar burning velocity attains its maximum value (see Figure 3.1).

It can be seen from Figures 6.21 and 6.22 that the maximum values of $\dot{\Omega}_F$ decreases with increasing Le_F (e.g. maximum value of $\dot{\Omega}_F$ is highest for the $Le_F = 0.8$ cases and the lowest in the $Le_F = 1.2$ case). In the $Le_F < 1$ case, fuel diffuses into the

reaction zone at a faster rate than the rate at which heat is conducted out. This leads to simultaneous presence of high temperature and reactant concentration, which increases the probability of finding high values of $\dot{\Omega}_F$ in the $Le_F = 0.8$ case in comparison to that in the $Le_F = 1.0$ case. Just the opposite mechanism give rise to smaller values of $\dot{\Omega}_F$ in the $Le_F = 1.2$ case in comparison to that in the unity fuel Lewis number case. These observed behaviour are present in both initial Gaussian and Bi-modal mixture distributions. The aforementioned effects of Le_F on $\dot{\Omega}_F$ are in good agreement with previous findings by Chakraborty *et al.* [48]. Figure 6.23 demonstrates that the fuel reaction rate magnitude distribution remains qualitatively similar following successful ignition and the same qualitative behaviours had been observed for other cases. A similar behaviour is observed for all other cases, which is also consistent with previous findings [48, 50, 51, 149, 212] in the context of localised forced ignition (also observed in Sections 5.2.5 and 5.3.5).

6.3.6 Extent of Burning

The temporal evolution of the mean and standard deviations of burned gas mass M_b are shown in Figures 6.24, 6.25 and 6.26 for $\phi' = 0.2$, $\phi' = 0.4$ and $\phi' = 0.6$ cases respectively from Table 6.3. It is evident from Figures 6.24, 6.25 and 6.26 that the extent of burning increases with decreasing Le_F for a given set of values of $\frac{u'}{S_{b(\phi=1)}}$, ${}^{l_\phi}/_{l_f}$ and ϕ' despite the nature of initial mixture distributions. The simultaneous existence of high fuel concentration in the high temperature reaction zone in the $Le_F < 1.0$ cases (e.g. $Le_F = 0.8$) give rise to higher extent of burning than the corresponding unity fuel Lewis number (i.e. $Le_F = 1.0$) cases. By contrast, heat diffuses faster than the rate at which fuel diffuses into the reaction zone in the $Le_F > 1.0$ cases (e.g. $Le_F = 1.2$) . And therefore a combination of fuel depletion due to slow mass diffusion rate and low temperature due to high thermal diffusion rate gives rise to smaller extent of burning in $Le_F = 1.2$ cases than the corresponding $Le_F = 1.0$ cases.

For the ease of understanding, this section 6.3.6 is further divided in different parts in order to illustrate the effects of $\frac{u'}{S_{b(\phi=1)}}$, ϕ' and ${}^{l_\phi}/_{l_f}$ with different values of Le_F on the extent of burning. Additionally, the effects of nature of initial mixture distribution remains qualitatively similar (see Section 5.3.6) in the presence of different Le_F cases, and therefore has not been repeated here.

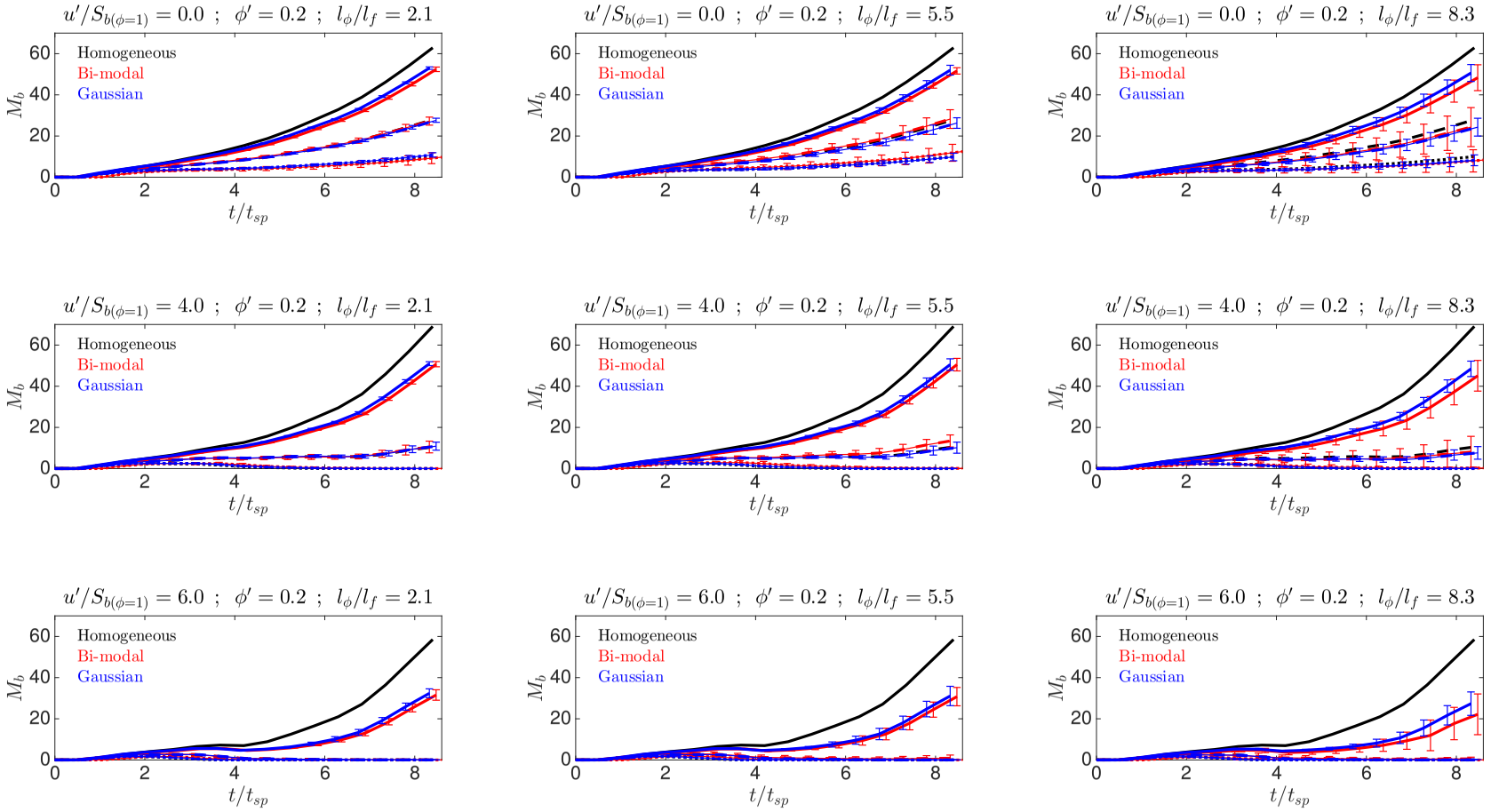

Figure 6.24: Temporal evolution of the mean and standard deviation of M_b for all the cases with $\phi' = 0.2$ listed in Table 6.3. [where 1^{st} column shows ${}^{l_\phi}/_{l_f} = 2.1$; 2^{nd} column shows ${}^{l_\phi}/_{l_f} = 5.5$; 3^{rd} column shows ${}^{l_\phi}/_{l_f} = 8.3$; additionally 1^{st} row shows $\frac{u'}{S_{b(\phi=1)}} = 0.0$; 2^{nd} row shows $\frac{u'}{S_{b(\phi=1)}} = 4.0$; 3^{rd} row shows $\frac{u'}{S_{b(\phi=1)}} = 6.0$, moreover $Le_F = 0.8$(——), $Le_F = 1.0$ (— — — —) and $Le_F = 1.2$ (- - - - - - -)]

Effects of $\frac{u'}{S_{b(\phi=1)}}$ with different Le_F

It can be observed from Figures 6.24, 6.25 and 6.26 that the $Le_F = 1.2$ cases eventually extinguish for initial values of $\frac{u'}{S_{b(\phi=1)}} = 4.0$ and $\frac{u'}{S_{b(\phi=1)}} = 6.0$ (also see Figures 6.9, 6.10 and 6.11), whereas all the $Le_F = 0.8$ cases with same initial $\frac{u'}{S_{b(\phi=1)}}$ exhibit self-sustained combustion. The higher extent of flame area generation and burning rate for turbulent $Le_F = 0.8$ homogeneous case eclipsed the enhanced heat transfer rate from the hot gas kernel, which directs higher value of M_b than corresponding quiescent case. Moreover, it is important to notice that the M_b attains at its maximum values for $Le_F = 0.8$ homogeneous cases in compare to that in $Le_F = 1.0$ and $Le_F = 1.2$ homogeneous cases. The favorable effects of $\frac{u'}{S_{b(\phi=1)}}$ can be observed in the extent of burning for $Le_F = 0.8$ homogeneous case (this effect has already been explained in Section 6.2.4). Additionally, the $Le_F = 1.0$ cases with initial values of $\frac{u'}{S_{b(\phi=1)}} = 6.0$ fail to sustain combustion once the igniter is switched off for initial values of $\phi' = 0.4$ and $\phi' = 0.6$ cases irrespective of the values of l_ϕ/l_f and nature of initial mixture distribution.

Moreover, Figures 6.24, 6.25 and 6.26 show that an increase in $\frac{u'}{S_{b(\phi=1)}}$ leads to a reduction in burning rate for all values of l_ϕ/l_f , ϕ' for the cases with $Le_F \geq 1.0$ irrespective the nature of initial mixture distribution. The probability of findings high values of c decreases with increasing $\frac{u'}{S_{b(\phi=1)}}$ due to enhanced heat transfer rate from the hot gas kernel for the $Le_F \geq 1.0$ cases. This is echoed in the smaller extent of burning for higher values of $\frac{u'}{S_{b(\phi=1)}}$ for the $Le_F \geq 1.0$ cases (e.g. all turbulent cases eventually extinguish for $Le_F = 1.2$) and the detrimental effect of $\frac{u'}{S_{b(\phi=1)}}$ on the extent of burning is consistent with previous experimental [96, 116], computational findings [46, 48, 50, 51, 109, 127, 149, 212] and has been discussed in Chapter 5 (Sections 5.2.6, 5.3.6, 5.4.2 and 5.5.4).

Effects of ϕ' with different Le_F

Moreover, Figures 6.24, 6.25 and 6.26 indicate that an increase in ϕ' leads to a decrease of M_b for all stratified cases irrespective of Le_F and the nature of initial mixture distributions. The burning rate of mixtures with $\phi < 1.0$ and $\phi \geq 1.10$ is smaller than that in the stoichiometric mixtures. The probability of finding $\phi < 1.0$ and $\phi \geq 1.10$ increases with increasing ϕ' and this gives rise to a reduction in burning rate for higher values of ϕ'. As, the unstrained laminar burning velocity attains its maximum value corresponding region $\phi \geq 1.0$ and $\phi \leq 1.10$ (see Figure 3.1). Additionally, the

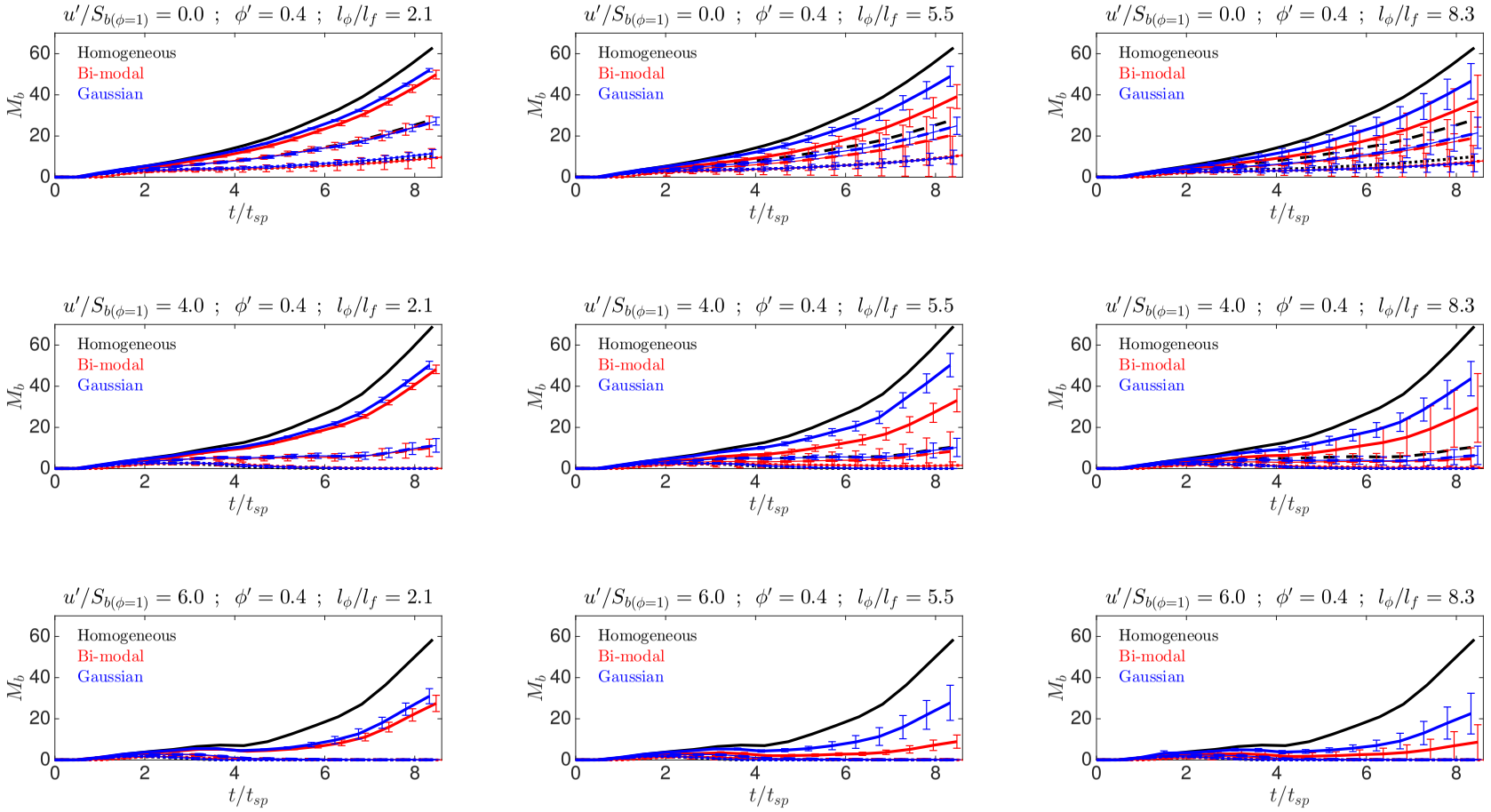

Figure 6.25: Temporal evolution of the mean and standard deviation of M_b for all the cases with $\phi' = 0.4$ listed in Table 6.3. [where 1^{st} column shows ${}^{l_\phi}/_{l_f} = 2.1$; 2^{nd} column shows ${}^{l_\phi}/_{l_f} = 5.5$; 3^{rd} column shows ${}^{l_\phi}/_{l_f} = 8.3$; additionally 1^{st} row shows $\frac{u'}{S_{b(\phi=1)}} = 0.0$; 2^{nd} row shows $\frac{u'}{S_{b(\phi=1)}} = 4.0$; 3^{rd} row shows $\frac{u'}{S_{b(\phi=1)}} = 6.0$, moreover $Le_F = 0.8$(——), $Le_F = 1.0$ (— — — —) and $Le_F = 1.2$ (·····)]

cases with initial Gaussian mixture distribution attained higher values of M_b for all ϕ' quiescent cases than that with initial Bi-modal mixture distribution irrespective of ${}^{l_\phi}/_{l_f}$ and Le_F. It can be seen from Figures 6.24, 6.25 and 6.26 that variation of $m_b(c \geq 0.9)$ between different realisations increases further with increasing ϕ' for all cases considered here. The reduction in burning rate due to mixture stratification in globally stoichiometric mixtures is found to be consistent with previous experimental [170], computational [88, 104, 128, 129, 149] and Chapter 5 findings.

Effects of ${}^{l_\phi}/_{l_f}$ with different Le_F

Furthermore, Figures 6.24, 6.25 and 6.26 show that M_b remains comparable for the quiescent cases with initial values of ${}^{l_\phi}/_{l_f}$ =5.5 and 8.3 (${}^{l_\phi}/_{l_f}$ =2.1, 5.5 and 8.3), and $\phi' = 0.2$ for the $Le_F = 1.0$ and 1.2 (Le_F =0.8) cases for initial Bi-modal distribution of ϕ. The probability of findings highly reactive mixtures corresponding to $1.10 \geq \phi \geq 1.0$ is greater in cases with initial values of ${}^{l_\phi}/_{l_f} = 5.5$ and ${}^{l_\phi}/_{l_f} = 8.3$ than in the initial ${}^{l_\phi}/_{l_f} = 2.1$ cases due to less efficient mixing for initial $\phi' = 0.2$ with $Le_F \geq 1.0$. This gives rise to greater rate of burning in the $Le_F \geq 1.0$ cases with initial values of ${}^{l_\phi}/_{l_f} = 5.5$ and ${}^{l_\phi}/_{l_f} = 8.3$ than in the initial ${}^{l_\phi}/_{l_f} = 2.1$ cases for initial $\phi' = 0.2$. However, the aforementioned effect is not strong in the $Le_F = 0.8$ cases due to higher mixing rate due to greater value of fuel mass diffusivity than in the $Le_F \geq 1.0$ cases. The probability of finding slow-burning mixtures ($\phi < 1.0$ and $\phi \geq 1.10$) is greater in the cases with initial ${}^{l_\phi}/_{l_f} = 5.5$ due to less efficient mixing then that in the initial ${}^{l_\phi}/_{l_f} = 2.1$ cases, and thus burning rate assumes greater values in the cases with ${}^{l_\phi}/_{l_f} = 2.1$ than the cases with initial ${}^{l_\phi}/_{l_f} = 5.5$ when initial ϕ' =0.4 and 0.6 (0.2, 0.4 and 0.6) for $Le_F \geq 1.0$ ($Le_F = 0.8$) cases. For the cases with ${}^{l_\phi}/_{l_f} = 8.3$ the clouds of mixture inhomogeneities are relatively big for both kinds of initial mixture distributions (see Figure 5.11), and as a result, there is a high probability of obtaining a large region of almost homogeneous mixture at the centre of igniter. If the igniter centre is located in the vicinity of a large cloud of $1.10 \geq \phi \geq 1.0$, which leads to higher burning rate for cases with ${}^{l_\phi}/_{l_f} = 8.3$ than in the cases with initial ${}^{l_\phi}/_{l_f} = 2.1$ when the ϕ' =0.4 and 0.6 (0.2, 0.4, and 0.6) for the $Le_F \geq 1.0$ ($Le_F = 0.8$) cases.

Figures 6.24, 6.25 and 6.26 reveals that for a given value of ${}^{l_\phi}/_{l_f}$, the burned gas mass M_b decreases with increasing ϕ', and the influence of ${}^{l_\phi}/_{l_f}$ on the extent of burning have been found to be non-monotonic and dependent on ϕ' and Le_F for initial Bi-modal distribution. On the other side for initial Gaussian distribution cases, the decreasing values of ${}^{l_\phi}/_{l_f}$ leads to increase in extend of burning for all initial values of ϕ' considered

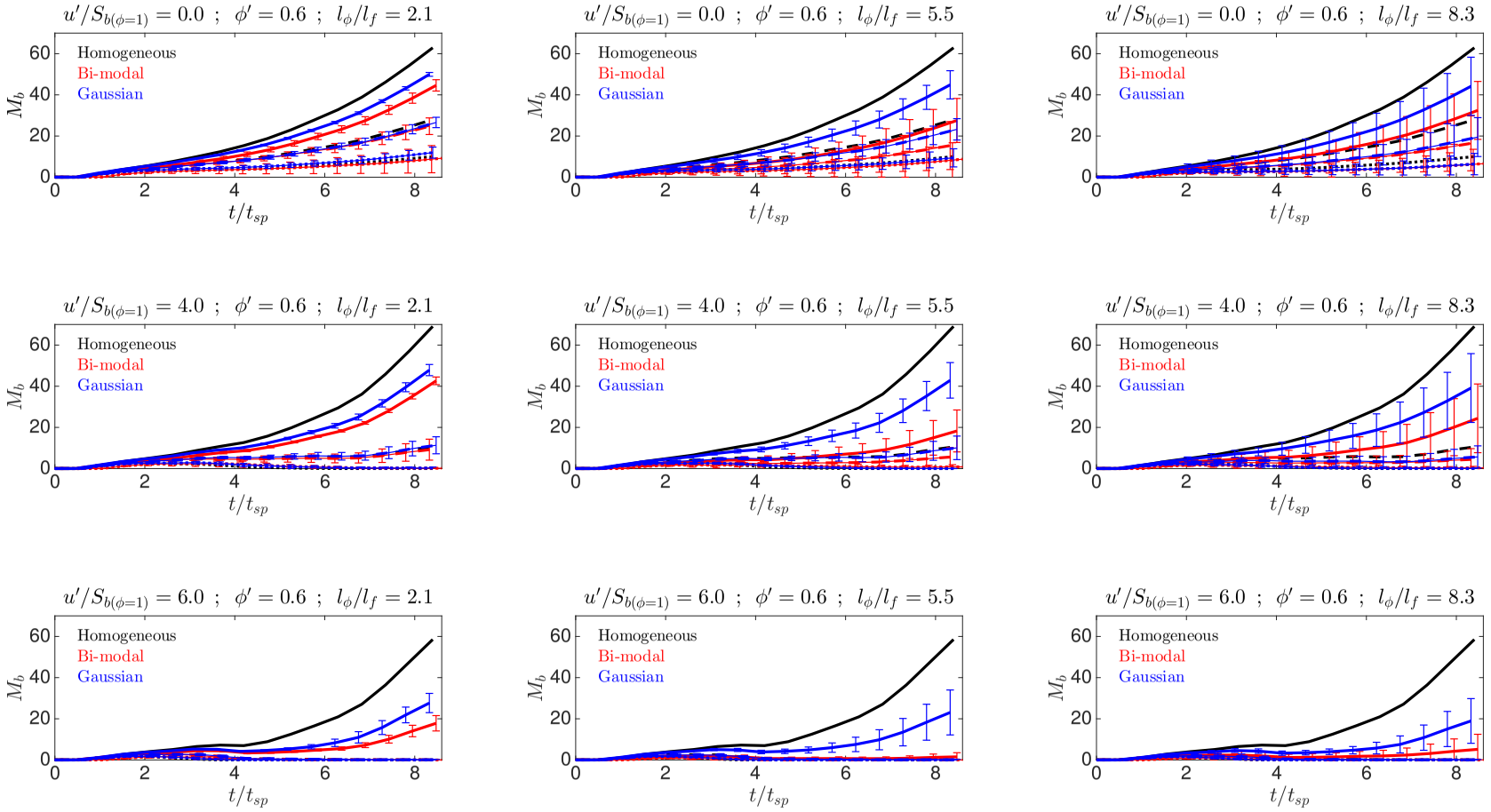

Figure 6.26: Temporal evolution of the mean and standard deviation of M_b for all the cases with $\phi' = 0.6$ listed in Table 6.3. [where 1^{st} column shows ${}^{l_\phi}/_{l_f} = 2.1$; 2^{nd} column shows ${}^{l_\phi}/_{l_f} = 5.5$; 3^{rd} column shows ${}^{l_\phi}/_{l_f} = 8.3$; additionally 1^{st} row shows $\frac{u'}{S_{b(\phi=1)}} = 0.0$; 2^{nd} row shows $\frac{u'}{S_{b(\phi=1)}} = 4.0$; 3^{rd} row shows $\frac{u'}{S_{b(\phi=1)}} = 6.0$, moreover $Le_F = 0.8$(——), $Le_F = 1.0$ (— — — —) and $Le_F = 1.2$ (·····)]

here irrespective of Le_F.

6.3.7 Summary

The Section 6.3 investigates the effects of ${}^{l_\phi}/_{l_f}$, ϕ' and ${}^{u'}/_{S_{b(\phi=1)}}$ on localised forced ignition of globally stoichiometric stratified mixtures for different initial mixture distribution (i.e. Gaussian and Bi-modal) and different values of fuel Lewis number Le_F ranging from 0.8 to 1.2. The flame resulting from localised forced ignition shows predominantly premixed mode of combustion although some region of non-premixed mode of combustion have also been observed for high values of ${}^{l_\phi}/_{l_f}$, ϕ' and Le_F. Additionally cases with initial Gaussian mixture distribution provides lower probability of finding non-premixed pockets in comparison to initial Bi-modal distribution cases, where the probability of finding $I_c < 0$ are higher. This aforementioned findings are in consistent agreement as observed in Chapter 5. The extent of burning M_b increases (decreases) with decreasing (increasing) Le_F for a given set of values of ${}^{l_\phi}/_{l_f}$, ϕ' and $\frac{u'}{S_{b(\phi=1)}}$, energy input and energy deposition duration. Simultaneous presence of high fuel concentration and temperature leads to greater magnitude of fuel reaction rate magnitude in the $Le_F = 0.8$ cases than in the corresponding $Le_F = 1.0$ cases. By contrast, the combination of the depletion of fuel due to slow fuel diffusion and rapid thermal diffusion rate in the reaction zone leads to weaker burning for the $Le_F = 1.2$ cases than in the corresponding $Le_F = 1.0$ cases.

The initial values of ${}^{l_\phi}/_{l_f}$ and ϕ' have shown to have significant influences on the self-sustained combustion and the extent of burning following successful ignition. In both initial distribution for given ${}^{l_\phi}/_{l_f}$, increasing ϕ' leads to decreasing burning rate irrespective of Le_F. But the influence of ${}^{l_\phi}/_{l_f}$ on the extent of burning shows non-monotonic behaviour and dependent of ϕ' and Le_F for initial Bi-modal distribution. On the other side for initial Gaussian distribution cases, the decreasing values of ${}^{l_\phi}/_{l_f}$ leads to increase in extend of burning rate for all initial values of ϕ' and Le_F considered here. The increase in heat transfer rate from hot gas kernel with an increase in $\frac{u'}{S_{b(\phi=1)}}$ leads to a decrease in the extent of burning irrespective of the values of ${}^{l_\phi}/_{l_f}$ and ϕ' for the $Le_F \geq 1.0$ cases but the burned gas mass increases with increasing $\frac{u'}{S_{b(\phi=1)}}$ for the homogeneous mixture with $Le_F = 0.8$ case. The findings observed in Section 6.3 demonstrate that the favourable conditions in terms of mixture inhomogeneity length scale (i.e. ${}^{l_\phi}/_{l_f}$) , mixture equivalence ratio variance (i.e. ϕ') and RMS values of velocity (i.e. $\frac{u'}{S_{b(\phi=1)}}$) for successful ignition and self-sustained combustion in stratified mixtures are dependent on fuel Lewis number Le_F.

6.4 Main Findings

Localised forced ignition and subsequent burning process of both turbulent homogeneous mixtures and stratified mixtures have been numerically investigated to study the effects of Le_F. The main findings can be summarised as follows:

- The MIE requirement for obtaining self-sustained combustion decreases with decreasing Le_F in the turbulent homogeneous mixtures. Higher rate of fuel diffusion into the reaction zone than the rate of thermal diffusion out of this region in the $Le_F = 0.8$ cases gives rise to simultaneous presence of high values of fuel concentration and temperature within the reaction layer, which in turn leads to greater magnitude of fuel reaction rate than in the corresponding $Le_F = 1.0$ cases. The combination of the depletion of fuel due to slow fuel diffusion and rapid thermal diffusion rate from the reaction zone leads to weaker burning for the $Le_F = 1.2$ cases than in the corresponding $Le_F = 1.0$ cases.

- The $Le_F \geq 1.0$ cases and the detrimental effects of $\frac{u'}{S_{b(\phi=1)}}$ are more critical in fuel-lean homogeneous mixture than in the stoichiometric homogeneous mixture due to its weaker heat release effects in the fuel-lean homogeneous mixtures. The enhanced rate of burning due to flame wrinkling may dominate over the augmented heat transfer rate in the $Le_F < 1.0$ cases under some conditions, which may give rise to an increase in the burned gas mass M_b with increasing $\frac{u'}{S_{b(\phi=1)}}$.

- Findings indicate that the laser ignition can be advantageous for obtaining successful ignition and self-sustained combustion in fuel-lean mixtures because the width of ignition energy distribution , duration of energy deposition and ignition energy parameters can be altered independently of each other (agreement with Chapter 4).

- The extent of burning M_b increases with decreasing Le_F for a given set of values of l_ϕ/l_f, ϕ' and $\frac{u'}{S_{b(\phi=1)}}$, energy input and energy deposition duration. For both nature of initial distribution of ϕ (i.e. Gaussian and Bi-modal) and given values of l_ϕ/l_f , increasing ϕ' leads to decreasing burning rate irrespective of Le_F.

- The influence of l_ϕ/l_f on the extent of burning is shows non-monotonic behaviour and dependent of ϕ' and Le_F for initial Bi-modal distribution. Besides for initial

Gaussian distribution cases, the decreasing values of l_ϕ/l_f leads to increase in extend of burning rate for all initial values of ϕ' and Le_F considered here.

- Furthermore, the conditions (e.g. a combination of high values of ϕ' and l_ϕ/l_f) which lead to large variability between different realisations should be avoided while designing industrial ignition systems for turbulent stratified mixtures. Thus, it is perhaps advantageous to have a feedback mechanism in cylinders of DI engines so that the fuel injection characteristics could be modulated to control l_ϕ/l_f and ϕ' to ensure successful ignition and self-sustained combustion depending on $\frac{u'}{S_{b(\phi=1)}}$ in the vicinity of the igniter. Moreover, it is desirable to avoid the combination of l_ϕ/l_f and ϕ' , which gives rise to large variability in the extent of burning between different realisations.

- The findings of this numerical investigation indicate that an ignition system for $Le_F < 1.0$ may not lead to successful ignition for heavier hydrocarbon-air mixtures with $Le_F > 1.0$ but the ignition systems designed for fuels with $Le_F > 1.0$ can successfully be used for lighter fuels with $Le_F < 1.0$.

In the following Chapter 7 of this thesis the summary of primary findings and suggestions for future investigation are provided.

Chapter 7

Conclusions and Future Work

In the present thesis, numerical simulations have been performed in order to gain improved physical understanding of localised forced ignition of turbulent combustible mixtures. The effects of turbulence and ignition energy deposition characteristics on localised forced ignition of turbulent homogeneous mixtures have been studied in Chapter 4. Furthermore Chapter 5 studied the numerical investigation of localised forced ignition of stratified fuel-air mixtures. The effects of fuel Lewis number (Le_F) on localised forced ignition of both homogeneous mixtures and stratified mixtures have been investigated in Chapter 6. This thesis also made an attempt to compare the present numerical findings with existing experimental results (Sections 4.2.7, 4.3.7 and 6.2.6). In this Chapter 7, a summary of primary findings and suggestions for future investigation are provided. In Section 7.4.1, the preliminary analysis results for localised forced ignition of stratified combustible mixtures in the presence of complex chemistry have been presented.

7.1 Parameters Influencing Localised Forced Ignition of Homogeneous Mixtures

In Chapter 4 (Section 4.2), the effects of ignition energy deposition characteristics (i.e. ignition energy, characteristic width of ignition energy deposition profile and duration of ignition energy deposition) on localised forced ignition of stoichiometric (i.e. $\phi = 1.0$) and fuel-lean (i.e. $\phi = 0.8$) homogeneous mixtures have been analysed using simplified chemistry 3D compressible DNS for different values of turbulent velocity fluctuation. Moreover, Chapter 4 (Section 4.3) investigates the ignitability of turbulent

homogeneous mixtures and the corresponding value of MIE in the case of localised forced ignition for different values of Karlovitz number Ka using 3D DNS.

It has been found that higher amount of ignition energy is necessary to obtain self-sustained combustion in fuel-lean cases than in the stoichiometric cases. Moreover, an increase in turbulent velocity fluctuation decreases the extent of burning and may lead to misfire for large values of $\frac{u'}{S_{b(\phi=1)}}$ when the augmentation of heat transfer due to turbulence dominates over the enhanced burning rate in turbulent flames. The detrimental effects of $\frac{u'}{S_{b(\phi=1)}}$ are more critical in the fuel-lean mixture than in the stoichiometric mixture because of weaker heat release effects in the fuel-lean mixture. The adverse effects of $\frac{u'}{S_{b(\phi=1)}}$ on burnt gas mass are in consistent agreement in both numerical [45, 50, 51, 78] and experimental findings [15, 96, 116]. The detrimental effects of high values of $\frac{u'}{S_{b(\phi=1)}}$ are more critical for high values of Ka. A decrease in the width of ignition energy deposition distribution acts to reduce the MIE requirement for both successful ignition and self-sustained combustion even for high values of Ka (i.e. thin-reaction regimes - see Figure 4.23). It is possible to ignite (successful ignition) fuel-lean mixtures with very high values of Ka and u', where MIE is dependent on u', Zel'dovich flame thickness l_f and also characteristic width of ignition energy deposition profile.

Moreover, an increase in the width of ignition energy deposition distribution and duration of ignition energy deposition for a given amount of input ignition energy has been found to have detrimental effects on the extent of burning and these effects can be critical especially for the ignition of fuel-lean mixtures. It has been found that the minimum amount of ignition energy required to obtain successful ignition and self-sustained combustion increases with increasing Ka. An increase in input ignition energy leads to increase in extent of burning irrespective of the values of Ka and u'. MIE requirement increases abruptly once Ka reaches a value of the order of ~ 10, which is crucial for fuel-lean mixtures to avoid unnecessary misfires. The findings indicate that it is possible to obtain self-sustained combustion and successful ignition by judicious choice of ignition energy deposition characteristics (i.e. width of ignition energy deposition distribution, duration of ignition energy deposition and amount of input ignition energy) and these parameters can be altered independently of each other in case of laser ignition. Thus, laser ignition can be more advantageous than the conventional spark ignition for the purpose of reducing the minimum ignition energy requirement and pollutant emission [63]. The computational findings for both the effects of ignition energy deposition characteristics (Section 4.2.7) and MIE re-

quirement for high values of $\frac{u'}{S_{b(\phi=1)}}$ (Section 4.3.7) have been found to be qualitatively consistent with previous experimental findings.

7.2 Parameters Influencing Localised Forced Ignition of Stratified Mixtures

In Chapter 5, localised forced ignition of stratified mixtures has been analysed using 3D DNS to study the effects of mixture inhomogeneity length scale l_ϕ/l_f and equivalence ratio fluctuation ϕ' (Section 5.2), the influences of nature of initial mixture distribution (Section 5.3), the effects of turbulent integral length scale L_{11}/l_f (Section 5.4) and the influences of global mean equivalence ratio $\langle\phi\rangle$ (Section 5.5).

The flame originating from localised forced ignition shows a predominantly premixed mode of combustion, however some pockets of non-premixed combustion have been observed and the probability of non-premixed combustion pockets increases with increasing ϕ' for all cases considered here. However, the cases with initial Gaussian distribution of ϕ provides lower probability of finding non-premixed pockets in comparison to initial Bi-modal mixture distribution, where the probability of finding non-premixed combustion are higher. The mixing process is slower for high values of l_ϕ/l_f for all cases considered here. The effects of l_ϕ/l_f on burnt gas mass shows non-monotonic trends and dependent of ϕ' for initial Bi-modal mixture distribution irrespective of the values of $\langle\phi\rangle$. However in the cases with initial Gaussian mixture distribution, lower values of l_ϕ/l_f lead to better mixing and thus increase the extent of burning for given values of ϕ' for $\langle\phi\rangle$ =0.8 and 1.0 mixture. The clouds of mixture inhomogeneities are relatively larger for high values of l_ϕ/l_f (see Figure 5.1), and as a result to this, it is highly possible that the igniter may encounter highly flammable and/or weakly flammable or even non-combustible mixture clouds which leads to large variations of burned gas mass between different realisations irrespective of the nature of initial mixture distribution. The variability in the extent of burning is relatively small for small values l_ϕ/l_f, and the degree of variability of burning increases with increasing ϕ'.

The results analysis demonstrates that an increase in ϕ' leads to reduction in the burned gas mass for all values of l_ϕ/l_f for $\langle\phi\rangle$ =0.8 and 1.0 mixture irrespective of the nature of initial mixture distributions (i.e. Gaussian or Bi-modal). The burning of the mixture with $1.0 \leq \phi \leq 1.10$ is highest (see Figure 3.1), and thus the probability of

Domain Size	$(3.0\,\text{mm})^3$
Discretised grids	$(128)^3$
Grid resolution	$23.6\ \mu m$
Stratified Fuel Mixture	$(n - C_7H_{16} + \text{air})$
$\langle\phi\rangle$	1.0
ϕ'	0.2
l_ϕ/l_f	5.5
L_{11}/l_f	3.36
$\frac{u'}{S_{b(\phi=1)}}$	4.0
Spark Duration	$0.23\,\mu s$
Spark Radius	0.424 mm
Spark Energy	$3.1\,mJ$
Initial temperature	$300\ K$
Initial pressure	1.0 bar

Table 7.1: Different parameters for the investigated case.

finding mixture with $\phi < 1.0$ and $\phi > 1.10$ increases with increasing ϕ'. The variation of burned gas mass between different realisations are lower in Gaussian distribution cases than those in Bi-modal distributions for all cases considered here. The cases with initial Bi-modal mixture distribution shows higher probabilities of finding $\phi < \langle\phi\rangle$ and $\phi > \langle\phi\rangle$ in comparison to initial Gaussian mixture distribution. The probability of finding $\phi \approx 1.0$ ($\phi \neq 1.0$) is greater for the cases with initial Gaussian (Bi-modal) mixture distribution then those with initial Bi-modal (Gaussian) mixture distribution for given sets of values of l_ϕ/l_f and $\frac{u'}{S_{b(\phi=1)}}$. The adverse effects of higher values of $\frac{u'}{S_{b(\phi=1)}}$ show an increase in heat transfer rate from the hot gas kernel, which further leads to a reduction in the burned gas mass irrespective values of $\langle\phi\rangle$, l_ϕ/l_f, ϕ' and nature of initial mixture distribution. This detrimental effects of $\frac{u'}{S_{b(\phi=1)}}$ on the extent of burning is in good consistent agreement with previous both homogeneous [96, 109, 116, 159] and inhomogeneous [4, 5, 15, 48, 50, 51] mixtures studies in the context of localised forced ignition. The initial value of $L_{11}/l_f = 3.36$ appears a better choice for obtaining higher values of M_b out of three different values considered here (i.e. L_{11}/l_f =2.52, 3.36 and 4.20). The better mixing process is associated with increasing (decreasing) values of $u'(l_\phi$ and $\phi')$ for given L_{11} despite the nature of initial mixture distribution. However decreasing values of L_{11} leads to increase in the mixing process for a given initial Bi-modal mixture distributions, suggesting effects of L_{11} are dependent on initial mixture distributions and initial values of ϕ'.

Once the igniter is switched off the hot gas kernel is in the vicinity of local mixture

gradient which is seriously affected by initial values of ${}^{l_\phi}/_{l_f}$, ϕ', $\frac{u'}{S_{b(\phi=1)}}$, ${}^{L_{11}}/_{l_f}$ and nature of initial mixture distribution profile of given $\langle\phi\rangle$. Therefore judicious control on ${}^{L_{11}}/_{l_f}$, ${}^{l_\phi}/_{l_f}$, ϕ', $\frac{u'}{S_{b(\phi=1)}}$ and monitoring initial mixture distribution can support achieving better quality of burning for a given combustion cycle. The variability of burned gas mass is routinely obtained in the cylinder of IC engines due to cycle-to-cycle variation. The findings reveal that the degree of variability of burning depends not only on u', ϕ' and ${}^{l_\phi}/_{l_f}$ but also on the nature of initial mixture distribution, which can be manipulated by careful design of the nozzle and fuel injection systems in IC engines. Moreover, in-cylinder turbulence along with injection characteristics can influence the values of u', ϕ' and ${}^{l_\phi}/_{l_f}$, and thus the effective control of mixing characteristics in IC engine combustion chamber can potentially play a pivotal role to ensure successful ignition and reduce the variability associated with the ignition event.

7.3 Fuel Lewis Number Effects on Localised Forced Ignition

In Chapter 6 (Section 6.2), 3D DNS are studied to investigate the influences of fuel Lewis number Le_F (ranging from 0.8 to 1.2) on the energy deposition characteristics on the localised forced ignition of both stoichiometric ($\phi = 1.0$) and fuel-lean ($\phi = 0.8$) homogeneous mixtures for different values of u'. Furthermore Chapter 6 (Section 6.3) also investigate the effects of Le_F on localised forced ignition of globally stoichiometric stratified mixtures, where the effects of mixture inhomogeneity length scale l_ϕ, equivalence ratio fluctuation ϕ', rms values of turbulent velocity u' and influences of initial nature of mixture distribution are examined for different value of Le_F (ranging from 0.8 to 1.2).

The extent of burning M_b has been found to increase with decreasing values of Le_F for a given set of parameters for energy deposition characteristics (i.e. width of ignition energy deposition distribution, duration of ignition energy deposition and amount of input ignition energy) and $\frac{u'}{S_{b(\phi=1)}}$. Moreover, the MIE requirement for self-sustained combustion decreases with decreasing Le_F. However, the enhanced rate of burning due to flame wrinkling may dominate over the augmented heat transfer rate in the $Le_F < 1.0$ cases under some conditions, which may give rise to an increase in the burned gas mass M_b with increasing $\frac{u'}{S_{b(\phi=1)}}$. The computational findings here (Section 6.2.6) are in good qualitative agreement with experimental findings in the context of

MIE.

The flame resulting from localised forced ignition shows predominantly premixed mode of combustion although some region of non-premixed mode of combustion have also been observed for high values of ${}^{l_\phi}/_{l_f}$, ϕ' and Le_F irrespective of nature of initial mixture distribution. The decay rate of ϕ' is stronger for decreasing values of Le_F (see Figure 6.15). The mass of the burned gas region decreases with increasing Le_F for a given set of values of ${}^{l_\phi}/_{l_f}$, ϕ' and $\frac{u'}{S_{b(\phi=1)}}$, energy input and energy deposition duration. The increase in heat transfer rate from hot gas kernel with an increase in $\frac{u'}{S_{b(\phi=1)}}$ leads to a decrease in the extent of burning irrespective of the values of ${}^{l_\phi}/_{l_f}$ and ϕ' for the $Le_F \geq 1.0$ cases but the burned gas mass increases with increasing $\frac{u'}{S_{b(\phi=1)}}$ for the homogeneous mixture with $Le_F = 0.8$ case.

Furthermore, the findings suggests that the conditions (e.g. a combination of high values of ϕ' and ${}^{l_\phi}/_{l_f}$) which lead to large variability between different realisations should be avoided while designing industrial ignition systems for turbulent stratified mixtures. Thus, it is perhaps advantageous to have a feedback mechanism in cylinders of DI engines so that the fuel injection characteristics could be modulated to control ${}^{l_\phi}/_{l_f}$ and ϕ' to ensure successful ignition and self-sustained combustion depending on $\frac{u'}{S_{b(\phi=1)}}$ in the vicinity of the igniter. Moreover, it is desirable to avoid the combination of ${}^{l_\phi}/_{l_f}$ and ϕ' , which gives rise to large variability in the extent of burning between different realisations. The findings of this numerical investigation indicate that an ignition system for $Le_F < 1.0$ may not lead to successful ignition for heavier hydrocarbon-air mixtures with $Le_F > 1.0$ but the ignition systems designed for fuels with $Le_F > 1.0$ can successfully be used for lighter fuels with $Le_F < 1.0$.

7.4 Future Investigations

The present thesis provides physical insight into various aspects of localised forced ignition and parameters influencing sustainability of combustion originating from successful ignition for both homogeneous and stratified turbulent combustible mixtures. In practical engineering applications, ignition and subsequent combustion takes place at higher values of Re_t and involves a large number of intermediate species which can lead to the back-diffusion of light radical (e.g. H radical) and post diffusion flames [144], which are not captured using simplified chemistry. Moreover, successful ignition often leads to momentum modification contribution, plasma formation and shock wave, which remain beyond the scope of the present DNS analysis. With improved

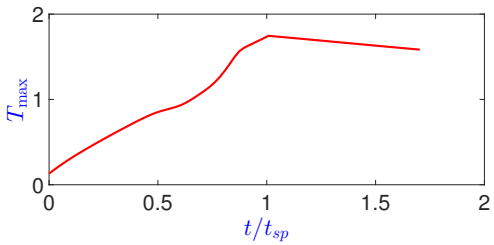

(a) Complex chemistry case from Table 7.1

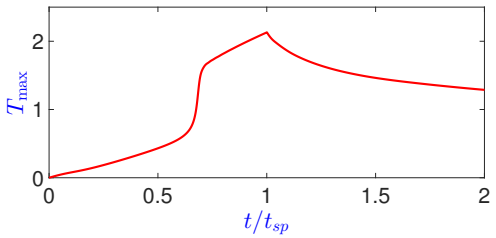

(b) Simplified chemistry case ST4AE from Table 5.1

Figure 7.1: Temporal distribution of $T_{\max}$ for case listed in Table 7.1 (left side) and case ST4AE from Table 5.1 (right side).

computational power and development of numerical capabilities, it is expected that three dimensional simulations with complex chemistry of industrially relevant fuels can be done for higher number of Re_t than used in the current simple chemistry simulation. Some of the possible research avenues for ignition in turbulent combustible mixtures are discussed in this section.

7.4.1 Preliminary Analysis in the Presence of Complex Chemistry

Numerical investigations in the presence of complex chemistry for localised forced ignition of turbulent stratified combustible mixtures have received limited consideration to date [51, 71, 149, 151]. In this analysis, some preliminary DNS simulations of localised forced ignition of stratified combustible mixtures have been conducted. The species inhomogeneity has been accounted for by a random bi-modal distribution of equivalence ratio ϕ for specified values of global mean equivalence ratio $\langle\phi\rangle$, rms fluctuations in equivalence ratio ϕ' and integral length scale of mixture inhomogeneity l_ϕ according to Eswaran and Pope [76]. In the current analysis globally stoichiometric (i.e. $\langle\phi\rangle = 1.0$) conditions have been considered. 3D DNS with complex chemistry for n-heptane has been used to extract physical information on the structure of igniting kernels following localised heat deposition in turbulent stratified mixtures. Here n-heptane is chosen as a fuel, as it is industrially relevant (e.g. main constitute of diesel oil).

The three-dimensional compressible DNS code SENGA2 [70, 103] including detailed chemistry has been used. Temperature dependent transport coefficient are eval-

uated through 5^{th}-order polynomials and molecular viscosity[145]. The values of Le_α for each species α were taken from the Lecture notes in Physics by Smooke and Giovangigli [190]. Here, n-heptane/Air combustion has been considered where the ignition was modelled by a source term in the energy equation, with a Gaussian energy deposition profile as described in Chapters 4, 5 and [50, 51]. The boundaries in the x-direction are partially non-reflecting and treated with Navier Stokes Characteristic Boundary Conditions (NSCBC). The transverse directions are periodic. A 4^{th}-order, low storage, explicit Runge-Kutta scheme [107], with a time-step of 5×10^{-9}[s] has been adopted here. The implicit solver VODPK [38] was then used for chemical reaction integration. A skeletal mechanism for n-heptane with 22 non-steady species undergoing 112 reactions, validated mostly for auto-ignition problems in non-premixed strained flows has been used [124]. Initial turbulent field was generated according to Batchelor-Townsend energy spectrum [24]. Details of different parameters for the investigated case are listed in Table 7.1.

7.4.1.1 Preliminary Results

The computational power required to run 3D simulations with complex chemistry are considerably high. The results presented in this section shows some preliminary results. The temporal evolution of the maximum values of non-dimensional temperature ($T_{\max}$) (Eq. 5.2) is shown in Figure 7.1. The temporal behaviour of $T_{\max}$ for complex chemistry mechanism case is in good qualitative agreement with simplified chemistry case simulation results. The quantity $T_{\max}$ rises with time during the energy deposition $0 \leq t \leq t_{sp}$ and thermal runaway seems to be appearing. The visualisation of flame kernel can be seen from Figure 7.2, where the distributions of T and $Y_{C_7H_{16}}$ are presented for the case analysed here. It can be seen from Figure 7.2 that the initial contour of T at $t \leq t_{sp}$ remains spherical during energy deposition and starts to deform as time progresses at $t = 1.50t_{sp}$. Prior to ignition phase, the contours of T principally determined by the diffusion of the deposited energy, but after the ignition, the contours of T depends on the magnitude of the reaction rate at the local mixture composition and flame stretch induced by the background of the fluid motion. Figure 7.3 demonstrates that ϕ' is decaying as time progresses. The above findings are in good qualitative agreement with the results obtained in Section 5.2. It is worth nothing that the complex chemistry case uses the stratified mixture of $n-C_7H_{16}+\text{Air}$, whereas the simplified chemistry case uses a generic chemical mechanism representative of CH_4-air combustion. The qualitative agreement between the present studied case (Table 7.1)

and simplified chemistry case studied in Chapter 5 (case ST4AE - Table 5.1) provides more confidence that the qualitative nature of flame propagation following localised forced ignition is not likely to change in the presence of detailed chemical kinetics.

7.4.2 Autoignition

The concept of homogeneous charge compression ignition (HCCI) engines have attracted vast amount of research interests. The hypothesis in HCCI engines, the reactant charges are very lean and nearly homogeneous and hence the ignition and combustion processes are controlled by the kinetically driven processes [177]. However, one of the key challenges in HCCI engines is to control the start of combustion and to ensure smooth heat generation during the cycle under various load conditions. Hence accurate predictive simulations of the ignition and subsequent combustion processes in an HCCI-like environment plays vital role in development of HCCI engines. The combustion mode in HCCI engines can be both volumetric and front-like, which is not well understood to date [98]. A major challenge for using HCCI method of combustion is to control the heat release rate, as it is required to spread it out over several crank angle degrees, suppressing the occurrence of rapid rate of pressure rise [54, 87]. Introducing temperature or mixture inhomogeneity to produce the desired heat release rate can be the possible control strategy [75, 187]. However, incomplete turbulent mixing and temperature stratification between bulk gases and cylinder wall can lead to a range of combustion modes, which are distinct from HCCI autoignition [54, 87]. Number of previous both experimental [120, 121] and numerical [20, 29, 54, 74, 87, 125, 177] investigations concentrate on effects of thermal stratification under HCCI conditions with fixed mean (i.e. $\langle T \rangle$) and RMS (i.e. T') of temperature field. The effects of non-zero RMS value of temperature field with different length scale of temperature inhomogeneity subjected to different RMS of turbulence velocity have received limited attention [54, 74, 87] in spite of its practical relevance.

The three-dimensional compressible DNS code SENGA [42] has been used here. All boundaries are taken to be periodic in nature and treated with Navier Stokes Characteristic Boundary Conditions (NSCBC). Simulations have been carried out for $t_{sim} \sim 6.6t_f$, where t_f is the characteristic chemical time scale. For the purpose of a detailed parametric analysis, a single step chemistry approach [197] has been considered here. Details of different parameters are listed in Table 7.2. The thermal inhomogeneity has been accounted for by a random Gaussian distribution of non-dimensional temperature for specified values of global mean temperature (i.e. $\langle T \rangle$),

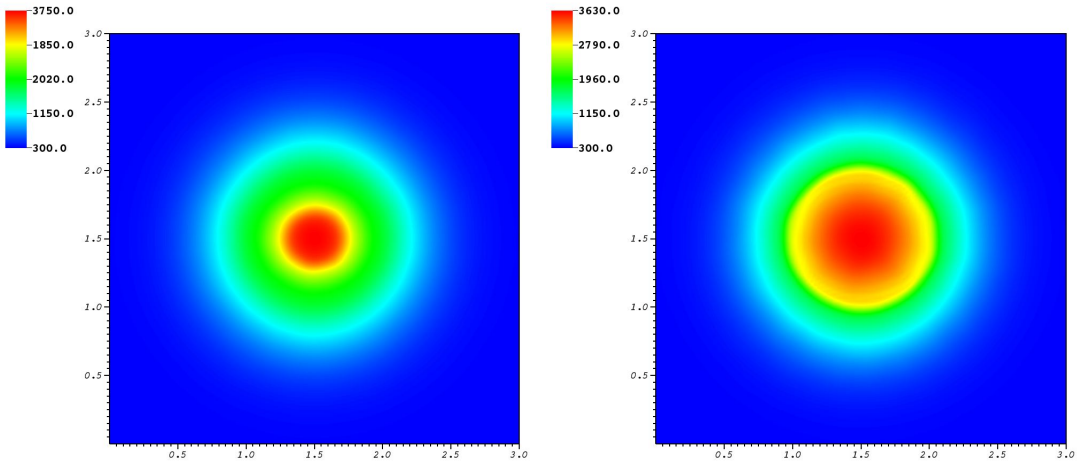

(a) Distribution of T on the central $x_1 - x_2$ plane.

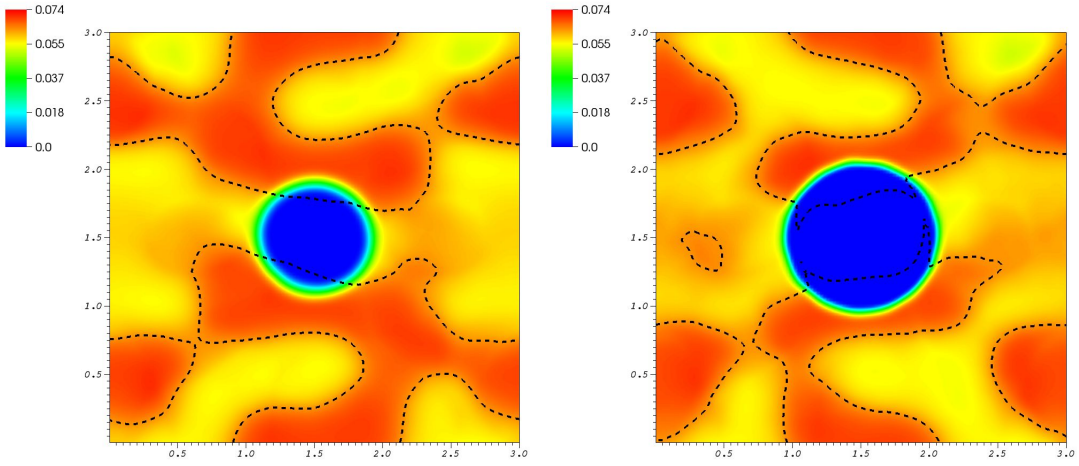

(b) Distribution of $Y_{C_7H_{16}}$ on the central $x_1 - x_2$ plane.

Figure 7.2: Distribution of T (a) and $Y_{C_7H_{16}}$ (b) for the case listed in Table 7.1. The black broken line shows $\xi = \xi_{st}$ where the left column shows $t = 0.8t_{sp}$ and right column shows $t = 1.50t_{sp}$.

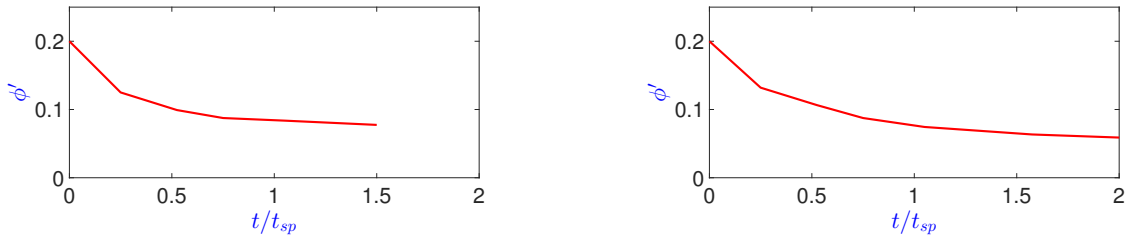

(a) Complex chemistry case from Table 7.1

(b) Simplified chemistry case ST4AE from Table 5.1

Figure 7.3: Temporal distribution of ϕ' calculated over whole computational domain for case listed in Table 7.1 (left column), case ST4AE ($\langle\phi\rangle = 1.0$, $\phi' = 0.2$, ${}^{l_\phi}/_{l_f} = 5.5$, $\frac{u'}{S_{b(\phi=1)}} = 4.0$) from Table 5.1 (right column).

Domain Size	$(33\, l_f)^3$
Discretised grids	$(200)^3$
Grid resolution	$\eta \geq 1.2\Delta x$
Homogeneous Fuel Mixture	$(CH_4 + \text{air})$
ϕ	0.5
$\langle T \rangle$	0.3
T'	0.2, 0.4, 0.6
${}^{l_T}/_{l_f}$	2.1, 5.5, 8.3
${}^{L_{11}}/_{l_f}$	3.36
$\frac{u'}{S_{b(\phi=1)}}$	1.5, 2.5, 4.0, 6.0, 10.0

Table 7.2: Domain, turbulence and temperature field characteristics for the investigated cases.

temperature fluctuation (i.e. T') and length scale of thermal inhomogeneity (i.e. ${}^{l_T}/_{l_f}$) [81]. For all cases, the mean temperature is taken as $\langle T \rangle = 0.3$, and the amplitude of T' is modulated, where $T = 1.0$ being an adiabatic flame temperature. Initial values of equivalence ratio (ϕ), $\langle T \rangle$ and $\frac{u'}{S_{b(\phi=1)}}$ are taken following previous studies [20, 29, 54, 74, 87, 125, 177].

7.4.2.1 Preliminary Results

The preliminary simulation results for specific cases with $\langle T \rangle = 0.3$; $T' = 0.6$; $\frac{u'}{S_{b(\phi=1)}} = 1.5$ and different ${}^{l_T}/_{l_f}$ (i.e. ${}^{l_T}/_{l_f}$ =2.1, 8.3) are shown in Figure 7.4, where volume rendered contours of $T = 1.0$ is shown at different time intervals. It is evident from Figure 7.4 that in both cases ${}^{l_T}/_{l_f}$ =2.1, 8.3, the flame kernel grows (originating from

multiple places) with time, indicating self-sustained combustion is possible for thermal stratification with very lean ($\phi = 0.5$) fuel-air mixture.

Additionally case with ${}^{l_T}/_{l_f} = 2.1$ exhibited more ignition sites in comparison with ${}^{l_T}/_{l_f} = 8.3$ case. As the clouds of thermal inhomogeneity are relatively small (big) for ${}^{l_T}/_{l_f} = 2.1$ (${}^{l_T}/_{l_f} = 8.3$), causing more ignition sites in ${}^{l_T}/_{l_f} = 2.1$ case. The values of T', ${}^{u'}/_{S_{b(\phi=1)}}$ also play an important roles in auto-ignition and subsequent combustion process. These analyses will form the basic of future research on auto-ignition and flame propagation with thermal inhomogeneities, which will contribute towards the understanding and modelling of combustion of future HCCI engines.

7.4.3 Numerical Model Integrating Physical Aspects of Forced Ignition

The details of the spark formation (momentum modification contribution, plasma formation and shock wave) remain beyond the scope of the present thesis analysis to keep this study computationally feasible. These aspects need to be understood further and simulation methodology for these processes need to be developed further for more comprehensive understanding and quantitative predictions from numerical simulations.

7.4.4 Feedback Loop Ignition Control for IC Engines

It could be advantageous to explore the feedback loop ignition control in future IC engines. The Chapter 5 identifies the effects of fuel injection characteristics to control mixture inhomogeneity to ensure successful ignition and self-sustained combustion. The feedback mechanism of controlling and sensing of combustion could provide design parameters for next generation engine configurations, moreover it extends the stratified GDI combustion to achieve reduced cycle-to-cycle variation and NO_X emission. This feedback mechanism could be used to explore how the dynamic selection of ignition, mixture inhomogeneity, fuel injection and control feedback parameters can be optimised for more efficient and cleaner combustion over wide range of engine operating conditions. Such conditions can be further analysed with the help of more detailed simulations and detailed experiments to create next to real engine environment.

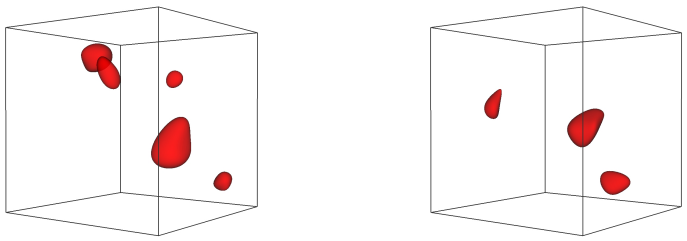

(a) $t = 1.05\, t_f$

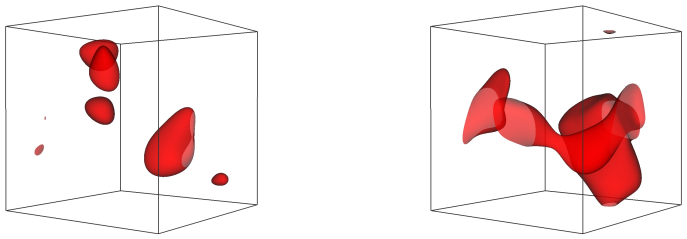

(b) $t = 2.10\, t_f$

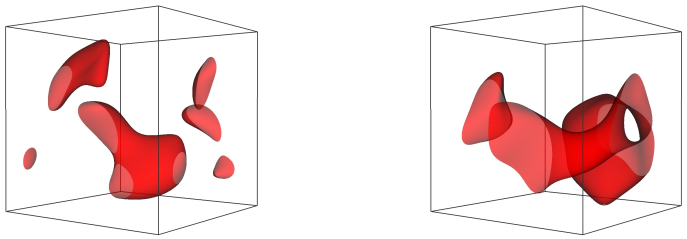

(c) $t = 4.20\, t_f$

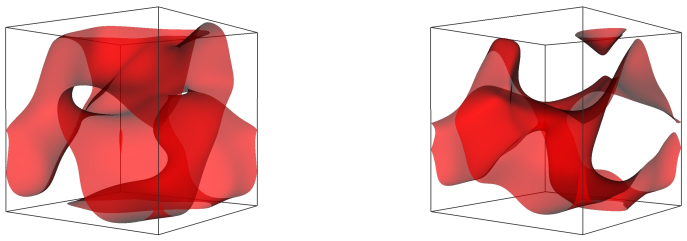

(d) $t = 6.30\, t_f$

Figure 7.4: Volume rendered contours of $T = 1.0$ within the domain $33l_f \times 33l_f \times 33l_f$ for cases with $\langle T \rangle = 0.3$; $T' = 0.6$; $\frac{u'}{S_{b(\phi=1)}} = 1.5$ showing ${}^{l_T}/_{l_f} = 2.1$ (left column) and ${}^{l_T}/_{l_f} = 8.3$ (right column) at different time instances from Table 7.2.

References

[1] Abdel-Gayed, R., Bradley, D., and Lung, F.-K. Combustion regimes and the straining of turbulent premixed flames. *Combustion and Flame*, **76** (1989), 213.

[2] Aggarwal, S. A review of spray ignition phenomena: present status and future research. *Progress in Energy and Combustion Science*, **24** (1998), 565.

[3] Ahmed, S. *Spark Ignition of Turbulent Non-premixed Flames.* Ph.D. thesis, Department of Engineering, University of Cambridge (2006).

[4] Ahmed, S., Balachandran, R., and Mastorakos, E. Measurements of ignition probability in turbulent non-premixed counterflow flames. *Proceedings of the Combustion Institute*, **31** (2007), 1507.

[5] Ahmed, S. and Mastorakos, E. Spark ignition of lifted turbulent jet flames. *Combustion and Flame*, **146** (2006), 215.

[6] Akindele, O., Bradley, D., Mak, P., and McMahon, M. Spark ignition of turbulent gases. *Combustion and Flame*, **47** (1982), 129.

[7] Aliramezani, M., Chitsaz, I., and Mozafari, A. Thermodynamic modeling of partially stratified charge engine characteristics for hydrogen-methane blends at ultra-lean conditions. *international journal of hydrogen energy*, **38** (2013), 10640.

[8] Alkidas, A. Combustion advancements in gasoline engines. *Energy Conversion and Management*, **48** (2007), 2751.

[9] Alvani, R. and Fairweather, M. Ignition characteristics of turbulent jet flows. *Chemical Engineering Research and Design*, **80** (2002), 917.

[10] Anselmo-Filho, P., Hochgreb, S., Barlow, R., and Cant, R. Experimental measurements of geometric properties of turbulent stratified flames. *Proceedings of the Combustion Institute*, **32** (2009), 1763.

[11] Aspden, A., Day, M., and Bell, J. Lewis number effects in distributed flames. *Proceedings of the Combustion Institute*, **33** (2011), 1473.

[12] Ballal, D. and Lefebvre, A. The influence of flow parameters on minimum ignition energy and quenching distance. vol. 15, pp. 1473–1481. Elsevier (1975). ISBN 0082-0784.

[13] Ballal, D. and Lefebvre, A. The influence of spark discharge characteristics on minimum ignition energy in flowing gases. *combustion and Flame*, **24** (1975), 99.

[14] Ballal, D. and Lefebvre, A. *Spark ignition of turbulent flowing gases.* American Institute of Aeronautics and Astronautics (1977).

[15] Ballal, D. and Lefebvre, A. Ignition and flame quenching of flowing heterogeneous fuel-air mixtures. *Combustion and Flame*, **35** (1979), 155.

[16] Ballal, D. and Lefebvre, A. Ignition and flame quenching of flowing heterogeneous fuel-air mixtures. *Combustion and Flame*, **35** (1979), 155.

[17] Ballal, D. and Lefebvre, A. Flame propagation in heterogeneous mixtures of fuel droplets, fuel vapor and air. In *Proceedings of the combustion Institute*, vol. 18, pp. 321–328. Elsevier (1981).

[18] Ballal, D. R. and Lefebvre, A. H. The influence of spark discharge characteristics on minimum ignition energy in flowing gases. *Combustion and Flame*, **24** (1975), 99.

[19] Balusamy, S., Cessou, A., and Lecordier, B. Laminar propagation of lean premixed flames ignited in stratified mixture. *Combustion and Flame*, **161** (2014), 427.

[20] Bansal, G. and Im, H. Autoignition and front propagation in low temperature combustion engine environments. *Combustion and Flame*, **158** (2011), 2105.

[21] Barbosa, S., Garcia, M. d. L. C., Ducruix, S., Labegorre, B., and Lacas, F. Control of combustion instabilities by local injection of hydrogen. *Proceedings of the combustion Institute*, **31** (2007), 3207.

[22] Batchelor, G. *The Theory of Homogeneous Turbulence*. Cambridge Science Classics. Cambridge University Press (1953). ISBN 9780521041171.

[23] Batchelor, G. and Townsend, A. Decay of turbulence in the final period. vol. 194, pp. 527–543. The Royal Society (1948). ISBN 1364-5021.

[24] Batchelor, G. K. and Townsend, A. A. The nature of turbulent motion at large wave-numbers. *Proceedings of the Royal Society of London A: Mathematical, Physical and Engineering Sciences*, **199** (1949), 238.

[25] Baum, M. and Poinsot, T. Effects of mean flow on premixed flame ignition. *Combustion Science and Technology*, **106** (1995), 19.

[26] Beduneau, J. and Ikeda, Y. Application of laser ignition on laminar flame front investigation. *Experiments in fluids*, **36** (2004), 108.

[27] Bilger, R., Pope, S., Bray, K., and Driscoll, J. Paradigms in turbulent combustion research. *Proceedings of the Combustion Institute*, **30** (2005), 21 .

[28] Birch, A., Brown, D., and Dodson, M. Ignition probabilities in turbulent mixing flows. In *Proceedings of the combustion Institute*, vol. 18, pp. 1775–1780. Elsevier (1981).

[29] Bisetti, F., Chen, J.-Y., Chen, J., and Hawkes, E. Differential diffusion effects during the ignition of a thermally stratified premixed hydrogen–air mixture subject to turbulence. *Proceedings of the Combustion Institute*, **32** (2009), 1465.

[30] Blanc, M., Guest, P., von Elbe, G., and Lewis, B. Ignition of explosive gas mixtures by electric sparks: Iii. minimum ignition energies and quenching distances ofmixtures of hydrocarbons and ether with oxygen and inert gases. In *Symposium on Combustion and Flame, and Explosion Phenomena*, vol. 3, pp. 363–367. Elsevier (1948).

[31] Böker, D. and Brüggemann, D. Advancing lean combustion of hydrogen–air mixtures by laser-induced spark ignition. *International Journal of Hydrogen Energy*, **36** (2011), 14759.

[32] Borghi, R. On the structure and morphology of turbulent premixed flames. In *Recent advances in the Aerospace sciences*, pp. 117–138. Springer (1985).

[33] Boyde, J., Le Clercq, P., Di Domenico, M., Rachner, M., Gebel, G., Mosbach, T., and Aigner, M. Numerical investigation of the parameter governing the ignitability of a spray flame. *Journal of Engineering for Gas Turbines and Power*, **135** (2013), 011506.

[34] Bradley, D. and Lung, F.-K. Spark ignition and the early stages of turbulent flame propagation. *Combustion and Flame*, **69** (1987), 71.

[35] Bray, K., Domingo, P., and Vervisch, L. Role of the progress variable in models for partially premixed turbulent combustion. *Combustion and Flame*, **141** (2005), 431 .

[36] Brequigny, P., Halter, F., Mounaïm-Rousselle, C., and Dubois, T. Fuel performances in spark-ignition (si) engines: Impact of flame stretch. *Combustion and Flame*, **166** (2016), 98.

[37] Brosh, T., Patel, D., Wacks, D., and Chakraborty, N. Numerical investigation of localised forced ignition of pulverised coal particle-laden mixtures: A direct numerical simulation (dns) analysis. *Fuel*, **145** (2015), 50.

[38] Brown, P. and Hindmarsh, A. Reduced storage matrix methods in stiff ode systems. *Applied Mathematics and Computation*, **31** (1989), 40.

[39] Calcote, H., Gregory, C., Barnett, C., and Gilmer, R. Spark ignition. effect of molecular structure. *Industrial & Engineering Chemistry*, **44** (1952), 2656.

[40] Cant, R. Direct numerical simulation of premixed turbulent flames. *Philosophical Transactions of the Royal Society of London A: Mathematical, Physical and Engineering Sciences*, **357** (1999), 3583.

[41] Cant, R. Initial conditions for direct numerical simulation of turbulence. technical report. Tech. rep., Cambridge University Engineering Department (2001).

[42] Cant, R. Senga, direct numerical simulation of combustion: User guide. Tech. rep., Cambridge University Engineering Department (2001).

[43] Cant, R. and Mastorakos, E. *An Introduction to Turbulent Reacting Flows*. Imperial College Press (2008). ISBN 9781860947780.

[44] Cardin, C., Renou, B., Cabot, G., and Boukhalfa, A. Experimental analysis of laser-induced spark ignition of lean turbulent premixed flames: New insight into ignition transition. *Combustion and Flame*, **160** (2013), 1414.

[45] Catlin, C., Fairweather, M., and Ibrahim, S. Predictions of turbulent, premixed flame propagation in explosion tubes. *Combustion and Flame*, **102** (1995), 115.

[46] Chakraborty, N. *Fundamental Study of Turbulent Premixed Combustion using Direct Numerical Simulation (DNS)*. Ph.D. thesis, University of Cambridge (2004).

[47] Chakraborty, N. and Cant, R. Unsteady effects of strain rate and curvature on turbulent premixed flames in an inflow–outflow configuration. *Combustion and flame*, **137** (2004), 129.

[48] Chakraborty, N., Hesse, H., and Mastorakos, E. Effects of fuel lewis number on localised forced ignition of turbulent mixing layers. *Flow, Turbulence and Combustion*, **84** (2010), 125.

[49] Chakraborty, N. and Mastorakos, E. Numerical investigation of edge flame propagation characteristics in turbulent mixing layers. *Physics of Fluids (1994-present)*, **18** (2006), 105103.

[50] Chakraborty, N. and Mastorakos, E. Direct numerical simulations of localised forced ignition in turbulent mixing layers: the effects of mixture fraction and its gradient. *Flow, Turbulence and Combustion*, **80** (2008), 155.

[51] Chakraborty, N., Mastorakos, E., and Cant, R. Effects of turbulence on spark ignition in inhomogeneous mixtures: a direct numerical simulation (dns) study. *Combustion Science and Technology*, **179** (2007), 293.

[52] Champion, M., Deshaies, B., Joulin, G., and Kinoshita, K. Spherical flame initiation: Theory versus experiments for lean propane-air mixtures. *Combustion and flame*, **65** (1986), 319.

[53] Chate, H. and Cant, R. Relevant scale in the corrugated flamelet regime. *Combustion and flame*, **74** (1988), 1.

[54] Chen, J., Hawkes, E., Sankaran, R., Mason, S., and Im, H. Direct numerical simulation of ignition front propagation in a constant volume with temperature inhomogeneities: I. fundamental analysis and diagnostics. *Combustion and flame*, **145** (2006), 128.

[55] Chin, J. Analysis of the effect of oxygen addition on minimum ignition energy. *Journal of energy*, **7** (1983), 710.

[56] Chung, S. Stabilization, propagation and instability of tribrachial triple flames. *Proceedings of the Combustion Institute*, **31** (2007), 877.

[57] Colwell, J. and Reza, A. Hot surface ignition of automotive and aviation fluids. *Fire technology*, **41** (2005), 105.

[58] Correa, S. Current problems in gas turbine combustion (1990). Paper Presented at the Fall Technical Meeting, The Combustion Institute, Estern States Section, Orlando, FL.

[59] Da Cruz, A. P., Dean, A., and Grenda, J. A numerical study of the laminar flame speed of stratified methane/air flames. *Proceedings of the Combustion Institute*, **28** (2000), 1925.

[60] Damköhler, G. Der einfluß der turbulenz auf die flammengeschwindigkeit in gasgemischen. *Zeitschrift für Elektrochemie und angewandte physikalische Chemie*, **46** (1940), 601.

[61] Danis, A., Namer, I., and Cernansky, N. Droplet size and equivalence ratio effects on spark ignition of monodisperse n-heptane and methanol sprays. *Combustion and flame*, **74** (1988), 285.

[62] De Soete, G. G. Overall reaction rates of no and n 2 formation from fuel nitrogen. In *Proceedings of the combustion Institute*, vol. 15, pp. 1093–1102. Elsevier (1975).

[63] Dearden, G. and Shenton, T. Laser ignited engines: progress, challenges and prospects. *Optics express*, **21** (2013), A1113.

[64] Defransure, F., Renou, B., Samson, E., Boukhalfa, A., and Veynante, D. Experimental and numerical studies of the laminar flame speed of stratified flames. In *Proceedings of 1st European Combustion Meeting, Orleans, France* (2003).

[65] Dharamshi, K., Pal, A., and Agarwal, A. Comparative investigations of flame kernel development in a laser ignited hydrogen–air mixture and methane–air mixture. *international journal of hydrogen energy*, **38** (2013), 10648.

[66] Dharamshi, K., Srivastava, D., and Agarwal, A. Combustion characteristics and flame-kernel development of a laser ignited hydrogen–air mixture in a constant volume combustion chamber. *International Journal of Hydrogen Energy*, **39** (2014), 593.

[67] Drake, M. and Haworth, D. Advanced gasoline engine development using optical diagnostics and numerical modeling. *Proceedings of the Combustion Institute*, **31** (2007), 99.

[68] Dreizler, A., Lindenmaier, S., Maas, U., Hult, J., Aldén, M., and Kaminski, C. Characterisation of a spark ignition system by planar laser-induced fluorescence of oh at high repetition rates and comparison with chemical kinetic calculations. *Applied Physics B*, **70** (2000), 287.

[69] Driscoll, J. Turbulent premixed combustion: Flamelet structure and its effect on turbulent burning velocities. *Progress in Energy and Combustion Science*, **34** (2008), 91.

[70] Dunstan, T. and Jenkins, K. The effects of hydrogen substitution on turbulent premixed methane–air kernels using direct numerical simulation. *International journal of hydrogen energy*, **34** (2009), 8389.

[71] Echekki, T. and Mastorakos, E. *Turbulent combustion modeling: Advances, new trends and perspectives*, vol. 95. Springer Science & Business Media (2010).

[72] Egolfopoulos, F., Cho, P., and Law, C. Laminar flame speeds of methane-air mixtures under reduced and elevated pressures. *Combustion and Flame*, **76** (1989), 375 .

[73] Eichenberger, D. and Roberts, W. Effect of unsteady stretch on spark-ignited flame kernel survival. *Combustion and flame*, **118** (1999), 469.

[74] El-Asrag, H. and Ju, Y. Direct numerical simulations of nox effect on multistage autoignition of dme/air mixture in the negative temperature coefficient regime for stratified hcci engine conditions. *Combustion and Flame*, **161** (2014), 256.

[75] Epping, K., Aceves, S., Bechtold, R., and Dec, J. The potential of hcci combustion for high efficiency and low emissions. Tech. rep., SAE Technical Paper (2002).

[76] Eswaran, V. and Pope, S. Direct numerical simulations of the turbulent mixing of a passive scalar. *Physics of Fluids (1958-1988)*, **31** (1988), 506.

[77] Foster, H. Effect of spark repetition rate on the ignition limits of a single tubular combustor. (1951).

[78] Fredi, A. and Sibulkin, M. Dependence of minimum ignition energy on ignition parameters. *Combustion science and technology*, **73** (1990), 395.

[79] Gashi, S., Hult, J., Jenkins, K., Chakraborty, N., Cant, R., and Kaminski, C. Curvature and wrinkling of premixed flame kernels—comparisons of oh plif and dns data. *Proceedings of the Combustion Institute*, **30** (2005), 809.

[80] Glassman, I. *Combustion*. Elsevier Science (1997). ISBN 9780080529417.

[81] Grout, R., Swaminathan, N., and Cant, R. Effects of compositional fluctuations on premixed flames. *Combustion Theory and Modelling*, **13** (2009), 823.

[82] Grune, J., Sempert, K., Kuznetsov, M., and Jordan, T. Experimental investigation of fast flame propagation in stratified hydrogen–air mixtures in semi-confined flat layers. *Journal of Loss Prevention in the Process Industries*, **26** (2013), 1442.

[83] Guan, Y., Zhao, G., and Xiao, X. Design and experiments of plasma jet igniter for aeroengine. *Propulsion and Power Research*, **2** (2013), 188.

[84] Han, I. and Huh, K. Roles of displacement speed on evolution of flame surface density for different turbulent intensities and lewis numbers in turbulent premixed combustion. *Combustion and Flame*, **152** (2008), 194.

[85] Han, I. and Huh, K. Effects of the karlovitz number on the evolution of the flame surface density in turbulent premixed flames. *Proceedings of the Combustion Institute*, **32** (2009), 1419.

[86] Hannebique, G., Sierra, P., Riber, E., and Cuenot, B. Large eddy simulation of reactive two-phase flow in an aeronautical multipoint burner. *Flow, turbulence and combustion*, **90** (2013), 449.

[87] Hawkes, E., Sankaran, R., Pébay, P., and Chen, J. Direct numerical simulation of ignition front propagation in a constant volume with temperature inhomogeneities: Ii. parametric study. *Combustion and Flame*, **145** (2006), 145.

[88] Haworth, D., Blint, R., Cuenot, B., and Poinsot, T. Numerical simulation of turbulent propane–air combustion with nonhomogeneous reactants. *Combustion and Flame*, **121** (2000), 395.

[89] Haworth, D., Cuenot, B., Poinsot, T., and Blint, R. Numerical simulation of turbulent propane-air combustion with non-homogeneous reactants: initial results. In *Center for Turbulence Research Proceedings of the Summer Program*, pp. 5–24 (1998).

[90] He, L. Critical conditions for spherical flame initiation in mixtures with high lewis numbers. *Combustion Theory and Modelling*, **4** (2000), 159.

[91] Hélie, J. and Trouvé, A. Turbulent flame propagation in partially premixed combustion. *Proceedings of the combustion Institute*, **27** (1998), 891.

[92] Hélie, J. and Trouvé, A. A modified coherent flame model to describe turbulent flame propagation in mixtures with variable composition. *Proceedings of the Combustion Institute*, **28** (2000), 193.

[93] Hesse, H., Malkeson, S., and Chakraborty, N. Displacement speed statistics for stratified mixture combustion in an igniting turbulent planar jet. *Journal of Engineering for Gas Turbines and Power*, **134** (2012), 051502.

[94] Hilbert, R. and Thevenin, D. Dns of multi-brachial structures with detailed chemistry and transport. In *Proceedings of the 9th International Conference on Numerical Combustion, Sorrento, Italy, Paper*, 064 (2002).

[95] Hoffmeyer, H. *Combustion Characteristics of Turbo Charged DISI-engines*. Logos Verlag Berlin (2012). ISBN 9783832530792.

[96] Huang, C., Shy, S., Liu, C., and Yan, Y. A transition on minimum ignition energy for lean turbulent methane combustion in flamelet and distributed regimes. *Proceedings of the Combustion Institute*, **31** (2007), 1401.

[97] Huang, Y. and Yang, V. Dynamics and stability of lean-premixed swirl-stabilized combustion. *Progress in Energy and Combustion Science*, **35** (2009), 293.

[98] Hultqvist, A., Christensen, M., Johansson, B., Richter, M., Nygren, J., Hult, J., and Aldén, M. The hcci combustion process in a single cycle-high-speed fuel tracer lif and chemiluminescence imaging. *SAE Technical Papers*, (2002).

[99] Im, H. and Chen, J. Structure and propagation of triple flames in partially premixed hydrogen–air mixtures. *Combustion and flame*, **119** (1999), 436.

[100] Im, H. and Chen, J. Effects of flow strain on triple flame propagation. *Combustion and Flame*, **126** (2001), 1384.

[101] In, B., Park, S., Kim, H., and Lee, K. Combustion and emission characteristics of a dual injection system applied to a disi engine. *Petroleum Science*, **11** (2014), 424.

[102] Jamrozik, A., Tutak, W., Kociszewski, A., and Sosnowski, M. Numerical simulation of two-stage combustion in si engine with prechamber. *Applied Mathematical Modelling*, **37** (2013), 2961.

[103] Jenkins, K. and Cant, R. Flame kernel interactions in a turbulent environment. Tech. rep., DTIC Document (2001).

[104] Jiménez, C., Cuenot, B., Poinsot, T., and Haworth, D. Numerical simulation and modeling for lean stratified propane-air flames. *Combustion and Flame*, **128** (2002), 1.

[105] Kaminski, C., Hult, J., Aldén, M., Lindenmaier, S., Dreizler, A., Maas, U., and Baum, M. Spark ignition of turbulent methane/air mixtures revealed by time-resolved planar laser-induced fluorescence and direct numerical simulations. *Proceedings of the combustion institute*, **28** (2000), 399.

[106] Kang, T. and Kyritsis, D. Methane flame propagation in compositionally stratified gases. *Combustion science and technology*, **177** (2005), 2191.

[107] Kennedy, C., Carpenter, M., and Lewis, R. Low-storage, explicit runge–kutta schemes for the compressible navier–stokes equations. *Applied numerical mathematics*, **35** (2000), 177.

[108] Kim, M., Won, S., and Chung, S. Effect of velocity gradient on propagation speed of tribrachial flames in laminar coflow jets. *Proceedings of the Combustion Institute*, **31** (2007), 901.

[109] Klein, M., Chakraborty, N., and Cant, R. Effects of turbulence on self-sustained combustion in premixed flame kernels: a direct numerical simulation (dns) study. *Flow, turbulence and combustion*, **81** (2008), 583.

[110] Ko, Y. and Chung, S. Propagation of unsteady tribrachial flames in laminar non-premixed jets. *Combustion and Flame*, **118** (1999), 151.

[111] Kono, M., Hatori, K., and Iinuma, K. Investigation on ignition ability of composite sparks in flowing mixtures. In *Proceedings of the combustion Institute*, vol. 20, pp. 133–140. Elsevier (1985).

[112] Kowalewicz, A. Combustion systems of the high speed internal combustion engines. *WKŁ, Warszawa*, (1980).

[113] Kravchik, T. and Sher, E. Numerical modeling of spark ignition and flame initiation in a quiescent methane-air mixture. *Combustion and flame*, **99** (1994), 635.

[114] Kumagai, S., Sakai, T., and Yasugahira, N. Calorimetry of spark energy. *Combustion Science and Technology*, **6** (1972), 233.

[115] Law, C. *Combustion Physics*. Cambridge University Press (2006). ISBN 9781139459242.

[116] Lefebvre, A. *GAS Turbine Combustion, Second Edition*. Combustion: An International Series. Taylor & Francis (1998). ISBN 9781560326731.

[117] Lewis, B. and Von Elbe, G. *Combustion, flames and explosions of gases*. Elsevier (2012).

[118] Lignell, D., Chen, J., Lu, T., and Law, C. Direct numerical simulation of extinction and reignition in a nonpremixed turbulent ethylene jet flame. Tech. rep., Sandia National Laboratories (SNL-CA), Livermore, CA (United States) (2007).

[119] Lim, K. *DNS of inhomogeneous reactants premixed combustion*. Ph.D. thesis, Fitzwilliam College, University of Cambridge, University of Cambridge (2014).

[120] Lim, O. Investigation of thermal stratification effect on n-heptane/iso-octane-air mixture hcci combustion. *International Journal of Automotive Technology*, **14** (2013), 843.

[121] Lim, O. and Iida, N. The investigation about the effects of thermal stratification in combustion chamber on hcci combustion fueled with dme/n-butane using rapid compression machine. *Experimental Thermal and Fluid Science*, **39** (2012), 123.

[122] Lipatnikov, A. *Fundamentals of Premixed Turbulent Combustion*. CRC Press (2012). ISBN 9781466510258.

[123] Lipatnikov, A. and Chomiak, J. Effects of premixed flames on turbulence and turbulent scalar transport. *Progress in Energy and Combustion Science*, **36** (2010), 1.

[124] Liu, S., Hewson, J., Chen, J., and Pitsch, H. Effects of strain rate on high-pressure nonpremixed n-heptane autoignition in counterflow. *Combustion and flame*, **137** (2004), 320.

[125] Lodier, G., Merlin, C., Domingo, P., Vervisch, L., and Ravet, F. Self-ignition scenarios after rapid compression of a turbulent mixture weakly-stratified in temperature. *Combustion and Flame*, **159** (2012), 3358.

[126] Lu, T. and Law, C. Toward accommodating realistic fuel chemistry in large-scale computations. *Progress in Energy and Combustion Science*, **35** (2009), 192.

[127] Malkeson, S. *Fundamental understanding and modelling of turbulent combustion in stratified mixtures using Direct Numerical Simulations (DNS).* Ph.D. thesis, School of Engineering, University of Liverpool (2011).

[128] Malkeson, S. and Chakraborty, N. A priori direct numerical simulation assessment of algebraic models of variances and dissipation rates in the context of reynolds-averaged navier-stokes simulations for low damköhler number partially premixed combustion. *Combustion Science and Technology*, **182** (2010), 960.

[129] Malkeson, S. and Chakraborty, N. Statistical analysis of displacement speed in turbulent stratified flames: A direct numerical simulation study. *Combustion Science and Technology*, **182** (2010), 1841.

[130] Malkeson, S. P. and Chakraborty, N. A-priori direct numerical simulation modelling of co-variance transport in turbulent stratified flames. *Flow, turbulence and combustion*, **90** (2013), 243.

[131] Maly, R. and Vogel, M. Initiation and propagation of flame fronts in lean ch4-air mixtures by the three modes of the ignition spark. In *Symposium (International) on Combustion*, vol. 17, pp. 821–831. Elsevier (1979).

[132] Mansour, M., Peters, N., and Schrader, L. Experimental study of turbulent flame kernel propagation. *Experimental Thermal and Fluid Science*, **32** (2008), 1396.

[133] Masri, A. Partial premixing and stratification in turbulent flames. *Proceedings of the Combustion Institute*, **35** (2015), 1115.

[134] Mastorakos, E. Ignition of turbulent non-premixed flames. *Progress in Energy and Combustion Science*, **35** (2009), 57 .

[135] Mastorakos, E., Baritaud, T., and Poinsot, T. Numerical simulations of autoignition in turbulent mixing flows. *Combustion and Flame*, **109** (1997), 198.

[136] McAllister, S., Chen, J., and Fernandez-Pello, A. *Fundamentals of Combustion Processes.* Mechanical Engineering Series. Springer New York (2011). ISBN 9781441979438.

[137] McIntyre, D. and Woodruff, S. Laser spark plug numerical design process with experimental validation. In *ASME 2011 Internal Combustion Engine Division Fall Technical Conference*, pp. 1–19. American Society of Mechanical Engineers (2011).

[138] Mercier, R., Auzillon, P., Moureau, V., Darabiha, N., Gicquel, O., Veynante, D., and Fiorina, B. Les modeling of the impact of heat losses and differential diffusion on turbulent stratified flame propagation: Application to the tu darmstadt stratified flame. *Flow, turbulence and combustion*, **93** (2014), 349.

[139] Mongia, H., Held, T., Hsiao, G., and Pandalai, R. Challenges and progress in controlling dynamics in gas turbine combustors. *Journal of Propulsion and Power*, **19** (2003), 822.

[140] Morgan, C. G. Laser-induced breakdown of gases. *Reports on Progress in Physics*, **38** (1975), 621.

[141] Morsy, M. Review and recent developments of laser ignition for internal combustion engines applications. *Renewable and Sustainable Energy Reviews*, **16** (2012), 4849.

[142] Mulla, I. and Chakravarthy, S. Flame speed and tangential strain measurements in widely stratified partially premixed flames interacting with grid turbulence. *Combustion and Flame*, **161** (2014), 2406.

[143] Mulla, I. A., Chakravarthy, S. R., Swaminathan, N., and Balachandran, R. Evolution of flame-kernel in laser-induced spark ignited mixtures: A parametric study. *Combustion and Flame*, **164** (2016), 303.

[144] Neophytou, A. Spark ignition and flame propagation in sprays (2010).

[145] Neophytou, A., Mastorakos, E., and Cant, R. Complex chemistry simulations of spark ignition in turbulent sprays. *Proceedings of the Combustion Institute*, **33** (2011), 2135.

[146] Neophytou, A., Richardson, E., and Mastorakos, E. Spark ignition of turbulent recirculating non-premixed gas and spray flames: A model for predicting ignition probability. *Combustion and Flame*, **159** (2012), 1503.

[147] Orrin, J., Vince, I., and Weinberg, F. A study of plasma jet ignition mechanisms. In *Proceedings of the combustion Institute*, vol. 18, pp. 1755–1765. Elsevier (1981).

[148] Park, C., Oh, H., Kim, S., Kim, H., Lee, S., and Bae, C. Evaluation and visualization of stratified ultra-lean combustion characteristics in a spray-guided type gasoline direct-injection engine. *International Journal of Automotive Technology*, **15** (2014), 525.

[149] Patel, D. and Chakraborty, N. Localised forced ignition of globally stoichiometric stratified mixtures: A numerical investigation. *Combustion Theory and Modelling*, **18** (2014), 627.

[150] Patel, D. and Chakraborty, N. Effects of energy deposition characteristics on localised forced ignition of homogeneous mixtures. *International Journal of Spray and Combustion Dynamics*, **7** (2015), 151.

[151] Patel, D. and Chakraborty, N. Effects of fuel lewis number on localised forced ignition of globally stoichiometric stratified mixtures: A numerical investigation. *Flow, Turbulence and Combustion*, **96** (2016), 1083.

[152] Patel, D. and Chakraborty, N. Effects of fuel lewis number on localised forced ignition of turbulent homogeneous mixtures: A numerical investigation. *International Journal of Spray and Combustion Dynamics*, **8(3)** (2016).

[153] Patel, D. and Chakraborty, N. Effects of mixture distribution on localised forced ignition of stratified mixtures: A direct numerical simulation study. *Combustion Science and Technology*, **188** (2016), 1904.

[154] Peng, M., Shy, Y., S.S.and Shiu, and Liu, C. High pressure ignition kernel development and minimum ignition energy measurements in different regimes of premixed turbulent combustion. *Combustion and Flame*, **160** (2013), 1755.

[155] Pera, A., Chevillard, S., and Reveillon, J. Effects of residual burnt gas heterogeneity on early flame propagation and on cyclic variability in spark-ignited engines. *Combustion and Flame*, **160** (2013), 1020 .

[156] Pera, C., Knop, V., and Reveillon, J. Influence of flow and ignition fluctuations on cycle-to-cycle variations in early flame kernel growth. *Proceedings of the Combustion Institute*, **35** (2015), 2897.

[157] Peters, N. Length and time scales in turbulent combustion. In *Turbulent Reactive Flows*, pp. 242–256. Springer (1989).

[158] Peters, N. *Turbulent Combustion*. Cambridge Monographs on Mechanics. Cambridge University Press (2000). ISBN 9781139428064.

[159] Poinsot, T., Candel, S., and Trouvé, A. Applications of direct numerical simulation to premixed turbulent combustion. *Progress in Energy and Combustion Science*, **21** (1995), 531.

[160] Poinsot, T. and Lele, S. Boundary conditions for direct simulations of compressible viscous flows. *Journal of computational physics*, **101** (1992), 104.

[161] Poinsot, T. and Veynante, D. *Theoretical and Numerical Combustion*. Edwards (2005). ISBN 9781930217102.

[162] Poinsot, T., Veynante, D., and Candel, S. Diagrams of premixed turbulent combustion based on direct simulation. In *Proceedings of the combustion Institute*, vol. 23, pp. 613–619. Elsevier (1991).

[163] Poinsot, T., Veynante, D., and Candel, S. Quenching processes and premixed turbulent combustion diagrams. *Journal of Fluid Mechanics*, **228** (1991), 561.

[164] Pratt and Canada, W. Pt6a engines. http://www.pwc.ca/en/engines/pt6a.

[165] Prosser, R. Improved boundary conditions for the direct numerical simulation of turbulent subsonic flows. i. inviscid flows. *Journal of Computational Physics*, **207** (2005), 736.

[166] Rao, H. and Lefebvre, A. Ignition of kerosine fuel sprays in a flowing air stream. *Combustion Science and Technology*, **8** (1973), 95.

[167] Rao, K. and Lefebvre, A. Minimum ignition energies in flowing kerosine-air mixtures. *Combustion and Flame*, **27** (1976), 1.

[168] Rashkovsky, S. Spark ignition in imperfectly mixed reactants. In *Proceedings of the 1st Mediterranean Combustion Symposium, Anatalya, Turkey,*, pp. 1403–1411 (1999).

[169] Ray, J., Najm, H., and McCoy, R. Ignition front structure in a methane-air jet. In *Proceedings of the 2nd Joint Meeting of the US Sections of the Combustion Institute, Oakland, CA, Paper*, 150 (2001).

[170] Renou, B., Samson, E., and Boukhalfa, A. An experimental study of freely propagating turbulent propane/air flames in stratified inhomogeneous mixtures. *Combustion science and technology*, **176** (2004), 1867.

[171] Richardson, E. *Ignition modelling for turbulent non-premixed flows*. Ph.D. thesis, University of Cambridge (2007).

[172] Richardson, E. and Mastorakos, E. Numerical investigation of forced ignition in laminar counterflow non-premixed methane-air flames. *Combustion science and technology*, **179** (2007), 21.

[173] Roberts, W., Driscoll, J., Drake, M., and Goss, L. Images of the quenching of a flame by a vortex—to quantify regimes of turbulent combustion. *Combustion and Flame*, **94** (1993), 58.

[174] Rogallo, R. Numerical experiments in homogeneous turbulence. Tech. rep., NASA Technical Memorandum 81315, NASA Ames Research Center, California (1984).

[175] Rosenberg, D. and Driscoll, J. A method to image flame index in partially premixed flames. In *50th AIAA Aerospace Sciences Meeting including the New Horizons Forum and Aerospace Exposition*, pp. 1–12 (2012).

[176] Samson, E. *Etude expérimentale de la propagation de flammes en expansion dans un milieu a richesse stratifiée*. Ph.D. thesis, INSA de Rouen (2002).

[177] Sankaran, R., Im, H., Hawkes, E., and Chen, J. The effects of non-uniform temperature distribution on the ignition of a lean homogeneous hydrogen–air mixture. *Proceedings of the Combustion Institute*, **30** (2005), 875.

[178] Savre, J., Carlsson, H., and Bai, X. Tubulent methane/air premixed flame structure at high karlovitz numbers. *Flow, turbulence and combustion*, **90** (2013), 325.

[179] Schmidt, D. *Laminar flame propagation in mixtures with compositional stratification at small length scales*. Ph.D. thesis, University of Illinois at Urbana-Champaign, University of Illinois at Urbana-Champaign (2011).

[180] Schmitt, M., Frouzakis, C. E., Tomboulides, A. G., Wright, Y. M., and Boulouchos, K. Direct numerical simulation of the effect of compression on the flow, temperature and composition under engine-like conditions. *Proceedings of the Combustion Institute*, **35** (2015), 3069.

[181] Schönfeld, T. and Poinsot, T. Influence of boundary conditions in les of premixed combustion instabilities. *Annual Research Briefs*, (1999), 73.

[182] Shy, S., Chen, Y., Yang, C., Liu, C., and Huang, C. Effects of h_2 or co_2 addition, equivalence ratio, and turbulent straining on turbulent burning velocities for lean premixed methane combustion. *Combustion and Flame*, **153** (2008), 510.

[183] Shy, S., Liu, C., Lin, J., Chen, L., Lipatnikov, A., and Yang, S. Correlations of high-pressure lean methane and syngas turbulent burning velocities: Effects of turbulent reynolds, damköhler, and karlovitz numbers. *Proceedings of the Combustion Institute*, **35** (2015), 1509.

[184] Shy, S., Liu, C., and Shih, W. Ignition transition in turbulent premixed combustion. *Combustion and flame*, **157** (2010), 341.

[185] Shy, S., Shih, W., and Liu, C. More on minimum ignition energy transition for lean premixed turbulent methane combustion in flamelet and distributed regimes. *Combustion Science and Technology*, **180** (2008), 1735.

[186] Sibulkin, M. and Siskind, K. Numerical study of initiation of a combustion wave by an ignition kernel. *Combustion and flame*, **69** (1987), 49.

[187] Sjöberg, M., Dec, J., and Cernansky, N. Potential of thermal stratification and combustion retard for reducing pressure-rise rates in hcci engines, based on multi-zone modeling and experiments. Tech. rep., SAE Technical Paper (2005).

[188] Smirnov, N., Nikitin, V., Dushin, V., Filippov, Y. G., Nerchenko, V., and Khadem, J. Combustion onset in non-uniform dispersed mixtures. *Acta Astronautica*, (2015).

[189] Smith, M., Birch, A., Brown, D., and Fairweather, M. Studies of ignition and flame propagation in turbulent jets of natural gas, propane and a

gas with a high hydrogen content. In *Proceedings of the combustion Institute*, vol. 21, pp. 1403–1408. Elsevier (1988).

[190] Smoke, M. D. and Giovangigli, V. *Formulation of the premixed and non-premixed test problems*, pp. 1–28. Springer (1991).

[191] Strehlow, R. *Fundamentals of combustion*. International Textbook Company Scranton, Pennsylvania (1968).

[192] Sutherland, J. and Kennedy, C. Improved boundary conditions for viscous, reacting, compressible flows. *Journal of computational physics*, **191** (2003), 502.

[193] Swaminathan, N., Grout, R., and Mastorakos, E. Direct simulation of forced ignition in stratified turbulent mixture. In *Proceeding of the Third European Combustion Meeting* (2007).

[194] Sweeney, M., Hochgreb, S., Dunn, M., and Barlow, R. The structure of turbulent stratified and premixed methane/air flames i: Non-swirling flows. *Combustion and flame*, **159** (2012), 2896.

[195] Sweeney, M., Hochgreb, S., Dunn, M., and Barlow, R. The structure of turbulent stratified and premixed methane/air flames ii: Swirling flows. *Combustion and Flame*, **159** (2012), 2912.

[196] Swett, C. Spark ignition of flowing gases using long-duration discharges. In *Proceedings of the combustion Institute*, vol. 6, pp. 523–532. Elsevier (1957).

[197] Tarrazo, E. F., Sánchez, A., Liñán, A., and Williams, F. A. A simple one-step chemistry model for partially premixed hydrocarbon combustion. *Combustion and Flame*, **147** (2006), 32.

[198] Tauer, J., Kofler, H., and Wintner, E. Laser-initiated ignition. *Laser & Photonics Reviews*, **4** (2010), 99.

[199] Teets, R. and Sell, J. Calorimetry of ignition sparks. Tech. rep., SAE Technical Paper (1988).

[200] Temperton, C. Self-sorting mixed-radix fast fourier transforms. *Journal of Computational Physics*, **52** (1983), 1 .

[201] Thevenin, D., Gicquel, O., De Charentenay, J., Hilbert, R., and Veynante, D. Two-versus three-dimensional direct simulations of turbulent methane flame kernels using realistic chemistry. *Proceedings of the Combustion Institute*, **29** (2002), 2031.

[202] Thiele, M., Warnatz, J., Dreizler, A., Lindenmaier, S., Schiessl, R., Maas, U., Grant, A., and Ewart, P. Spark ignited hydrogen/air mixtures: two dimensional detailed modeling and laser based diagnostics. *Combustion and flame*, **128** (2002), 74.

[203] Thiele, M., Warnatz, J., and Maas, U. Geometrical study of spark ignition in two dimensions. *Combustion Theory and Modelling*, **4** (2000), 413.

[204] Thompson, K. W. Time dependent boundary conditions for hyperbolic systems. *Journal of computational physics*, **68** (1987), 1.

[205] Tromans, P. and Furzeland, R. An analysis of lewis number and flow effects on the ignition of premixed gases. In *Proceedings of the combustion Institute*, vol. 21, pp. 1891–1897. Elsevier (1988).

[206] Turns, S. *An Introduction to Combustion: Concepts and Applications*. McGraw-Hill series in mechanical engineering. McGraw-Hill (2012). ISBN 9780071086875.

[207] Vázquez-Espi, C. and Liñán, A. Fast, non-diffusive ignition of a gaseous reacting mixture subject to a point energy source. *Combustion Theory Modelling*, **5** (2001), 485.

[208] Vázquez-Espi, C. and Liñán, A. Thermal-diffusive ignition and flame initiation by a local energy source. *Combustion Theory Modelling*, **6** (2002), 297.

[209] Vena, P., Deschamps, B., Guo, H., and Johnson, M. Effects of stratification on locally lean, near-stoichiometric, and rich iso-octane/air turbulent v-flames. *Combustion and Flame*, **162** (2015), 4231.

[210] Wandel, A. Extinction predictors in turbulent sprays. *Proceedings of the Combustion Institute*, **34** (2013), 1625.

[211] Wandel, A. Influence of scalar dissipation on flame success in turbulent sprays with spark ignition. *Combustion and Flame*, **161** (2014), 2579.

[212] Wandel, A., Chakraborty, N., and Mastorakos, E. Direct numerical simulations of turbulent flame expansion in fine sprays. *Proceedings of the Combustion Institute*, **32** (2009), 2283.

[213] Warris, A. and Weinberg, F. Ignition and flame stabilization by plasma jets in fast gas streams. vol. 20, pp. 1825–1831. Elsevier (1985). ISBN 0082-0784.

[214] Weinberg, F., Hom, K., Oppenheim, A., and Teichman, K. Ignition by plasma jet. (1978).

[215] Wilsted, H. and Armstrong, J. Preliminary results of turbojet-engine altitude-starting investigation. (1951).

[216] Won, S., Kim, J., Hong, K., Cha, M., and Chung, S. Stabilization mechanism of lifted flame edge in the near field of coflow jets for diluted methane. *Proceedings of the Combustion Institute*, **30** (2005), 339.

[217] Wu, F., Saha, A., Chaudhuri, S., and Law, C. K. Propagation speeds of expanding turbulent flames of c 4 to c 8 n-alkanes at elevated pressures: Experimental determination, fuel similarity, and stretch-affected local extinction. *Proceedings of the Combustion Institute*, **35** (2015), 1501.

[218] Wu, W., Zhou, X., Yang, L., He, C., Peng, F., Ji, J., and Zhong, C. Experimental study on the effect of the igniter position on piloted ignition of polymethylmethacrylate. *Journal of Fire Sciences*, (2012), 0734904112447598.

[219] Yamashita, H., Shimada, M., and Takeno, T. A numerical study on flame stability at the transition point of jet diffusion flames. In *Proceedings of the combustion Institute*, vol. 26, pp. 27–34. Elsevier (1996).

[220] Yoo, C. and Im, H. Transient dynamics of edge flames in a laminar nonpremixed hydrogen–air counterflow. *Proceedings of the Combustion Institute*, **30** (2005), 349.

[221] Zhang, H., Hawkes, E. R., Chen, J., and Kook, S. A numerical study of the autoignition of dimethyl ether with temperature inhomogeneities. *Proceedings of the Combustion Institute*, **34** (2013), 803.

[222] Zheng, X. and Mantzaras, J. An analytical and numerical investigation of hetero-/homogeneous combustion with deficient reactants having larger than unity lewis numbers. *Combustion and Flame*, **161** (2014), 1911.

[223] Zhou, J., Nishida, K., Yoshizaki, T., and Hiroyasu, H. Flame propagation characteristics in a heterogeneous concentration distribution of a fuel-air mixture. Tech. rep., SAE Technical Paper (1998).

[224] Zhou, R., Balusamy, S., Sweeney, M., Barlow, R., and Hochgreb, S. Flow field measurements of a series of turbulent premixed and stratified methane/air flames. *Combustion and Flame*, **160** (2013), 2017.